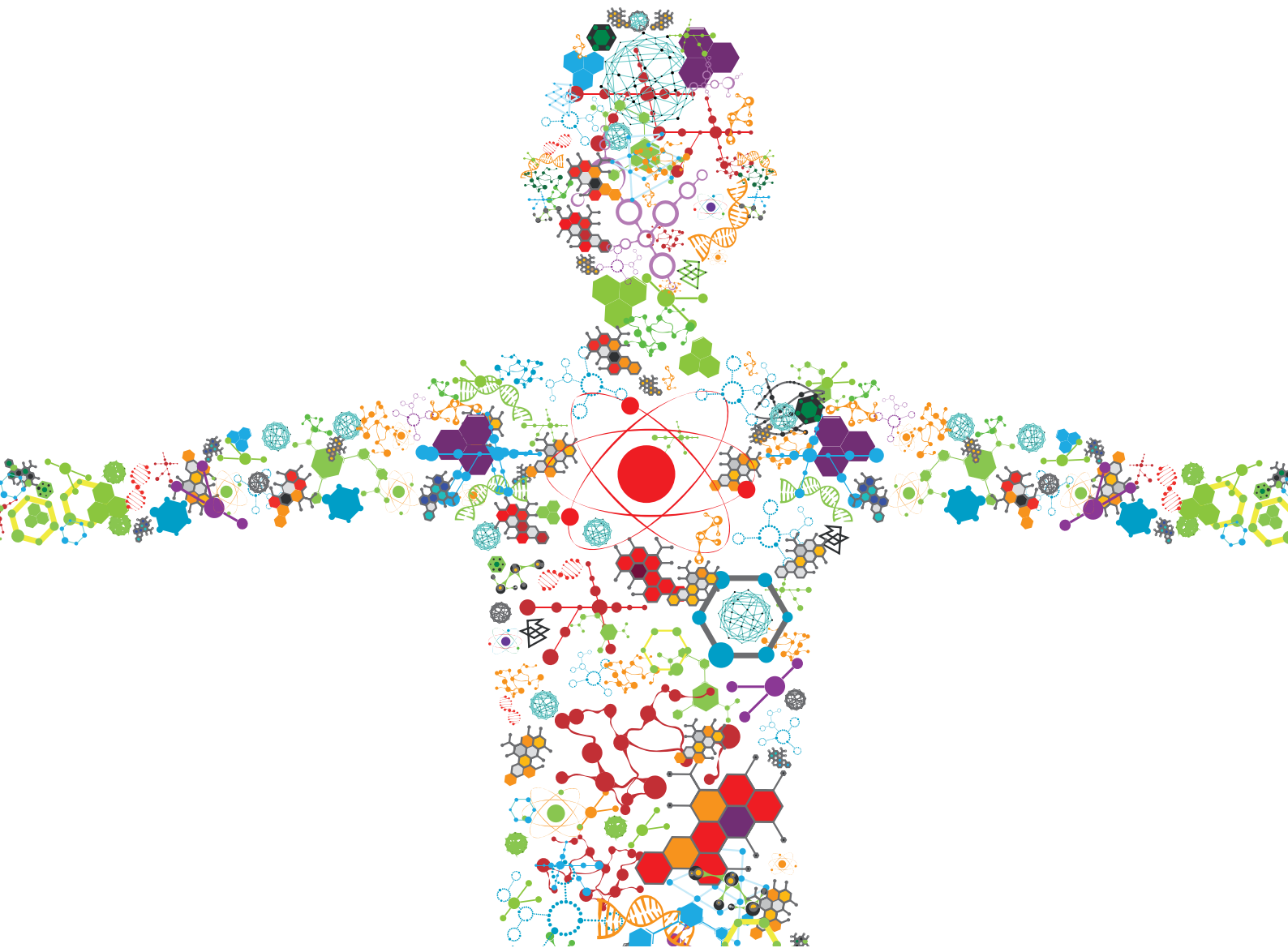


BIOMATERIALS FOR SKIN WOUND REPAIR: TISSUE ENGINEERING, GUIDED REGENERATION, AND WOUND SCARRING PREVENTION

EDITED BY: Ubaldo Armato, Bing Tang and Giuliano Freddi
PUBLISHED IN: Frontiers in Bioengineering and Biotechnology





frontiers

Frontiers eBook Copyright Statement

The copyright in the text of individual articles in this eBook is the property of their respective authors or their respective institutions or funders. The copyright in graphics and images within each article may be subject to copyright of other parties. In both cases this is subject to a license granted to Frontiers.

The compilation of articles constituting this eBook is the property of Frontiers.

Each article within this eBook, and the eBook itself, are published under the most recent version of the Creative Commons CC-BY licence.

The version current at the date of publication of this eBook is CC-BY 4.0. If the CC-BY licence is updated, the licence granted by Frontiers is automatically updated to the new version.

When exercising any right under the CC-BY licence, Frontiers must be attributed as the original publisher of the article or eBook, as applicable.

Authors have the responsibility of ensuring that any graphics or other materials which are the property of others may be included in the CC-BY licence, but this should be checked before relying on the CC-BY licence to reproduce those materials. Any copyright notices relating to those materials must be complied with.

Copyright and source acknowledgement notices may not be removed and must be displayed in any copy, derivative work or partial copy which includes the elements in question.

All copyright, and all rights therein, are protected by national and international copyright laws. The above represents a summary only. For further information please read Frontiers' Conditions for Website Use and Copyright Statement, and the applicable CC-BY licence.

ISSN 1664-8714

ISBN 978-2-88971-329-5

DOI 10.3389/978-2-88971-329-5

About Frontiers

Frontiers is more than just an open-access publisher of scholarly articles: it is a pioneering approach to the world of academia, radically improving the way scholarly research is managed. The grand vision of Frontiers is a world where all people have an equal opportunity to seek, share and generate knowledge. Frontiers provides immediate and permanent online open access to all its publications, but this alone is not enough to realize our grand goals.

Frontiers Journal Series

The Frontiers Journal Series is a multi-tier and interdisciplinary set of open-access, online journals, promising a paradigm shift from the current review, selection and dissemination processes in academic publishing. All Frontiers journals are driven by researchers for researchers; therefore, they constitute a service to the scholarly community. At the same time, the Frontiers Journal Series operates on a revolutionary invention, the tiered publishing system, initially addressing specific communities of scholars, and gradually climbing up to broader public understanding, thus serving the interests of the lay society, too.

Dedication to Quality

Each Frontiers article is a landmark of the highest quality, thanks to genuinely collaborative interactions between authors and review editors, who include some of the world's best academicians. Research must be certified by peers before entering a stream of knowledge that may eventually reach the public - and shape society; therefore, Frontiers only applies the most rigorous and unbiased reviews.

Frontiers revolutionizes research publishing by freely delivering the most outstanding research, evaluated with no bias from both the academic and social point of view. By applying the most advanced information technologies, Frontiers is catapulting scholarly publishing into a new generation.

What are Frontiers Research Topics?

Frontiers Research Topics are very popular trademarks of the Frontiers Journals Series: they are collections of at least ten articles, all centered on a particular subject. With their unique mix of varied contributions from Original Research to Review Articles, Frontiers Research Topics unify the most influential researchers, the latest key findings and historical advances in a hot research area! Find out more on how to host your own Frontiers Research Topic or contribute to one as an author by contacting the Frontiers Editorial Office: frontiersin.org/about/contact

BIOMATERIALS FOR SKIN WOUND REPAIR: TISSUE ENGINEERING, GUIDED REGENERATION, AND WOUND SCARRING PREVENTION

Topic Editors:

Ubaldo Armato, University of Verona, Italy

Bing Tang, First Affiliated Hospital of Sun Yat-sen University, China

Giuliano Freddi, Other, Italy

Dr. Giuliano Freddi is Chief Scientific Officer and co-founder of the company Silk Biomaterials srl. All other Guest Editors declare no competing interests with regards to the Topic subject.

Citation: Armato, U., Tang, B., Freddi, G., eds. (2021). Biomaterials for Skin Wound Repair: Tissue Engineering, Guided Regeneration, and Wound Scarring Prevention. Lausanne: Frontiers Media SA. doi: 10.3389/978-2-88971-329-5

Table of Contents

- 04 Editorial: Biomaterials for Skin Wound Repair: Tissue Engineering, Guided Regeneration, and Wound Scarring Prevention**
Ubaldo Armato and Giuliano Freddi
- 07 The Correlation Between Quality of Life and Acceptability of Disability in Patients With Facial Burn Scars**
Xiuni Zhang, Yuan Liu, Xiaohong Deng, Chengsong Deng, Yunfeng Pan and Ailing Hu
- 14 A Systematic Review and Meta-Analysis of Clinical Effectiveness and Safety of Hydrogel Dressings in the Management of Skin Wounds**
Lijun Zhang, Hanxiao Yin, Xun Lei, Johnson N. Y. Lau, Mingzhou Yuan, Xiaoyan Wang, Fangyingnan Zhang, Fei Zhou, Shaohai Qi, Bin Shu and Jun Wu
- 30 Three-Layered Silk Fibroin Tubular Scaffold for the Repair and Regeneration of Small Caliber Blood Vessels: From Design to in vivo Pilot Tests**
Antonio Alessandrino, Anna Chiarini, Marco Biagiotti, Ilaria Dal Prà, Giulia A. Bassani, Valentina Vincoli, Piergiorgio Settembrini, Pasquale Pierimarchi, Giuliano Freddi and Ubaldo Armato
- 47 Preparation of Antimicrobial Hyaluronic Acid/Quaternized Chitosan Hydrogels for the Promotion of Seawater-Immersion Wound Healing**
Xinlu Wang, Pengcheng Xu, Zexin Yao, Qi Fang, Longbao Feng, Rui Guo and Biao Cheng
- 67 Electrospun Nanofibrous Poly (Lactic Acid)/Titanium Dioxide Nanocomposite Membranes for Cutaneous Scar Minimization**
Teresa C. O. Marsi, Ritchelli Ricci, Tatiane V. Toniato, Luana M. R. Vasconcellos, Conceição de Maria Vaz Elias, Andre D. R. Silva, Andre S. A. Furtado, Leila S. S. M. Magalhães, Edson C. Silva-Filho, Fernanda R. Marciano, Andrea Zille, Thomas J. Webster and Anderson O. Lobo
- 81 Application of 3D Printed Models of Complex Hypertrophic Scars for Preoperative Evaluation and Surgical Planning**
Peng Liu, Zhicheng Hu, Shaobin Huang, Peng Wang, Yunxian Dong, Pu Cheng, Hailin Xu, Bing Tang and Jiayuan Zhu
- 88 Selection of Appropriate Wound Dressing for Various Wounds**
Chenyu Shi, Chenyu Wang, He Liu, Qiuju Li, Ronghang Li, Yan Zhang, Yuzhe Liu, Ying Shao and Jincheng Wang
- 105 Electrospun Biomaterials in the Treatment and Prevention of Scars in Skin Wound Healing**
Eoghan J. Mulholland
- 120 Targeting Tunable Physical Properties of Materials for Chronic Wound Care**
Yuzhen Wang, Ubaldo Armato and Jun Wu
- 134 Anatomical Characteristics of Cutaneous Branches Extending From the Second Dorsal Metacarpal Artery**
Peng Liu, Zhongyuan Deng, Tao Zhang and Xiaojian Li



Editorial: Biomaterials for Skin Wound Repair: Tissue Engineering, Guided Regeneration, and Wound Scarring Prevention

Ubaldo Armato^{1,2*} and Giuliano Freddi³

¹Department of Burns and Plastic Surgery, 2nd People's Hospital, Shenzhen University, Shenzhen, China, ²Department of Surgery, Dentistry, Paediatrics and Gynaecology, Medical School, University of Verona, Verona, Italy, ³Silk Biomaterials S.r.l., Lomazzo, Italy

Keywords: skin wounds, burns, ulcers, tissue engineering, biomaterial-guided regeneration, scar hypertrophy, scar retraction

Editorial on the Research Topic

Biomaterials for Skin Wound Repair: Tissue Engineering, Guided Regeneration, and Wound Scarring Prevention

Although laypersons may not realize it, the skin or integument is the largest and heaviest organ of our body. It is of the utmost importance that as a boundary organ it keeps its integrity and functions. True, the skin's esthetic role crucially mediates social and emotional interactions. But there is much more than this: wounds due to any factor or agent impair the integument's barrier function allowing the entry of infectious agents and the concurrent loss of blood and interstitial fluid components. Wounds' severity is proportional to their extent and depth. Still other etiologic factors drive acute and chronic diseases also altering the skin's barrier. Most importantly, bidirectional pathophysiological links exist between the skin and internal organs. A diseased organ can alter skin's structure and function. For example, immune reactions to foreign or endogenous antigens or malignancy may drive a diffuse urticaria (hives). As an example of the reverse, extensive deep burn wounds both favor infections and release toxins inducing multiple organs failure and jeopardizing patients' survival.

Prevalence of severe skin wounds varies according to countries and ongoing socioeconomic (e.g., urbanization) and political factors (skin burns—and not bullet lesions—are the commonest injuries affecting wounded soldiers). Such wounds impact on the patients' survival odds, length of hospital stays, healing with hypertrophied scars (keloids) and functional impairments from scar retraction. Serious burns also alter patients' body image, which results in psychological reverberations due to more difficult social and emotional interactions with third persons, and job-, and daily tasks coping-related hurdles. Moreover, chronic skin wounds or ulcers often concur with lifestyle-related metabolic disorders and are a growing worldwide issue causing a huge financial burden on healthcare systems.

Sen (2021) recently reviewed the available data on the economic impact of chronic wounds in the United States, pointing out that wound management is still an open clinical problem and that it will continue to be a substantial clinical, social, and economic challenge for the future. The coronavirus pandemic made this problem even worse, due to the dramatic disruption that caused in the healthcare systems worldwide. In fact, higher risks of more severe symptoms or even of death have been observed for patients with chronic wounds and related comorbidities left untreated or improperly managed.

The paper of Sen C.K. systematically reviews the most recent epidemiological data about the incidence of wound diseases, not only chronic wounds, but also pressure, foot, and venous ulcers, acute wounds, as well as diabetes-, obesity-, and infection-associated diseases. Moreover, it presents estimates about the percentage of population involved, healthcare costs, market size, and trend of care products consumption.

OPEN ACCESS

Edited and reviewed by:

Hasan Uludag,
University of Alberta, Canada

*Correspondence:

Ubaldo Armato
uarmato@me.com

Specialty section:

This article was submitted to
Biomaterials,
a section of the journal
Frontiers in Bioengineering and
Biotechnology

Received: 08 June 2021

Accepted: 07 July 2021

Published: 19 July 2021

Citation:

Armato U and Freddi G (2021)
Editorial: Biomaterials for Skin Wound
Repair: Tissue Engineering, Guided
Regeneration, and Wound
Scarring Prevention.
Front. Bioeng. Biotechnol. 9:722327.
doi: 10.3389/fbioe.2021.722327

As an example, here they report some data on the impact of chronic wounds, which are mostly seen in the elderly population (over 65 years). In the United States, 3% of these people have open wounds. It is foreseen that chronic wound will continue to be an increasingly persistent problem owing to the estimate of elderly population increase over the next decades. Accordingly, the wound care market is projected to reach \$18.7 billion by 2027, with a Compound Annual Growth Rate (CAGR) of 6.6%.

As the author keenly suggests, several social, economic, environmental, psychological determinants are known to interact with the biology of the individual and to determine health outcomes such as disease development, wound healing, and life expectancy. Thus, for an integrated approach to be successful, investments are needed in welfare, education, healthcare, and research, with a patient-centered view aimed at establishing an interdisciplinary environment able to address the still open challenges.

Last decades' scientific progress has made a remarkable impression on basic research attempts to clarify the intricate pathophysiological mechanisms involved in skin wound healing and on the clinical management of acute and chronic skin wounds. Both types of endeavors have been aiming at improving the clinical upshots of severe skin wounds and at mitigating their healthcare, economic, and social consequences. In keeping with these trends, this Research Topic updates the results of recent basic and applied research in the complex field of wound repair.

A first group papers explores innovative approaches to prevent or treat or mitigate wound's hypertrophic and retracting scars and their unpleasant consequences.

To start with, the study of Liu et al. deals with the cutaneous distribution of the branches of the second dorsal metacarpal artery, which supply a skin flap frequently used to surgically repair hand and fingers wounds. Defining the courses of such cutaneous branches is crucial to the flap's therapeutic success. The authors examined specimens from 16 subjects to assess and measure the origin, and course of the said artery branches and their relative location in the hand with respect to the dorsal branch of the radial nerve. They conclude that three clusters in the distal branches of the second dorsal metacarpal artery must be used as the flap's pedicles to successfully repair wounds of the hand and fingers.

A second paper by Liu et al. concerns the novel preoperative use of 3D printed models to plan and conduct the surgical removal of complex hypertrophic scars, which cause multiple joint contractures and deformities. By availing themselves of cross-sectional computed tomography (CT) scan data the authors produced 3D printed reduced-scale models accurately reproducing the patients' keloids. Preoperative simulations using such 3D printed models allowed to successfully remove each scar. Therefore, using such preoperative 3D printed models not only will allow surgeons to fully excise keloids but also will advance young doctors' training and patients' confidence.

Moreover, Zhang et al. tackle another clinically relevant facet of cutaneous scars. They investigated whether and how much the life quality of patients bearing facial burn scars depends on acceptance of their disability. The results showed that the overall quality of life of such patients is positively correlated with the degree of their disability acceptance. Therefore, the authors suggest that a primary therapeutic target of the medical and nursing staff is heightening the patients' disability acceptance.

The second group of papers deals with the selection, production, and testing of novel biomaterials targeted for more therapeutically advantageous wound bandages and with the development of novel 3D biomaterial scaffolds for tissue and vascular engineering/regeneration.

Wound healing is a dynamic process going through succeeding stages deeply influenced by concurring local (e.g., infection), general (e.g., diabetes), and therapeutic (e.g., specific bandages) factors. In this framework, Wang et al. deal with the all-important topic of chronic wounds due to diabetes, infections, or radiation exposure, which altogether constitute a worldwide growing medical problem. The authors mention recent studies showing that physical cues significantly impact on both stem cells fate and bacterial resistance. Therefore, it would be beneficial to tune up the physical properties of the biomaterials—particularly of those made of nanoparticles (NPs)—used for chronic wounds. To improve the latters' care and healing upshots, the authors analyze the tunable physical (i.e., mechanical-, structural- and size-related) properties of both dermal matrixes and wound bandages. Moreover, they discuss the physical and structural factors governing stem cells' fate. Next, they survey wound dressings according to the size-related properties of their components (i.e., metal NPs, lipid NPs, and polymeric NPs). Finally, they focus on the known problem caused by AgNPs cytotoxicity proposing size-, dose-, and time-dependent solutions to prevent it.

From another relevant standpoint, Shi et al. examine the rational criteria that should govern an optimal selection of dressings for each type of wounds in clinical settings. To improve the readers' understanding of the topic, they summarize wound dressings' developmental history and classify the current bandage's types. Next, they expound the clinical guidelines to select the best wound dressings according to wound types. In doing this, they focus on burn wounds and on chronic ulcers caused by diabetes, pressure, and/or varicose veins. Usefully, the authors discuss in detail the pros and cons underlying the dressing choices for each wound type.

Two more contributions examine the clinical effectiveness and safety of hydrogel-based dressings as skin wounds therapeutics. On the one hand, Zhang et al. undertake a systematic review and meta-analysis of 43 clinical trials that compared hydrogel bandages vs. non-hydrogel dressings. The results showed that the hydrogel dressings were therapeutically advantageous under several respects, including pain alleviation, both for acute and chronic skin injuries. Therefore, the authors posit that hydrogel dressings are effective and safe therapeutics for skin wounds management. On the other hand, Wang et al. describe a novel set of composite hydrogels made of oxidized and/or hydrazide hyaluronic acid (HA) and quaternized chitosan (QCS). The authors investigated whether HA/QCS hydrogels did prevent bacterial infections and promote the healing of seawater-immersed wounds. The results of *in vitro* and *in vivo* tests showed that HA/QCS hydrogels were biocompatible and inhibited bacterial growth. *In vivo*, these hydrogels also efficiently promoted the repair of seawater-immersed wounds. Therefore the authors postulate that HA/QCS hydrogels advance the healing of chronic wounds from various causes.

Concerning another field of endeavor, Mulholland provides recent details about the electrospinning technique that rapidly and cost-effectively allows to produce nanofibers from a wide variety of (bio)polymers. The nanofibers' exceedingly high surface area makes them excellent components of novel wound dressings. The author points out that using electrospun biomaterials can confer an enhanced tensile strength to the engineered/regenerated skin and prevent or mitigate hypertrophic scar development. Since electrospun biomaterials hold such enticing promises, the author suggests refining the electrospinning technique to combine it with innovative gene therapies to boost tissue repair and minimize scarring.

In the same context, Marsi et al. report on the electrospinning of a classical biomaterial component, i.e., poly(lactic acid) (PLA) combined with titanium dioxide (TiO₂). PLA is biodegradable, biocompatible, easy to manage, and suitable to form composites. Due to its favorable characteristics and low cost, the use of PLA for skin tissue engineering/regeneration has been increasing with time. The authors prepared electrospun PLA/TiO₂ nanofibrous composites and minutely analyzed their properties and biocompatibility using various *in vitro* and *in vivo* preclinical assays. Importantly, the PLA/TiO₂ nanopolymers exhibited a nanoporous structure mimicking cellular environments and were not cytotoxic at all. Altogether, the results supported the view that PLA/TiO₂ nanomembranes may hinder scarring.

Purified silk fibroin (SF), a biomacromolecule produced by domesticated *Bombyx mori* silkworm and other insects, is also amenable to electrospinning. SF lends itself to be formed as 2D membranes or 3D scaffolds made of microfibers or nanofibers, or hydrogels. SF's popularity as biomaterial is due to a remarkable set of features. First, SF is highly biocompatible and rightly so: about 50 human proteins own conserved homology sequences of *Bombyx mori*'s SF (Armato et al., 2011). Second, SF is neither persistently inflammagenic nor profibrogenic nor cytotoxic. Third, once grafted SF does not induce any foreign body response (Dal Prà et al., 2005; Chiarini et al., 2016). Fourth, SF-adhering human fibroblasts cultured *in vitro* persistently release exosomes carrying heightened amounts of various angiogenic factors (Hu et al., 2021). Obviously, to become manifest all these advantageous properties strictly require using a very highly purified SF. In this context, Alessandrino

et al. report on the properties of a newly multi-layered SF tubular scaffold, named SilkGraf, designed to substitute, repair, or regenerate small peripheral arteries. SilkGraf samples kept for 20 days *in vitro* promoted the adhesion, survival, metabolism, and growth of human coronary artery endothelial cells, aortic smooth muscle cells, and aortic adventitial fibroblasts. Notably, the SilkGraf-attached aortic fibroblasts synthesized much smaller amounts of type I procollagen than they did on polystyrene, further strengthening the view (Dal Prà et al., 2005; Chiarini et al., 2016) that SF hinders fibrogenesis and hypertrophic scarring. Moreover, the SilkGraf-attached three cell types did not secrete any proinflammatory cytokines. In addition, SilkGraf samples exhibited a good hemocompatibility. Finally, *in vivo* pilot trials identified the sheep as the animal model apt for future medium-to-long term preclinical trials with SilkGraf.

CONCLUSION

On a personal note, I wish to state that editing these paper in this Research Topic was profitable under both the scientific and human relationship standpoints. On a more general note, I expect that this Research Topic of innovative research works will inspire the readers to conceive, produce, and experimentally evaluate novel dermal matrixes and/or wound dressings based upon even more advanced design strategies to further improve skin wounds' therapeutic management.

AUTHOR CONTRIBUTIONS

The authors confirms being the sole contributor of this work and have approved it for publication.

ACKNOWLEDGMENTS

We thank the co-Editor of this Research Topic, Bing Tang for his cooperation. We also express our deep gratitude to Anna Chiarini and Ilaria Dal Prà, who have been very valuably collaborating with us for nearly 3 decades. No funding to be acknowledged.

REFERENCES

- Armato, U., Dal Prà, I., Chiarini, A., and Freddi, G. (2011). Will Silk Fibroin Nanofiber Scaffolds Ever Hold a Useful Place in Translational Regenerative Medicine?. *Int. J. Burns Trauma* 1 (1), 27–33.
- Chiarini, A., Freddi, G., Liu, D., Armato, U., and Dal Prà, I. (2016). Biocompatible Silk Noil-Based Three-Dimensional Carded-Needled Nonwoven Scaffolds Guide the Engineering of Novel Skin Connective Tissue. *Tissue Eng. A* 22 (15–16), 1047–1060. doi:10.1089/ten.TEA.2016.0124
- Dal Prà, I., Freddi, G., Minic, J., Chiarini, A., and Armato, U. (2005). De Novo Engineering of Reticular Connective Tissue *In Vivo* by Silk Fibroin Nonwoven Materials. *Biomaterials* 26 (14), 1987–1999. doi:10.1016/j.biomaterials.2004.06.036
- Hu, P., Chiarini, A., Wu, J., Freddi, G., Nie, K., Armato, U., et al. (2021). Exosomes of Adult Human Fibroblasts Cultured on 3D Silk Fibroin Nonwovens Intensely Stimulate Neovascularization. *Burns & Trauma* 9, tkab003. doi:10.1093/burnst/tkab003
- Sen, C. K. (2021). Human Wound and its Burden: Updated 2020 Compendium of Estimates. *Adv. Wound Care* 10 (5), 281–292. doi:10.1089/wound.2021.0026

Conflict of Interest: Author GF is a cofounder and shareholder of Silk Biomaterials s.r.l.

The remaining author declares that the work was conducted in the absence of any commercial or financial relationships that could be construed as a potential conflict of interest.

Copyright © 2021 Armato and Freddi. This is an open-access article distributed under the terms of the Creative Commons Attribution License (CC BY). The use, distribution or reproduction in other forums is permitted, provided the original author(s) and the copyright owner(s) are credited and that the original publication in this journal is cited, in accordance with accepted academic practice. No use, distribution or reproduction is permitted which does not comply with these terms.



The Correlation Between Quality of Life and Acceptability of Disability in Patients With Facial Burn Scars

Xiuni Zhang^{1†}, Yuan Liu^{2†}, Xiaohong Deng^{2†}, Chengsong Deng², Yunfeng Pan^{2*} and Ailing Hu^{2*}

¹ Department of Trauma and Orthopaedics, Guangzhou Panyu Central Hospital, Guangzhou, China, ² Third Affiliated Hospital of Sun Yat-sen University, Guangzhou, China

OPEN ACCESS

Edited by:

Bing Tang,
First Affiliated Hospital of Sun Yat-sen
University, China

Reviewed by:

Narendra Pal Singh Chauhan,
Bhopal Nobles University, India
Jianxun Ding,
Changchun Institute of Applied
Chemistry (CAS), China

*Correspondence:

Yunfeng Pan
p-yunfeng@163.com
Ailing Hu
h-ailing@163.com

[†]These authors have contributed
equally to this work and share first
authorship

Specialty section:

This article was submitted to
Biomaterials,
a section of the journal
Frontiers in Bioengineering and
Biotechnology

Received: 23 August 2019

Accepted: 29 October 2019

Published: 14 November 2019

Citation:

Zhang X, Liu Y, Deng X, Deng C,
Pan Y and Hu A (2019) The
Correlation Between Quality of Life
and Acceptability of Disability in
Patients With Facial Burn Scars.
Front. Bioeng. Biotechnol. 7:329.
doi: 10.3389/fbioe.2019.00329

The purpose of our research is to understand the status of the quality of life and level of disability acceptance in patients with facial burn scars and to explore the correlation between quality of life and disability acceptance and how to improve nursing care for these patients. Patients with facial burn scars were investigated in an outpatient clinic of tertiary hospitals from September 2015 to February 2016. A cross-sectional survey was conducted. The questionnaires used included demographic data and investigations using the burn scars table, Burn-Specific Health Scale-Brief (BSHS-B), and acceptance disability scale (ADS). Differences between participants in terms of demographic characteristics, quality of life, and disability acceptance were assessed using two-tailed independent *t*-tests. The total score of quality of life and disability acceptance in facial burn scar patients was 137.06 ± 17.05 and 185.68 ± 23.74 , respectively. The results of Spearman correlation analysis showed that the overall quality of life score of facial burn scar patients was positively correlated with disability acceptance ($r = 0.245$, $p = 0.007$). The quality of life of facial burn scar patients will improve with the improvement of disability acceptance level. Therefore, medical staff can improve the quality of life of patients by improving their disability acceptance level.

Keywords: quality of life, acceptability of disability, facial, burn scars, nursing

INTRODUCTION

Burns are generally caused by high-intensity currents, high temperatures, chemicals, physical rays, etc. (Simons et al., 2018; Van Lieshout et al., 2018). With continuous mechanization and urbanization, the incidence of burns continues to increase. Although the government's efforts in prevention and treatment have reduced the mortality of burn, the disability rate of burn patients has not decreased. It is reported that the annual incidence of burns in China is ~2% (Brewin and Homer, 2018), which occupies the second highest mortality rate among accidents. As an obvious exposed part of the body, facial burns account for more than half of all burn incidents.

The loose subcutaneous adipose tissue and complex vascular nerves in facial areas makes it easier for body fluids to accumulate in the interstitial space. At the same time, the body's own oral and nasal secretions increase the incidence of infection in facial burns, resulting in hypertrophic scars or keloids during the tissue repair process (Kowal-Vern and Criswell, 2005). Deep second degree burns usually leave scars of different sizes, and when the wounds are not treated properly, shallow second degree burns or even degree I burns may form scars.

Scars after burns can cause dysfunction and disfigurement, which greatly affects the patient's daily life and social interaction. Patients often feel disappointment, fear, inferiority, anxiety, loneliness, suspiciousness, and mental disorders due to changes in their appearance. Disfigurement can also lead to social escape. Some patients still cannot accept themselves after long-term recovery and even have a suicidal tendency (Yurdalan et al., 2018).

Burns can produce negative emotions such as anxiety and depression, which in turn affect the quality of life (Kowal-Vern and Criswell, 2005; Miller et al., 2013; Cakir et al., 2015; Spronk et al., 2018a). Studies have shown that the quality of life of patients with burn scars is moderate. A survey (Palmu et al., 2015) showed that the quality of life (QOL) in patients with small burns was higher than the QOL in patients with a total burn area of 30%. At the same time, most patients agree that face and hand burns have a greater impact on the patient's QOL than the actual burn area does. Salvador-Aanza et al. found that different burn patients have different changes in their body, in mental function and in other dimensions. There are many studies on the psychological function of patients after burns at home and away, but systematic research on the QOL in patients with facial burn scars is rarely reported. Some current studies have shown that the factors affecting the quality of life of patients with facial burn scars are as follows (Finnerty et al., 2016; Polychronopoulou et al., 2018): social factors [gender, marital status, occupation, and economic status (Levi et al., 2018; Spronk et al., 2018a)] disease-related factors [effects of scarring on facial function, the degree of influence, the degree of burn, and the duration of disease (Watson et al., 2018)] and psychosocial factors (stress, suppression, social support, and disability acceptance) (Garcia et al., 2016).

Disability acceptance refers to the degree to which a patient builds his or her own knowledge by integrating his or her lifestyle into an experience of dealing with disability. Patients with a higher level of disability acceptance can truly understand the meaning of existence and the ability of the group at the present stage by realizing the loss of their own value and group value due to their disabilities (Nicholls et al., 2012). Therefore, the degree of disability acceptance can predict an individual's ability to respond to attitudes against disability. The obvious exposure of facial burn scars and the importance of appearance characteristics may easily lead to a feeling of inferiority in patients with facial burn scars. Additional research efforts should be made toward understanding the relevant psychological changes after discharge from the hospital, such as the acceptance of disability.

Researchers have studied the correlation between quality of life and disability acceptance. Some studies have shown that quality of life is affected by the acceptance of disability. The level of patient disability acceptance increases with the duration of disability, and the patient is better able to adapt to life after the illness, so the quality of life also has a significant upward trend. The quality of life also increases significantly (Garcia et al., 2016). The reasons may be as follows. (a) Patients are more able to adapt to life after a longer duration of disability. (b) The effect of rehabilitation therapy is more obvious over time, and the degree of patient disability also improves. There are also

studies (Nicholls et al., 2012; Baldwin et al., 2018) that indicate that there is a positive correlation between quality of life and disability acceptance.

In summary, it may have a special relationship between Quality of life and disability acceptance in patients with facial burn. However, there is no quantitative study between the two factors. Therefore, we conducted a case investigation to understand the status of the quality of life and level of disability acceptance in patients with facial burn scars and to explore the correlation between quality of life and disability acceptance and how to improve nursing care for these patients.

METHODS

Participants

Patients with facial burn scars were investigated in an outpatient clinic of tertiary hospitals from September 2015 to February 2016. All participants are voluntary and signed informed consent before investigation.

The inclusion criteria were as follows:

- (1) Patient age ≥ 18 years old
- (2) Patients with facial damage caused only by heat, current, chemicals, laser exposure, radiation, etc., and the wound had a hypertrophic scar or keloid of $>2\text{ cm}^2$ after healing
- (3) Conscious patients
- (4) Patients with an educational level of primary school and above

The exclusion criteria were as follows:

- (1) Patients with disabilities in other parts of the body
- (2) Patients with heart failure, severe liver disease, stroke, and other serious physical illnesses
- (3) Patients with a history of mental illness

All participants are voluntary and signed informed consent before investigation.

Investigation

In this study, a cross-sectional survey was conducted to investigate the demographic information, quality of life, disability acceptance, and related factors of patients with facial burn scars after discharge. The questionnaires used included demographic data and investigations using the burn scars table, Burn-Specific Health Scale-Brief (BSHS-B), and acceptance disability scale (ADS). This study was approved by the ethics committee of the central hospital of Panyu District, Guangzhou.

Measures

Demographic Data and Survey on Burn Scarring

An investigation was conducted by a self-designed questionnaire, which includes 10 questions (gender, age, educational level, pre-burn occupation, current occupation, marital status, place of residence, per capita monthly income of the family, average monthly treatment cost, and mode of payment for medical expenses). The disease and treatment-related information questionnaire included eight questions [cause of burn, time of scar formation, scar site, scar area, whether the patient thinks

the burn scar affects facial function (e.g., facial function, sweat gland function, etc.), observation of scar by the patient, length of hospitalization, and presence of burns on other body parts].

Burn-Specific Health Scale-Brief (BSHS-B)

The Burn-Specific Health Scale-Brief was used to investigate the quality of life. The scale includes 9 dimensions and 40 items, including body image, work, heat sensitivity, treatment regimens, simple abilities, interpersonal relationships, hand function, affect, and sexuality. Each item of the scale has 5 rating options for each dimension score, and the Likert 5-point scale was adopted. The scale of 1–5 points for items 1–9 represents 5 levels of “failure to achieve.” The scale of 1–5 for items 10–40 represent 5 grades of “conformity,” from complete conformity to non-conformity. The lower the score of each dimension is, the lower the quality of life (Chin et al., 2018). Previous studies have shown that the scale has good reliability and validity [83], and the Chinese version of the simplified burn health scale BSHS-B has a total Cronbach's α reliability coefficient of 0.968 and Cronbach's α coefficient of 0.795–0.940 after being evaluated by relevant professionals (Gandolfi et al., 2018).

Acceptance Disability Scale (ADS)

The scale includes four dimensions called transformation, enlargement, containment and subordination, with a total of 50 items, in which 35 items are scored in a negative direction (one point representing “agree very much” and six points representing “disagree very much”). The remaining 15 items were scored positively. The total score of the scale ranged from 50 to 300. Low acceptance level is defined as a total score of 50–133, and scores ranging from 134 to 217 and 218 to 300 were for moderate and high acceptance levels, respectively. The subordination dimension ranges from 5 to 30 points, in which the ranges of 5–12, 13–22, and 23–30 are defined as low, moderate and high acceptance levels, respectively. The containment dimension ranges from 16 to 96 points, in which the ranges of 16–42, 43–79, and 80–96 are defined as low, moderate and high acceptance levels, respectively. The transformation dimension ranges from 15 to 90 points, in which the ranges of 15–40, 41–65, and 66–90 are defined as low, moderate and high acceptance levels, respectively. The enlargement dimension ranges from 14 to 84 points, in which the ranges of 14–37, 38–61, and 62–84 are defined as low, moderate and high acceptance levels, respectively. The Cronbach's α value of this scale is 0.95 (Nicholls et al., 2012).

Sample Size Calculation

The sample size was calculated according to the total number of scale dimensions used. The empirical formula is sample size = [Max (dimension degree) \times (10–20)] \times [1 + (10%–15%)]. Among the questionnaires used in this survey, the Chinese version of the BSHS-B has the highest dimensionality coefficient, with a dimensionality of 9; therefore, the dimensionality of this scale is used as the benchmark for the sample size. Considering some invalid questionnaires, the sample size required for this survey is finally defined as 130 patients.

Quality Control

Before the investigation, the specialist nurses were given unified training on the scoring methods of the BSHS-B, ADS and disability acceptance scale, and the contents of the questionnaires were explained in the same words without guidance. Researchers and trained specialist nurses handed out and recycled all questionnaires used at the site. In the process of completing the questionnaires, unclear questions were explained, checked and supplemented in time. During the investigation, the subjects were strictly selected according to the inclusion criteria and exclusion criteria. The content and purpose of the survey were explained to the volunteers first, and then the questionnaires were collected on the premise of their informed consent. The researcher answered the questions one by one within the specified time. The investigators were required to read the answers one by one for those who could not fill in the answers by themselves, and the volunteers made their own choices without intervention.

The questionnaires were evaluated after collection. Invalid questionnaires were removed, and two teams input the data to a computer-independent order to avoid entry error. Ten percent of the data were checked through random inspection, and the unqualified rate of random inspection was controlled below 0.5%. The qualified rate of this sampling inspection was 100%.

Data Analysis

General Demographic and Disease-Related Conditions data about Facial Burn Scar Patients were described by frequency and percentage. The Quality of Life Score was summarized as maximum, minimum, mean, and standard deviation. Each dimension of Acceptance Disability was defined as low, moderate and high acceptance and described by frequency and percentage. Differences between participants in terms of demographic characteristics, quality of life, and disability acceptance were assessed using variance analysis. Spearman correlation analysis was conducted on the quality of life score and disability acceptance.

$$\rho_{QoL,ADS} = \frac{Cov(QoL,ADS)}{\sqrt{D(QoL)}\sqrt{D(ADS)}} \quad (1)$$

In, which, $\rho_{QoL,ADS}$, $Cov(QoL,ADS)$, $\sqrt{D(QoL)}$, $\sqrt{D(ADS)}$ stands for the correlation, covariance between the quality of life score and disability acceptance, and their own standard variance, respectively. $P < 0.05$ was considered as significantly difference, and, all the analysis was performed using R version 3.4.3.

RESULTS

General Demographic Data of Facial Burn Scar Patients

A total of 130 people were investigated in this survey, 121 valid questionnaires were recovered, and the effective questionnaire recovery rate was 93.08%. The age of the facial burn scar patients ranged from 18 to 83 years, with an average age of 42.77 ± 13.82 years old. The majority of patients were male (63.6%) and married (86%). The ratio of males to females was $\sim 1.75:1$. The education levels of patients were 12.4, 35.5, 47.9,

and 4.1% for primary school, junior high school, senior high school, junior college, and undergraduate or above, respectively. In total, 82.6% of patients live in cities. Unemployed persons before burning accounted for 1.7% of the total number, while the proportion increased to 17.4% after burning. Approximately 63.6% of families have a monthly income of 2,000~4,000 yuan per capita. The average monthly treatment cost was 620.74 yuan. A total of 66.9% of patients did have medical insurance (Table 1).

Disease Related Information of Facial Burn Scar Patients

In total, 113 people (93.4%) suffered from thermal burns. The average scar formation time of facial burns was 116.72 days, ranging from 15 to 427 days, of which 96 patients exhibited scars within 6 months and 25 exhibited scars after 6 months. Submandibular scars were the most common scar formation sites among the facial burns, accounting for 71.9% of 87 patients. Fifty-seven patients had a burn scar area $\geq 5 \text{ cm}^2$, accounting for 47.1% of patients. A total of 7.4% of the patients believed that the impact of their scars was significant. A total of 34.7% of patients often have sensation of their facial burn scars, while only 3.3% of patients have no sensation of facial burn scars. The first hospital stay of facial burn scar patients was 2–74 days in duration, with an average of 20.31 ± 17.82 days. Three (1.7%) patients suffered from facial burns alone; 71 (58.7%) were complicated with trunk burns; 67 (55.4%) were complicated with upper limb burns; and 31 patients (25.6%) were complicated with lower limb burns (Table 2).

Quality of Life

Among 121 patients, 28.93% (35/121) had a score of quality of life greater than 145, 47.22% (57/121) had a quality of life between 130–145, and 23.97% (29/121) had a quality of life below 130. The total score of quality of life in facial burn scar patients was 137.06 ± 17.05 . The scores of body image, work, heat sensitivity, simple abilities, interpersonal relationships, hand function, affect, and sexuality were 12.31 ± 2.52 , 12.60 ± 3.27 , 16.01 ± 3.57 , 16.31 ± 2.90 , 10.61 ± 2.77 , 14.29 ± 1.97 , 18.00 ± 4.42 , 25.49 ± 4.32 , and 11.44 ± 1.50 , respectively (Table 3). There's significantly difference between each dimension of quality of life ($F = 271.53$, $P < 0.01$).

Acceptance Disability Scale (ADS)

The total score of disability acceptance was 185.68 ± 23.74 . Among the scoring items, the scores for transformation, enlargement, dimension, containment and subordination were 58.64 ± 9.31 , 54.12 ± 7.54 , 58.04 ± 8.62 , and 14.88 ± 2.75 , respectively. The degree of disability acceptance and its dimensions are divided into three levels: low, medium, and high. In the distribution of the total disability acceptance score of the study subjects, 91.7% of patients were at the moderate acceptance level, while 22.3% of patients in the compliance dimension scored at the low acceptance level (Table 4).

Correlation Analysis of Quality of Life and Handicap Acceptance

Spearman correlation analysis was conducted on the quality of life score and disability acceptance. The results are shown in Table 5. The results showed that the overall quality of life score of

TABLE 1 | General demographic of facial burn scar patients ($n = 121$).

Variable name	Frequency	Percentage (%)
Gender		
Male	77	63.6
Female	44	36.4
Age (years)		
18–30	28	23.1
31–44	43	35.5
45–59	32	26.4
60–83	18	14.9
Education level		
Primary school	15	12.4
Junior high school	43	35.5
High school	58	47.9
College, undergraduate or above	5	4.1
Pre-burn occupation		
Workers	40	33.1
Farmers	23	19.0
Individuals, businessmen, enterprises, government	40	33.1
Housewives	11	9.1
Unemployed	2	1.7
Students	5	4.1
Current occupation		
Workers	28	23.1
Farmers	22	18.2
Individual, business, enterprise, government, service	32	26.4
Housewives	12	9.9
Unemployed	21	17.4
Students	5	4.1
Other	1	0.8
Marital status		
Unmarried	15	12.4
Married	104	86.0
Divorced/separated	2	1.7
Residence		
City	100	82.6
Countryside	21	17.4
Per capita monthly income (yuan)		
<2,000	6	5.0
2,000–4,000	77	63.6
>4,000	38	31.4
Payment method of medical expenses		
At their own expense	81	66.9
Medical insurance	40	33.1

TABLE 2 | Disease-related conditions of facial burn scar patients ($n = 121$).

Variable	Frequency	Percentage (%)
Cause of burn		
Thermal burns	113	93.4
Chemical burns	6	5.0
Others (radiation burns)	2	1.7
Combined with burns on other body parts		
Trunk	71	58.7
Limb	67	55.4
Lower limb	31	25.6
No combined burns	3	2.5
Scar formation time		
Within 6 months	96	79.3
More than 6 months	25	20.7
Facial scar formation site		
Frontal compartment	11	9.1
Face	26	21.5
Submandibular area	87	71.9
Eyelid	18	14.9
Mouth	10	8.3
Nasal area	1	0.8
Scar area of facial burns		
2~4 cm ²	64	52.9
5~15 cm ²	46	38.0
>15 cm ²	11	9.1
Number of days of first hospitalization		
>9 days	36	29.8
More than 9 days	61	50.4
≥30 days	24	19.8
Observation of facial scar by patients		
Regular observation	42	34.7
Sometimes observation	36	29.8
Occasional observation	43	35.5
Does the patient think the burn scar will affect his or her facial function		
Basically no	72	59.5
Little influence	40	33.1
Great influence	9	7.4

facial burn scar patients was positively correlated with disability acceptance ($r = 0.245$, $p = 0.007$).

DISCUSSION

In this survey, the overall quality of life of patients with facial burn scars was divided into 77~160 points with an average score of 137.0 ± 17.05 points, indicating that the quality of life of patients with facial burn scars is at a moderate or low level. However, some researchers scored 182.43 ± 48.6 points in the study on the quality of life of patients in the burn rehabilitation period. This result may be because the face is a special area where once burned, it can easily be observed by other people, so burns on the face have a substantial effect the quality of life of

TABLE 3 | The quality of life score of facial burn scar patients ($n = 121$).

Item	$X \pm s$	Average score of the single entry
Total score	137.06 ± 17.05	3.43
Body image	12.31 ± 2.52	3.08
Work	12.60 ± 3.27	3.15
Heat sensitivity	1601 ± 357	3.2
Treatment regimens	16.31 ± 2.90	3.26
Simple abilities	10.61 ± 2.77	3.54
Interpersonal relationships	14.29 ± 1.97	3.57
Hand function	18.00 ± 4.42	3.6
Affect	25.49 ± 4.32	3.64
Sexuality	11.44 ± 1.50	3.81

patients. At the same time, facial burn scarring can increase the psychological pressure of the patient and cause great interference to his or her work and life, which may lead to a moderate-to-low quality of life (Spronk et al., 2018b).

According to the Appraisal Standard for Disability Degree of Industrial Injury and Occupational Disease of Workers, the subjects of this study have disabilities ranging from grade 4 to grade 10. The results of this study show that the total score of disability acceptance of facial burn scar patients is 185.68 ± 23.74 , which is close to the score of other subjects (181.46 ± 39.45) and higher than score range of the low level of acceptance. This finding indicates that the disability acceptance of burn scar patients is at a medium level and still needs to be improved. According to the grading distribution of the total score of disability acceptance for facial burn scar patients, 91.7% of the patients were at a moderate acceptance level. The low acceptance level was 3.3%. Patients with a high acceptance level only accounted for 5%.

To our knowledge, there's still no report about the relationship between quality of life and the acceptance of disability in facial burn patients, and the acceptance of disability plays a significant role in mediating the correlation between general self-efficacy and depression/general quality of life in mild traumatic brain injury patients (Yehene et al., 2019). The results of this survey show that disability acceptance in facial burn patients is a factor affecting the quality of life of patients, and there is a positive correlation between the two factors. Similar to the research results, the reasons may be as follows. (1) The overall quality of life improvement level in patients is not only affected by the treatment level during hospitalization but also has a great correlation with the attitude in coping with their own disability. Through reasonable cognition, patients can adopt logical thinking to overcome the belittling of self-esteem, create a good life, adapt to their environments with a reasonable outlook on life, and improve their effective adaptability to their disabilities. Patients need reasonable cognition to guide adaptive behavior in the process of social reintegration after burn. Patients can identify new role orientations and self-definitions and then

TABLE 4 | Acceptance disability level of facial burn scar patients ($n = 121$).

Variable quantity	Low acceptance		Moderate acceptance		High acceptance	
	N	Percentage (%)	N	Percentage (%)	N	Percentage (%)
Transformation	9	7.4	87	71.9	25	20.7
Enlargement	4	3.3	94	77.7	23	19
Containment	7	5.8	114	94.2	0	0
Subordination	27	22.3	91	75.2	3	2.5
Total score of disability acceptance	4	3.3	111	91.7	6	5.0

TABLE 5 | Correlation between quality of life and disability acceptance in patients with facial burn scar ($n = 121$).

BSHS-B dimensions	Transformation	Enlargement	Containment	Subordination	Total score
Total score of quality of life	0.203*	0.277**	0.235**	-0.264**	0.245**
Simple abilities	0.062	0.132	0.059	-0.280**	0.073
Hand function	0.137	0.248**	0.078	-0.331**	0.130
Affect	0.301**	0.347**	0.357**	-0.287**	0.345**
Interpersonal relationships	0.160	0.165	0.184*	-0.299**	0.165
Sexuality	0.276**	0.402**	0.250**	-0.431**	0.279**
Body image	-0.053	0.008	0.051	0.022	0.017
Heat sensitivity	0.138	0.105	0.185*	-0.046	0.170
Treatment regimens	0.155	0.177	0.198*	-0.053	0.190*
Work	0.075	0.301	0.083	0.079	0.619

* $P < 0.05$, ** $P < 0.01$.

adopt adaptive behaviors to promote the recovery of body functions and the improvement of various skills and abilities. The improvement of disability acceptance level is conducive to further improving the physical condition of patients. (2) Improvement in the degree of disability acceptance changes patients' cognition to a certain extent, improves patients' control over their own emotions, and allows them to perceive less negative psychological emotions, thus guiding patients to actively change their self-value and attitude toward life. The continuous improvement in disability acceptance indicates that patients can actively change their self-value recognition and self-cognition, thus improving their quality of life.

Our study found that the affect dimension in the quality of life of facial burn scar patients has a correlation with all dimensions of disability acceptance, of which the correlation coefficient with the containment dimension was the largest, suggesting that the affect dimension has the closest relationship with the control dimension. According to Maslow's hierarchy of needs theory, after human beings have satisfied their physiological and safety needs, they will pursue the satisfaction of the needs of emotion and belonging (Kowal-Vern and Criswell, 2005); emotional needs are more delicate than physiological needs are, and at the same time, emotional needs have a certain relationship with individual physiological characteristics, social education, personal experience, and religious beliefs. If patients can rationally view facial burn scars and control the negative effects caused by facial burn scars so that they do not exceed the actual damage range to the body, the patient's emotion can be expressed more smoothly, and the demand level of

emotion and belonging can be realized, thus improving the patient's acceptance of his or her disability. The sex life dimension of the quality of life of patients with facial burn scars is correlated with all dimensions of disability acceptance, of which the correlation coefficient with the compliance dimension is the largest, indicating that the sex life dimension is most closely related to the compliance dimension. By analyzing the reasons, patients cannot accept their current appearance changes and do not obey their current physical conditions. They still attach great importance to the facial appearance changes caused by sudden accidents and show higher attention to their own abilities and appearance. Patients will be more inclined to think that burn scars lead to the disability of their bodily functions, thus affecting their sex life (Capek et al., 2018).

CONCLUSION AND CLINICAL SIGNIFICANCE

The quality of life of facial burn scar patients will improve with the improvement of disability acceptance level. Therefore, medical staff can improve the quality of life of patients by improving their disability acceptance level. Medical staff can assist patients to find control and management methods of the body, expand the scope of patients' values, establish a correct evaluation of their appearance, obey the changes brought about by facial burn scars, assist patients to reconstruct their internal aesthetics, and help patients to rediscover their own

value orientation and meaning of life by guiding patients to formal medical institutions for scar treatment consultation and follow-up.

DATA AVAILABILITY STATEMENT

The datasets generated for this study are available on request to the corresponding author.

REFERENCES

- Baldwin, S., Yuan, H., Liao, J., Grieve, B., Heard, J., and Wibbenmeyer, L. A. (2018). Burn survivor quality of life and barriers to support program participation. *J. Burn Care Res.* 5, 823–830. doi: 10.1093/jbcr/irx058
- Brewin, M. P., and Homer, S. J. (2018). The lived experience and quality of life with burn scarring—the results from a large-scale online survey. *Burns* 7, 1801–1810. doi: 10.1016/j.burns.2018.04.007
- Cakir, U., Terzi, R., Abaci, F., and Aker, T. (2015). The prevalence of post-traumatic stress disorder in patients with burn injuries, and their quality of life. *Int. J. Psychiatry Clin. Pract.* 1, 56–59. doi: 10.3109/13651501.2014.981545
- Capek, K. D., Culnan, D. M., Desai, M. H., and Herndon, D. N. (2018). Fifty years of burn care at shriners hospitals for children, Galveston. *Ann. Plast. Surg.* 3 (Suppl. 2), S90–S94. doi: 10.1097/SAP.0000000000001376
- Chin, T. L., Carrougher, G. J., Amtmann, D., McMullen, K., Herndon, D. N., Holavanahalli, R., et al. (2018). Trends 10 years after burn injury: a burn model system national database study. *Burns* 8, 1882–1886. doi: 10.1016/j.burns.2018.09.033
- Finnerty, C. C., Jeschke, M. G., Branski, L. K., Barret, J. P., Dziewulski, P., Herndon, D. N. (2016). Hypertrophic scarring: the greatest unmet challenge after burn injury. *Lancet* 10052, 1427–1436. doi: 10.1016/S0140-6736(16)31406-4
- Gandolfi, S., Carloni, R., Bertheuil, N., Grolleau, J. L., Auquit-Auckbur, I., and Chaput, B. (2018). Assessment of quality-of-life in patients with face-and-neck burns: the burn-specific health scale for face and neck (BSHS-FN). *Burns* 6, 1602–1609. doi: 10.1016/j.burns.2018.03.002
- Garcia, L. P., Huang, A., Corlew, D. S., Aeron, K., Aeron, Y., Rai, S. M., et al. (2016). Factors affecting burn contracture outcome in developing countries. *Ann. Plast. Surg.* 3, 290–296. doi: 10.1097/SAP.0000000000000856
- Kowal-Vern, A., and Criswell, B. K. (2005). Burn scar neoplasms: a literature review and statistical analysis. *Burns* 4, 403–413. doi: 10.1016/j.burns.2005.02.015
- Levi, B., Kraft, C. T., Shapiro, G. D., Trinh, N. T., Dore, E. C., Jeng, J., et al. (2018). The associations of gender with social participation of burn survivors: a life impact burn recovery evaluation profile study. *J. Burn Care Res.* 6, 915–922. doi: 10.1093/jbcr/iry007
- Miller, T., Bhattacharya, S., Zamula, W., Lezotte, D., Kowalske, K., Herndon, D., et al. (2013). Quality-of-life loss of people admitted to burn centers, United States. *Qual. Life Res.* 9, 2293–2305. doi: 10.1007/s11136-012-0321-5
- Nicholls, E., Lehan, T., Plaza, S. L., Deng, X., Romero, J. L., Pizarro, J. A., et al. (2012). Factors influencing acceptance of disability in individuals with spinal cord injury in Neiva, Colombia, South America. *Disabil. Rehabil.* 13, 1082–1088. doi: 10.3109/09638288.2011.631684

AUTHOR CONTRIBUTIONS

XZ, YL, and AH contributed to the conception and design of the study. XZ and XD organized the database. YL, CD, and YP performed the statistical analysis. XZ wrote the first draft of the manuscript. YL, XD, and CD wrote sections of the manuscript. All authors contributed to manuscript revision, read, and approved the submitted version.

- Palmu, R., Partonen, T., Suominen, K., Vuola, J., and Isometsa, E. (2015). Return to work six months after burn: a prospective study at the Helsinki Burn Center. *Burns* 6, 1152–1160. doi: 10.1016/j.burns.2015.06.010
- Polychronopoulou, E., Herndon, D. N., and Porter, C. (2018). The long-term impact of severe burn trauma on musculoskeletal health. *J. Burn Care Res.* 6, 869–880. doi: 10.1093/jbcr/iry035
- Simons, M., Lim, P. C. C., Kimble, R. M., and Tyack, Z. (2018). Towards a clinical and empirical definition of burn scarring: a template analysis using qualitative data. *Burns* 7, 1811–1819. doi: 10.1016/j.burns.2018.04.006
- Spronk, I., Legemate, C., Oen, I., van Loey, N., Polinder, S., van Baar, M. (2018b). Health related quality of life in adults after burn injuries: a systematic review. *PLoS ONE* 5:e0197507. doi: 10.1371/journal.pone.0197507
- Spronk, I., Legemate, C. M., Dokter, J., van Loey, N. E. E., van Baar, M. E., Polinder, S. (2018a). Predictors of health-related quality of life after burn injuries: a systematic review. *Crit. Care* 1:160. doi: 10.1186/s13054-018-2071-4
- Van Lieshout, E. M., Van Yperen, D. T., Van Baar, M. E., Polinder, S., Boersma, D., Cardon, A. Y., et al. (2018). Epidemiology of injuries, treatment (costs) and outcome in burn patients admitted to a hospital with or without dedicated burn centre (Burn-Pro): protocol for a multicentre prospective observational study. *BMJ Open* 11:e023709. doi: 10.1136/bmjopen-2018-023709
- Watson, E. J. R., Nenadlová, K., Clancy, O. H., Farag, M., Nordin, N. A., Nilsen, A., et al. (2018). Perioperative research into memory (PRiMe): cognitive impairment following a severe burn injury and critical care admission, part 1. *Burns* 5, 1167–1178. doi: 10.1016/j.burns.2018.04.011
- Yehene, E., Lichtenstern, G., Harel, Y., Druckman, E., and Sacher, Y. (2019). Self-efficacy and acceptance of disability following mild traumatic brain injury: a pilot study. *Appl. Neuropsychol. Adult* 2, 1–10. doi: 10.1080/23279095.2019.1569523
- Yurdalan, S. U., Unlu, B., Seyyah, M., Senyildiz, B., Cetin, Y. K., and Cimen, M. (2018). Effects of structured home-based exercise program on depression status and quality of life in burn patients. *Burns* 5, 1287–1293. doi: 10.1016/j.burns.2018.02.015

Conflict of Interest: The authors declare that the research was conducted in the absence of any commercial or financial relationships that could be construed as a potential conflict of interest.

Copyright © 2019 Zhang, Liu, Deng, Deng, Pan and Hu. This is an open-access article distributed under the terms of the Creative Commons Attribution License (CC BY). The use, distribution or reproduction in other forums is permitted, provided the original author(s) and the copyright owner(s) are credited and that the original publication in this journal is cited, in accordance with accepted academic practice. No use, distribution or reproduction is permitted which does not comply with these terms.



A Systematic Review and Meta-Analysis of Clinical Effectiveness and Safety of Hydrogel Dressings in the Management of Skin Wounds

Lijun Zhang^{1†}, Hanxiao Yin^{1†}, Xun Lei², Johnson N. Y. Lau³, Mingzhou Yuan¹, Xiaoyan Wang¹, Fangyingnan Zhang¹, Fei Zhou¹, Shaohai Qi¹, Bin Shu^{1*} and Jun Wu^{1*}

¹ Department of Burns, The First Affiliated Hospital, Sun Yat-sen University, Guangzhou, China, ² School of Public Health and Management, Chongqing Medical University, Chongqing, China, ³ University of Hong Kong, Hong Kong Polytechnic University, Kowloon, China

OPEN ACCESS

Edited by:

Ubaldo Armato,
University of Verona, Italy

Reviewed by:

Maria Grazia Raucchi,
Italian National Research Council
(CNR), Italy
Jingning Huan,
Shanghai Jiao Tong University, China

*Correspondence:

Bin Shu
shubin29@sina.com
Jun Wu
junwupro@126.com

[†]These authors have contributed
equally to this work

Specialty section:

This article was submitted to
Biomaterials,
a section of the journal
Frontiers in Bioengineering and
Biotechnology

Received: 28 September 2019

Accepted: 04 November 2019

Published: 21 November 2019

Citation:

Zhang L, Yin H, Lei X, Lau JNY,
Yuan M, Wang X, Zhang F, Zhou F,
Qi S, Shu B and Wu J (2019) A
Systematic Review and Meta-Analysis
of Clinical Effectiveness and Safety of
Hydrogel Dressings in the
Management of Skin Wounds.
Front. Bioeng. Biotechnol. 7:342.
doi: 10.3389/fbioe.2019.00342

The purpose of this systematic review and meta-analysis is to assess the clinical effectiveness and safety of the medical hydrogel dressings used in skin wounds and therefore to weight the evidence for their clinical application. PubMed/Medline (1980–2019), Cochrane Library (1980–2019), ClinicalTrials.gov, Cochrane CENTRAL, Chinese Journal Full-text Database (CNKI, 1994–2019), and China Biomedicine Medicine disc (CBM, 1978–2019), Chinese Scientific Journal Database (VIP, 1989–2019), and Wanfang Database (WFDATA, 1980–2019) were searched to identify relevant clinical trials and studies. Forty-three studies that assessed hydrogel vs. non-hydrogel dressings were identified. Compared to the latter, hydrogel dressings associated with a significantly shortened healing time of degree II burn (superficial and deep) wounds, diabetic foot ulcers, traumatic skin injuries, radioactive skin injuries, dog bites, and body surface ulcers. In addition, hydrogel dressing obviously increased the cure rate of diabetic foot ulcers, surgical wounds, dog bites, and body surface ulcers. Moreover, hydrogel dressing significantly relieved pain in degree II burn (superficial and deep) wounds, traumatic skin injuries, and laser treatment-induced wounds. However, no significant differences obtained between hydrogel and non-hydrogel dressings in the healing time of surgical wounds, the cure rate of inpatients' pressure ulcers, and phlebitis ulcers. This comprehensive systematic review and meta-analysis of the available evidence reveals that the application of hydrogel dressings advances the healing of various wound types and effectively alleviates the pain with no severe adverse reactions. These results strongly indicate that hydrogel products are effective and safe in wound management.

Keywords: hydrogel, wound dressing, wound healing, pain relief, meta-analysis, systematic review

INTRODUCTION

Skin is the largest human organ as it reaches almost 10% of the total body mass (Grice et al., 2009) and acts as a key protective barrier against the outside environment. Normally, the human body heal skin injuries via a set of complex and interactive processes that include hemostasis, inflammation, proliferation, and remodeling. However, this healing process can be impaired by

various local and systemic factors causing more severe complications and a lower quality of life (Nourian Dehkordi et al., 2019). Plenty of wound care products have been created and developed in the latest decades aimed at promoting wound healing and improving the life quality of the patients afflicted by skin wounds (Metcalf and Ferguson, 2007; Gil et al., 2013; Chattopadhyay and Raines, 2014; Garg et al., 2015; Xu et al., 2015; Das and Baker, 2016). Therefore, surgeons must specifically select wound treatment products according to the factors impeding wounds healing.

Since the 1960s, wound dressing was considered to play a positive role in wound healing. Wound dressing could establish and maintain an environment apt for wound repair. Winter (1962) were the pioneers of this field by initiating the concept of functional active dressings. According to them, the ideal advanced wound dressing should provide and maintain a moist environment, adequate gaseous exchange, and thermal insulation in the absence of toxic contaminants; it should protect against secondary infections, induce tissue regeneration, relieve wound pain, and promote wound healing quality; finally, it should be elastic, non-antigenic, and allow to manage wound exudate (Purna and Babu, 2000). Considering all the just mentioned factors, hydrogel products have the capacity to act as promising candidates as wound dressings for applications in clinical settings (Qu et al., 2018).

In 1960, Wichterle and Lim prepared the first hydrogels by cross-linking 2-hydroxyethyl methacrylate, thus initiating the application and practice of hydrogels in the biomedical field (Wichterle and Lim, 1960). Hydrogels are extremely hydrophilic. Advanced hydrogel materials are environment-sensitive or stimuli-sensitive, as they start swelling under certain conditions and respond to definite stimuli (Qiu and Park, 2001). They can absorb exudate from the wound surface and promote fibroblast proliferation and cell migration and keratinization. In addition, hydrogels' dense meshes can prevent bacteria from invading the wound while effectively transporting bioactive molecules (such as antibacterial agents and drugs) to the wound surface (Mohan et al., 2007; Tsao et al., 2010; Schwartz et al., 2012; Mao et al., 2017). At the same time, the unique mechanical properties of hydrogels i.e., elasticity and flexibility, allow for their adaptation to different parts of the wound, making them suitable for both wound care and tissue engineering (Huang et al., 2015).

Being a novel category of wet dressings, hydrogel products have been gradually perfected in recent years. Their clinical application has become rather extensive, ranging from dry scab wounds to multiple treatments of skin ulcers, burn wounds, animal bites, bed sores, etc. (Sood et al., 2014). Medicinal hydrogel dressings are endowed with a three-dimensional (3D) crosslinked network structure, which contains three main

components, a high-molecular weight compound, propylene glycol, and water. High-molecular weight compounds such as Carboxy Methyl Cellulose (CMC) can double the absorption of wound exudate and necrotic tissue fluid (Roy et al., 2010). Propylene glycol can kill bacteria and prevent bacterial proliferation. In turn, the water in hydrogel dressings can create a relatively moist environment that prevents the wound from drying up (Fan et al., 2014). Therefore, although necrotic tissues in the making go through a slow hydration, the hydrogel dressing ensures a strong absorption of wound exudate. Concurrently, it promotes the debridement of water-soluble materials and absorbs wound carrion to provide a localized moist environment advancing wound healing (Qu et al., 2018). Besides, hydrogels' micro-acidic and hypoxic environment can attract cells involved in wound repair, help inhibit bacterial growth, and promote neoangiogenesis at the wound site (Dong et al., 2016).

Managing wounds through the use of hydrogels has been an accepted practice for decades. At present, many forms of hydrogel and non-hydrogel products are available aimed at managing wounds caused by various injuries. However, the benefits of multiple options also entail many challenges to the clinicians. The purpose of this systematic review and meta-analysis is to assess the clinical effectiveness and safety of the medicinal hydrogel dressings in treating multiple skin wounds compared to non-hydrogel dressings in terms of wound healing time, wound cure rate, pain reduction, and incidence of adverse reactions.

METHODS

Systematic Review Eligibility Criteria

A systematic review was conducted according to the Preferred Reporting Items for Systematic Reviews and Meta-analyses (PRISMA) guidelines (Shamseer et al., 2015). It was based on the planned Participants, Intervention, Control, Outcome, and Study design (PICOS) elements outlined in **Table 1**.

Search Strategy

We sought to identify suitable studies by searching the following online databases: PubMed/Medline (1980–2019), Cochrane Library (1980–2019), ClinicalTrials.gov, Cochrane CENTRAL, Chinese Journal Full-text Database (CNKI, 1994–2019), and China Biomedicine disc (CBM, 1978–2019), Chinese Scientific Journal Database (VIP, 1989–2019), and Wanfang Database (WFDATA, 1980–2019). With the combination of subject words and free words, the search terms included two categories: (1) “hydrogel,” “polymeric hydrophilic compound,” “guar gum,” “guar bean,” and “polyvinylpyrrolidone (PVP);” (2) “wound,” “wound surface,” and “burn.” The logical relationship was created with “OR” and “AND,” and the search formula was thereafter developed according to the characteristics of the different databases. The search strategy was improved through a pre-retrieval process. Meanwhile, unpublished studies and conference materials were manually searched, and references of the included literature were also tracked. No language limits were applied.

Abbreviations: GRADE, Grading of Recommendations Assessment, Development and Evaluation; PRISMA, Preferred Reporting Items for Systematic Reviews and Meta-Analyses; RCT, Randomized Controlled Trial; PICOS, Participants, Intervention, Control, Outcome and Study design; PVP, Polyvinylpyrrolidone; CMC, Carboxy Methyl Cellulose; EPOC, Effective Practice and Organization of Care Group; WMD, Weighted Mean Difference; SSD, Silver Sulphadiazine; VAS, Visual Analog Scale; SMSDAR, State Monitoring System of Drug Adverse Reactions; JW scale, Jun Wu scale.

TABLE 1 | Inclusion and exclusion criteria.

Criteria	Inclusion	Exclusion
Type of study	RCTs, quasi-RCTs, CCTs	Review, case study, mechanism study, research and development, preparation and storage of materials, animal experiment, marketing strategy, editorials, news, and registered clinical trials with unfinished/unreported results.
Participants	Patients with skin wounds provoked by various causes (e.g., burns, surgery, body surface ulcers, etc.).	Patients with deep burns (degrees III and IV), treatment for bone wounds, pre-operation preparation, patients using biological tissue synthesis substitutes, and patients with autologous skin cultured transplants.
Interventions	Various types of hydrogel dressings [polymeric hydrophilic compounds such as guar gum and Lengningkang ^a (Wound Caring)].	The hydrogel is used as a non-wound dressing such as an <i>in vivo</i> drug release carrier, contact lens, tissue filling material, medical sensor, etc.
Control	Any other dressing, treatment, placebo, or blank control.	Comparison of functions before and after using hydrogel dressings or comparison between different hydrogels.
Outcomes	Effective indicators including wound healing time, wound healing rate, pain score, pain level, etc. Safety indicators referring to the incidence rate of adverse reactions including skin allergy, skin dryness, tight skin, pruritus, and fever.	Long-term follow-up results such as quality of life.

^a The commercial name of a hydrogel dressing.

Study Selection

Two reviewers carried out the preliminary screening by independently reading titles and abstracts to exclude literature that obviously did not conform with the inclusion criteria. As a further screening they read the full texts of the literature that might meet the inclusion criteria. When the two researchers' opinions differed, they consulted and discussed with a third researcher to reach a final decision. During the full-text screening, the information below would be extracted: authors, date of publication, study type, subject characteristics, sample number, loss to or withdrawal from follow-up, intervention measures, and measuring indicators, etc. In case of multiple studies in a single published work, data based on study contents would be extracted as needed. With regard to repeatedly reported studies, only the latest or the most comprehensive one was included.

Quality Evaluation

The quality of the methodology employed by the included studies was evaluated according to the Effective Practice and Organization of Care Group (EPOC) improved scoring standard recommended by The Cochrane Collaboration. The evaluation package included randomization methods, allocation concealment, blinding use, control of loss to follow-up, baseline information, outcome data, etc. Scores of 5–6 were classified as grade A, 2–4 as grade B, and 0–1 as grade C.

Meta-Analysis

Meta-analysis was carried out by using the RevMan5.0 software recommended by The Cochrane Collaboration. Subgroups were divided according to patient (wound) types and types of outcome variables. The relative risk (RR) was taken as the combined effect size for categorical data, while the weighted mean difference (WMD) as the combined effect size for measuring data. Each effect size was shown as 95% CI. The heterogeneity of the study results was tested by χ^2 test. When studies showed a statistical homogeneity ($P > 0.1$, $I^2 < 50\%$), a fixed-effect

model would be used; otherwise, a random effect model was adopted. For subgroups containing a single study, description, and comparative analysis would be conducted on their results.

RESULTS

Study Selection and Characteristics

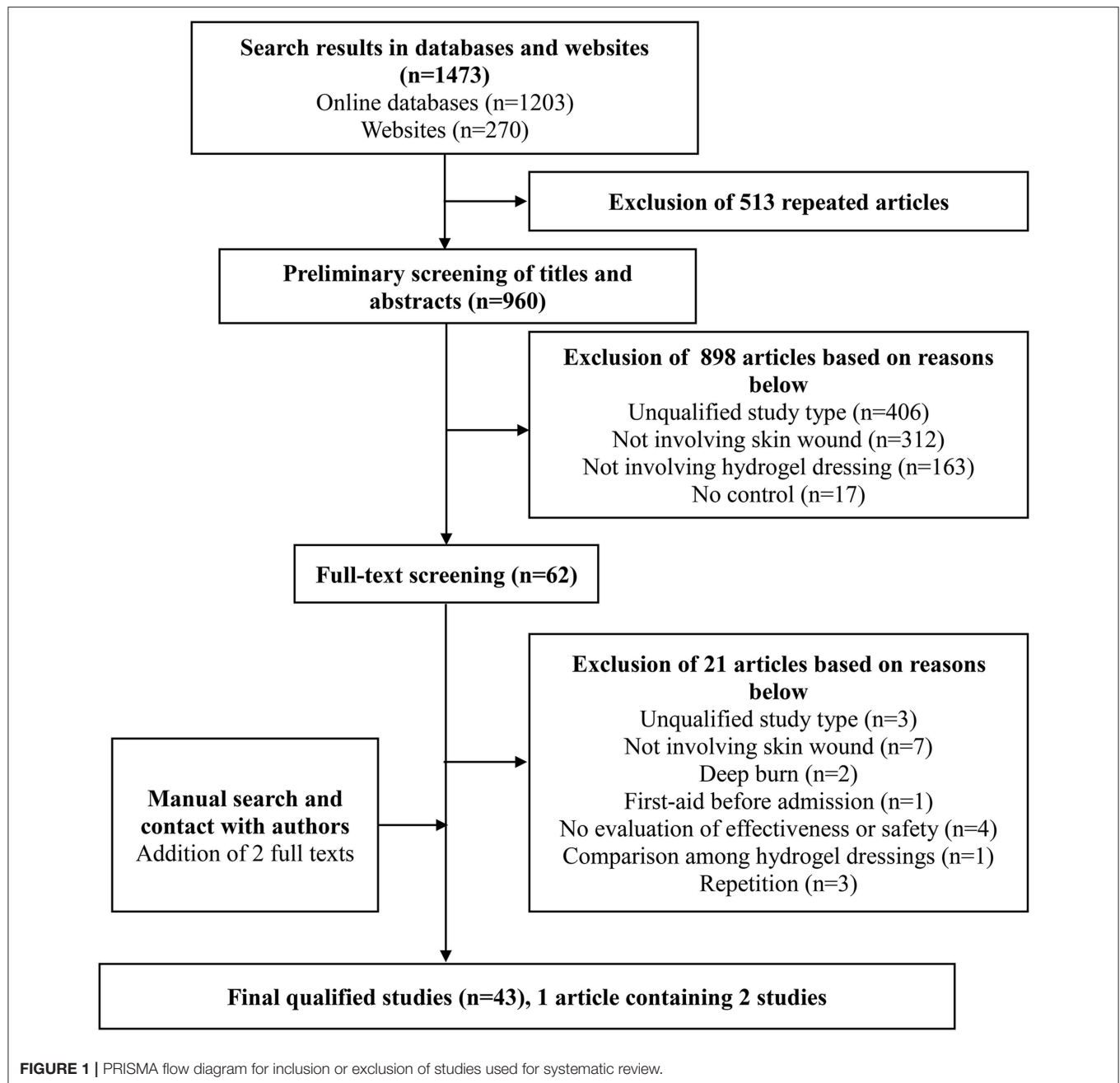
One thousand four hundred and seventy three studies were selected by the preliminary screening. Only 43 studies were kept after screening titles, abstracts, and full-texts (**Figure 1**), including 29 randomized controlled trials (RCTs) and 14 clinical controlled trials (CCTs) with a total of 3,521 patients. The basic characteristics of the included studies and the results of methodological quality evaluations are shown in **Table 2**. In all studies, patients' basic situations were comparable between intervention groups and control groups ($P > 0.05$).

Data Synthesis

Healing Times Comparison of Degree-II Superficial and Deep Burn Wounds

Eleven studies, reported by Cui et al. (2007), Jiang et al. (2008), Gong et al. (2009), Jin et al. (2009), Wang et al. (2011), Diao et al. (2012), Liu and Ye (2014), Liu (2015), Jin et al. (2017), Li and Wu (2018), Lin et al. (2018), compared the healing times of degree-II superficial burn wounds treated with hydrogel dressings or other treatments. There existed a statistical heterogeneity among the study results ($P < 0.0001$, $I^2 = 76\%$). Therefore, the random effect model was applied for meta-synthesis (**Figure 2A**). The results showed that on average the wound healing time of the hydrogel dressings group was shortened by 2.87 days as compared with the control group and that the difference had a high statistical significance (MD = -2.87 , 95% CI: -3.35 to -2.38 , $P < 0.00001$).

Twelve studies, reported by Cui et al. (2007), Jiang et al. (2008), Gong et al. (2009), Jin et al. (2009), Cai et al. (2010), Wang



et al. (2011), Wang et al. (2013), Liu and Ye (2014), Lan and Duan (2015), Liu (2015), Shang (2015), and Jin et al. (2017), compared the healing times of degree-II deep burn wounds treated with hydrogel dressings or other therapeutics. There existed a statistical heterogeneity among the study results ($P < 0.00001$, $I^2 = 83\%$). Hence, the random effect model was applied for meta-synthesis (Figure 2B). The results revealed that on average the wound healing time of the hydrogel dressings group was shortened by 5.04 days as compared with the control group and that statistically this difference was highly significant (MD = -5.04, 95% CI: -5.81 to -4.26, $P < 0.00001$).

WHO Pain Ratings of Burn Wounds

Five studies, reported by Jiang et al. (2008), Jin et al. (2009), Wang et al. (2011), Jin et al. (2017), and Li and Wu (2018), compared the pain ratings difference of burn wounds after treatment with hydrogel dressings or other therapeutic means. There occurred no statistical heterogeneity among the study results ($P = 0.57$). Consequently, the fixed effect model was applied for meta-synthesis (Figure 3). The results brought to light that patients suffering either grade 0 or grade I pain accounted for a higher proportion among those treated with hydrogel dressings and that statistically the

TABLE 2 | Characteristics of the studies employing hydrogel dressings vs. non-hydrogel dressings.

References	Study design	Country	Participants	Sample size	Quality level
Cai et al., 2010	CCT	China	Degree-II deep burn wounds	60 patients Chitosan hydrogel = 30 SSD = 30	B
Jiang et al., 2008	RCT	China	degree-II superficial and deep burn wounds	90 patients Hydrogel = 45 SSD = 45	B
Wang et al., 2011	RCT	China	Degree-II superficial and deep burn wounds	560 patients Hydrogel with silver = 280 SSD = 280	B
Jin et al., 2009	CCT	China	Degree-II superficial and deep burn wounds	72 patients Hydrogel = 42 Iodine solution = 30	B
Wang et al., 2013	RCT	China	Degree-II burn wounds	76 patients Hydrogel = 38 Entiodine and petrolatum gauze = 38	B
Liu, 2015	CCT	China	Degree-II superficial and deep burn wounds	120 patients Hydrogel and Lithosin solution = 60 Lithosin solution = 60	B
Jin et al., 2017	CCT	China	Degree-II superficial and deep burn wounds	92 patients Hydrogel = 48 SSD = 44	B
Diao et al., 2012	RCT	China	Degree-II superficial burn wounds	60 patients Hydrogel with silver = 30 SSD = 30	A
Lin et al., 2018	RCT	China	Degree-II superficial burn wounds	66 patients Hydrogel with silver = 33 SSD = 33	B
Liu and Ye, 2014	RCT	China	Degree-II superficial and deep burn wounds	80 patients Hydrogel = 40 Lithosin oil = 40	A
Shang, 2015	RCT	China	Degree-II deep burn wounds	68 patients Hydrogel = 34 Petrolatum gauze = 34	B
Li and Wu, 2018	CCT	China	Degree-II superficial and deep burn wounds	120 patients Hydrogel = 60 SD-Zn = 60	B
Lan and Duan, 2015	RCT	China	Degree-II deep burn wounds	60 patients Hydrogel with silver = 30 MEBO = 30	B
Gong et al., 2009	RCT	China	Degree-II superficial and deep burn wounds	104 patients Hydrogel with silver = 52 SSD and petrolatum gauze = 52	B
Cui et al., 2007	RCT	China	Degree-II superficial and deep burn wounds	44 patients Hydrogel = 22 SSD and Petrolatum gauze = 22	B
Xiang et al., 2012	CCT	China	Non-gangrenous diabetic foot ulcers	86 patients Alginate hydrogel with silver = 43 Polyvidone iodine = 43	B
Liu et al., 2017	RCT	China	Diabetic foot ulcers	30 patients Hydrogel = 15 Gentamicin dressing = 15	B
Teng, 2010	RCT	China	Diabetic foot ulcers	43 patients Hydrogel with silver = 23 Petrolatum gauze = 20	B

(Continued)

TABLE 2 | Continued

References	Study design	Country	Participants	Sample size	Quality level
Shao et al., 2015	CCT	China	Diabetic foot ulcers	78 patients Hydrogel = 39 Glauber and Lidocaine hydrochloride = 39	B
Li et al., 2015	CCT	China	Diabetic foot ulcers	40 patients Hydrogel = 20 Iodophor oil and gauze = 20	B
Nie et al., 2015	RCT	China	Diabetic foot ulcers	65 patients Hydrogel with silver = 34 Petrolatum gauze = 31	B
Wang et al., 2008	RCT	China	Diabetic foot ulcers	43 patients Hydrogel with silver = 23 Petrolatum gauze = 20	A
Mao, 2010	RCT	China	Diabetic foot ulcers	44 patients Hydrogel with silver = 22 Silver dressing = 22	B
Zhang et al., 2012	RCT	China	Diabetic foot ulcers	126 patients Hydrogel with silver = 63 Silver dressing = 63	B
Chen et al., 2015	CCT	China	Diabetic foot ulcers	66 patients Hydrogel with silver = 33 Saline and petrolatum gauze = 33	B
D'Hemecourt et al., 1998	RCT	USA	Diabetic foot ulcers	138 patients Hydrogel = 70 Non-hydrogel = 68	A
Jensen et al., 1998	RCT	USA	Diabetic foot ulcers	31 patients Hydrogel = 14 Non-hydrogel = 17	B
Vandeputte and Gryson, 1997	RCT	Belgium	Diabetic foot ulcers	31 patients Hydrogel = 14 Non-hydrogel = 17	B
Huang et al., 2017	CCT	China	Pressure ulcers	45 patients Hydrogel = 23 Iodine and gauze = 22	B
Wen, 2015	RCT	China	Pressure ulcers	40 patients Hydrogel = 20 Betadine ointment = 20	B
Jiang et al., 2018	RCT	China	Radioactive skin injuries	108 patients Hydrogel = 54 Gauze = 54	B
Hu et al., 2015	RCT	China	Radioactive skin injuries	76 patients Hydrogel = 32 Gauze = 44	B
Shi et al., 2016	CCT	China	Phlebitis patients	73 patients Hydrogel = 38 Magnesium sulfate solution = 35	B
He et al., 2008	RCT	China	Phlebitis patients	60 patients Hydrogel = 30 Saline gauze = 30	B
Huang et al., 2016	RCT	China	Traumatic skin injuries	42 patients Hydrogel = 21 Multi-source therapy device = 21	B
Chen et al., 2015	CCT	China	Traumatic skin injuries	66 patients Hydrogel with silver = 35 Multi-source therapy device = 31	B
Zeng and Li, 2016	RCT	China	Traumatic skin injuries	44 patients Hydrogel = 22 Myogenic silicone = 22	A

(Continued)

TABLE 2 | Continued

References	Study design	Country	Participants	Sample size	Quality level
Zeng and Li, 2016	RCT	China	Traumatic skin injuries	44 patients Hydrogel = 22 Myogenic cream and gauze = 22	A
Lu et al., 2017	CCT	China	Surgical wounds	62 patients Hydrogel with silver = 31 Gauze = 31	B
Fan et al., 2013	RCT	China	Surgical wounds	100 patients Hydrogel with silver = 42 Gauze = 58	A
Wang et al., 2008	RCT	China	Canine bites	40 patients Hydrogel with silver = 20 Saline and gauze = 20	A
Fang et al., 2011	CCT	China	Body surface ulcers	72 patients Hydrogel with silver = 36 Iodine, hydrogen peroxide, and petrolatum gauze = 36	B
Fan et al., 2014	RCT	China	Laser treatments	200 patients Hydrogel = 100 Non-hydrogel = 100	B

difference was highly significant (OR = 4.93, 95% CI: 4.06–5.98, $P < 0.00001$).

VAS Pain Scores of Degree-II Superficial and Deep Burn Wounds

Four studies, reported by Diao et al. (2012), Liu and Ye (2014), Liu (2015), and Lin et al. (2018), compared visual analog scale (VAS) pain scores of the burn wounds treated with hydrogel dressings or other therapeutics. There occurred a statistical heterogeneity among the study results ($P < 0.00001$, $I^2 = 87\%$). Accordingly, the random effect model was applied for meta-synthesis (Figure 4A). The results showed that on average the VAS score of the hydrogel dressings group was 3.31 points lower than the control group, and that the difference had a high statistical significance (MD = -3.31, 95% CI: -4.16 to -2.46, $P < 0.00001$).

Four studies, reported by Liu and Ye (2014), Lan and Duan (2015), Liu (2015), and Shang (2015), compared VAS pain scores of burn wounds treated with hydrogel dressings or other medicaments. A statistical heterogeneity turned up among the study results ($P < 0.00001$, $I^2 = 98\%$). For that reason, the random effect model was applied for meta-synthesis (Figure 4B). The results made clear that on average the VAS score of the hydrogel dressings group was 2.74 points lower than that of the control group and that the difference was statistically significant (MD = -2.74, 95% CI: -4.74 ~ -0.74, $P = 0.007$).

Wound Healing Times of Diabetic Foot Ulcers

Seven studies, reported by Wang et al. (2008), Mao (2010), Teng (2010), Xiang et al. (2012), Zhang et al. (2012), Chen (2015), and Nie et al. (2015), compared the healing times of diabetic foot ulcer wounds treated with hydrogel dressing or other ministrations. There occurred a statistical heterogeneity among the study results ($P < 0.00001$, $I^2 = 99\%$). Therefore, the random effect model was applied for meta-synthesis (Figure 5). The results made plain

that on average the healing time of the hydrogel dressings group was 7.28 days shorter than that of the control group and that the difference had a high statistical significance (MD = -7.28, 95% CI: -11.01 to -3.55, $P < 0.0001$).

Wound Cure Rates of Diabetic Foot Ulcers

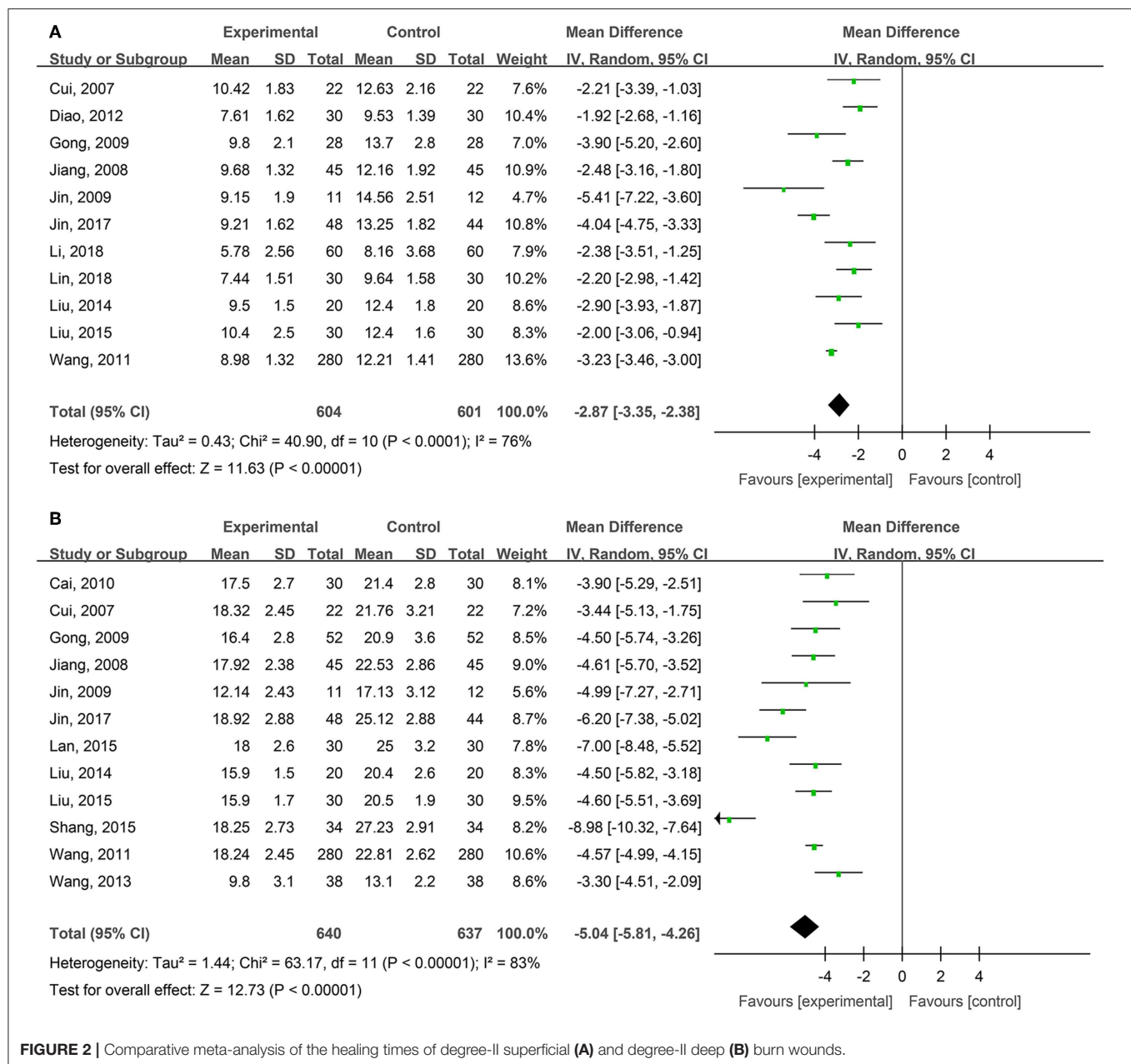
Nine studies, reported by Vandeputte and Gryson (1997), D'Hemecourt et al. (1998), Jensen et al. (1998), Xiang et al. (2012), Zhang et al. (2012), Chen (2015), Li et al. (2015), Shao et al. (2015), and Liu et al. (2017), compared the wound cure rates of diabetic foot ulcers treated with hydrogel dressing or other therapeutics. There existed a statistical heterogeneity among the study results ($P = 0.002$, $I^2 = 67\%$). Hence, the random effect model was applied for meta-synthesis (Figure 6). The results proved that the cure rate of diabetic foot ulcers was higher in the hydrogel dressings group than in the control group and that the difference was statistically significant (RR = 1.57, 95% CI: 1.13–2.17, $P = 0.007$).

Healing Times of Traumatic Skin Injuries

Four studies, reported by Chen et al. (2015), Huang et al. (2016), and Zeng and Li (2016), compared the healing times of traumatic skin injuries treated with hydrogel dressings or other therapeutics. There occurred a statistical heterogeneity among the study results ($P < 0.00001$, $I^2 = 97\%$). Consequently, the random effect model was applied for meta-synthesis (Figure 7). The results revealed that on average the healing time of traumatic skin injuries was 5.28 days shorter in the hydrogel dressing group than in the control group and that the difference reached statistical significance (MD = -5.28, 95% CI: -10.49 to -0.07, $P = 0.05$).

WHO Pain Ratings of Traumatic Skin Injuries

Two studies, reported by Chen et al. (2015) and Huang et al. (2016), compared the WHO pain ratings difference



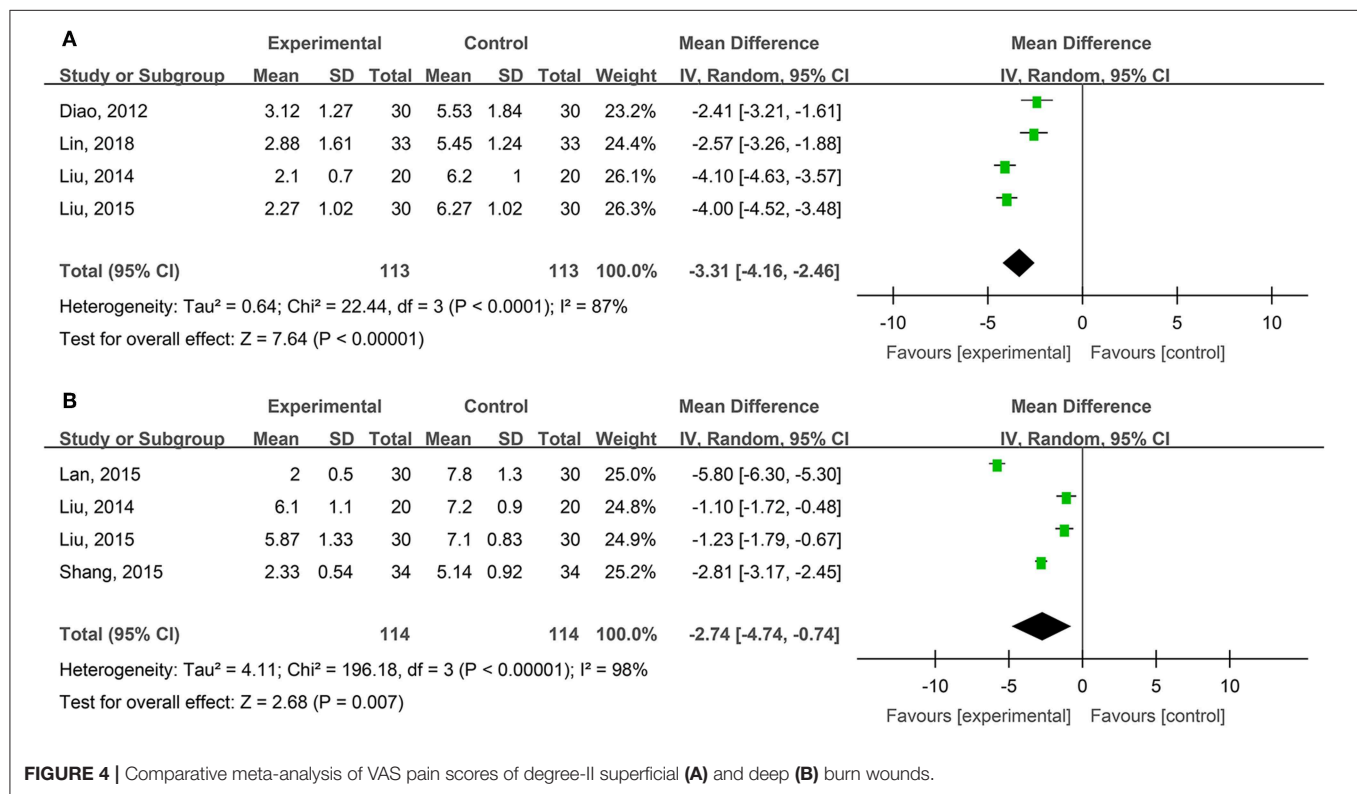
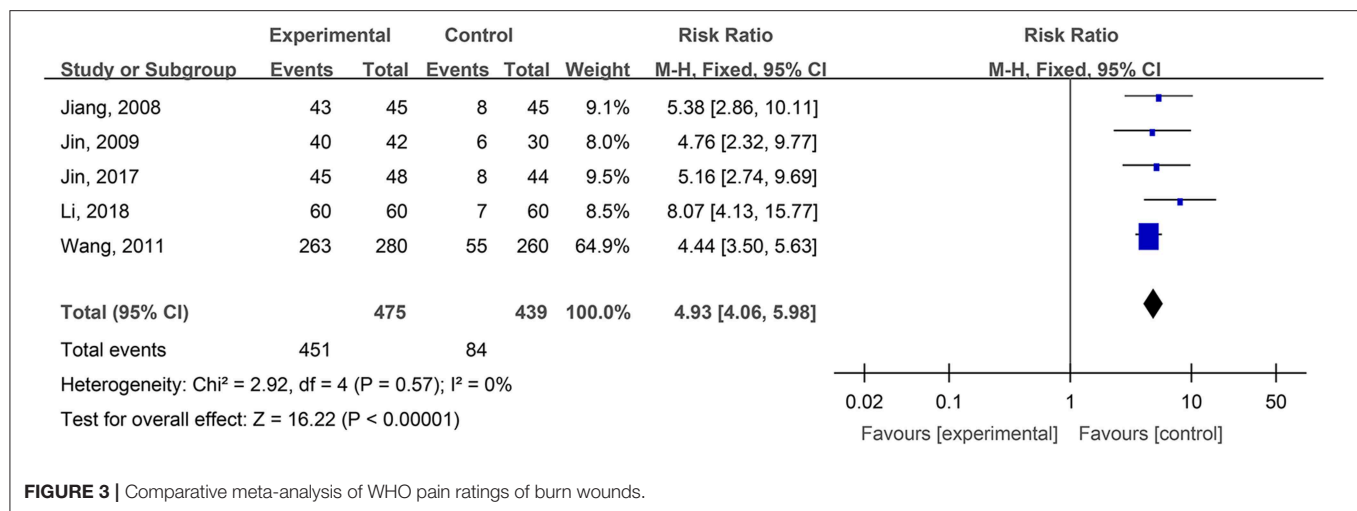
after treatment with hydrogel dressings or other therapeutic interventions. There existed no statistical heterogeneity among the study results ($P = 0.63$). In consequence, the fixed effect model was applied for meta-synthesis (Figure 8). The results disclosed that patients suffering grade-0 and grade-I pain accounted for a higher proportion than the control group did and that the difference was statistically significant ($RR = 25.70$, 95% CI: 3.33–198.43, $P = 0.002$).

Healing Times and Cure Rates of Surgical Wounds

Two studies, reported by Fan et al. (2013) and Lu et al. (2017), compared the healing times of surgical wounds treated with hydrogel dressing or other ministrations. There existed a

statistical heterogeneity among the study results ($P < 0.00001$, $I^2 = 98\%$). Therefore, the random effect model was applied for meta-synthesis (Figure 9A). The results showed that as the healing time of surgical wounds was concerned no statistically significant difference ($P = 0.28$) intervened between the hydrogel dressings group and the control group.

Two studies, reported by Fan et al. (2013) and Lu et al. (2017), compared the cure rates of surgical wounds medicated with hydrogel dressing or other treatments. There existed no statistical heterogeneity among the study results ($P = 0.08$). Consequently, the fixed effect model was applied for meta-synthesis (Figure 9B). The results demonstrated that the cure rate of surgical wounds in the hydrogel dressings group was 20.85% higher than in the



control group and that statistically the difference was highly significant (MD = 20.85%, 95% CI: 20.04–21.65%, $P < 0.00001$).

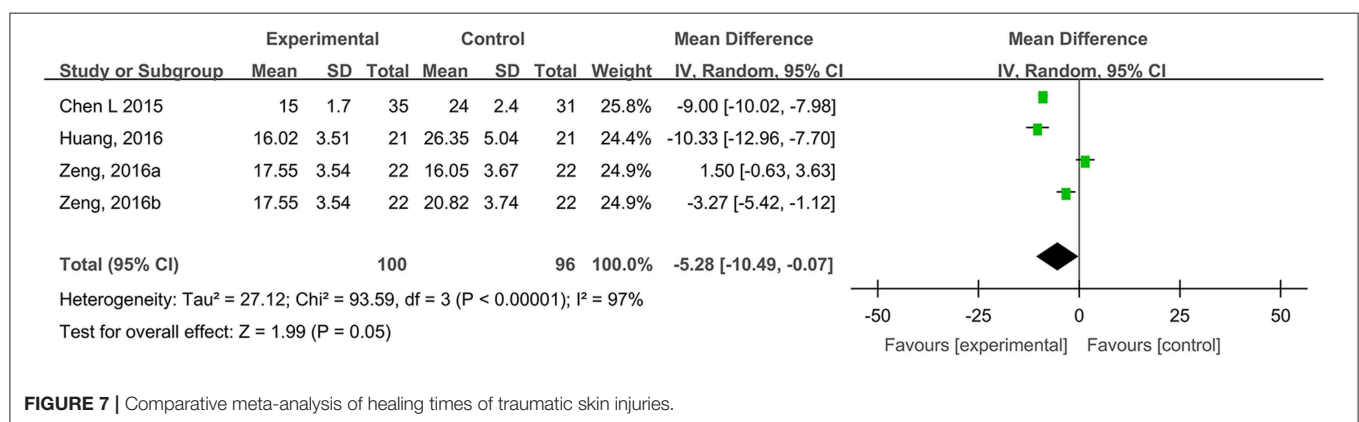
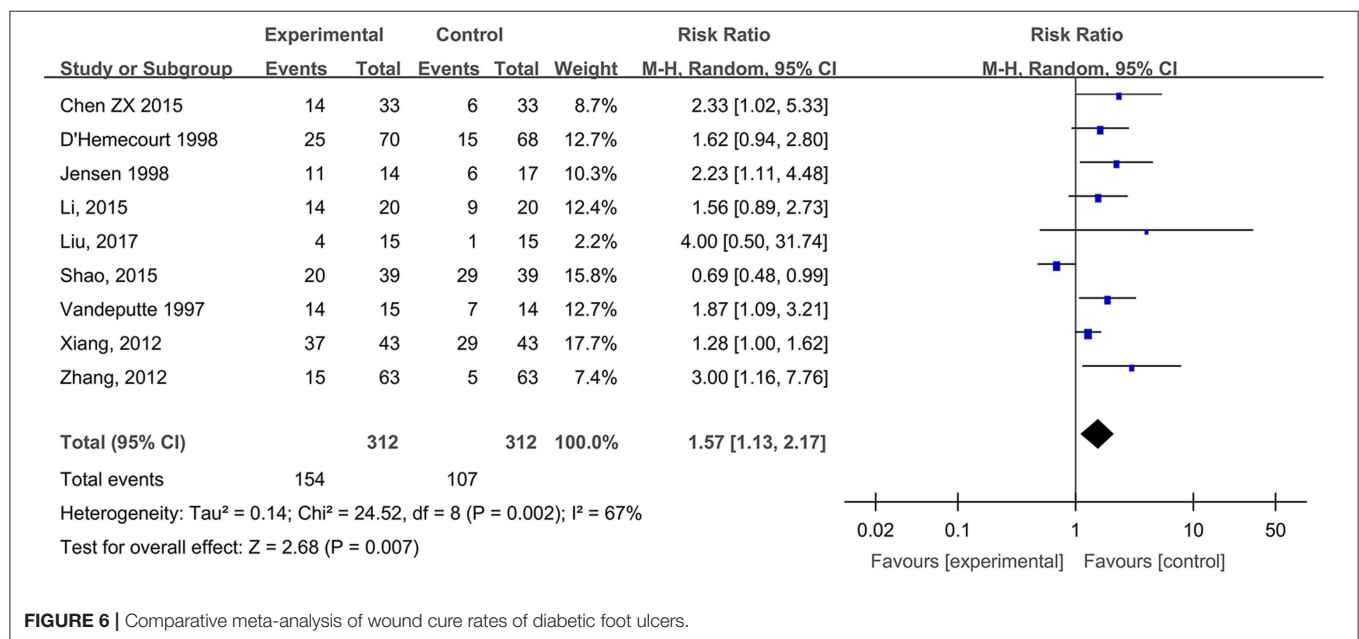
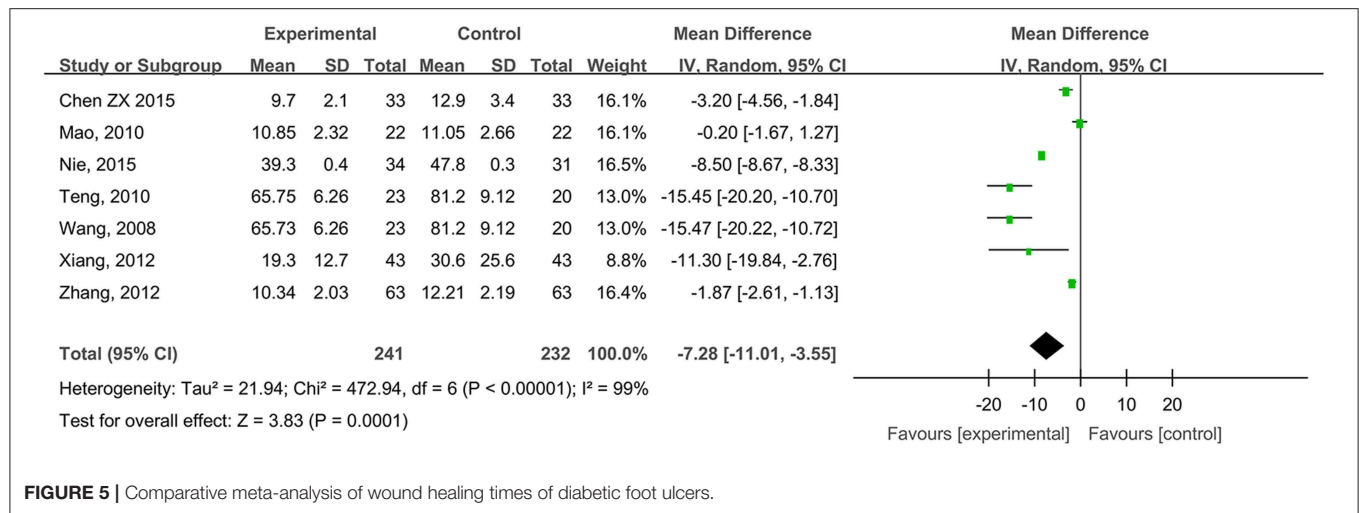
The Cure Rates of Inpatients' Pressure Ulcers

Two studies, reported by Wen (2015) and Huang et al. (2017), compared the cure rates of inpatients' pressure ulcers treated with hydrogel dressings or other therapeutic means. There existed a statistical heterogeneity among the study results ($P = 0.002$, $I^2 = 81\%$). Hence, the random effect model was applied for meta-synthesis (Figure 10). The results revealed that there occurred no statistically significant difference between the hydrogel dressing

group and the control group ($P = 0.08$) in the cure rate of inpatients' pressure ulcers.

Healing Times of Radioactive Skin Injuries

Two studies, reported by Hu et al. (2015) and Jiang et al. (2018), compared the healing times of radioactive skin injuries treated with hydrogel dressings or other medicaments. There occurred no statistical heterogeneity among the study results ($P = 0.95$). In consequence, the fixed effect model was applied for meta-synthesis (Figure 11). The results demonstrated that on average the healing time of the hydrogel dressings group



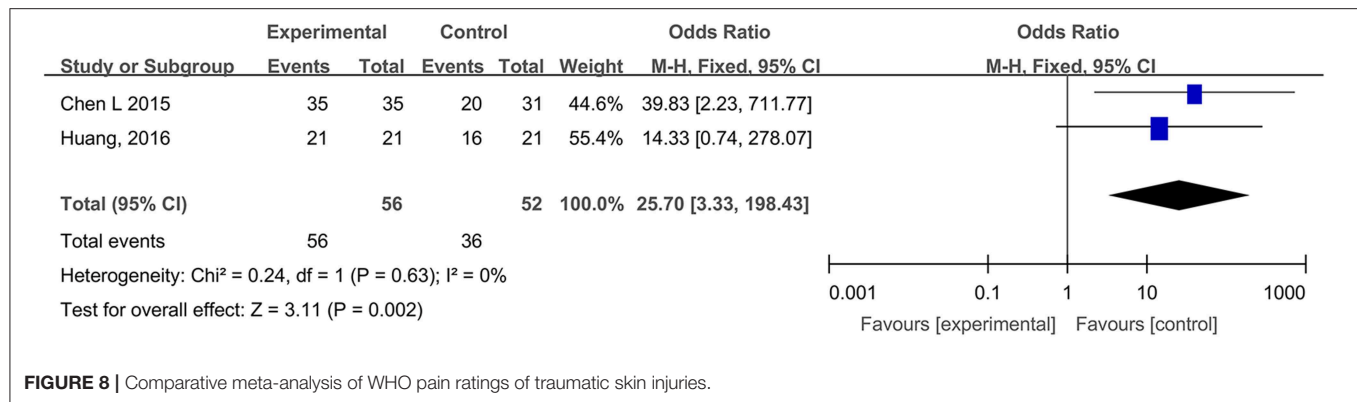


FIGURE 8 | Comparative meta-analysis of WHO pain ratings of traumatic skin injuries.

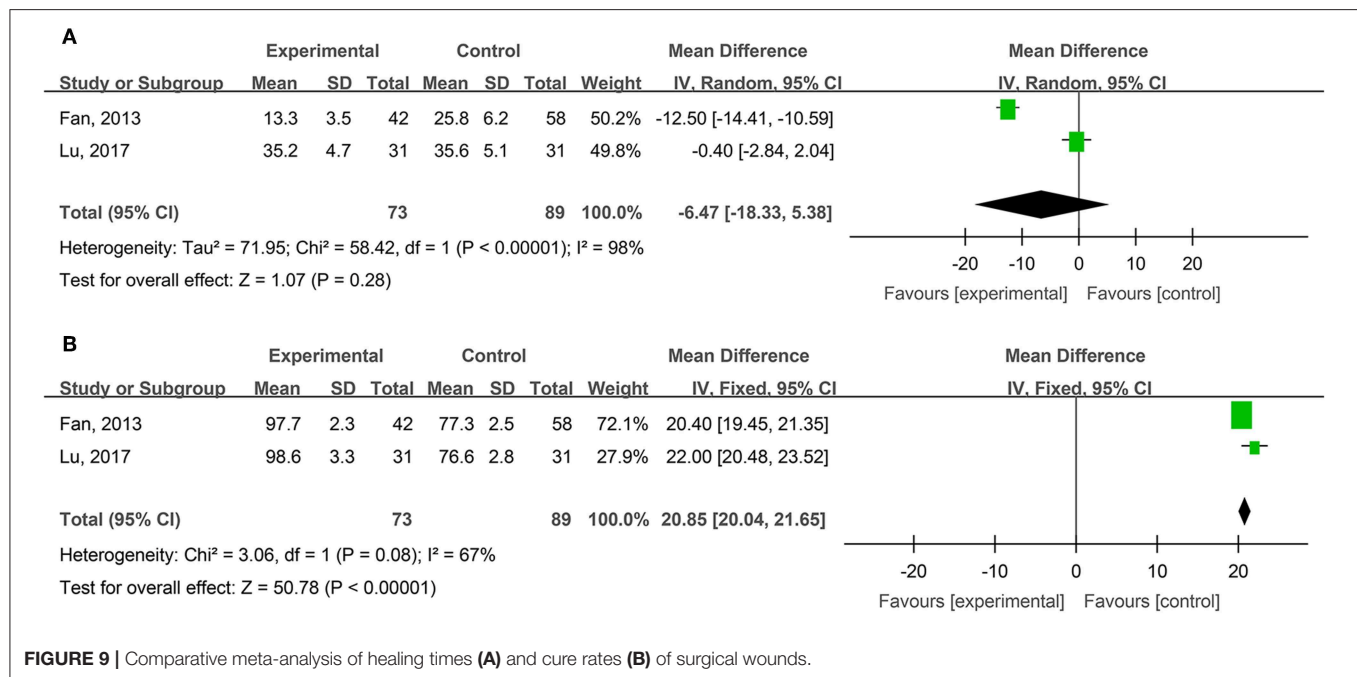


FIGURE 9 | Comparative meta-analysis of healing times (A) and cure rates (B) of surgical wounds.

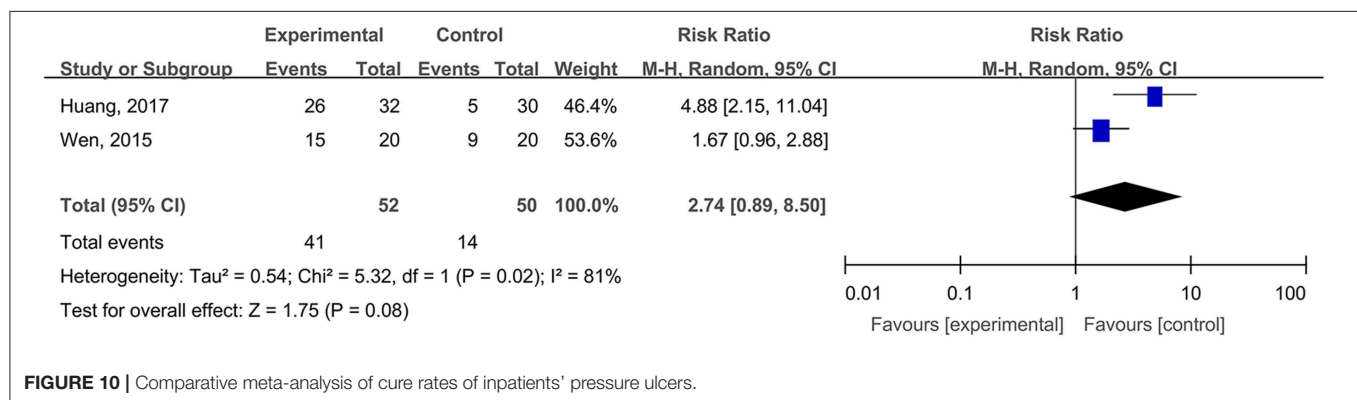


FIGURE 10 | Comparative meta-analysis of cure rates of inpatients' pressure ulcers.

was shortened by 9.46 days as compared with that of the control group and that the difference had a high statistical significance (MD = -9.46 , 95% CI: -10.90 to -8.01 , $P < 0.00001$).

The Cure Rates of Phlebitis Ulcers (Cure and Effectiveness)

Two studies, reported by He et al. (2008) and Shi et al. (2016), compared the cure rates of phlebitis ulcers treated with hydrogel

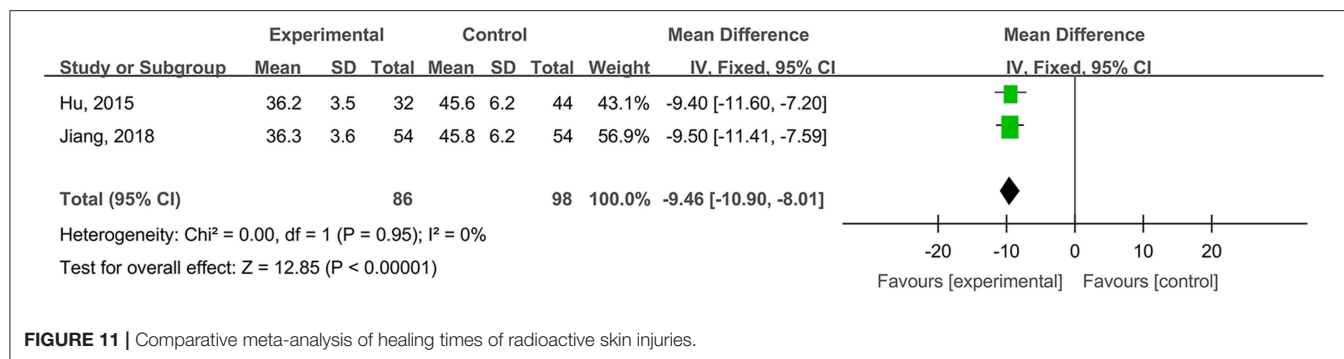


FIGURE 11 | Comparative meta-analysis of healing times of radioactive skin injuries.

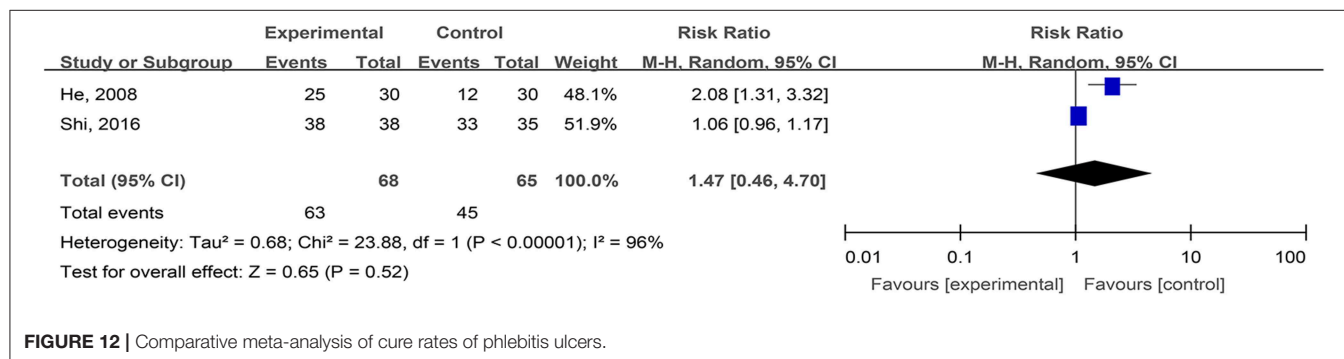


FIGURE 12 | Comparative meta-analysis of cure rates of phlebitis ulcers.

dressings and other ministrations. There existed a statistical heterogeneity among the study results ($P < 0.00001$, $I^2 = 96\%$). Consequently, the random effect model was applied for meta-synthesis (Figure 12). The results indicated that the difference in cure rates between the hydrogel dressings group and the control group of patients with phlebitis ulcers was not statistically significant ($P = 0.52$).

Dog Bite Wounds, Body Surface Ulcers, and Laser Treatment-Induced Wounds

Only one study, reported by Wang and Teng (2008), compared the cure rates of dog bite wounds treated with hydrogel dressings or saline gauze. The results made known that the healing time of the hydrogel dressings group was 4.0 days shorter than that of controls ($t = -16.54$, $P < 0.001$); in addition, the average cure rate of the wounds was 24.8% higher ($t = 27.8$, $P < 0.001$) than the controls.

Then again, a single study, reported by Fang et al. (2011), compared the cure rates of body surface ulcers treated with hydrogel dressings or conventional therapy with Iodophor or hydrogen peroxide plus Vaseline gauze. The results revealed that the healing time of the hydrogel dressings group was 18.4 days shorter than that of the controls ($t = -5.29$, $P < 0.001$); moreover, the total wound cure rate was also significantly higher than that of the control group ($\chi^2 = 13.78$, $P < 0.001$).

Finally, a lone study, reported by Xin et al. (2014), compared the wound care of patients categorized as hydrogel dressings group and blank control group bearing laser treatment-induced wounds. Concerning VAS scores, as contrasted with the blank control group, the pain score of the hydrogel dressings group

was 1.63 lower ($t = -6.47$, $P < 0.001$), the burning sensation score was 1.10 lower ($t = -8.65$, $P < 0.001$) and the stimulating sensation score was 1.46 lower ($t = -10.78$, $P < 0.001$) than the controls.

Data Set of Complaints and Adverse Events

Data Source

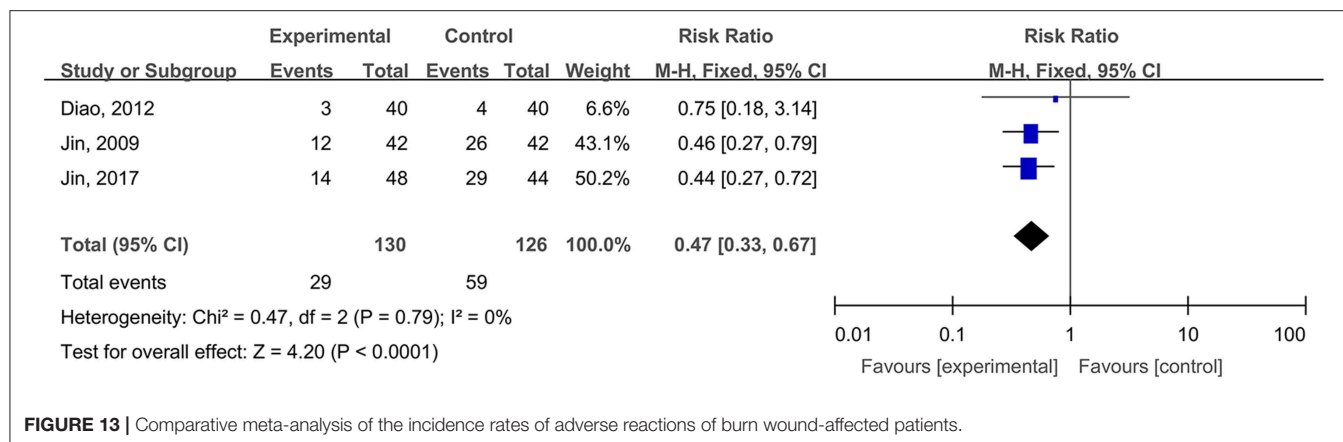
Besides the mentioned above Chinese and English databases, a supplementary search was carried out in the State Monitoring System of Drug Adverse Reactions (SMSDAR; <http://www.adrs.org.cn/>).

Data Synthesis and Analysis

To perform Meta-analyses about the incidence rate of adverse reactions RevMan5.0 software was used and the relative risk was taken as a combined effect size. The heterogeneity of the study results was tested by χ^2 -test. When the study showed a statistical homogeneity ($P > 0.1$, $I^2 < 50\%$), a fixed effect model was applied, otherwise a random effect model was adopted.

Analysis Result

Three studies, reported by Jin et al. (2009), Diao et al. (2012), and Jin et al. (2017), compared the adverse reaction rates in cases of burn wounds treated with hydrogel dressings or other therapeutics. No statistical heterogeneity was detected among the study results ($P = 0.79$). Therefore, the random effect model was applied for meta-synthesis (Figure 13). The results disclosed that the incidence rate of adverse reactions—including skin dryness, swelling, pruritus, and fever—was lower in the hydrogel



dressings group than in the control group, and that statistically the difference was highly significant ($RR = 0.47$, 95% CI: 0.33–0.67, $P < 0.0001$). Other included studies reported no details about patients' adverse reactions.

No reports on adverse reactions of using medicinal hydrogels were found in the State Monitoring System of Drug Adverse Reactions (SMSDAR).

DISCUSSION

This study attempted to adopt the Cochrane systematic evaluation and Meta-analysis to assess the effectiveness and safety of hydrogel dressings employed in the management of skin wounds. The results brought to light that the application of medicinal hydrogel dressings can significantly shorten the healing time of skin wounds such as superficial degree-II burns (Figure 2A), deep degree-II burns (Figure 2B), diabetic foot ulcers (Figure 5), traumatic skin injuries (Figure 7), radioactive skin injuries (Figure 11), dog bites ($t = -5.29$, $P < 0.001$), and body surface ulcers ($t = -5.29$, $P < 0.001$). Hydrogel dressings can also effectively improve the cure rate of diabetic foot ulcers (Figure 6), surgical wounds (Figure 9B), dog bites ($t = 27.8$, $P < 0.001$), and body surface ulcers ($\chi^2 = 13.78$, $P < 0.001$). These advantageous effects are likely due to the nearly ideal moist environment that hydrogel dressings provide once applied to skin wounds. This promotes cell viability and physiological functioning and subsequently wound healing. In addition, hydrogel dressings reduce the loss of body fluids while absorbing wound's exudate and advancing autolytic debridement in necrotic wounds and granulating wounds. The hydrogels' swelling property has been proved to decrease the excessive fluid accumulation between the wound surface and the dressing. On the other hand, the hydrogel owns a soft texture and tends to adhere to the wound surface tightly and evenly, which prevents bacterial invasion and reduces soreness as well.

In recent years, with the appearance of new antibiotics and drugs applied to wounds, bactericidal and bacteriostatic substances such as silver ions have been combined with dressings to control local infections and accelerate wound healing. Nanocrystalline silver modulates the inflammatory response

through its antimicrobial activity, thereby reducing the infections incidence and leading to an improved wound healing outcome. Furthermore, a faster re-epithelialization occurred in the wounds treated with nanocrystalline silver-coupled dressing rather than with a standard antibiotic solution (Demling and DeSanti, 2002; Nherera et al., 2017).

Study results also indicate that medicinal hydrogels can effectively alleviate the pain and burning and irritating sensations typical of skin wounds. The WHO pain rating of burn wounds (Figure 3) and traumatic skin injuries was significantly lower in the hydrogel dressing treatment studies. In addition, when hydrogel dressings were compared with non-hydrogel treatments, the VAS pain score was obviously lower in superficial degree-II burns (Figure 4A), deep degree-II burns (Figure 4B), and laser treatment-induced wounds. Concurrently, adverse reactions such as wound dryness, swelling, pruritus, and fever were significantly reduced (Figure 13). The benefits brought by hydrogel dressings to wounds might be related to the hydrogel-induced microenvironment that minimizes secondary injuries and alleviates pain by generating a cool feeling and by protecting any exposed peripheral nerve terminals. Our data also indicated that the guar gum-based hydrogel (CQ-01) is safe and can effectively alleviate the intractable pruritus otherwise affecting the patients [the score of Jun Wu scale (JW scale) pruritus rating scale for CQ-01 group was significantly lower than that of the traditional dressing group]. This further supports the clinical antipruritic effect of hydrogel dressings (Wu et al., 2016).

Meta-analysis is an observational study, thus, biases are somehow inevitable (Easterbrook et al., 1991). Among 43 original studies only 8 of them were graded A according to EPOC quality grading, which may potentially prejudice the results. Moreover, some hydrogel dressings were used in combination with other dressings, for example, silver dressings or with Lithosin solution. None of these trials assessed the effects of these combinations. It should be noted that hydrogel dressings are supposed to be applied singly rather than in combination with other therapeutics and that when used in combination their effectiveness and safety cannot be evaluated from individual dressing data. On the other hand, in the result of healing times comparison of burn wounds and others, there existed a statistical heterogeneity among the

study results. The main reason for statistical heterogeneity of selected studies is that the sample size of each selected study varies greatly. In addition, clinical heterogeneity may also cause heterogeneity in statistical analysis, such as differences in baseline characteristics and medical conditions of burn patients in various studies, which may affect treatment outcomes.

The limitation of this meta-analysis is that, various dressings were applied in control groups included in this review, such as SSD, Iodine solution, Entoiodine and petrolatum gauze, Lithosin solution and oil, SD-Zn, Petrolatum gauze, Polyvidone iodine, Gentamicin dressing, etc. which may affect the outcomes and potentially add the biases to the study as well.

The main limitation of this review is the potential publication bias in terms of safety assessment of hydrogel dressings. Although we endeavored to collect quite a number of clinical trials by searching both publication databases and SMSDAR, in this systematic review only three studies compared the adverse reactions between hydrogel dressings and other medicinal products. The poor reporting of adverse reactions could be generalizable to the study purpose of clinical trials, which are commonly designed to explore the effectiveness of a dressing in promoting wound healing while they do not focus on the wound site responses to the dressing tested. On the other hand, it is sometimes hard to distinguish an adverse reaction from events related to wound healing.

CONCLUSIONS

This evidence-based systematic review and meta-analysis from RCTs and CCTs studies suggests that the use of hydrogel dressings results in a significant decrease in wound healing time, an obvious increase in cure rate, and a satisfying relief of pain as compared to non-hydrogel dressings. All the above-reported results strongly indicate that hydrogel products are effective and safe in wound management. Furthermore, there is a need

for high-quality and international multi-center RCTs reporting adverse reactions to help clinicians make informed decisions on the best options for patients suffering from skin wounds.

DATA AVAILABILITY STATEMENT

All datasets generated for this study are included in the article/supplementary material.

AUTHOR CONTRIBUTIONS

Study design and conception of this manuscript were due to JW and BS. Literature retrieving and studies selection were performed by XL and JL. MY and XW carried out the quality evaluation of the study. Mathematical modeling and meta-analysis were conducted by FZha and FZho. Results analysis and interpretation were done by LZ, HY, and SQ. The manuscript was drafted by LZ and HY. All authors read and approved the final manuscript.

FUNDING

This work was supported by 100 Talents Program of Sun Yat-Sen University (Y61216), the Three-Three Project of the First Affiliated Hospital, Sun Yat-sen University (Y70214), National Natural Science Foundation of China (NSFC 81601624), China Postdoctoral Science Foundation Grant (2018M631028), and Doctoral Innovation Project of Shenzhen Health and Family Planning System Research Project (201605007).

ACKNOWLEDGMENTS

We would like to thank Prof. Ji Wang and Prof. Xuyang Feng for their useful comments.

REFERENCES

- Cai, L., Lv, G., and Chen, J. (2010). Clinical study of photocrosslinked chitosan hydrogel film in the treatment of deep second degree burn wounds. *Chin. J. Inj. Repair* 5, 61–65.
- Chattopadhyay, S., and Raines, R. T. (2014). Review collagen-based biomaterials for wound healing. *Biopolymers* 101, 821–833. doi: 10.1002/bip.22486
- Chen, L., Ning, N., and Chen, H. (2015). Clinical observation of skin wound wet healing treatment. *Huaxi Med.* 30, 1811–1813.
- Chen, Z. X. (2015). Observation on the effect of silver ion dressing combined with hydrogel in the treatment of diabetic foot. *Mod. Med.* 15, 82–83.
- Cui, Z., Liu, L., and Li, J. (2007). Treatment of 42 cases of wounds in burn and plastic donor area with cold Lengningkang dressing. *Chin. J. Injury Repair Wound Healing, Electronic Edn.* 2, 36–37.
- Das, S., and Baker, A. B. (2016). Biomaterials and nanotherapeutics for enhancing skin wound healing. *Front. Bioeng. Biotechnol.* 4:82. doi: 10.3389/fbioe.2016.00082
- Demling, R. H., and DeSanti, M. D. L. (2002). The rate of re-epithelialization across meshed skin grafts is increased with exposure to silver. *Burns* 28, 264–266. doi: 10.1016/S0305-4179(01)00119-X
- D'Hemecourt, P. A., Smiell, J. M., and Karim, M. R. (1998). Sodium carboxymethyl cellulose aqueous-based gel vs becaplermin gel in patients with nonhealing lower extremity diabetic ulcers. *Wound* 10, 69–75.
- Diao, Y., Wang, S., and Chen, M. (2012). Application of hydrogel dressing Ai Kangye silver in the treatment of shallow second degree burn wounds. *J. Southeast Univ.* 31, 729–731.
- Dong, R., Zhao, X., Guo, B., and Ma, P. X. (2016). Self-healing conductive injectable hydrogels with antibacterial activity as cell delivery carrier for cardiac cell therapy. *ACS Appl. Mater. Interfaces* 8, 17138–17150. doi: 10.1021/acsami.6b04911
- Easterbrook, P. J., Berlin, J. A., Gopalan, R., and Matthews, D. R. (1991). Publication bias in clinical research. *Lancet* 337, 867–872. doi: 10.1016/0140-6736(91)90201-Y
- Fan, X., Xiao, M., and Wu, Y. (2013). A prospective study of the effect of silver ion combined with hydrogel dressing on postoperative infection wounds. *Chin. J. Basic Clin. Med.* 20, 102–104.
- Fan, Z., Liu, B., Wang, J. Q., Zhang, S., Lin, Q., Gong, P., et al. (2014). A novel wound dressing based on ag/graphene polymer hydrogel: effectively kill bacteria and accelerate wound healing. *Adv. Funct. Mater.* 24, 3933–3943. doi: 10.1002/adfm.201304202

- Fang, Q., Zhang, C., and Cai, X. (2011). Effect of wet therapy on the treatment of surface ulcers. *J. Nurs. Train.* 26, 2076–2077.
- Garg, T., Rath, G., and Goyal, A. K. (2015). Biomaterials-based nanofiber scaffold: targeted and controlled carrier for cell and drug delivery. *J. Drug Target.* 23, 202–221. doi: 10.3109/1061186X.2014.992899
- Gil, E. S., Panilaitis, B., Bellas, E., and Kaplan, D. L. (2013). Functionalized silk biomaterials for wound healing. *Adv. Healthc. Mater.* 2, 206–217. doi: 10.1002/adhm.201200192
- Gong, Z., Yao, J., and Ji, J. (2009). Effects of silver ion dressing combined with hydrogel on wound healing of second-degree burns. *J. Clin. Rehabil. Tissue Eng. Res.* 13, 8373–8376.
- Grice, E. A., Kong, H. H., Conlan, S., Deming, C. B., Davis, J., Young, A. C., et al. (2009). Topographical and temporal diversity of the human skin microbiome. *Science* 324 1190–1192. doi: 10.1126/science.1171700
- He, Q., Wu, G., and Yu, B. (2008). Early results of wound healing hydrogel in the treatment of chronic lower extremity varicose ulcers. *Chin. J. Reconstr. Surg.* 22, 311–313.
- Hu, Y., Xiao, H., and Fu, L. (2015). Study on the effect of new hydrogel dressings on the treatment of wet peeling after radiotherapy. *Chin. Nurs. Res.* 29, 1635–1637.
- Huang, G., Liu, L., and Rongfen, W. (2016). Treatment and nursing observation of 42 cases of acute skin abrasion and contusion. *J. Yangtze Univ.* 13, 67–68.
- Huang, Y., Han, W., and Weng, L. (2017). Application of wet healing therapy in stage III and IV severe pressure ulcers. *Modern Clin. Care* 16, 46–48.
- Huang, Y., Wang, Y., Sun, L., Agrawal, R., and Zhang, M. (2015). Sundew adhesive: a naturally occurring hydrogel. *J. R. Soc. Interface* 12:12. doi: 10.1098/rsif.2015.0226
- Jensen, J. L., Seeley, J., and Gilin, B. (1998). A controlled, randomized comparison of two moist wound healing protocols: carrasyn hydrogel wound dressing and wet-to-moist saline gauze. *Adv. Wound Care* 11, 323–327.
- Jiang, J., Yu, S., and Shen, X. (2008). Treatment of burn wound pain by Lengningkang dressing. *Chin. J. Inj. Repair Wound Heal. (Electronic Edition)* 3, 200–202.
- Jiang, X., Sun, R., and Li, J. (2018). Observation on the effect of hydrogel dressing on radiation-induced skin injury. *J. Pract. Clin. Nurs.* 3, 91–100.
- Jin, A., Cai, L., and Chen, Y. (2017). Comparison of curative effect between hydrogel wound dressing and silver sulfadiazine on bromine burn wounds. *Zhejiang Med. J.* 39, 1474–1475+1482.
- Jin, A., Shi, S., and Lu, J. (2009). “Application of Lengningkang in facial burn wounds,” in *Zhejiang Medical Association Burns Surgery Academic Annual Conference Papers* (Zhejiang Medical Association).
- Lan, Y., and Duan, N. (2015). Observation on the effect of new dressing for debridement and treatment of deep II burn wounds. *Contemp. Nurse* 5, 116–117.
- Li, L., and Wu, B. (2018). Clinical study of early external HD series medical hydrogel wound dressing for small area burn wounds. *Chin. J. Damage Restor.* 13, 376–377.
- Li, P., Chen, Y., and Wo, H. (2015). Clinical efficacy of Sanhuang wet compress hydrogel in the treatment of diabetic foot ulcer wounds. *Inner Mongolia Tradition. Chin. Med.* 12, 18–19.
- Lin, Z., Yang, R., Shubin, R., Yan, L., Zhang, F., Xiong, X., et al. (2018). Analysis of the role of hydrogel dressing in the treatment of superficial second degree burn wounds. *J. Gannan Med. College* 38, 358–360.
- Liu, B. (2015). *Comparative Study on the Clinical Efficacy of Wet Protective Dressing for the Treatment of Second Degree Burn Wounds*. Ningxia Medical University.
- Liu, B., and Ye, L. (2014). Application of hydrogel dressing combined with compound comfrey oil in second degree burn wounds. *Chin. J. Aesthetic Med.* 23, 1330–1333.
- Liu, L., Wang, S., and Cheng, C. (2017). Clinical observation of collagen-loaded nerve growth factor in the treatment of diabetic foot ulcer. *J. Armed Police Log. Univ.* 26, 421–423.
- Lu, L., Xie, C., and Lu, J. (2017). Efficacy evaluation of cefuroxime sodium combined with silver ion and hydrogel dressing for wound healing in patients with postoperative infection. *Anti-infected Pharm.* 14, 1310–1312.
- Mao, C., Xiang, Y., Liu, X., Cui, Z., Yang, X., Yeung, K. W. K., et al. (2017). Photo-inspired antibacterial activity and wound healing acceleration by hydrogel embedded with Ag/AgCl/ZnO nanostructures. *ACS Nano* 11, 9010–9021. doi: 10.1021/acsnano.7b03513
- Mao, L. (2010). Therapeutic effect of silver ion dressing combined with hydrogel and moist treatment wound dressing on diabetic foot infection. *Chin. J. Misdiagn.* 10:8348.
- Metcalfe, A. D., and Ferguson, M. W. (2007). Tissue engineering of replacement skin: the crossroads of biomaterials, wound healing, embryonic development, stem cells and regeneration. *J. R. Soc. Interface* 4, 413–437. doi: 10.1098/rsif.2006.0179
- Mohan, Y. M., Lee, K., Premkumar, T., and Geckeler, K. E. (2007). Hydrogel networks as nanoreactors: a novel approach to silver nanoparticles for antibacterial applications. *Polymer* 48, 158–164. doi: 10.1016/j.polymer.2006.10.045
- Nherera, L. M., Trueman, P., Roberts, C. D., and Berg, L. (2017). A systematic review and meta-analysis of clinical outcomes associated with nanocrystalline silver use compared to alternative silver delivery systems in the management of superficial and deep partial thickness burns. *Burns* 43, 939–948. doi: 10.1016/j.burns.2017.01.004
- Nie, H., Li, K., and Zhang, Q. (2015). Application of wet dressing in dressing change of elderly diabetic foot ulcer. *Inner Mongolia Tradition. Chin. Med.* 35, 3582–3584.
- Nourian Dehkordi, A., Mirahmadi Babaheydari, F., Chehelgerdi, M., and Raeisi Dehkordi, S. (2019). Skin tissue engineering: wound healing based on stem-cell-based therapeutic strategies. *Stem Cell Res. Ther.* 10:111. doi: 10.1186/s13287-019-1212-2
- Purna, S. K., and Babu, M. (2000). Collagen based dressings—a review. *Burns* 26, 54–62. doi: 10.1016/S0305-4179(99)00103-5
- Qiu, Y., and Park, K. (2001). Environment-sensitive hydrogels for drug delivery. *Adv. Drug Deliv. Rev.* 53, 321–339. doi: 10.1016/S0169-409X(01)00203-4
- Qu, J., Zhao, X., Liang, Y., Zhang, T., Ma, P. X., and Guo, B. (2018). Antibacterial adhesive injectable hydrogels with rapid self-healing, extensibility and compressibility as wound dressing for joints skin wound healing. *Biomaterials* 183, 185–199. doi: 10.1016/j.biomaterials.2018.08.044
- Roy, N., Saha, N., Kitano, T., and Saha, P. (2010). Novel hydrogels of PVP-CMC and their swelling effect on viscoelastic properties. *J. Appl. Polym. Sci.* 117, 1703–1710. doi: 10.1002/app.32056
- Schwartz, V. B., Thetiot, F., Ritz, S., Puetz, S., Choritz, L., Lappas, A., et al. (2012). Antibacterial surface coatings from zinc oxide nanoparticles embedded in poly(N-isopropylacrylamide) hydrogel surface layers. *Adv. Funct. Mater.* 22, 2376–2386. doi: 10.1002/adfm.201102980
- Shamseer, L., Moher, D., Clarke, M., Ghersi, D., Liberati, A., Petticrew, M., et al. (2015). Preferred reporting items for systematic review and meta-analysis protocols (PRISMA-P) 2015: elaboration and explanation. *BMJ* 350:g7647. doi: 10.1136/bmj.g7647
- Shang, N. (2015). *Application of Hydrogel Dressing in Wound Healing After Grinding*. Shandong University.
- Shao, M., Chen, H., and Chen, Q. (2015). Effects of pain during incision dressing on wound healing in diabetic foot. *Chin. J. Modern Nurs.* 21, 1522–1524.
- Shi, S., LuTing, W., and Wang, Y. (2016). Therapeutic effect of Lengningkang HD-M hydrogel dressing on PICC-associated phlebitis. *Hainan Med. J.* 27, 2221–2222.
- Sood, A., Granick, M. S., and Tomaselli, N. L. (2014). Wound dressings and comparative effectiveness. *Data.* 3, 511–529. doi: 10.1089/wound.2012.0401
- Teng, Y. (2010). *Evidence-Based Research on Clinical Treatment of Chronic Wounds*. Lanzhou: Lanzhou University.
- Tsao, C. T., Chang, C. H., Lin, Y. Y., Wu, M. F., Wang, J. L., Han, J. L., et al. (2010). Antibacterial activity and biocompatibility of a chitosan-gamma-poly (glutamic acid) polyelectrolyte complex hydrogel. *Carbohydr. Res.* 345, 1774–1780. doi: 10.1016/j.carres.2010.06.002
- Vandeputte, J., and Gryson, L. (1997). “Diabetic foot infection controlled by immuno-modulating hydrogel containing 65% glycerine. Presentation of a clinical trial,” in *6th European Conference on Advances in Wound Management, Vol. 1997* (Amsterdam), 50–53.
- Wang, J., and Teng, Y. (2008). Local treatment of canine bite wound III with silver ion dressing combined with hydrogel: randomized controlled group. *Chin. J. Tissue Eng. Res. Clin. Rehab.* 12, 2659–2662.

- Wang, J., Yan, X., and Teng, Y. (2008). Local treatment of diabetic foot wound with silver ion dressing combined with hydrogel. *J. Chongqing Med. Univ.* 33, 747–749.
- Wang, J., Yan, X., and Teng, Y. (2013). A prospective study of the effect of silver ion combined with hydrogel dressing on postoperative infection wounds. *J. Chongqing Med. Univ.* 20, 102–104.
- Wang, L., Lin, X., and Xiang, X. (2011). Clinical application and safety of Lengningkang dressing in the treatment of burn wounds. *China Pharmaceutic.* 20, 64–65.
- Wen, S. (2015). Nursing experience of hydrogel combined with insulin for the treatment of patients with acne. *World's Latest Med. Inform. Abst.* 15, 221–226.
- Wichterle, O., and Lim, D. (1960). Hydrophilic gels for biological use. *Nature* 185, 117–118. doi: 10.1038/185117a0
- Winter, G. D. (1962). Formation of the scab and the rate of epithelization of superficial wounds in the skin of the young domestic pig. *Nature* 193, 293–294. doi: 10.1038/193293a0
- Wu, J., Xu, R., Zhan, R., Luo, G., Niu, X., Liu, Y., et al. (2016). Effective symptomatic treatment for severe and intractable pruritus associated with severe burn-induced hypertrophic scars: a prospective, multicenter, controlled trial. *Burns* 42, 1059–1066. doi: 10.1016/j.burns.2015.09.021
- Xiang, Y., Zhang, H., and Zou, J. (2012). Clinical study on innovative dressing for the treatment of diabetic foot ulcer. *Chin. Pharm.* 23, 2063–2064.
- Xin, F., Liu, L., and An, Y. (2014). Application of medical hydrogel in laser therapy and multi-center clinical efficacy observation. *J. Pract. Dermatol.* 7, 193–195.
- Xu, R., Luo, G., Xia, H., He, W., Zhao, J., Liu, B., et al. (2015). Novel bilayer wound dressing composed of silicone rubber with particular micropores enhanced wound re-epithelialization and contraction. *Biomaterials* 40, 1–11. doi: 10.1016/j.biomaterials.2014.10.077
- Zeng, Y., and Li, Y. (2016). Application of Shengji ointment combined with silicone dressing in wound care. *Contemp. Nurses*, 5, 78–80.
- Zhang, L., Ma, J., and Zhang, H. (2012). Comparison of silver ion dressing combined with hydrogel and wet treatment wound dressing for the treatment of diabetic foot infection. *Chin. J. Nosocomiol.* 22, 4002–4003.

Conflict of Interest: The authors declare that the research was conducted in the absence of any commercial or financial relationships that could be construed as a potential conflict of interest.

Copyright © 2019 Zhang, Yin, Lei, Lau, Yuan, Wang, Zhang, Zhou, Qi, Shu and Wu. This is an open-access article distributed under the terms of the Creative Commons Attribution License (CC BY). The use, distribution or reproduction in other forums is permitted, provided the original author(s) and the copyright owner(s) are credited and that the original publication in this journal is cited, in accordance with accepted academic practice. No use, distribution or reproduction is permitted which does not comply with these terms.



Three-Layered Silk Fibroin Tubular Scaffold for the Repair and Regeneration of Small Caliber Blood Vessels: From Design to *in vivo* Pilot Tests

Antonio Alessandrino¹, Anna Chiarini², Marco Biagiotti¹, Ilaria Dal Prà², Giulia A. Bassani¹, Valentina Vincoli¹, Piergiorgio Settembrini³, Pasquale Pierimarchi⁴, Giuliano Freddi^{1*} and Ubaldo Armato²

OPEN ACCESS

Edited by:

Masoud Mozafari,
University of Toronto, Canada

Reviewed by:

Sajjad Ashraf,
Mount Sinai Hospital, University of
Toronto, Canada
Fatemeh Kabirian,
Materials and Energy Research
Center, Iran

*Correspondence:

Giuliano Freddi
giuliano@silkbioaterials.com

Specialty section:

This article was submitted to
Biomaterials,
a section of the journal
Frontiers in Bioengineering and
Biotechnology

Received: 30 July 2019

Accepted: 08 November 2019

Published: 29 November 2019

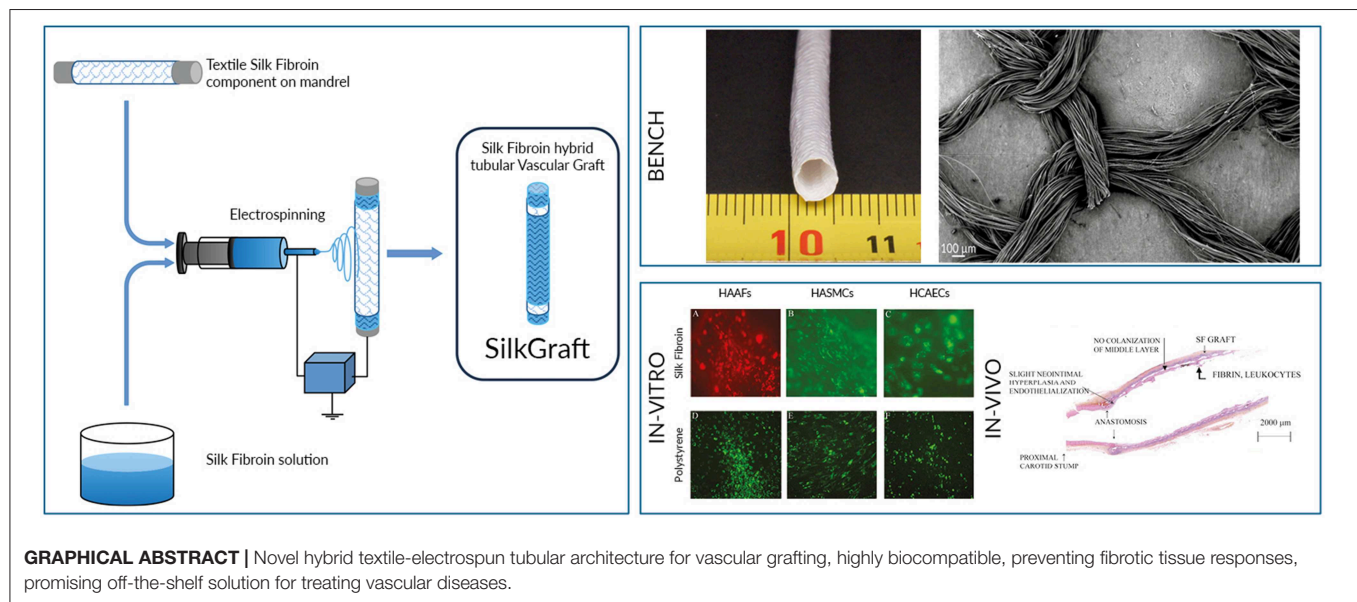
Citation:

Alessandrino A, Chiarini A, Biagiotti M,
Dal Prà I, Bassani GA, Vincoli V,
Settembrini P, Pierimarchi P, Freddi G
and Armato U (2019) Three-Layered
Silk Fibroin Tubular Scaffold for the
Repair and Regeneration of Small
Caliber Blood Vessels: From Design to
in vivo Pilot Tests.
Front. Bioeng. Biotechnol. 7:356.
doi: 10.3389/fbioe.2019.00356

¹ Silk Biomaterials Srl, Lomazzo, Italy, ² Human Histology & Embryology Section, Department of Surgery, Dentistry, Pediatrics & Gynecology, University of Verona Medical School, Verona, Italy, ³ Department of Vascular Surgery, San Carlo Borromeo Hospital, Milan, Italy, ⁴ Institute of Translational Pharmacology, National Research Council, Rome, Italy

Silk fibroin (SF) is an eligible biomaterial for the development of small caliber vascular grafts for substitution, repair, and regeneration of blood vessels. This study presents the properties of a newly designed multi-layered SF tubular scaffold for vascular grafting (SilkGraf). The wall architecture consists of two electrospun layers (inner and outer) and an intermediate textile layer. The latter was designed to confer high mechanical performance and resistance on the device, while electrospun layers allow enhancing its biomimicry properties and host's tissues integration. *In vitro* cell interaction studies performed with adult Human Coronary Artery Endothelial Cells (HCAECs), Human Aortic Smooth Muscle Cells (HASMCs), and Human Aortic Adventitial Fibroblasts (HAAFs) demonstrated that the electrospun layers favor cell adhesion, survival, and growth. Once cultured *in vitro* on the SF scaffold the three cell types showed an active metabolism (consumption of glucose and glutamine, release of lactate), and proliferation for up to 20 days. HAAF cells grown on SF showed a significantly lower synthesis of type I procollagen than on polystyrene, meaning a lower fibrotic effect of the SF substrate. The cytokine and chemokine expression patterns were investigated to evaluate the cells' proliferative and pro-inflammatory attitude. Interestingly, no significant amounts of truly pro-inflammatory cytokines were secreted by any of the three cell types which exhibited a clearly proliferative profile. Good hemocompatibility was observed by complement activation, hemolysis, and hematology assays. Finally, the results of an *in vivo* preliminary pilot trial on minipig and sheep to assess the functional behavior of implanted SF-based vascular graft identified the sheep as the more apt animal model for next medium-to-long term preclinical trials.

Keywords: silk fibroin, small caliber vascular graft, morphological structure, mechanical performance, *in vitro* biocompatibility, *in vivo* pilot test



INTRODUCTION

Cardiovascular pathologies are the leading cause of death worldwide (World Health Organization, 2012), with very high overall incidence on health expenditures. As the vascular diseases progress with age, the related burden is likely to increase with the global rise in life expectancy. Thus, the availability of grafts for the treatment of vascular diseases becomes a real and urgent need. In the vascular surgery field of either coronary or peripheral bypass procedures, there is a crucial necessity of novel viable solutions, which might complement or even replace current surgical approaches, based on autografts, or synthetic grafts (Catto et al., 2014; Hiob et al., 2017; Sugiura et al., 2017). Autografts (using native vessels such as superficial veins or rarely umbilical veins) still remain the standard clinical approach for the replacement of small diameter blood vessels. However, there are some factors which may strongly curb the use of autografts: absence of a usable graft, significative atherosclerosis of the arteries, previous usage of an autograft for surgical procedures, or angiographic approaches (Catto et al., 2014).

Nowadays, small caliber synthetic grafts are made of polyethylene terephthalate (PET) or expanded polytetrafluoroethylene (ePTFE). Their use leads to possible multiple complications like aneurysm, intimal hyperplasia, calcification, thrombosis, infection, and lack of growth potential for pediatric applications. These drawbacks are mainly correlated to the regeneration of a non-functional endothelium and a mismatch between the mechanical properties of grafts and native blood vessels leading to the development of an intimal hyperplasia with subsequent reduction of the patency rate (Catto et al., 2014 and references therein cited).

As a biodegradable and biocompatible natural polymer Silk Fibroin (SF) has the potential to become the biomaterial of choice for the development of a range of medical applications,

including small caliber blood vessel grafts (Altman et al., 2003; Thurber et al., 2015; Wang et al., 2017). The starting material can be easily purified and processed in different 2D/3D shapes. It is not immunogenic in humans (preliminary proteomic data revealed that several human proteins expressed by both epithelial and connective tissue cells exhibit homology sequences with SF Armato et al., 2011) and favors angiogenesis, an essential feature for tissue repair/regeneration (Dal Prà et al., 2005).

Manufacturing technologies of SF-based small caliber tubular grafts span from filament winding (Enomoto et al., 2010; Nakazawa et al., 2011), braiding (Ding et al., 2016; Zamani et al., 2017), and knitting (Yagi et al., 2011; Yamamoto et al., 2016), which are textile techniques making use of native microfiber yarns as starting material, to electrospinning (Wang et al., 2010; Liu et al., 2011; Xiang et al., 2011), and gel spinning (Lovett et al., 2008, 2010), which lead to various formats of regenerated SF tubular scaffolds. A recent research trend is to simulate in the scaffold the three-layered structure of the native blood vessel. Thus, designing multi-layered tubular scaffolds is seen as an effective way to mimic not only the native architecture but also to approach functional features of the artery. In particular, the aim is to create regionally selective environments in favor of the infiltration, adhesion, and spreading of cells conducive to the regeneration of neo-tissues with biological features and mechanical behaviors similar to the native ones.

The simplest technical approach to create at least an additional layer is to coat the textile tubular scaffold with a film-forming biocompatible polymer (SF or gelatin) (Fukayama et al., 2015; Yamamoto et al., 2016). The use of SF microfibers as scaffold material and of SF aqueous solution as coating showed advantages in terms of enhanced *in vivo* endothelialization, which corresponded to improved graft performance (e.g., medium-to-long term patency). Addition of crosslinking agents, like poly(ethylene glycol diglycidyl ether), to aqueous SF

enhanced stability, and protected the scaffold from rapid degradation when implanted *in vivo* (Yagi et al., 2011).

Building a 3D sponge-like layer on one or both sides of the tubular braided/knitted textile core may represent a step forward in approaching more complex scaffold architectures (Aytemiz et al., 2013; Liu et al., 2013, 2018; Ding et al., 2016; Zamani et al., 2017; Tanaka et al., 2018). The manufacturing techniques used by various authors, albeit with minor variations, share common steps: immersion of the tubular textile core in a mold, pouring a polymer solution, freeze-drying, and possible solvent consolidation of the just created layer. Crosslinking agents can be added to modulate porosity, strength, elasticity, and degradation rate; functional molecules, most often anti-thrombogenic agents, can also be loaded into the sponge. *In vivo* implantation up to 1 year in dogs (Aytemiz et al., 2013) and rabbits (Liu et al., 2018), and up to 3 months in rats (Tanaka et al., 2018) resulted in high patency rate, absence of thrombus, aneurysm, or infection, and a physiological level of endothelialization of the internal lumen of the graft with no signs of intimal hyperplasia.

The three-layered concept for the wall structure of the graft was approached by Enomoto et al. (2010), who fabricated a tubular scaffold by combining two kinds of native SF microfibers, i.e., a thin silk thread and cocoon filaments, which were successively arranged around a cylindrical core. The final consolidation step consisted in dipping the scaffold into a SF solution. The scaffold implanted into the abdominal aorta of male Sprague-Dawley rats showed very good patency at 1 year, organization of endothelial and medial layers, formation of *vasa-vasorum* in the adventitia, regenerating a vascular-like structure. These findings highlighted the importance of SF as a promising material to develop vascular grafts for smaller caliber blood vessels.

Wu et al. (2018) and McClure et al. (2012) engineered three-layered tubular scaffolds using only electrospinning as the manufacturing technology. Combinations of natural (SF, collagen, elastin) and biodegradable synthetic polymers [polycaprolactone, poly(L-lactide-co-caprolactone), and poly(lactide-co-glycolide)], alone or as blends, were used to build layers with finely tuned morphological and mechanical properties. The devices were fully characterized from the mechanical point of view, but the authors reported no *in vivo* functional tests. One of the devices was subcutaneously implanted for 10 weeks in rats (Wu et al., 2018) showing a propensity to promote cell infiltration from the outside environment into the interior of the graft.

Electrospinning has the ability to mimic the nanoscale properties of fibrous components (collagen and elastin fibrils) of the extracellular matrix and to realize a range of biochemical, topographical, and mechanical properties conducive to improved cell interactions (Babitha et al., 2017). Our previous studies focused on the development of small caliber vascular grafts made of electrospun SF (Marelli et al., 2009, 2010, 2012; Cattaneo et al., 2013; Catto et al., 2015). SF tubular matrices with inner diameter of about 5 mm had a pressurized burst strength of 576 ± 17 mmHg, higher than physiological and pathological pressure thresholds, but still lower than that of human arteries

($\sim 5,000$ mmHg for carotids). The compliance value of about 3.5 (radial deformation/mmHg 10^{-2}) was considered very interesting since it is higher than synthetic grafts (<2) and closer to the physiological values for saphenous (4.4) and umbilical vein (3.7), the gold standard for autologous replacement of small caliber arteries. *In vitro* studies (Marelli et al., 2009, 2010, 2012; Catto et al., 2015) showed good integration of cells with the SF matrix, while functional implants in the abdominal aorta of Lewis rats proved short term patency of the grafts (Cattaneo et al., 2013). The cellular intimal thickening showed a structure similar to the tunica of native arterial vessel, with elastin and intimal layers reminiscent of the native inner vascular structure. Small blood vessels with the morphology of *vasa-vasorum* were found in the thin layer of tissue grown on the outer surface of the graft. Taken together, all these results showed that small caliber SF vascular grafts produced by electrospinning may be promising matrices for vascular tissue replacement, without requiring cell seeding before implantation.

This study reports the chemical, morphological, physical, and mechanical properties of a novel multi-layered SF tubular scaffold (SilkGraft). The hybrid architecture was designed to optimize not only production and pre-surgery manipulation of the device, but also stitching at the site of implantation, biological integration with host's tissues, and biomechanical performance (compliance, resistance to radial stresses, biodegradation rate, etc.). A wide range of *in vitro* cell interaction studies with human adult fibroblasts, endothelial cells, and smooth muscle cells were performed to investigate the biological response to the device. The cytokine and chemokine expression patterns were investigated to evaluate the cells' proliferative and/or pro-inflammatory attitude. The SilkGraft interaction with blood components was studied by means of the complement cascade activation assay, the change of the leucocyte and erythrocyte counts, and the hemolysis assay. Additionally, the results of *in vivo* preliminary pilot tests on large animals aimed at evaluating the handling of the device during the surgical procedure and identifying the more apt animal model for next medium-to-long term preclinical trials will be presented and discussed.

MATERIALS AND METHODS

Fabrication of the Three-Layered Tubular Scaffold

The vascular graft is a hybrid three-layered tubular device comprising inner and outer electrospun layers (ES), and an intermediate textile layer (TEX). The TEX layer was manufactured by warp needle braiding technology using degummed SF yarn. The ES nanofibrous layers were produced via electrospinning using pupae-free silk cocoons as starting material. Cocoons were degummed in autoclave at 120°C for 30 min and extensively washed with warm water. Pure SF microfibers thus obtained were dissolved with an aqueous solution of 9.3 M lithium bromide at 60°C for 3 h. The salt was removed by dialysis and aqueous SF was cast in Petri dishes at 35°C in a ventilated oven until complete evaporation of water to produce SF films, which were then dissolved in Formic Acid

(8% w_{SF}/v_{FA}) to prepare the spinning dope. Electrospinning was performed as previously reported (Marelli et al., 2010) using the following experimental parameters: voltage 25 kV, flow rate 0.8 ml/h, spinneret-collector distance 15 mm. Coupling of TEX and ES layers was made during electrospinning, according to a patented process (Alessandrino, 2016), with the use of an ionic liquid (1-ethyl-3-methylimidazolium acetate, Sigma Aldrich) as welding agent. Hybrid ES-TEX-ES tubular devices were finally purified by extraction with ethanol under microwave heating at 50°C for 60 min to remove processing aids, immersed in distilled water overnight, dried, packaged under laminar flow cabinet, and sterilized with ethylene oxide (EtO). Henceforth, the final three-layered SF-based ES-TEX-ES vascular graft is identified by the name “SilkGraft.”

Materials and Scaffolds Characterization

Morphological and Geometrical Properties

Morphological analyses were performed with a scanning electron microscope (SEM; Zeiss EVO MA10) on Au/Pd sputter-coated samples (Desk IV, Denton Vacuum, LLC), at 10 kV acceleration voltage, 100 μ A beam current, and 15 mm working distance.

Geometrical properties of SilkGraft were characterized by determining the weight per unit length, the wall thickness, and the inner diameter. Wall thickness was measured according to the ISO 7198:2016 standard method. The tubular device was cut longitudinally, flattened and measured with a thickness tester MarCator 1075R (Mahr) equipped with a constant load thickness gauge of 1 cm² foot area that exerts a pressure of 1 kPa. Dry state inner diameter was determined from SEM images of tubular cross-sections mounted on stubs, using the SEM software measuring tools.

Amino Acid Analysis

The amino acid composition was performed after hydrolysis with HCl 6N, under vacuum, for 24 h. Free amino acids were quantitatively determined by Ion Exchange Chromatography using external standard calibration. Samples were analyzed in duplicate.

Attenuated Total Reflectance Fourier Transform Infrared Spectroscopy (ATR-FTIR)

ATR-FTIR spectra were made with an ALPHA FTIR spectrometer equipped with an ATR Platinum Diamond accessory, at a resolution of 4 cm⁻¹, in the infrared range of 4,000–400 cm⁻¹. Spectra were corrected with a linear baseline and normalized to the CH₂ bending peak at about 1,445 cm⁻¹. This peak was selected because it's not sensitive to SF molecular conformation.

Differential Scanning Calorimetry (DSC)

Thermal analyses were performed with a DSC 3500 Sirius (Netzsch). Samples (3–5 mg) were closed in Aluminum pans and subjected to a heating cycle from 50 to 400°C, at a heating rate of 10°C/min, under N₂ atmosphere (flow rate: 20 ml/min).

Circumferential Tensile Tests

Tests were performed according to ISO 7198:2016 using an All Electric Dynamic Test Instrument ElectroPuls E3000 (Instron),

equipped with a load cell of 250 N, a thermostatic bath (BioPuls), and appropriate grips fabricated *ad hoc*. Samples (length = 10 mm, $n = 3$) were cut carefully, mounted on the grips, conditioned in water at 37°C for 5 min, and tested while submerged at a crosshead speed of 50 mm/min. Due to the difficulty in determining the correct size of the resistant cross-sectional area, the results are expressed in terms of load and not of the usual stress values.

Pressurized Burst Strength

The test was carried out according to ISO 7198:2016. A balloon was placed inside the tubular graft (length = 100 mm; $n = 3$) and filled with test fluid at a measured rate of pressure change until the sample burst or test was discontinued. Before testing, samples were conditioned in the test fluid (distilled water) at 37°C for 20 min. No sample pre-stretching was applied, but axial displacement (axial elongation of the sample) was allowed. The test was performed with the sample submerged in the testing fluid. A gear pump provided a flow through the sample and pressure was measured just upstream the sample. The rise in pressure and the pressure at which sample burst or test was discontinued were measured and recorded.

In vitro Cellular Studies

Preparation of Substrates for in vitro Cell Cultures

SilkGraft samples were washed, transversally cut into 1.5 cm long pieces, and opened lengthwise in order to obtain small squares with an apparent surface area of about 300 mm². After autoclave sterilization (121°C for 30 min), they were aseptically transferred to 2.2 cm-diameter culture plates (Falcon-Becton Dickinson). Heat-sterilized stainless-steel rings were applied onto the upper surface of the pieces to keep them flat at the bottom of the plates.

Pre-culture Intravital Cell Staining

Cells were stained with fluorescent lipophilic membrane dyes (tracers) such as the red-orange fluorescent DiC₁₈(3) (1,1'-Diocadecyl-3,3,3',3'-tetramethyl-indocarbocyanine perchlorate; maximum fluorescence excitation 549 nm and emission 565 nm; Thermo Fisher Scientific, USA) or the green fluorescent DiOC₁₈(3) (3,3'-Diocadecyl oxacarbocyanine perchlorate; maximum fluorescence excitation 484 nm and emission 590 nm; Thermo Fisher Scientific, USA) dissolved in DMSO according to seller's instructions. At intervals of 3 days, cultured specimens were observed under an inverted fluorescence microscope (IM 35, Zeiss) equipped with proper excitation and emission filters according to the intravital stain used, and digitally photographed with a DP10 Camera (Olympus, Japan).

Cell Cultures

Adult Human Coronary Artery Endothelial Cells (HCAECs), Human Aortic Smooth Muscle Cells (HASMCs), and Human Aortic Adventitial Fibroblasts (HAAF) were provided by ScienCell Research Laboratories (Carlsbad, CA, USA). The supplier company guaranteed the cells characteristics we required via Cell Applications Inc. (San Diego, CA, USA).

For the adhesion studies, 2×10^4 human intravital pre-stained cells were separately seeded onto SilkGraft samples.

HCAECs were seeded onto the inner ES layer, whereas HASMCs or HAAFs were seeded onto the outer ES layer. In parallel, the three cell types were separately seeded on 2D polystyrene plates as controls. All the tests were performed in triplicate and repeated in three separate experiments. Cell cultures were kept in an incubator at 37°C in 95 vol% air plus 5 vol% CO₂. The growth media used were: HCAECs, ready to use Endothelial Cell Medium; HAAFs, Fibroblast Medium; HASMCs, Smooth Muscle Cell Medium (all from ScienCell Research Laboratories, USA). Every 3 days the growth media were changed with fresh ones and the cell-conditioned media collected and stored at -80°C to be subsequently analyzed. The cultures were kept going for at least 20 consecutive days.

Cells Counts

Cells counts on polystyrene plates were first performed using an inverted light microscope (IM35, Zeiss) (Armato et al., 1986). On the same samples, cell number was determined by means of the Cell Titer-Blue® Cell Viability Assay (Promega, USA) fluorescence assay based on the ability of living cells to convert a redox dye (resazurin) into a final fluorescent product (resorufin). Correlating microscopic findings with resorufin Promega assay data allowed to construct cell type-specific standard curves to be used to determine total cell numbers on SilkGrafts.

Assays of Cell Metabolites

Three metabolites (D-glucose, L-glutamine, lactate) were assayed in the cell-conditioned growth medium samples from each of the three types of cells separately cultured on SilkGraft or on polystyrene surfaces. The data corrected for actual cell numbers were expressed as means ± SE of the respective time-related cumulative curves.

Cell D-glucose consumption was assessed by means of a glucose oxidase assay using the Amplex® Red Glucose/Glucose Oxidase Assay Kit (Invitrogen-USA). L-glutamine uptake/consumption was determined using the L-glutamine assay kit developed by Megazyme (Ireland). The lactic acid release was assessed via the colorimetric enzymatic Lactate Assay Kit (Sigma Aldrich).

Assay of the Extracellular C-Telopeptide of Procollagen Type I

The extracellular release (and subsequent assembly of fibers) of type I collagen was assessed by evaluating the amount of the C-telopeptide, which is released into the cell-conditioned growth medium in stoichiometrically equal amounts from precursor procollagen type I molecules. The samples were assayed using the EIA kit developed by Takara Bio Inc. (Shiga, Japan). The sensitivity of this assay is 10 ng/ml.

Human Proinflammatory Cytokines and Chemokines Antibody Array

The secretion of various cytokines/chemokines into the growth medium was assessed by using the Human Inflammation Antibody Array, C-Series (RayBiotech-USA) in three distinct experiments. In detail, 1.0 ml medium sampled between day 18th and 20th, was used. After a treatment for 60 min with blocking

solution (Odyssey Blocking Buffer™ (LI-COR) with 0.05% Tween 20), the cytokines and chemokines antibody array membranes were incubated with the medium samples overnight at 4°C. Next, the membranes were washed and incubated at room temperature for 2 h with 1.0 ml of primary biotin-conjugated antibody diluted 1:250 in blocking solution. This was followed by an incubation at room temperature for 1 h with 2 ml of DyLight800-Labeled streptavidin (KPL, USA) diluted 1:7,500 in blocking solution. The immunofluorescent signals were acquired by means of an Odyssey Imager™ (LI-COR) scanner and quantified using the Image Studio™ software. The resulting intensity values from each array were normalized per 1,000 cells grown on either substrate. The array kit sensitivity is 4–25 pg/ml and the coefficient of variation of the intensity of the spots is 5–10%.

Hemocompatibility

The interaction between SilkGraft and blood components, i.e., the activation of the complement cascade and the alteration of the leucocyte count, the changes on erythrocyte count, and the presence of hemolysis, was studied according to the ISO 10993-4:2017 standard. As suggested by the regulation, the induction of thrombosis was assessed during the *in vivo* pilot trials. The tests reported below were performed in compliance with Good Laboratory Practices.

Activation of the Complement System

SilkGraft was incubated in human serum at 37 ± 1°C for 90 min with a surface/volume ratio of 3 cm²/ml. Zymosan A from *Saccharomyces cerevisiae* served as positive control, human serum alone as negative control and polypropylene material as negative reference material. Serum Complement Membrane Attack Complex (Sc5b-9) and Complement Component 3 (C3a) concentrations were determined with a commercial ELISA (MicroVue™ SC5b-9 Plus EIA and MicroVue™ C3a Plus EIA, Quidel Corporation).

Hemolysis

The blood was collected from three adult rabbits in test tube with anti-coagulant Sodium Citrate 3.2% (ratio 1+9 v/v Sodium Citrate/Blood). Equal quantities of blood from each rabbit were pooled and diluted with Mg- and Ca-free PBS to obtain a final hemoglobin concentration of 1,000 mg/dl.

For indirect contact assay, SilkGraft samples were dipped in Mg- and Ca-free PBS in order to reach a surface/volume ratio of 3 cm²/ml and incubated for 72 h at 50 ± 2°C. Seven milliliter of extract were added to 1 ml of diluted rabbit blood. For direct contact assay, SilkGraft samples were dipped in diluted rabbit blood and in Mg- and Ca-free PBS in order to reach a surface/volume ratio of 3 cm²/ml for SilkGraft/PBS and 0.14 ml/ml for diluted blood/PBS. Negative control (USP reference standard high-density polyethylene), positive control (water for injection) and blank (PBS) were tested.

All the samples (direct and indirect contact) were incubated in a water bath for 3 h at 37 ± 1°C and agitation was inverted twice every 30 min. After centrifugation at 800 G for 15 min, the concentration of hemoglobin in the supernatant was determined with the automatic chemistry analyzer Konelab 20 (DASIT).

Hematology

The effect of SilkGraft on red blood and white blood cells counts was evaluated after immersion in human whole blood in order to reach a surface/volume ratio of 3 cm²/ml and incubation for 15 min at 37 ± 1°C under dynamic conditions. An automatic counter Sysmex KX-21N (DASIT) was used. As control, the remaining part of the blood that did not come in contact with SilkGraft was used.

In vivo Animal Pilot Studies

Animal Care

Pilot animal experiments were performed at NAMSA (Lyon, France), an AAALAC internationally accredited firm. The study protocol was approved by the NAMSA Ethical Committee and the French Ministry of Education, Higher Education, and Research. The study conditions conformed to the guidelines of the European Union's Directive EU/2010/63 for animal experiments. One sheep (Blanche du Massif Central) and one minipig (Göttingen) were used. Animals were kept under controlled conditions. The animal housing room temperature and relative humidity were recorded daily. Staff involved was properly qualified and trained. Standard veterinary medical care was also provided.

Pharmacological Treatment

Starting 3 days prior to the operation, the animals received daily antiaggregant treatment (sheep: oral acetylsalicylic acid, Bayer; minipig: Clopidogrel, Sanofi) to prevent thrombosis. Twenty hours before surgery the animals were weighed and Enrofloxacin (5% Baytril®, Bayer) and/or Amoxicillin (Duphamox® LA, Zoetis) were administered. After anesthesia was induced, heparin (Heparin Choay®, Sanofi) was injected into the femoral artery via an introducer sheath and Activated Clotted Time (ACT) was evaluated using a Hemochron Junior 2 (International Technidyne Corp., USA) instrument. Analgesic, anti-inflammatory drugs and antibiotic treatments were administered during surgery and the follow up period. Animals were also maintained under prophylactic anticoagulant/antiaggregant therapy for the 4 weeks of observation until termination.

Surgical Grafting Procedure and Follow-Up

A 2.5 cm (minipig) or 8.0 cm (sheep) segment of the carotid artery was excised and replaced by end-to-end anastomosis with a piece of sterilized SilkGraft (nominal 5 mm inner diameter) of corresponding length. Surgery was unilateral in the minipig and bilateral in the sheep. Angiography and doppler ultrasound controls were performed before and after the grafting procedure and just prior to sacrifice using Iomeron 400 (Bracco Imaging, France) as contrast medium.

After surgery, the animals were transferred to a recovery area and monitored for 1 h prior to be brought back to their housing. The supply of water and food was reinstalled. Animals were monitored for 4 weeks and then euthanized.

Histopathology

At autopsy, the grafts, their connected carotid stumps, and surrounding tissues were excised, endoluminal blood was

removed from the carotids by gently flushing it out first with heparinized saline and then with 10% neutral buffered formalin (NBS). To complete fixation explanted samples were dipped into 10% NBS. The fixed tissues were dehydrated in ethanol solutions of increasing strength, cleared in xylene, and embedded in paraffin. Microtome sections (4–7 µm thick) were cut from each paraffin block for histopathological analysis. After removing the paraffin and rehydrating, the sections were stained with Safranin-Hematoxylin-Eosin (SHE). Histopathology analysis concerned graft endothelialization, intimal hyperplasia, thrombi, graft recellularization, potential occlusion and the presence and type of inflammatory cells.

Statistical Analysis

Data were expressed as mean values ± SE and their level of statistical significance assessed by means of one-way ANOVA followed by Holm-Sidak's *post hoc* test. A *P* < 0.05 was taken as significant.

RESULTS

Morphological, Chemical, Physical, and Mechanical Characterization

The SilkGraft device (**Figure 1A**) is a hybrid tubular structure consisting of two electrospun (ES) layers (inner and outer) and an intermediate textile (TEX) layer (**Figures 1B,C**). It is made of pure SF, present in the final device in form of native microfibers (TEX) with an average diameter of 12–14 µm (**Figure 1D**), and electrospun nanofibers (ES), whose diameter falls in the 400–600 nm range (**Figure 1E**) (Marelli et al., 2009).

To verify whether the processing steps, including the sterilization with EtO, altered the chemical structure and properties of the constituent biopolymer, the amino acid composition of the sterilized SilkGraft device, as well as that of two constituent materials, i.e., TEX microfibers, and ES nanofibers, was determined and compared to that of native SF microfibers. The results demonstrated that there were no differences in the amino acid composition, indicating that neither processing conditions nor sterilization with EtO (Zhao et al., 2011) altered the intrinsic properties of SF materials (**Table S1**).

Structural properties of SilkGraft were characterized by ATR-FTIR. The spectra of TEX microfibers and ES nanofibers (**Figure 1F**) display the typical profile of β-sheet crystalline materials (Marelli et al., 2010; Chiarini et al., 2016), as indicated by the position, shape, and intensity of the Amide bands (Amide I at 1,620 cm⁻¹, with shoulder at 1,691 cm⁻¹; Amide II at 1,512 cm⁻¹; Amide III at 1,227 cm⁻¹, and 1,262 cm⁻¹). The crystallinity index of ES nanofibers, expressed as intensity ratio between the two Amide III components at 1,227 and 1,262 cm⁻¹ (CI = I₁₂₂₇/I₁₂₆₂), was 0.58 ± 0.03, close to that determined on native SF microfibers (CI ≈ 0.60) (Chiarini et al., 2016), thus confirming the completion of the conformational transition from a prevalently random coil structure of as-spun nanofibers to a fully crystallized SF material.

Thermal properties of SilkGraft were investigated by DSC analysis. Thermograms of TEX microfibers, ES nanofibers, and final tubular device are shown in **Figure 1G**. TEX

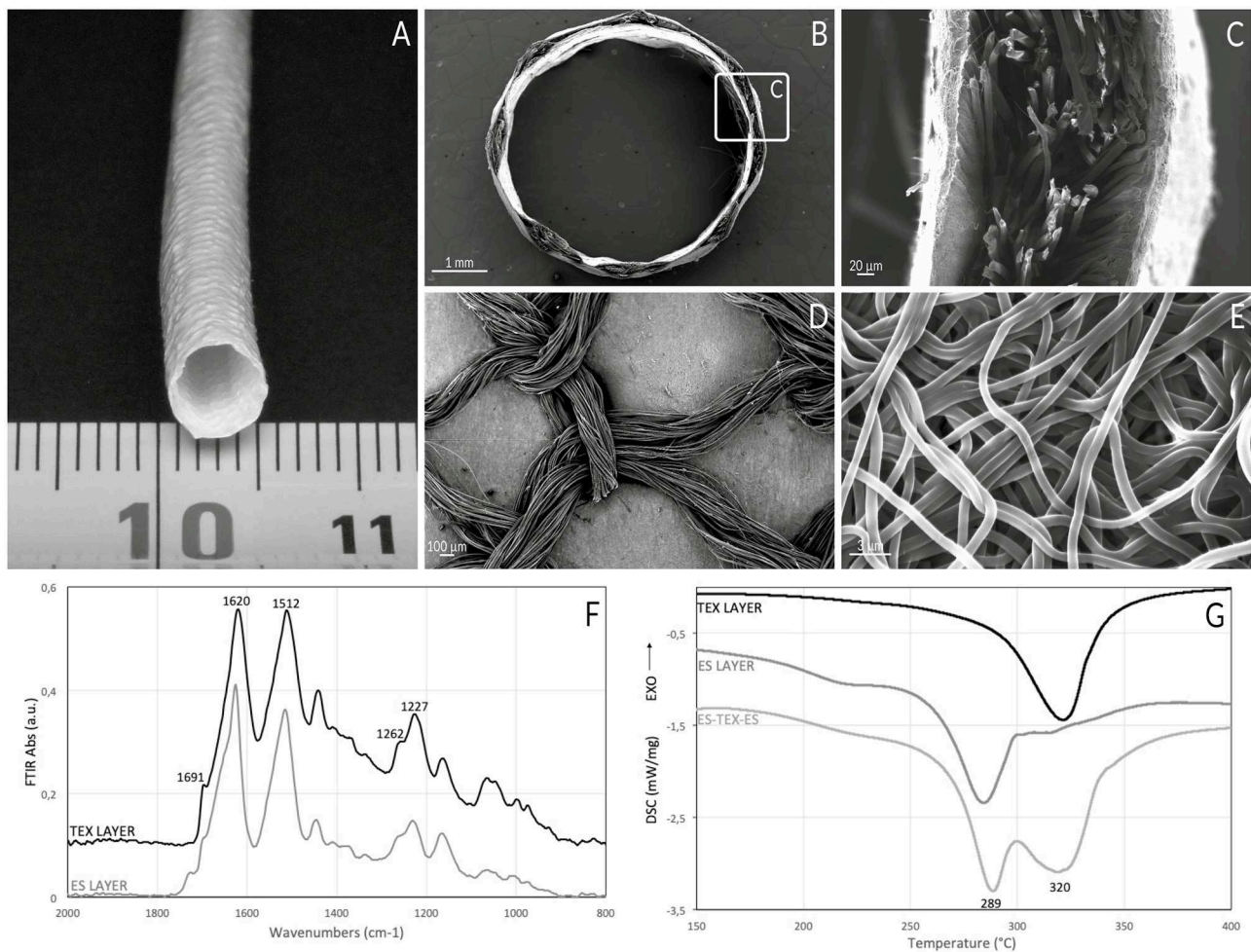


FIGURE 1 | Morphological and physico-chemical structure of SilkGraft. **(A)** Picture of a SilkGraft device with 5 mm nominal inner diameter (ruler in mm). **(B)** SEM cross-section of the graft showing the two inner and outer ES layers that enclose the intermediate TEX layer (scale bar, 1 mm). **(C)** Detail of **(B)** showing a magnification of the wall structure (scale bar 20 μm). **(D)** TEX layer coupled to an ES layer, visible in the background. The texture of the braided mesh is characterized by the presence of voids (scale bar 100 μm). **(E)** SEM detail of SF nanofibers of the ES layer (scale bar, 3 μm). **(F)** ATR-FTIR spectra of TEX and ES layers in the 2,000–800 cm^{-1} range. **(G)** DSC thermograms of TEX layer, ES layer, and SilkGraft finished device (marked ES-TEX-ES) in the 150–400°C temperature range.

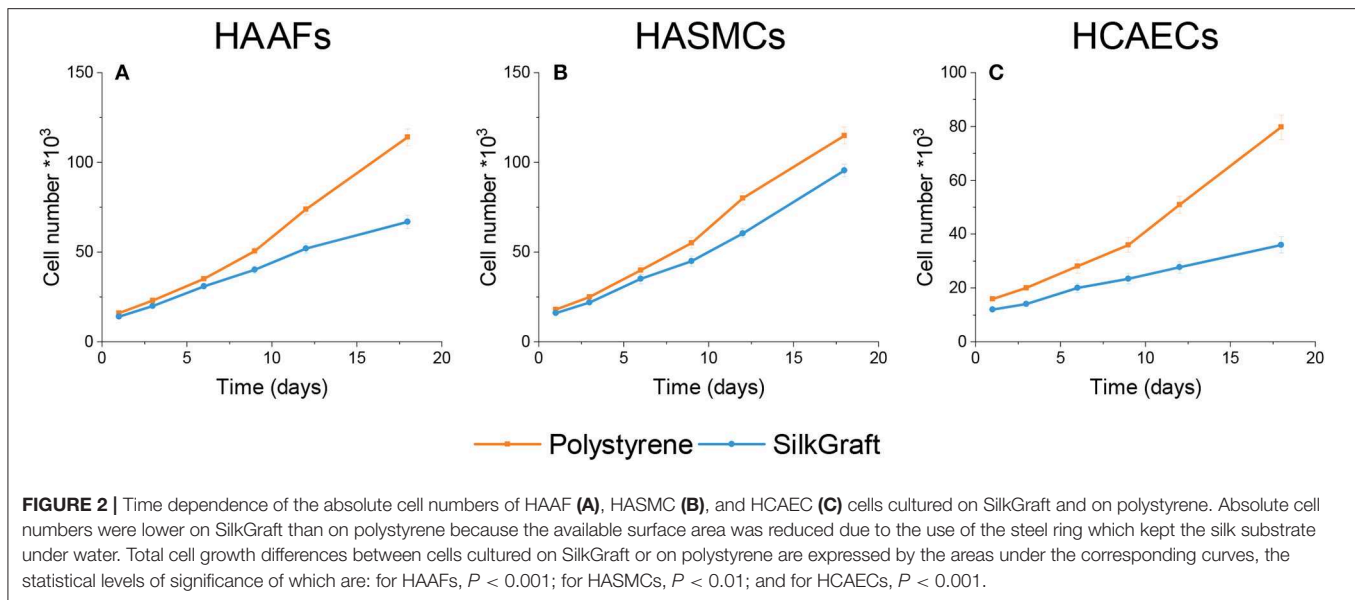
TABLE 1 | Geometrical and mechanical properties of SilkGraft (nominal $\varnothing_{\text{inner}} = 5 \text{ mm}$).

Wall thickness (mm)	Unit weight (mg cm^{-1})	Weight (%)		Circumferential tensile tests		Burst pressure (mmHg)
		ES layers	TEX layer	Breaking Load (N)	Strain at break (mm/mm)	
0.59 ± 0.03	11.9 ± 0.5	61 ± 2	39 ± 2	29.5 ± 1.0	1.60 ± 0.05	$2,308 \pm 88$

microfibers displayed a high thermal stability, with a main endothermic transition peaking at about 320°C, attributed to melting/degradation of highly crystalline and oriented SF microfibers (Chiarini et al., 2016). ES nanofibers, as many other regenerated SF materials, showed a marked low-temperature shift of the same transition, with a peak at about 289°C (Marelli et al., 2010). The DSC profile of the SilkGraft device was the sum of the individual components, with two discrete peaks corresponding to the thermal transitions of ES and TEX layers.

The enthalpy associated with the thermal degradation of TEX ($\Delta H = -402 \pm 41 \text{ J/g}$) and ES ($\Delta H = -307 \pm 32 \text{ J/g}$) was used to estimate the weight contribution of each component in the final device. ES nanofibers account for about 60% by weight, while the remaining 40% is represented by the TEX layer (Table 1).

Geometrical parameters and mechanical properties of SilkGraft with a nominal inner diameter of 5 mm are listed in Table 1. The weight per unit length of the device is very low, about 5 times lower than that of a commercial ePTFE vascular



graft with similar inner diameter and wall thickness. While the ePTFE graft has a full thickness wall, the middle TEX layer of SilkGraft shows the typical structure of a braided mesh, with many voids that contribute to make the structure lighter (Figure 1D). The values of breaking load, which are about 30 times higher than those of similar grafts made only of electrospun SF nanofibers (Marelli et al., 2010), confirm that the TEX layer is the load bearing component of the graft. The contribution of the ES layers, which are solidly attached to the TEX layer through numerous welding points, is negligible. The results of burst pressure further confirm the significant contribution of the TEX layer to the mechanical performance of the multi-layered graft. The value of 2,308 mmHg is significantly larger than that of electrospun SF tubes with the same diameter (Marelli et al., 2010) and of the same order of magnitude of the values reported for internal mammary artery ($3,196 \pm 1,264$ mmHg) and saphenous vein ($1,599 \pm 877$ mmHg) (Konig et al., 2009).

In vitro Biocompatibility Studies

The biocompatibility of SilkGraft was tested using the three most representative cell types of human peripheral arteries, namely endothelial cells (HCAECs), smooth muscle cells (HASMCs), and adventitial fibroblasts (HAAFs). To assure the full significance and relevance of the results, we chose and applied a stringent set of selective criteria. To be eligible, the human cells had to originate from disease-free human subjects, to be of recent isolation (i.e., within the second passage *in vitro*), to be free from contaminating cells of other types, to be diploid and unprocessed, to be free from viral infections (particularly HIV-1, HHVB, HHVC), and to express cell type-specific markers.

Cell Adhesion, Survival and Proliferation Studies

DiIC₁₈(3) or DiOC₁₈(3) intravitaly stained cells were carefully seeded on the internal (HCAECs) or external (HASMCs or HAAFs) surfaces of SilkGraft and, in parallel, onto polystyrene.

Next, the fluorescent cells were observed daily under an inverted microscope for up to 3 weeks of staying *in vitro*. Examples of the three types of cells grown on SilkGraft and on polystyrene substrates are shown in Figure S1. An adhesion fraction of $61 \pm 5\%$ for each cell type was detected 3 h after seeding, which was 2.1-fold ($P < 0.001$) the fraction of the same cells adhering to polystyrene surfaces at the same time point. Morphological indicators of apoptosis (e.g., cells with a shrunk or blebbing cytoplasm and substrate-adhering or free-floating spherical apoptotic bodies) were very rarely observed. Alike data were reported previously in the case of human dermal fibroblasts isolated from adult subjects and grown on SF-covered poly(carbonate)-urethane vs. polystyrene (Chiarini et al., 2003). Our present findings show that with respect to a polystyrene surface, SilkGraft neatly favors the adhesion of isolated human cells. As is well-known, adhesion to a substrate favors the survival and growth of untransformed (normal) cells.

The absolute numbers of each cell type grown on either substrate are shown and compared in Figure 2. Throughout 20 days HAAFs seeded onto SilkGraft increased their number by 4-fold, HCAECs by 3-fold, and HASMCs by 6.5-fold ($P < 0.001$ vs. 0 time in all instances). On polystyrene, the increases in numbers of the same cell types were greater, i.e., 7.5-fold for HAAFs, 5-fold for HCAECs, and nearly 7-fold for HASMCs ($P < 0.001$ vs. 0 time in all instances). However, if data are normalized to the apparent surface area available for growth (lower on SilkGraft due to the steel ring applied onto its surface), after 20 days HAAFs and HASMCs reached significantly ($P < 0.001$) greater cell densities on SilkGraft than on polystyrene, whereas HCAECs densities were similar between the two substrates ($P > 0.05$) (Table 2).

Evaluation of Cell Metabolism

The results concerning the studies on glucose and glutamine consumption, and the extracellular release of lactate were

normalized per 1,000 cells and are reported in **Figure 3** and **Table 3**. Cumulative HAAFs consumption of glucose on SilkGraft was greater than on polystyrene, the difference being much

TABLE 2 | Living cells density/mm² of apparent surface area after 21 days of *in vitro* culture.

Cell type	Polystyrene (PS) plate	SilkGraft (SF)	Ratio SF/PS
HAAFs	363 ± 31	692 ± 63*	1.9 ± 0.1*
HASMCs	366 ± 28	1222 ± 106*	3.3 ± 0.2*
HCAECs	254 ± 23	232 ± 19 ^{ns}	0.91 ± 0.1 ^{ns}

Data are normalized to the apparent surface area available for growth. Levels of statistical significance of the differences between the values on SilkGraft and on polystyrene: * $P < 0.001$; ns, $P > 0.05$.

more remarkable during the first 12 days of culture *in vitro* (**Figure 3A**). Conversely, the cumulative HAAFs consumption of glutamine on polystyrene was greater than on SilkGraft (**Figure 3D**), the difference becoming remarkable only after the first 12 days. On the other hand, the release of lactate into the medium was the same whichever the substrate considered (**Figure 3G**).

HASMCs cumulative consumption of glucose (**Figure 3B**) and glutamine (**Figure 3E**) and the release of lactic acid into the medium (**Figure 3H**) were not significantly affected by their attachment to either substrate.

Glutamine oxidation is the main source of energy for HCAECs. On SilkGraft the cumulative consumption of glutamine was typically much higher than on polystyrene (**Figure 3F**). The cumulative consumption of glucose was

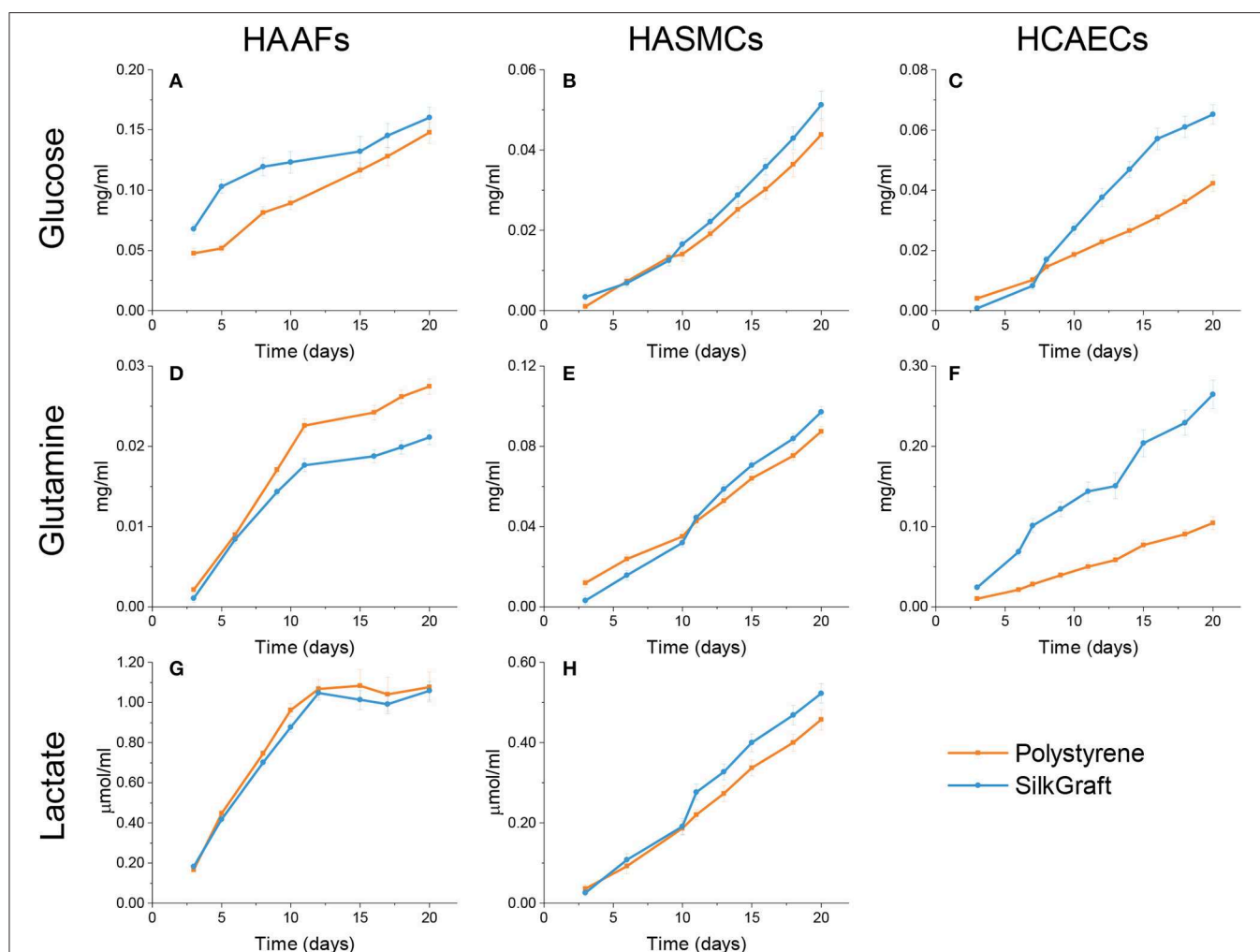


FIGURE 3 | Cumulative consumption of glucose and glutamine and release of lactate. Results were normalized per 10³ cells. (A–C) The cumulative glucose consumption was higher for HAAFs ($P < 0.05$) and HCAECs ($P < 0.001$) seeded on SilkGraft, whereas it showed only marginal differences between the two substrates for HASMCs ($P > 0.05$). (D–F) Glutamine consumption was lower for HAAFs ($P < 0.05$) seeded on SilkGraft, similar for HASMCs ($P > 0.05$) cultured on the two substrates, and significantly larger for HCAECs ($P < 0.001$) grown on the silk substrate. (G,H) The cumulative amount of lactate released by HAAFs and HASMCs was the same whichever the substrate ($P > 0.05$). Lactate release could not be assessed for HCAECs because the released lactate was re-uptaken and used for metabolic purposes. The statistical analysis of these data is shown in **Table 3**.

TABLE 3 | Comparison of metabolic parameters* of the different cell types cultured on SilkGraft and polystyrene.

	Polystyrene	SilkGraft	$\Delta\%$	P
HAAFs				
Glucose uptake	1.642 \pm 0.098	2.122 \pm 0.150	+29.2	0.021
Glutamine uptake	0.316 \pm 0.013	0.251 \pm 0.012	-20.6	0.003
Lactate release	14.664 \pm 0.783	13.947 \pm 0.545	-4.9	0.465
Procollagen C-Telopeptide	1.500 \pm 0.078	0.993 \pm 0.072	-33.8	<0.001
HCAECs				
Glucose uptake	0.368 \pm 0.026	0.572 \pm 0.039	+55.4	<0.001
Glutamine uptake	0.919 \pm 0.083	2.504 \pm 0.198	+172.4	<0.001
HASMCs				
Glucose uptake	0.336 \pm 0.030	0.385 \pm 0.032	+14.6	0.276
Glutamine uptake	0.794 \pm 0.042	0.807 \pm 0.041	+1.6	0.827
Lactate release	4.016 \pm 0.311	4.652 \pm 0.328	+15.8	0.181

*The parameters are the areas under the respective cumulative curves shown in Figures 3, 4.

also greater than on polystyrene (Figure 3C). Undetectable levels of lactate were released into the medium by HCAECs, whichever the substrate considered, due to the known fact that endothelial cells can uptake and use lactate as an additional source of energy (Krützfeldt et al., 1990; Vegran et al., 2011).

Synthesis of Type I Collagen by HAAFs

Type I procollagen synthesis is a specific biomarker of HAAFs (Dal Prà et al., 2006). The release of the C-telopeptide of the procollagen is a stoichiometric index of the amount of collagen type I secreted, which subsequently undergoes fiber assembly. Thus, when HAAFs were grown on SilkGraft their cumulative release of C-telopeptide significantly decreased vs. that on polystyrene (Figure 4). A quantitative comparison of type I collagen synthesis on the two substrates is listed in Table 3.

Cytokine and Chemokine Expression

After 20 days of staying *in vitro*, each cell type exhibited its own specific pattern of secreted cytokines and chemokines (Figure 5). No substantial qualitative differences emerged when comparing the expression patterns of each cell type in relation to the culture substrate. However, substrate-related significant differences in the quantitative secretion of some cytokines and chemokines could be detected.

HAAFs seeded on SilkGraft exhibited a higher secretion of IL-6 (+22%), MCP-1 (+13%), and TIMP-2 (+19%), whereas IP-10 (-26%), MCP-2 (-50%), Eotaxin-1 (-41%), and RANTES (-72%) were released at lesser extent than on polystyrene.

HCAECs grown on SilkGraft released higher amounts of IP-10 (+43%), MCP-1 (+27%), and TNF- β (+84%) as compared to polystyrene. RANTES and IL-6 were released to a lesser extent, while TIMP-2 and MIP-1 β did not change significantly between the two substrates.

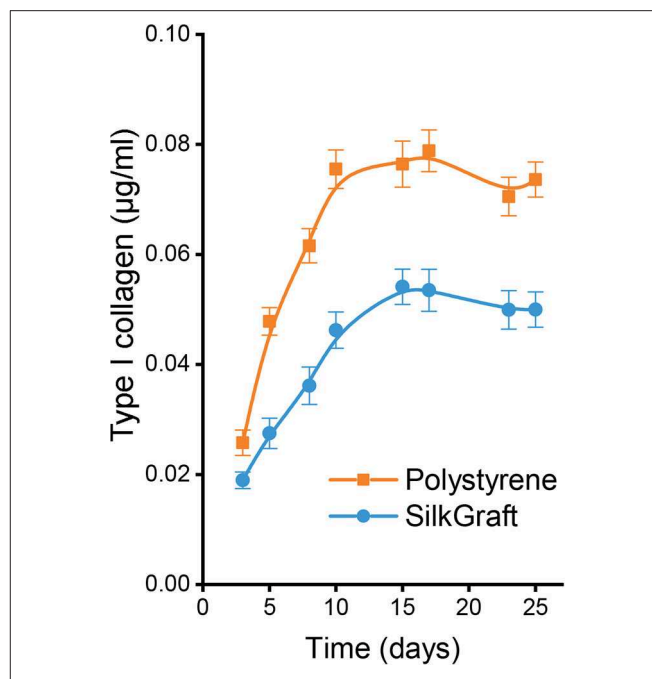


FIGURE 4 | The cumulative assembly of collagen type I (indirectly measured as the stoichiometrically released C-telopeptide of procollagen) was significantly ($P < 0.001$) lower for HAAFs cultured on SilkGraft than on polystyrene surfaces. Results were normalized per 10^3 cells. The statistical analysis of these data is shown in Table 3.

Finally, HASMCs discretely secreted a wider set of cytokines/chemokines. Interestingly, GM-CSF (+766%), MCP-2 (+557%), IL-1 α (+561%), IL-1 β (+390%), and Eotaxin-1 (+315%) were secreted at much higher levels on SilkGraft than on polystyrene, the secretion of ICAM-1 and RANTES only raised by +30%, whereas the release of IL-6, MIP-1 β , TIMP-2, MCP-1, and IP-10 fell by -10/30% vs. the corresponding levels on polystyrene.

Hemocompatibility

Regarding the complement activation, a statistically significant increase ($p < 0.05$) in Sc5b-9 was noted (Table S2). However, the Sc5b-9 values of SilkGraft were still inside the range of the control data of a normal standard population (334–1,672 ng/ml). Based on this, the increase was regarded as not biologically relevant. The C3a concentration was comparable to that of the negative control (Table S2). In conclusion, it can be stated that SilkGraft did not induce a biologically relevant activation of the complement system. Both indirect and direct contact hemolysis assays showed that SilkGraft exerted no hemolytic activity (hemolytic indexes < 2%) (Table S3). SilkGraft did not cause any alteration of red and white blood cells counts because the difference with the respective controls was <4 and <7%, respectively (Table S4).

Pilot Animal Studies

The purposes of the pilot studies were first to assess which animal model would be better to use for future medium-to-long term trials, and then to establish the suitability of the surgical

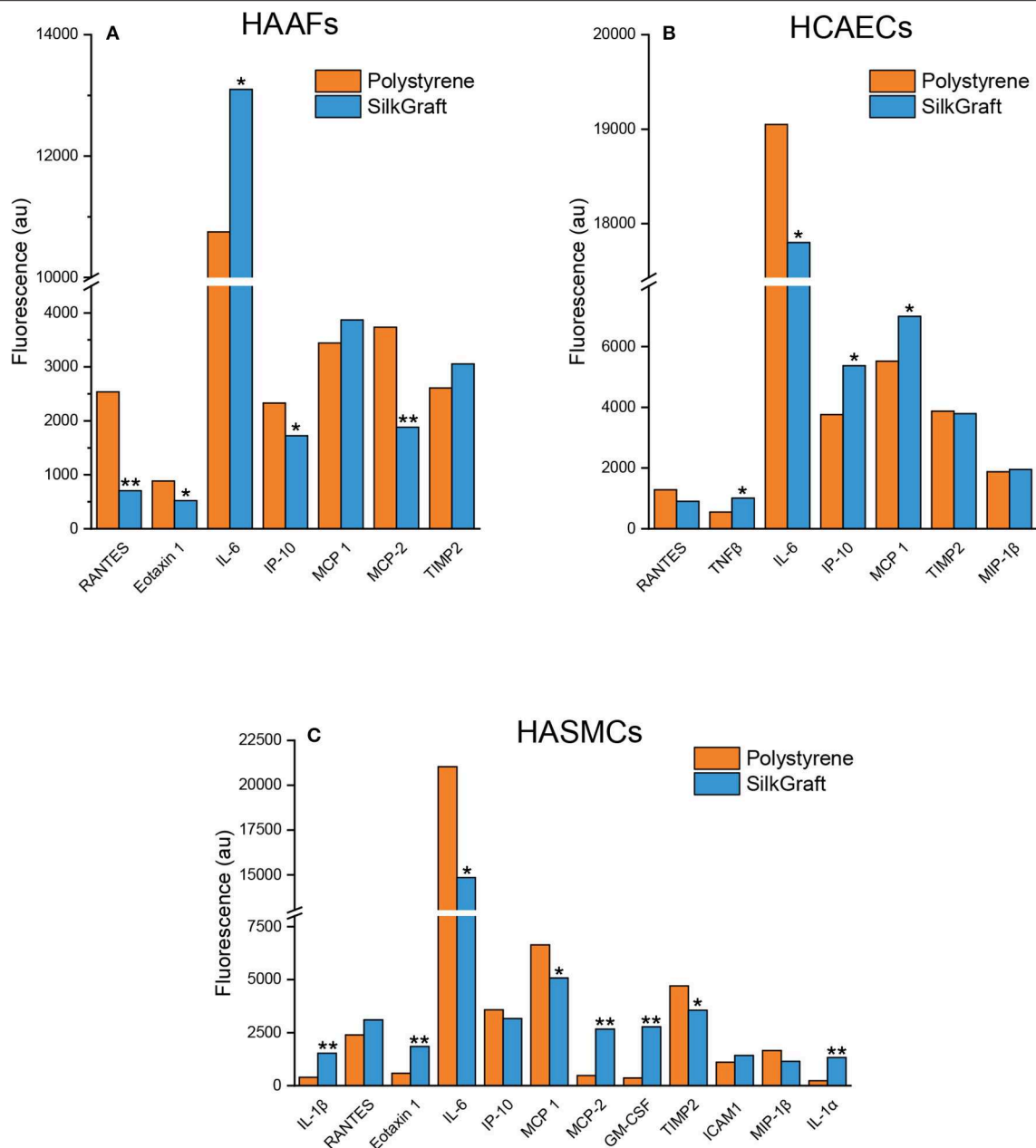


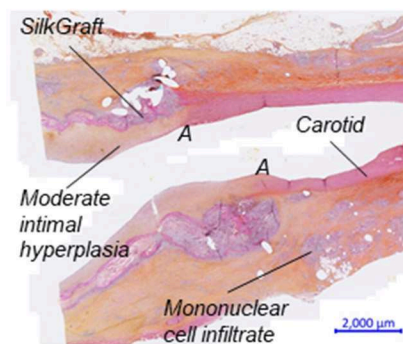
FIGURE 5 | Relevant cytokines and chemokines secreted by each cell type cultured between 18 and 20 days on SilkGraft and polystyrene: HAAFs (A), HCAECs (B), and HASMCs (C). Results of immunofluorescence intensities were normalized to 10^3 cells. IL-6: Interleukin-6; MCP-1: Monocyte chemoattractant protein-1; TIMP-2: Tissue inhibitor of metal proteinases-2; IP-10: Interferon gamma-induced protein-10; MCP-2: Monocyte chemoattractant protein-2; Eotaxin-1; RANTES: Regulated on activation normal T cell expressed and secreted; MIP-1β: Macrophage inflammatory protein-1β; TNF-β: Tumor necrosis factor-β; GM-CSF: Granulocyte-macrophage colony stimulating factor; IL-1α: Interleukin-1α; IL-1β: Interleukin-1β; ICAM-1: Intercellular adhesion molecule-1. The bars are the mean values of three independent experiments corrected for cell numbers. * $P < 0.01$; ** $P < 0.001$. SEMs, not shown, ranged between 5 and 10% of corresponding mean values.

model, to evaluate handling characteristics, aptness to stitching, patency, formation of thrombi, first signs of degradation, local tissue effects, and the general performance of SilkGraft. Resected portions of the carotid arteries of one minipig (unilateral) and one sheep (bilateral) were replaced with SilkGraft, the animals were sacrificed 4 weeks later, and histopathology of explants was examined.

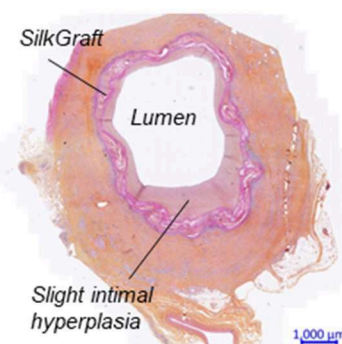
Surgery was done without major difficulty on both minipig and sheep. SilkGraft preparation, handling, stitching suitability, and anastomosis capacity were overall considered as good. Moderate bleeding at the suture holes was observed. The animals survived for 4 weeks with no unwanted side effects prior to be euthanized. No graft-related clinical or macroscopic abnormalities were noted at the site of implantation or

MINIPIG

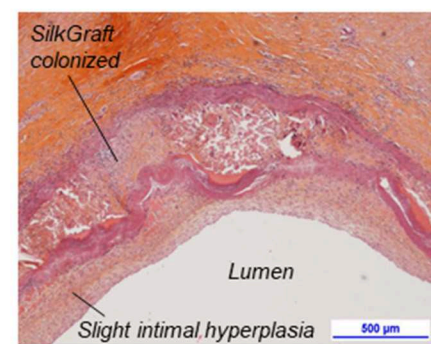
A Proximal anastomosis



B Central section

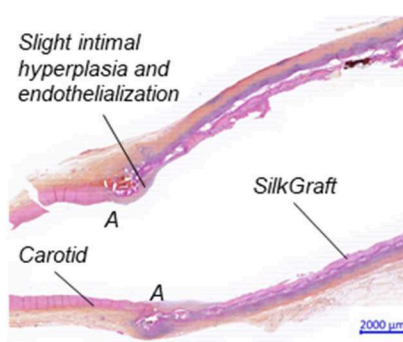


C Central section

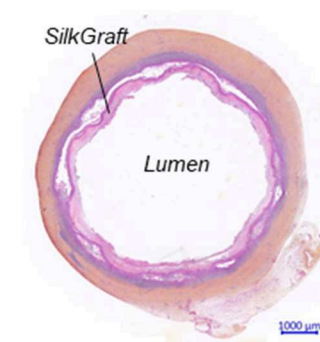


SHEEP

D Proximal anastomosis



E Central section



F Central section

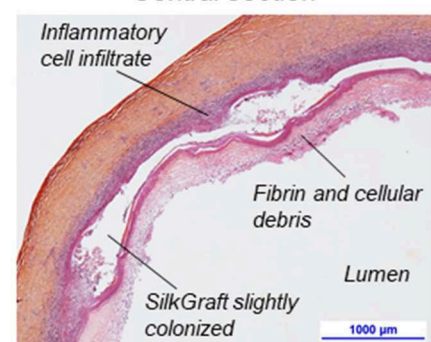


FIGURE 6 | Histopathological analysis of a SilkGraft stitched end-to-end on the carotid artery of minipig and sheep 4 weeks after grafting. Staining: Safranin-Hematoxylin-Eosin. Minipig: **(A)** Longitudinal cut in correspondence of the proximal anastomosis showing a pervious lumen (A, anastomotic line). **(B)** Representative cross-sectional cut of the central part of the graft. The lumen is pervious, though moderately reduced by an intimal hyperplasia. **(C)** Detail of the graft wall: perivascular cell infiltrates are visible; the inner and outer ES layers appear compact, whereas the TEX layer is penetrated by growing vessels and collagen-producing fibroblasts; endothelialization is visible at the inner graft surface. Sheep: **(D)** Typical longitudinal sections of the proximal end-to-end anastomotic sites (A, anastomotic line); the lumen is pervious and devoid of any stenosis. Endothelialization is restricted to a 3 mm-wide area beyond the anastomotic sites. **(E)** Representative cross-section of the central part of the graft; the lumen is pervious while endothelialization, neointimal hyperplasia, and stenosis are absent. **(F)** Detail of the graft wall: an inflammatory infiltrate envelops the graft; a newly-formed vascularized connective tissue only partly colonizes the middle TEX layer.

in distant organs during the test period. Ultrasound and angiographic examination at day 13 and 24 after surgery showed patent carotids, no aneurysm, dilation, dissection, blood collection or signs of infection. No stenosis was identified for the sheep, whereas a slight stenosis near the proximal anastomosis was identified for the minipig. Normal blood flow was also noted at termination. The external surface of the grafts explanted from the sheep was covered by a moderate amount of thin and soft tissue, while that recovered from the minipig was surrounded by a thicker layer of soft tissue.

The histopathological analysis of the minipig explant showed that inside the graft and its attached carotid stumps the lumen was still pervious and totally devoid of thrombi (**Figure 6A**). Histopathology also confirmed the presence of a slight yet diffuse stenosis of the graft's lumen (**Figure 6B**). Endothelial-like cells lined the whole surface of the newly-formed graft's

intima (**Figure 6C**). Collagen fibers, fibroblasts, macrophages, and multinucleated giant cells together with a lesser number of lymphocytes, plasma cells, and neutrophils filled the voids of the middle TEX layer. Colonizing cells circumferentially infiltrated the graft's outer nanofibrous ES layer. Moreover, the abundant periarterial tissue was infiltrated by lymphocytes and plasma cells. Altogether, these features suggested an ongoing foreign body response (FBR), as reported for other SF-based scaffolds (Dal Prà et al., 2005; Chiarini et al., 2016).

Grafted sheep carotids were pervious to blood flow and did not show any luminal stenosis (**Figures 6D,E**). Endothelialization was restricted to a 3 mm-wide area beyond the end-to-end anastomotic sites. Only a thin fibrin layer and margined leukocytes adhered to the remaining inner nanofibrous surfaces of the grafts. Also, differently from the minipig, in the long portion of the graft intervening between the anastomotic sites no newly-formed neointimal connective

tissue was present. The middle TEX layer was only partially colonized by newly-formed vascularized connective tissue (**Figure 6F**). A thick infiltrate made up by lymphocytes, mononuclear macrophages, polynucleated giant cells, and neutrophils enveloped the graft's external nanofibrous layer, being less crowded around the proximal and distal arterial stumps. This picture indicated an ongoing FBR, but with no concurring subendothelial hyperplasia and no damage to neighboring tissues.

DISCUSSION

Electrospun scaffolds may suffer from some limitations when biomimicry must be coupled with a high level of mechanical performance, such as in the case of vascular grafts. An affordable solution is therefore to couple electrospinning and textile technologies (like weaving, knitting, braiding, etc.), with the aim to take advantage of both of them for realizing biomimetic scaffolds able to withstand mechanical stresses in tensile, compression, and bending modes. Zhang et al. (2017) reported the fabrication of a three-layered vascular graft where the intima and media layers were obtained by sequentially electrospinning SF and poly(L-lactide-co- ϵ -caprolactone), while the outer adventitia-like layer was built up by braiding SF yarns. In another study (Mi et al., 2015), a polyurethane (PU)/SF three-layered small diameter tubular scaffold was fabricated by combining electrospinning (inner PU layer) and braiding (middle SF layer) technologies. In addition, a spongy PU layer was built as third outer layer by molding and freeze drying. Both scaffolds underwent extensive mechanical and *in vitro* cytocompatibility characterization, but no *in vivo* functional tests were reported.

Coupling electrospun and textile SF matrices for the production of multi-layered tubular scaffolds is recognized as a valid approach to overcome bottlenecks due to lack of mechanical attributes of the electrospun SF scaffolds. However, the achievement of a strong adhesion between electrospun and textile layers might be a challenge, because textile surfaces onto which electrospun fibers are deposited are not homogeneously flat, but present microscopic rough or sunken sites that prevent a continuous contact between the two surfaces. This results in poor adhesion strength, as demonstrated by the fact that the electrospun layer can be easily peeled off by applying a mild strength. Risks associated with poor adhesion between electrospun and textile layers may have very serious consequences on the performance of an implantable device, such as creation of morphological and mechanical discontinuities between layers, yielding and/or collapse of weaker layers, loss of geometric characteristics, thus leading to ultimate failure, especially under the stressing working conditions experienced *in vivo*.

To overcome these problems, we have developed an advanced manufacturing technology aimed at achieving an effective hybridization between electrospun and textile matrices (Alessandrino, 2016). Coating of the TEX surface with the ionic liquid before electrospinning ensures perfect welding between

the electrospun and textile matrices. In fact, as soon as the first electrospun fibers reach the TEX surface, the still plastic fibers melt in contact with the ionic liquid. A dense network of strong welding points between the growing electrospun layer and the textile substrate is created. Adhesion tests showed that a force of 0.5–1 N is needed to peel off one layer from the other (Alessandrino, 2016). Therefore, the multi-layered wall of the tubular scaffold behaves as if it were made of a single piece, while harmonizing the high resistance to mechanical stresses of native SF microfibers with the enhanced biomimicking attitude of regenerated SF nanofibers. The load bearing component is the TEX layer, which confers a high mechanical resistance on the device. When stressed under wet conditions the inner and outer ES layers become very elastic. Under increasing load, they undergo extensive stretching deformation without fracturing or breaking. Interestingly, ES and TEX layers remain strongly attached to each other until the ultimate breaking point is reached, thus confirming the effectiveness of the patented coupling technology, which allows the formation of a dense network of welding points between the ES layers and the meshes of the TEX layer.

The production technology allows the fabrication of SilkGraft in a wide range of inner diameters, overlapping those of currently marketed small caliber synthetic vascular grafts. Compared to available ePTFE and PET vascular devices, SilkGraft is characterized by a design which results in a light but mechanically resistant structure. The light weight is likely to bring biological advantages because the burden of foreign material at the site of implantation is significantly reduced, thus avoiding excessive stresses to surrounding tissues during remodeling. This feature doesn't seem to negatively impact on the mechanical performance, as demonstrated by the values of circumferential breaking load and burst strength. In fact, if the breaking load reported in **Table 1** is normalized to the cross-section surface, a stress value of about 3 MPa is obtained, which underestimates the real value due to the open texture of the wall of the device (see: **Figure 1D**). The stress value is significantly larger than that reported for the human descending mid-thoracic aorta with roughly similar inner diameter (1.72 ± 0.89 MPa) (Mohan and Melvin, 1982). Interestingly, the value of strain falls in the same range of that reported for human aorta (1.53 ± 0.28) (Mohan and Melvin, 1982).

The manufacturing protocol of SilkGraft includes various washing treatments with hydro-alcoholic solutions, which are aimed not only at achieving the complete removal of processing aids, but also at consolidating as-spun SF nanofibers that are still prevalently amorphous and more sensitive to physical, (bio)chemical, and mechanical stresses. The IR crystallinity index confirmed that nanofibers in the final device are fully crystallized. Actually, this structural feature is very important for the functionality of the device because, according to unanimous consensus, the degree of crystallinity of regenerated SF scaffolds strongly impacts on the rate of *in vivo* biodegradation (Thurber et al., 2015). In our case, the nanofibers are expected to undergo remodeling in the medium term, while in the meantime supporting neo-vascular tissue formation. To this purpose, fully

crystalline ES nanofibers are more favorable to ensure a slow degradation rate in the biological environment.

The results of the *in vitro* studies on SilkGraft showed a high biocompatibility of the device, which was evaluated by seeding the three main types of cells inhabiting the arterial wall (HCAECs, HASMCs, and HAAFs). Cell adhesion to SilkGraft was in all instance superior to polystyrene, in keeping with previous observations (Chiarini et al., 2003; Dal Prà et al., 2006). The preferential energy source for both HASMCs and HCAECs was glutamine, while it was glucose for HAAFs (Wu et al., 2000; Eelen et al., 2013). HAAFs and HASMCs also secreted large amounts of lactic acid into the medium, whereas HCAECs released none. This occurred because HCAECs have the metabolic capability to convert lactate into pyruvate and to use it for oxidative metabolism, thus saving glucose which they cede to the surrounding tissues (Dal Prà et al., 2005; Chiarini et al., 2016). It should be noted that the cumulative curves of consumed glucose and glutamine and of released lactate proper of HAAFs and HASMCs exhibited similar patterns, matching the metabolic activities and the expansion of the respective cell populations.

Notably, addition of serum suppresses the contact inhibition of growth in HASMCs (Krützfeldt et al., 1990; Viñals and Pouyssegur, 1999). This may explain why they reached the highest density when seeded on SilkGraft, which did not happen for HCAECs. Moreover, the observed behavioral differences could be due to unlike cell sizes (endothelial cells > fibroblasts > smooth muscle cells), morphological features, and regulatory mechanisms intrinsic to each cell type. In addition, the different characteristics of SilkGraft and polystyrene surfaces, including the adhesiveness for cells and the somewhat broader surface area offered by the nanofibers, also had an impact. Having larger sizes, the HCAECs seeded on the inner nanofibrous surface reached the confluence and the contact inhibition of growth at an earlier time and more permanently than the other two cell types. This could be beneficial because *in vivo* HCAECs, once they had reached confluence on the surface of the graft, would stop proliferating and thus keep the lumen pervious to the flowing blood. Moreover, according to our previous observations concerning HAAFs grown on SF microfibers (Chiarini et al., 2003), the present results strengthen the view that HAAFs growing on an SF substrate significantly curtail their *de novo* production of type I collagen, which translates into a remarkable antifibrogenic upshot and could be significantly relevant in the clinical settings. In other words, it can be concluded that the SF substrate in a nanofibrous format exerts a neat antifibrotic effect on HAAFs.

Some cytokines and/or chemokines are cell type-specific biomarkers. The pattern of cytokines and chemokines secreted into the growth medium under the conditions examined would reveal the proliferative and/or pro-inflammatory proclivities of the cells. In particular, released chemokines may attract circulating leukocytes. Moreover, cytokines and chemokines play important roles in several cellular processes like growth, differentiation, apoptosis, angiogenesis, inflammation, and innate immunity. Among the identified cytokines and chemokines, IL-6 stands out, being the most intensely secreted one by each of the three cell types both on

SilkGraft and on polystyrene. IL-6 is considered a biomarker of cell proliferation, differentiation and survival (Morimoto et al., 1991; Krishnaswamy et al., 1998; Kyurkchiev et al., 2014). Similarly, the basal secretion of MCP-1 and/or MCP-2 is indicative of a cell proliferation capacity. MCP-1 promotes the arteriogenesis associated with the induction of Vascular Endothelial Growth Factor (VEGF)-A expression (Keeley et al., 2008). Among the other important chemokines secreted by the three cell types, we mention here IP-10, known for its antifibrotic and angiostatic properties, and RANTES protein, known for its ability to regulate leucocyte diapedesis, angiogenesis and some scarring processes (Bujak et al., 2009; Lin et al., 2018). In human aorta-derived SMCs, RANTES increased the expression of cell cycle regulatory proteins and of markers of their synthetic phenotype (Lin et al., 2018). GM-CSF is constitutively expressed by HASMCs and an elevation in GM-CSF expression associates with the HASMCs synthetic phenotype (Plenz et al., 1997). As well, the cellular adhesion molecule ICAM-1 and the HASMCs basal secretion of cytokines IL-1 α and IL-1 β can influence and potentiate cellular proliferation by playing an autocrine role (Braun et al., 1999; Schultz et al., 2007; Bonin et al., 2009). The low secretion of TNF- β from HCAECs on polystyrene surged significantly when the cells were grown on SilkGraft. Notably, TNF- β signals control the proper development and maintenance of endothelial cells (Zindl et al., 2009).

All the three cell types, once cultured on either SilkGraft or polystyrene, exhibited similarly low basal levels of TIMP-2, a metalloprotease blocker which regulates extracellular matrix (ECM) remodeling processes and interactions between cells and ECM, as well as cell proliferation by an autocrine mechanism (Hayakawa et al., 1994). On the other hand, it is important to note that no significant amounts of truly pro-inflammatory cytokines, such as Tumor Necrosis Factor- α (TNF- α), or of profibrotic cytokines, such as Transforming growth factor- β (TGF- β) were secreted by any of the three cell types grown on either substrate. Therefore, the patterns of cytokines and chemokines secreted by the three cell types cultured on SilkGraft suggest a proliferative attitude while neatly excluding a pro-inflammatory and/or pro-fibrogenic proclivity.

The complement system is part of the innate immune system and may be involved in promoting and accelerating hemolysis, platelet and leukocyte activation and thrombosis on device material surfaces, while hemolysis is the liberation of hemoglobin following disruption of the erythrocytes. The hemocompatibility assays demonstrated that SilkGraft did not activate the Sc5b-9 and C3a components of the complement system, did not result in hemolytic effects, and did not alter the counts of red and white blood cells. Moreover, no thrombi formation was observed during the *in vivo* pilot trials. The latter parameter will be further controlled during the on-going long-term studies (up to 1 year).

Finally, the pilot animal study showed the feasibility of using SilkGraft as small caliber vessel graft *in vivo*. Due to the size of the graft, a large animal model with vessels similar in size to human's was needed to allow appropriate placement and evaluation in view of future clinical use. Both minipig and sheep are used as appropriate animal models to evaluate performance, and local tissue effects after vascular implantation (Byrom et al., 2010).

Carotid implantation was chosen to mimic clinical use and to avoid anatomical limitations (carotids are straighter and with less branches than femoral arteries). Advantages associated with using sheep as the animal model are: (i) blood vessels easily accessible and more superficial; (ii) slower endothelialization, more similar to human; (iii) ability to perform blood tests and eco-doppler with animals awake, which translates into the possibility to perform more exams with less stress for the animal; and last but not least (iv) the sheep model allows to evaluate a longer graft, up to 10 cm. Therefore, long-term studies (up to 1 year) aimed at assessing the patency and wall restructuration ability of the graft are already under course in sheep, to demonstrate the feasibility of testing SilkGraft in human clinical settings.

CONCLUSIONS

SilkGraft is a small caliber vascular graft entirely made of pure silk fibroin. The fabrication technology was progressively refined through recursive testing and optimization procedures which led to a standardized production protocol. Particular attention was devoted to the careful selection of starting materials and processing aids (e.g., size of the SF yarn, texture and mechanical performance of the TEX layer, chemical properties and efficacy of the welding medium, etc.), as well as to fine-tuning key processing parameters (e.g., electrospinning, strategy of coupling TEX and ES layers, consolidation of the hybrid structure, final purification before sterilization, etc.). The process development led to a tubular device where the inner and outer ES layers and the middle TEX layer are perfectly integrated at the structural and functional level and respond as a single body to mechanical stresses, without showing any mutual slipping or separation. In fact, the main target was to manufacture a multi-layered scaffold characterized by an easy handling during surgery and, when implanted, able to achieve top level biomimicking performance with the surrounding living tissues while avoiding the onset of any biomechanical mismatch with the native artery.

In vitro studies with three main types of cells inhabiting the arterial wall, i.e., HCAECs, HASMCs, and HAAFs, showed that SilkGraft exhibited a high degree of biocompatibility and a level of cell adhesion superior to polystyrene. The trends of specific metabolic markers, like consumption of glucose and glutamine and release of acid lactic into the medium, confirmed the intense metabolic activities and the expansion of the cell populations cultured on SilkGraft coupled with a curtailed production of collagen and with no secretion of pro-inflammatory or pro-fibrotic cytokines and chemokines. Furthermore, blood hemocompatibility was corroborated by the lack of complement activation, hemolysis, and alteration of cell counts assays.

The results of pilot animal studies indicated the sheep as the model of choice to carry out the preclinical *in vivo* tests before the clinical trials in humans and confirmed that the device is easy to handle and surgically stitch. Finally, it is important to highlight that in our setting, thanks to its promising biological responses,

SilkGraft is intended as an “off-the-shelf” device, no longer requiring pre-seeding with cells, thus eliminating related time delays and costs and minimizing the steps for graft preparation before implantation.

DATA AVAILABILITY STATEMENT

The raw data supporting the conclusions of this manuscript will be made available by the authors, without undue reservation, to any qualified researcher.

ETHICS STATEMENT

The animal study was reviewed and approved by the NAMSA Ethical Committee and the French Ministry of Education, Higher Education, and Research.

AUTHOR CONTRIBUTIONS

This is a multi-disciplinary project that has been conducted by three groups coordinated by GF. Biomaterial development group: AA and GF led the conception and design of the project. MB, GB, and VV contributed to designing, planning, and executing all the experimental activities. Data interpretation responsibility was collectively shared by the entire group. *In vitro* preclinical study group: UA, AC, and ID were responsible for the design and planning of the *in vitro* tests. The experimental execution was performed by AC and ID, who also acquired and validated the results under the supervision of UA. *In vivo* preclinical/clinical study group: PS and PP designed the experimental approach for the *in vivo* pilot study. They shared the responsibility of selecting models, addressing surgical techniques, and evaluating the histological results. GF was responsible for drafting the text of the biomaterial development part of the work, as well as for collecting and critically revising the text contributions drafted by the other two participating groups and gathering the final approval of all authors for the publishable version. All authors ensure that questions related to the accuracy or integrity of any part of the work are appropriately investigated and resolved.

FUNDING

This study was entirely funded by Silk Biomaterials Srl, whose stock owners and employees were deeply involved in study design, data collection and analysis, decision to publish, preparation of the manuscript, and decision about submission.

ACKNOWLEDGMENTS

The authors express their deep gratitude to Dr. Hu Peng (from the First Affiliated Hospital of Zunyi Medical University, China and currently Ph.D. Student in Verona's Laboratory, Italy) for his skillful handling of human cell lines. The authors would like to address heartfelt thanks to Dr. Alberto Settembrini (Department

of Vascular Surgery, Fondazione Ca' Granda Ospedale Maggiore, Milan) for his fruitful contribution to the development of the device and to the execution of the *in vivo* tests. This research did not receive any specific grant from funding agencies in the public, commercial, or not-for-profit sectors.

REFERENCES

- Alessandrino, A. (2016). *Process for the Production of a Hybrid Structure Consisting of Coupled Silk Fibroin Microfibers and Nanofibers, Hybrid Structure Thus Obtained and Its Use as Implantable Medical Device*. WIPO/PCT Patent No. WO 2016/067189 A1. World Intellectual Property Organization.
- Altman, G. H., Diaz, F., Jakuba, C., Calabro, T., Horan, R. L., Chen, J., et al. (2003). Silk-based biomaterials. *Biomaterials*. 24, 401–416. doi: 10.1016/S0142-9612(02)00353-8
- Armato, U., Dal Prà, I., Chiarini, A., and Freddi, G. (2011). Will silk fibroin nanofiber scaffolds ever hold a useful place in translational regenerative medicine? *Int. J. Burn Trauma*. 1, 27–33.
- Armato, U., Romano, F., Andreis, P. G., Paccagnella, L., and Marchesini, C. (1986). Growth stimulation and apoptosis induced in cultures of neonatal rat liver cells by repeated exposures to epidermal growth factor/urogastrone with or without associated pancreatic hormones. *Cell Tissue Res*. 245, 471–480. doi: 10.1007/BF00218546
- Aytemiz, D., Sakiyama, W., Suzuki, Y., Nakaizumi, N., Tanaka, R., Ogawa, Y., et al. (2013). Small-diameter silk vascular grafts (3 mm diameter) with a double-raschel knitted silk tube coated with silk fibroin sponge. *Adv. Health. Mater.* 2, 361–368. doi: 10.1002/adhm.201200227
- Babitha, S., Rachita, L., Karthikeyan, K., Shoba, E., Janani, I., Poornima, B., et al. (2017). Electrospun protein nanofibers in healthcare: a review. *Int. J. Pharm.* 523, 52–90. doi: 10.1016/j.ijpharm.2017.03.013
- Bonin, P. D., Fic, G. J., and Singh, P. (2009). Interleukin-1 promotes proliferation of vascular smooth muscle cells in coordination with PDGF or a monocyte derived growth factor. *Exp. Cell Res.* 181, 475–482. doi: 10.1016/0014-4827(89)90104-3
- Braun, M., Pietsch, P., Schrör, K., Baumann, G., and Felix, S. B. (1999). Cellular adhesion molecules on vascular smooth muscle cells. *Cardiovasc. Res.* 41, 395–401. doi: 10.1016/S0008-6363(98)00302-2
- Bujak, M., Dobaczewski, M., Gonzalez-Quesada, C., Xia, Y., Leucker, T., Zymek, P., et al. (2009). Induction of the CXC chemokine interferon-gamma-inducible protein 10 regulates the reparative response following myocardial infarction. *Circ. Res.* 105, 973–983. doi: 10.1161/CIRCRESAHA.109.199471
- Byrom, M. J., Bannon, P. G., and White, G. H., M.K.C. (2010). Animal models for the assessment of novel vascular conduits. *J. Vasc. Surg.* 52, 176–195. doi: 10.1016/j.jvs.2009.10.080
- Cattaneo, I., Figliuzzi, M., Azzollini, N., Catto, V., Farè, S., Tanzi, M. C., et al. (2013). *In vivo* regeneration of elastic lamina on fibroin biodegradable vascular scaffold. *Int. J. Artif. Organs*. 36, 166–174. doi: 10.5301/ijao.5000185
- Catto, V., Farè, S., Cattaneo, I., Figliuzzi, M., Alessandrino, A., Freddi, G., et al. (2015). Small diameter electrospun silk fibroin vascular grafts: mechanical properties, *in vitro* biodegradability, and *in vivo* biocompatibility. *Mater. Sci. Eng. C*. 54, 101–111. doi: 10.1016/j.msec.2015.05.003
- Catto, V., Farè, S., Freddi, G., and Tanzi, M. C. (2014). Vascular tissue engineering: recent advances in small diameter blood vessel regeneration. *ISRN Vasc. Med.* 923030. doi: 10.1155/2014/923030
- Chiarini, A., Freddi, G., Liu, D., Armato, U., and Dal Prà, I. (2016). Biocompatible silk noil-based three-dimensional carded-needled nonwoven scaffolds guide the engineering of novel skin connective tissue. *Tissue Eng. Part A*. 22, 1047–1060. doi: 10.1089/ten.tea.2016.0124
- Chiarini, A., Petrini, P., Bozzini, S., Dal Prà, I., and Armato, U. (2003). Silk fibroin/poly(carbonate)-urethane as a substrate for cell growth: *in vitro* interactions with human cells. *Biomaterials* 24, 789–799. doi: 10.1016/S0142-9612(02)00417-9
- Dal Prà, I., Chiarini, A., Boschi, A., Freddi, G., and Armato, U. (2006). Novel dermo-epidermal equivalents on silk fibroin-based formic acid-crosslinked three-dimensional nonwoven devices with prospective applications in human tissue engineering/regeneration/repair. *Int. J. Mol. Med.* 18, 241–247. doi: 10.3892/ijmm.18.2.241
- Dal Prà, I., Freddi, G., Minic, J., Chiarini, A., and Armato, U. (2005). *De novo* engineering of reticular connective tissue *in vivo* by silk fibroin nonwoven materials. *Biomaterials*. 26, 1987–1999. doi: 10.1016/j.biomaterials.2004.06.036
- Ding, X., Zou, T., Gong, X., Ren, C., Kang, H., Xu, P., et al. (2016). Trilayered sulfated silk fibroin vascular grafts enhanced with braided silk tube. *J. Bioact. Compat. Polym.* 31, 613–623. doi: 10.1177/0883911516643107
- Eelen, G., Cruys, B., Welti, J., De Bock, K., and Carmeliet, P. (2013). Control of vessel sprouting by genetic and metabolic determinants. *Trends Endocrinol. Metab.* 24, 589–596. doi: 10.1016/j.tem.2013.08.006
- Enomoto, S., Sumi, M., Kajimoto, K., Nakazawa, Y., Takahashi, R., Takabayashi, C., et al. (2010). Long-term patency of small-diameter vascular graft made from fibroin, a silk-based biodegradable material. *J. Vasc. Surg.* 51, 155–164. doi: 10.1016/j.jvs.2009.09.005
- Fukayama, T., Ozai, Y., Shimokawadoko, H., Aytemiz, D., Tanaka, R., Machida, N., et al. (2015). Effect of fibroin sponge coating on *in vivo* performance of knitted silk small diameter vascular grafts. *Organogenesis* 11, 137–151. doi: 10.1080/15476278.2015.1093268
- Hayakawa, T., Yamashita, K., Ohuchi, E., and Shinagawa, A. (1994). Cell growth-promoting activity of tissue inhibitor of metalloproteinases-2 (TIMP-2). *J. Cell Sci.* 107, 2373–2379.
- Hiob, M. A., She, S., Muiznieks, L. D., and Weiss, A. S. (2017). Biomaterials and modifications in the development of small-diameter vascular grafts. *ACS Biomater. Sci. Eng.* 3, 712–723. doi: 10.1021/acsbomaterials.6b00220
- Keeley, E. C., Mehrad, B., and Strieter, R. M. (2008). Chemokines as mediators of neovascularization. *Arterioscler. Thromb. Vasc. Biol.* 28, 1928–1936. doi: 10.1161/ATVBAHA.108.162925
- König, G., McAllister, T. N., Dusserre, N., Garrido, S. A., Iyican, C., Marini, A. (2009). Mechanical properties of completely autologous human tissue engineered blood vessels compared to human saphenous vein and mammary artery. *Biomaterials* 30, 1542–1550. doi: 10.1016/j.biomaterials.2008.11.011
- Krishnaswamy, G., Smith, J. K., Mukkamala, R., Hall, K., Joyner, W., Yerra, L., et al. (1998). Multifunctional cytokine expression by human coronary endothelium and regulation by monokines and glucocorticoids. *Microvasc. Res.* 55, 189–200. doi: 10.1006/mvres.1998.2079
- Krützfeldt, A., Spahr, R., Mertens, S., Siegmund, B., and Piper, H. M. (1990). Metabolism of exogenous substrates by coronary endothelial cells in culture. *J. Mol. Cell. Cardiol.* 22, 1393–1404. doi: 10.1016/0022-2828(90)90984-A
- Kyurkchiev, D., Bochev, I., Ivanova-Todorova, E., Mourdjeva, M., Oreshkova, T., Belemezova, K., et al. (2014). Secretion of immunoregulatory cytokines by mesenchymal stem cells. *World J. Stem Cells*. 6, 552–570. doi: 10.4252/wjsc.v6.i5.552
- Lin, C. S., Hsieh, P. S., Hwang, L. L., Lee, Y. H., Tsai, S. H., Tu, Y. C., et al. (2018). The CCL5/CCR5 axis promotes vascular smooth muscle cell proliferation and atherogenic phenotype switching. *Cell. Physiol. Biochem.* 47, 707–720. doi: 10.1159/000490024
- Liu, H., Li, X., Zhou, G., Fan, H., and Fan, Y. (2011). Electrospun sulfated silk fibroin nanofibrous scaffolds for vascular tissue engineering. *Biomaterials* 32, 3784–3793. doi: 10.1016/j.biomaterials.2011.02.002
- Liu, S., Dong, C., Lu, G., Lu, Q., Li, Z., Kaplan, D. L., et al. (2013). Bilayered vascular grafts based on silk proteins. *Acta Biomater.* 9, 8991–9003. doi: 10.1016/j.actbio.2013.06.045

SUPPLEMENTARY MATERIAL

The Supplementary Material for this article can be found online at: <https://www.frontiersin.org/articles/10.3389/fbioe.2019.00356/full#supplementary-material>

- Liu, Y., Tu, F., Li, H., Shi, P., Yin, Y., Dong, F., et al. (2018). Preparation, characterization and *in vivo* graft patency of a silk fibroin tubular scaffold. *Mater. Technology*. 33, 227–234. doi: 10.1080/10667857.2017.1405889
- Lovett, M. L., Cannizzaro, C. M., Vunjak-Novakovic, G., and Kaplan, D. L. (2008). Gel spinning of silk tubes for tissue engineering. *Biomaterials* 29, 4650–4657. doi: 10.1016/j.biomaterials.2008.08.025
- Lovett, M. L., Eng, G., Kluge, J. A., Cannizzaro, C. M., Vunjak-Novakovic, G., and Kaplan, D. L. (2010). Tubular silk scaffolds for small diameter vascular grafts. *Organogenesis* 6, 217–224. doi: 10.1016/j.org.6.4.13407
- Marelli, B., Achilli, M., Alessandrino, A., Freddi, G., Tanzi, M. C., Farè, S., et al. (2012). Collagen-reinforced electrospun silk fibroin tubular construct as small calibre vascular graft. *Macromol. Biosci.* 12, 1566–1574. doi: 10.1002/mabi.201200195
- Marelli, B., Alessandrino, A., Farè, S., Freddi, G., Mantovani, D., and Tanzi, M. C. (2010). Compliant electrospun silk fibroin tubes for small vessel bypass grafting. *Acta Biomater.* 6, 4019–4026. doi: 10.1016/j.actbio.2010.05.008
- Marelli, B., Alessandrino, A., Farè, S., Tanzi, M. C., and Freddi, G. (2009). Electrospun silk fibroin tubular matrixes for small vessel bypass grafting. *Mater. Technol.* 24, 52–57. doi: 10.1179/175355509X417945
- McClure, M. J., Simpson, D. G., and Bowlin, G. L. (2012). Tri-layered vascular grafts composed of polycaprolactone, elastin, collagen, and silk: optimization of graft properties. *J. Mech. Behav. Biomed. Mater.* 10, 48–61. doi: 10.1016/j.jmbbm.2012.02.026
- Mi, H.-Y., Jing, X., Yu, E., McNulty, J., Peng, X.-F., and Turng, L.-S. (2015). Fabrication of triple-layered vascular scaffolds by combining electrospinning, braiding, and thermally induced phase separation. *Mater. Lett.* 161, 305–308. doi: 10.1016/j.matlet.2015.08.119
- Mohan, D., and Melvin, J. W. (1982). Failure properties of passive human aortic tissue. I-Uniaxial tension tests. *J. Biomech.* 15, 887–902. doi: 10.1016/0021-9290(82)90055-0
- Morimoto, S., Nabata, T., Koh, E., Shiraishi, T., Fukuo, K., Imanaka, S., et al. (1991). Interleukin-6 stimulates proliferation of cultured vascular smooth muscle cells independently of interleukin-1 beta. *J. Cardiovasc. Pharmacol.* 17 (Suppl. 2), S117–118. doi: 10.1097/00005344-199117002-00026
- Nakazawa, Y., Sato, M., Takahashi, R., Aytemiz, D., Takabayashi, C., Tamura, T., et al. (2011). Development of small-diameter vascular grafts based on silk fibroin fibers from *Bombyx mori* for vascular regeneration. *J. Biomater. Sci. Polym. Ed.* 22, 195–206. doi: 10.1163/092050609X12586381656530
- Plenz, G., Koenig, C., Severs, N. J., and Robenek, H. (1997). Smooth muscle cells express Granulocyte-Macrophage Colony-Stimulating Factor in the undiseased and atherosclerotic human coronary artery. *Arterioscl. Thromb. Vasc. Biol.* 17, 2489–2499. doi: 10.1161/01.ATV.17.11.2489
- Schultz, K., Murthy, V., Tatrow, J. B., and Beasley, D. (2007). Endogenous interleukin-1 alpha promotes a proliferative and proinflammatory phenotype in human vascular smooth muscle cells. *Am. J. Physiol. Heart. Circ. Physiol.* 292, H2927–H2934. doi: 10.1152/ajpheart.00700.2006
- Sugiura, T., Lee, A. Y., and Shinoka, T. (2017). “Tissue engineering in vascular medicine,” in *Frontiers in Stem Cell and Regenerative Medicine Research*, Vol 4, eds A.-U. Rahman and S. Anjum (Sharjah: Bentham Science Publisher), 3–35. doi: 10.2174/9781681084756117050003
- Tanaka, T., Uemura, A., Tanaka, R., Tasei, Y., and Asakura, T. (2018). Comparison of the knitted silk vascular grafts coated with fibroin sponges prepared using glycerin, poly(ethylene glycol diglycidyl ether) and poly(ethylene glycol) as porogens. *J. Biomater. Appl.* 32, 1239–1252. doi: 10.1177/0885328218758276
- Thurber, A. E., Omenetto, F. G., and Kaplan, D. L. (2015). *In vivo* bio responses to silk proteins. *Biomaterials*. 71, 145–157. doi: 10.1016/j.biomaterials.2015.08.039
- Vegran, F., Boidot, R., Michiels, C., Sonveaux, P., and Feron, O., and (2011). Lactate influx through the endothelial cell monocarboxylate transporter MCT1 supports an NF-kappaB/IL-8 pathway that drives tumor angiogenesis. *Cancer Res.* 71, 2550–2560. doi: 10.1158/0008-5472.CAN-10-2828
- Viñals, F., and Pouyssegur, J. (1999). Confluence of vascular endothelial cells induces cell cycle exit by inhibiting p42/p44 mitogen-activated protein kinase activity. *Mol Cell Biol.* 19, 2763–2772. doi: 10.1128/MCB.19.4.2763
- Wang, D., Liu, H., and Fan, Y. (2017). Silk fibroin for vascular regeneration. *Microsc. Res. Tech.* 80, 280–290. doi: 10.1002/jemt.22532
- Wang, S.-D., Zhang, Y.-Z., Yin, G.-B., Wang, H. W., and Dong, Z.-H. (2010). Fabrication of a composite vascular scaffold using electrospinning technology. *Mater. Sci. Eng. C*. 30, 670–676. doi: 10.1016/j.msec.2010.02.021
- World Health Organization (2012). *Cardiovascular Diseases*. Fact Sheet No. 317.
- Wu, G., Haynes, T. E., Li, H., and Meininger, C. J. (2000). Glutamine metabolism in endothelial cells: ornithine synthesis from glutamine via pyrroline-5-carboxylate synthase. *Comp. Biochem. Physiol. A Mol. Integr. Physiol.* 126, 115–123. doi: 10.1016/S1095-6433(00)00196-3
- Wu, T., Zhang, J., Wang, Y., Li, D., Sun, B., El-Hamshary, H., et al. (2018). Fabrication and preliminary study of a biomimetic tri-layer tubular graft based on fibers and fiber yarns for vascular tissue engineering. *Mater. Sci. Eng. C*. 82, 121–129. doi: 10.1016/j.msec.2017.08.072
- Xiang, P., Li, M., Zhang, C.-Y., Chen, D.-L., and Zhou, Z.-H. (2011). Cytocompatibility of electrospun nanofiber tubular scaffolds for small diameter tissue engineering blood vessels. *Int. J. Biol. Macromol.* 49, 281–288. doi: 10.1016/j.ijbiomac.2011.05.004
- Yagi, T., Sato, M., Nakazawa, Y., Tanaka, K., Sata, M., Itoh, K., et al. (2011). Preparation of double-raschel knitted silk vascular grafts and evaluation of short-term function in a rat abdominal aorta. *J. Artif. Organs*. 14, 89–99. doi: 10.1007/s10047-011-0554-z
- Yamamoto, S., Okamoto, H., Haga, M., Shigematsu, K., Miyata, T., Watanabe, T., et al. (2016). Rapid endothelialization and thin luminal layers in vascular grafts using silk fibroin. *J. Mater. Chem. B*. 4, 938–946. doi: 10.1039/C5TB.02528A
- Zamani, M., Khafaji, M., Naji, M., Vossoughi, M., Alemzadeh, I., and Haghighipour, N. (2017). A biomimetic heparinized composite silk-based vascular scaffold with sustained antithrombogenicity. *Sci. Rep.* 7:4455. doi: 10.1038/s41598-017-04510-1
- Zhang, J., Huang, H., Ju, R., Chen, K., Li, S., Wang, W., et al. (2017). *In vivo* biocompatibility and hemocompatibility of a polytetrafluoroethylene small diameter vascular graft modified with sulfonated silk fibroin. *Am. J. Surg.* 213, 87–93. doi: 10.1016/j.amjsurg.0.2016.04.005
- Zhao, Y., Yan, X., Ding, F., Yang, Y., and Gu, X. (2011). The effects of different sterilization methods on silk fibroin. *Biomed. Sci. J. Eng.* 4, 397–402. doi: 10.4236/jbise.2011.45050
- Zindl, C. L., Kim, T. H., Zeng, M., Archambault, A. S., Grayson, M. H., Choi, K., et al. (2009). The lymphotoxin LTalpha(1)beta(2) controls postnatal and adult spleen marginal sinus vascular structure and function. *Immunity* 30, 408–420. doi: 10.1016/j.immuni.2009.01.010

Conflict of Interest: The study was sponsored by Silk Biomaterials srl; GF and AA are stock owners and employees of the sponsoring organization. GB, MB, and VV are employees of the sponsoring organization. UA, AC, ID, and PS are consultants of the sponsoring organization. PP was a former member of the Board of Directors of the sponsoring organization.

Copyright © 2019 Alessandrino, Chiarini, Biagiotti, Dal Prà, Bassani, Vincoli, Settembrini, Pierimarchi, Freddi and Armato. This is an open-access article distributed under the terms of the Creative Commons Attribution License (CC BY). The use, distribution or reproduction in other forums is permitted, provided the original author(s) and the copyright owner(s) are credited and that the original publication in this journal is cited, in accordance with accepted academic practice. No use, distribution or reproduction is permitted which does not comply with these terms.



Preparation of Antimicrobial Hyaluronic Acid/Quaternized Chitosan Hydrogels for the Promotion of Seawater-Immersion Wound Healing

OPEN ACCESS

Edited by:

Bing Tang,

First Affiliated Hospital of Sun Yat-sen University, China

Reviewed by:

Baolin Guo,

Xi'an Jiaotong University

(XJTU), China

Zhengwei Mao,

Zhejiang University, China

*Correspondence:

Rui Guo

guorui@jnu.edu.cn

Biao Cheng

chengbiaocheng@163.com

[†]These authors have contributed equally to this work

Specialty section:

This article was submitted to

Biomaterials,

a section of the journal

Frontiers in Bioengineering and

Biotechnology

Received: 23 September 2019

Accepted: 12 November 2019

Published: 10 December 2019

Citation:

Wang X, Xu P, Yao Z, Fang Q, Feng L,

Guo R and Cheng B (2019)

Preparation of Antimicrobial

Hyaluronic Acid/Quaternized Chitosan

Hydrogels for the Promotion of

Seawater-Immersion Wound Healing.

Front. Bioeng. Biotechnol. 7:360.

doi: 10.3389/fbioe.2019.00360

Xinlu Wang^{1,2†}, Pengcheng Xu^{2†}, Zexin Yao^{2,3}, Qi Fang¹, Longbao Feng⁴, Rui Guo^{5*} and Biao Cheng^{2*}

¹ The First Clinical Hospital of Guangzhou Medical University, Guangzhou, China, ² Department of Plastic Surgery, General Hospital of Southern Theater Command, PLA, Guangzhou, China, ³ Department of Public Health, Guangdong Pharmaceutical University, Guangzhou, China, ⁴ Beogene Biotech (Guangzhou) Co., Ltd., Guangzhou, China, ⁵ Key Laboratory of Biomaterials of Guangdong Higher Education Institutes, Department of Biomedical Engineering, Guangdong Provincial Engineering and Technological Research Center for Drug Carrier Development, Jinan University, Guangzhou, China

Wound immersion in seawater with high salt, high sodium, and a high abundance of pathogenic bacteria, especially gram-negative bacteria, can cause serious infections and difficulties in wound repair. The present study aimed to prepare a composite hydrogel composed of hyaluronic acid (HA) and quaternized chitosan (QCS) that may promote wound healing of seawater-immersed wounds and prevent bacterial infection. Based on dynamic Schiff base linkage, hydrogel was prepared by mixing oxidized hyaluronic acid (OHA) and hyaluronic acid-hydrazide (HA-ADH) under physiological conditions. With the addition of quaternized chitosan, oxidized hyaluronic acid/hyaluronic acid-hydrazide/quaternized chitosan (OHA/HA-ADH/O-HACC and OHA/HA-ADH/N-HACC) composite hydrogels with good swelling properties and mechanical properties, appropriate water vapor transmission rates (WVTR), and excellent stability were prepared. The biocompatibility of the hydrogels was demonstrated by *in vitro* fibroblast L929 cell culture study. The results of *in vitro* and *in vivo* studies revealed that the prepared antibacterial hydrogels could largely inhibit bacterial growth. The *in vivo* study further demonstrated that the antibacterial hydrogels exhibited high repair efficiencies in a seawater-immersed wound defect model. In addition, the antibacterial hydrogels decreased pro-inflammatory factors (TNF- α , IL-1 β , and IL-6) but enhanced anti-inflammatory factors (TGF- β 1) in wound. This work indicates that the prepared antibacterial composite hydrogels have great potential in chronic wound healing applications, such as severe wound cure and treatment of open trauma infections.

Keywords: quaternized chitosan, hydrogel, hyaluronic acid, seawater immersion, wound healing

INTRODUCTION

With the extensive use of high-tech weapons, especially precision-guided missiles on the battlefield, the trauma and burns caused by high-energy explosion in naval battle have become the most important and challenging healthcare issues (Zhu et al., 2017; Chen et al., 2019). In modern high-tech naval warfare, the unavoidable exposure of open traumas to seawater with high salt, high sodium, and a high abundance of pathogenic bacteria, especially gram-negative bacteria, can cause serious infections and wound-repair difficulties (Zhang et al., 2017). Current traditional antimicrobials such as antibiotics, iodine, silver, and zinc oxide are effective in preventing bacterial infection of skin wounds, but they cause resistance to last-line antibiotics and cause significant damage to vital organs (Chung et al., 2017; Lin et al., 2019). Considering these imperfect treatments, the development of new and more effective antimicrobials is still highly desired in clinical application.

Chitosan is a kind of natural polymer that has the characteristics of biodegradability, biocompatibility, and antimicrobial activity (Thattaruparambil et al., 2016; Liang et al., 2019a). It meets the requirements of environmental protection and has become one of the research hotspots in the development of natural antimicrobial agents (Sarhan et al., 2016). The antimicrobial mechanism of chitosan is based on the positive charge of the amino group at the C-2 position after protonation at a pH below 6, which can interact with the surface of bacteria and cause bacterial death (Pires et al., 2013; Yildirim-Aksoy and Beck, 2017). However, chitosan is insoluble in neutral and alkaline aqueous solutions with pH values of >6.5 , which greatly limits its application (Mohamed et al., 2017). Recently, quaternized chitosan (QCS) has received more attention from researchers, as it can replace traditional antimicrobials and reduce organ damage (Thanou et al., 2002; You et al., 2016). The addition of quaternary amino groups in chitosan greatly enhances the water solubility of chitosan, and quaternized chitosan with antimicrobial activity combines with polyatomic amino groups to form double antimicrobial active groups, which greatly improves its antimicrobial field of application.

In wound treatment, wound dressing materials with superior properties are typically used to facilitate wound healing, of which hydrogels that have high water content, flexible mechanical properties, and good biocompatibility are considered promising candidates for practical application (Li et al., 2018, 2019; Yi et al., 2018). Firstly, by providing a porous structure and having a suitable swelling ratio, a hydrogel matrix can allow the presence of oxygen, remove wound exudates, and maintain a moist wound bed to promote wound healing (Kaoru et al., 2010; Rakhshaei and Namazi, 2017). Secondly, the antibacterial property of traditional dressing is endowed by antibiotics encapsulated in the hydrogel matrix (Li et al., 2016). However, hydrogels with inherent antimicrobial properties have received widespread interest among biomaterial researchers (Gonzálezhenríquez et al., 2017; Zhao et al., 2017; Kumar et al., 2018). Thirdly, unlike traditional wound dressings (gauze and cotton wool), biodegraded hydrogel dressings are easy to peel off and degrade spontaneously,

which avoids pain and secondary trauma during dressing changes (Yang et al., 2018).

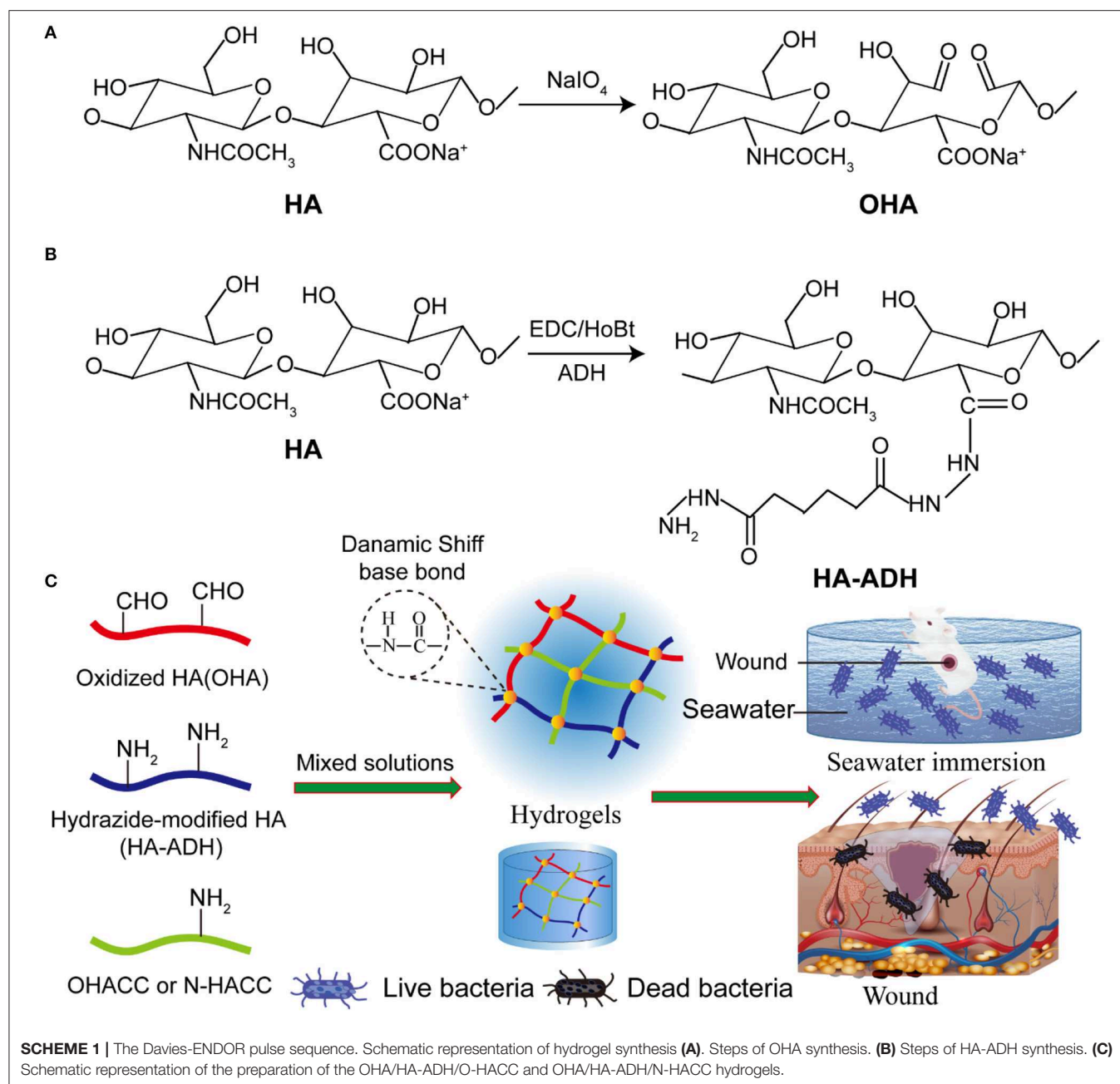
Inspired by the concept of moist wound healing, numerous novel hydrogels have been designed, and these play an important role in the treatment of various wounds (Blacklow et al., 2019; Wang et al., 2019). The majority of hydrogels are prepared from natural polymer materials (e.g., alginate, carboxymethylcellulose, dextran, gelatin, collagen, and hyaluronic acid) and synthetic polymer materials [e.g., methoxy polyethylene glycol, poly(vinyl alcohol), peptide, and polyamidoamine] because of their excellent biocompatibility and biodegradability (Travan et al., 2016). Hyaluronic acid (HA), the main component of the extracellular membrane (ECM), can increase cell-matrix interaction and initiate the signal transduction essential for cell survival and function and has been widely used in the biomedical materials field because of its property of easily peeling, excellent biocompatibility, and high water retention (Purcell et al., 2012; Julia et al., 2013; Zhu et al., 2018a; Liang et al., 2019b).

In this work, biocompatible hydrogel wound dressings with inherent antibacterial properties were prepared by dynamic Schiff base linkage (**Scheme 1**). We furthermore demonstrated that these hydrogel dressings greatly promoted the healing process in a seawater-immersed full-thickness skin defect model. The hydrogels were prepared by mixing quaternized chitosan/hyaluronic acid-hydrazide (HA-ADH) solutions and oxidized hyaluronic acid (OHA) solution under physiological conditions. Hyaluronic acid (HA) was chosen as a hydrogel substrate due to its advantageous properties of high water retention performance and good biocompatibility (Li et al., 2017; Park et al., 2019). In this work, the addition of quaternized chitosan enhanced the mechanical properties of OHA/HA-ADH hydrogel. The hydrogels exhibited excellent antibacterial performance compared to the previous reported antibacterial hydrogels *in vitro* and *in vivo*. Furthermore, the results for the wound contraction area, bacteria in wound, histopathological examinations, collagen analysis, and pro-inflammatory factors (TNF- α , IL-1 β , and IL-6) and anti-inflammatory factors (TGF- β 1) in wound were employed to evaluate the *in vivo* therapeutic effect. The results indicated that these antibacterial hydrogels have good biocompatibility and show great potential as wound dressings, especially for the healing of severe wounds and open trauma infections.

MATERIALS AND METHODS

Reagents and Materials

Chitosan (CS, Mw = 3 kDa, degree of deacetylation = 95%) was obtained from Nantong Lushen Bioengineering Co., Ltd. (Jiangsu, China). Benzaldehyde, Glycidyltrimethylammonium chloride (GTMAC), (3-chloro-2-hydroxypropyl) trimethylammonium chloride S, and ethylene glycol was purchased from Sinopharm Chemical Reagent Co., Ltd. (Shanghai, China). Hyaluronic acid (HA, Mw = 200 kDa) was purchased from Bloomage Freda Biopharm Co., Ltd. (Shangdong, China). Adipic dihydrazide (ADH), hydroxy-benzotriazole (HOBt), and dimethyl sulfoxide (DMSO) were purchased from Aladdin



Chemical Company (Shanghai, China). Sodium periodate, 1-ethyl-3-(3-dimethylaminopropyl)-carbodiimide (EDC), and hyaluronidase were obtained from Shanghai Yuanye Bio-Technology Co., Ltd. (Shanghai, China). The organic silicon film (BD film KYQ-500) was purchased from Hangzhou Baoerde New Materials Technology Co., Ltd (Hangzhou, China).

The L929 fibroblast cell line was obtained from Beogene Biotechnology Co., Ltd. (Guangzhou, China). Cell Counting Kit-8 (CCK8) was obtained from Beyotime Biotechnology Co., Ltd. (Shanghai, China). Live/dead cell staining kits were purchased from BestBio Bio-Technology Co., Ltd. (Shanghai,

China). The bacteria strains of *Escherichia coli* (*E. coli*, CMCCB 44102) and *Staphylococcus aureus* (*S. aureus*, CMCCB 26003) were purchased from Guangdong Institute of Microbiology (Guangzhou, Guangdong). VRBA-MUG selection medium, Mannitol salt agar, and Pseudomonas agar base/CN-AGAR were obtained from HuanKai Microbial Biotechnology Co., Ltd (Guangzhou, China). The other reagents were listed as follows: Dulbecco's modified Eagle's medium (DMEM, Gibco, USA), fetal bovine serum (FBS, HyClone, USA), trypsin (Amresco, USA), and dimethyl sulfoxide (DMSO, Sigma-Aldrich, USA). All other reagents were analytical grade unless otherwise noted.

Synthesis of Quaternized Chitosan (QCS)

O-HACC and N-HACC were synthesized according to the previous literature with slight modifications (Hu et al., 2010; Xin et al., 2015; Mohamed et al., 2017). The synthesis route of O-HACC and N-HACC polymer is presented in **Scheme 2**.

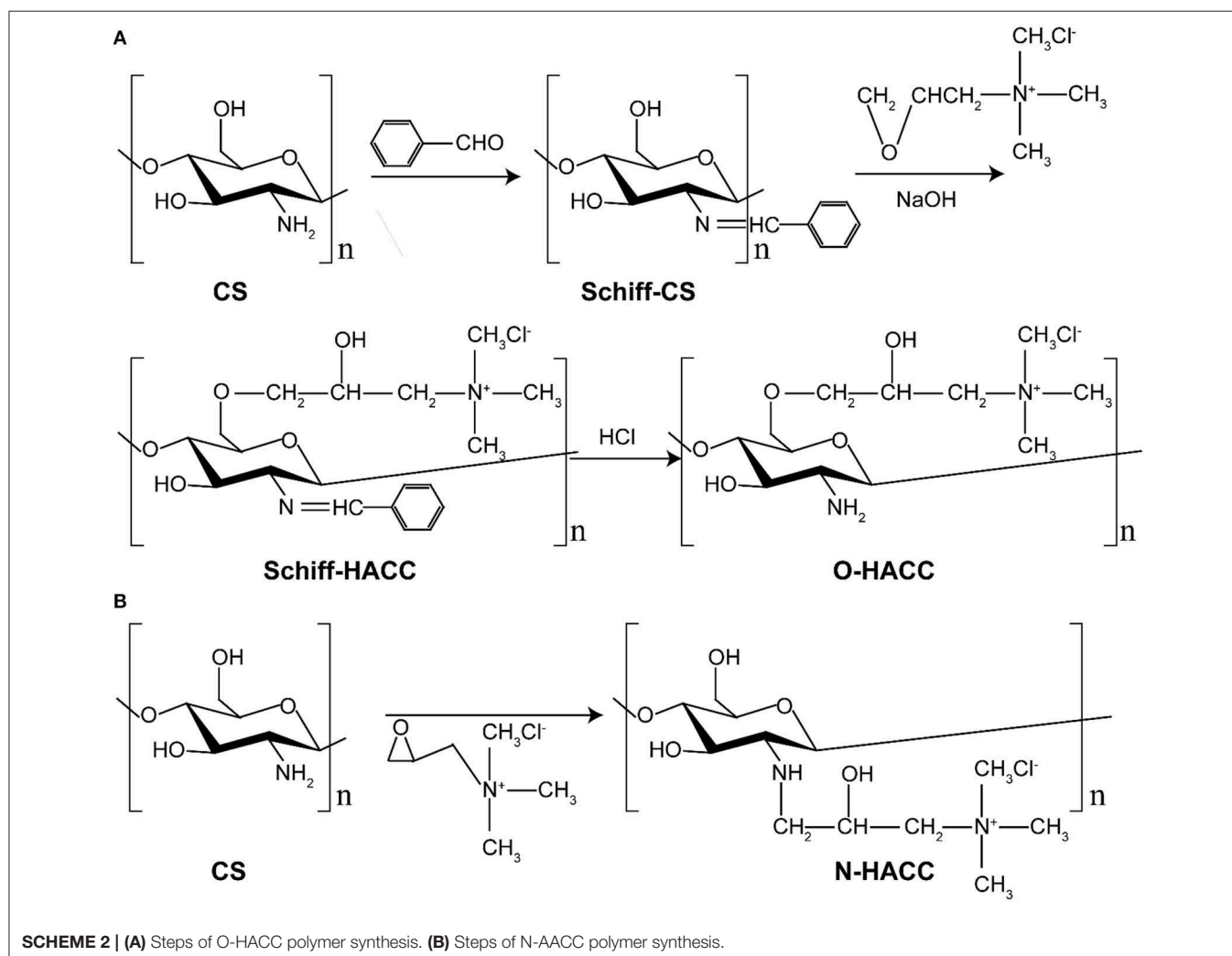
Synthesis of O-HACC

Briefly, 0.3 g of chitosan powder was dissolved in 120 mL of 10% acetic acid for 4 h, 40 mL ethanol was added, and then 15.8 g benzaldehyde was added to the mixed solutions with continuous stirring. After the mixed solutions had been heated and reacted at 60°C for 20 h, the pH was adjusted to pH 7.0 using NaOH solution. The mixture was precipitated, filtered, and washed fully with methanol. The yellow powder chitosan imine Schiff base (Schiff-CS) was obtained by vacuum drying. A quantity of 2.5 g chitosan imine Schiff base and 7.5 g 2,3-epoxypropyl trimethylammonium chloride (ETA) were placed in a straight glass cylinder. Then, 0.02 g NaOH was dissolved in 10 mL water. The mixture was dissolved with the 10 mL 0.2 wt% NaOH solution with continuous stirring to obtain a viscous crude product. The product was precipitated by ethanol,

filtered, and washed with 80% ethanol aqueous solution. The crude product was extracted by Soxhlet extractor with absolute ethyl alcohol as the solvent for 24 h and dried in a vacuum. The solid powder product was obtained and named O-HACC. The degree of quaternization (DQ) of the obtained O-HACC was 65.2%.

Synthesis of N-HACC

Briefly, 3.0 g of chitosan powder was suspended in 27 mL of isopropanol for a 4-h period at 8°C, and then 35 wt.% GTMAC was added dropwise to the suspension with continuous stirring. The pH of the mixed solutions was then adjusted to pH 7.0 using NaOH solution. After reaction at 80°C for 7 h, the mixture was poured into cold acetone, and stirring was continued for 12 h at 4°C. The mixture was washed three times with cold acetone and dialyzed in a dialysis sack (8–12 KDa molecular weight (MW) cut-off) for 3 days. The purified product was obtained by overnight lyophilization of the dialysate, and the fine powder collected was named N-HACC. The degree of quaternization (DQ) of the N-HACC obtained was 98.4%.



Characterization of O-HACC and N-HACC Water Solubility

Chitosan (20 mg) was dissolved in 2 mL distilled water and 2 mL 1% (w/v) acetic acid solution at 25°C for 2 h with constant stirring, respectively. O-HACC (20 mg) and N-HACC (20 mg) was dissolved in 2 mL distilled water at 25°C for 2 h with constant stirring, respectively. The clarity of the solution was examined and photographed.

pH Dependence of the Water Solubility

The solubility was assessed for the pH range 3.0–12.0 via the turbidimetric titration method. O-HACC (40 mg) and N-HACC (40 mg) were dissolved in 20 mL of 1% acetic acid, and the solution was gradually titrated (20 μ L) with NaOH (1 mol/L) to the final pH, with constant stirring. Absorbance measurements of the solutions were recorded using a UV spectrophotometer (UV-2550, Shimadzu, Tokyo, Japan) at $\lambda = 600$ nm.

Characterization of ^1H NMR and FT-IR

The chemical structure of the synthetic O-HACC and N-HACC was performed by ^1H NMR (AVANCE III 600M, Bruker, Germany). FT-IR spectral data were recorded with a Fourier transform-infrared spectrometer (FT-IR; Spectrum One, Perkin Elmer, Norwalk, USA). The samples were pressed with KBr.

Minimum Inhibitory Concentration (MIC) Measurements

The MIC of O-HACC and N-HACC were determined using a broth microdilution method, as described previously (Chin et al., 2018). Briefly, 50 μ L deionized water solution of O-HACC and N-HACC with different concentrations was placed into each well of a 96-well microplate. Then, 50 μ L of bacterial TSB solution (3×10^5 CFU/mL) was added into each well containing the polymer solution. A bacterial TSB solution without O-HACC and N-HACC was used as the control. The 96-well plate was kept in an incubator at 37°C under constant shaking at 100 rpm for 18 h. The MIC was taken as the concentration of the polymer at which no microbial growth was observed with unaided eyes and with the microplate reader at the end of 18-h incubation. All measurements were repeated three times in the same assay plate.

Preparation of the Antimicrobial Composite Hydrogels

Oxidized HA Synthesis (OHA)

OHA was synthesized according to a previously reported method, with a slight modification (Taichi et al., 2007). HA (1 g, 2.48 mmol) was dissolved in 150 mL distilled water, and then 5 mL NaIO_4 solution (0.5 mol/L) was added. The mixed solution was stirred at room temperature for 2 h, protected from light. The reaction was terminated by adding 1 mL ethylene glycol and stirring for an additional 1 h. The solution was dialyzed in a dialysis sack (MWCO 8,000–15,000) for 3 days against distilled water, changing the water three times per day, and then OHA was obtained by freeze-drying.

Hydrazide-Modified HA Synthesis (HA-ADH)

Hydrazide-modified HA (HA-ADH) was synthesized according to a previously established carbodiimide chemical process (Jia et al., 2004). In brief, HA (500 mg, 1.24 mmol) was dissolved in 125 mL distilled water, and then 8 g ADH was added. Subsequently, 10 mL DMSO/ H_2O solution (V:V = 1:1) with 750 mg EDC and 660 mg HoBt was added into the previous HA solution, and the HA was reacted with ADH at a pH 4.75 for 4 h. The reaction was terminated by increasing the solution pH to 7.5 by adding NaOH solution. The HA-ADH solution was precipitated in ethanol, and the precipitate was re-dissolved in distilled water and dialyzed in a dialysis sack (MWCO 80,00–15,000) for 3 days against distilled water, changing the water three times per day, and then HA-ADH was obtained by freeze-drying.

Preparation of Composite Hydrogels

The hydrogels were fabricated by dynamic chemical bonding (Schiff base) of OHA and HA-ADH in a distilled solution. For the preparation of antimicrobial composite hydrogels, 4% (w/v) OHA and 4% (w/v) HA-ADH were fully dissolved in deionized water. Subsequently, 20 mg O-HACC (or 10 mg N-HACC) was added into 0.4 mL HA-ADH solution. After thorough gentle mixing, the mixture was transferred into a 48-well plate as a cylindrical mold. The resultant hydrogels were termed OHA/HA-ADH/O-HACC (or OHA/HA-ADH/N-HACC). The whole preparation processes of OHA/HA-ADH hydrogel was the same as for OHA/HA-ADH/O-HACC except for the addition of O-HACC.

Physical and Mechanical Properties

Swelling Ratio of the Hydrogels

The swelling behavior of the hydrogels was determined using the equilibrium swelling ratio (ESR). Briefly, hydrogels were weighed before the test and then immersed in phosphate-buffered saline (PBS) (pH 7.4, 37°C). At each measurement time point, the hydrogels were removed, gently blotted with filter paper to remove the excess surface water, and immediately weighed. The degree of swelling (DS) was calculated using the formula

$$\text{DS} = \frac{W_t - W_0}{W_0} \times 100\%$$

where W_t and W_0 are the weight of the hydrogel at time t and the weight of the hydrogel at $t = 0$, respectively.

Rheological Studies

Rheological measurements of the hydrogels were performed using a TA rheometer instrument (Kinexus, Ma Erwen instruments, Britain). For oscillatory time sweep experiments, the storage modulus (G') and loss modulus (G'') were measured at a 10% strain, 1 Hz frequency, and 0.5 mm gap (CD mode) for 300 s. For the characterization of the linear viscoelastic range, a dynamic strain sweep test was run at frequencies ranging from 0.1 to 100 Hz.

Compression Test

Compression tests of the hydrogels were performed using a universal testing machine (model 5543; Instron, Norwood,

MA). The hydrogel samples (8 mm in diameter and 4 mm in thickness) were prepared in advance and equilibrated in PBS. The compressive strain rate was set at 1 mm min^{-1} with a 5 N load cell under 40% constraint. The measurements were performed three times ($n = 3$).

Water Vapor Transmission Rate (WVTR)

The moisture permeability of the hydrogels was determined by measuring their WVTR according to the American Society for Testing and Materials (ASTM) standard. Briefly, the hydrogel samples mounted on the mouth of a cylindrical vial (diameter 9.67 mm) containing 5 mL of deionized water, and then placed into a 37°C incubator at 79% relative humidity. The WVTR of the hydrogels was calculated using the formula

$$\text{WVTR} \left(\text{g/m}^2\text{day}^{-1} \right) = \frac{\Delta m}{A \times \text{time}}$$

where Δm is the weight of moisture loss for 24 h (g) and A is the effective transfer area (m^2).

In vitro Degradation of the Hydrogels

The hydrogels were placed in PBS (pH 7.4) containing either 0 or 100 U/mL of hyaluronidase solution in a horizontal shaker at 37°C for 28 days. The samples were carefully removed at predetermined time intervals of 3, 7, 14, 21, and 28 days. The remaining gels were taken out, washed with distilled water, and lyophilized. The percentage of degradation of hydrogels was calculated using the formula

$$\text{Degradation} = \frac{W_t}{W_0} \times 100\%$$

where W_0 is the initial weight of the freeze-dried hydrogels and W_t is the weight of the freeze-dried hydrogel at time t . All tests were performed on five samples ($n = 5$).

In vitro Biocompatibility Test

Hydrogels pre-treated with radiation for sterilization were immersed in DMEM with 10% fetal calf serum and 1% (v/v) penicillin/streptomycin at 37°C for 24 h to obtain the leach liquor. The L929 cells were seeded on a 96-well plate at a density of 2×10^4 cells per well and maintained with 100 μL of leach liquor. DMEM medium was cultured with L929 cells as controls. The leach liquor and DMEM medium were changed every 2 days. After 1, 2, and 3 days of incubation, the relative cell viabilities of the different experimental groups were measured via live/dead staining and CCK-8 colorimetric assay.

For the live/dead staining, the cells attached in each well were rinsed twice with PBS, and then 100 μL of live/dead staining stock solution was added to each well in a dark environment at 4°C for 15 min. Afterward, fluorescent images of the cells were examined using an inverted fluorescence microscope (TE2000-S, Nikon, Japan). For the CCK-8 assay, the cell culture medium was replaced by 100 μL of DMEM medium containing 10% CCK8

solution and was added to each well at 37°C for 1–1.5 h. The absorbance at 450 nm was read immediately on a microplate reader (SH1000, Corona, Japan).

In vitro Antimicrobial Evaluation

A 100- μL bacteria suspension (density = 10^6 CFU/mL) of *S. aureus* was added onto 400 μL of aseptically prepared OHA/HA-ADH, OHA/HA-ADH/O-HACC and OHA/HA-ADH/N-HACC hydrogels in 48-well plates and incubated for 1 h. Subsequently, 500 μL of LB broth was added to the hydrogels. After incubation for different durations (0, 8, and 16 h) at 37°C , the hydrogels were washed three times with PBS. The hydrogels were fixed with 4% (w/w) paraformaldehyde for 30 min. The hydrogels were further dehydrated with graded ethanol series (25, 50, 75, 90, and 100% ethanol) for 15 min each, and the samples were dried under a glass dryer. The specimens were pre-coated with gold and imaged using SEM.

Evaluation of the Anti-seawater Immersion and Wound Healing Efficacy of the Hydrogels in vivo

All animal studies were approved by the Institutional Animal Care and Use Committee (IACUC) of the General Hospital of the Southern Theater Command of the PLA, and the animals were treated according to the regulations. Adult male Sprague Dawley rats (200–250 g) were used for the study *in vivo*. Fifty receptor SD rats were randomly assigned to five groups: the organic silicon film control group (group I, the negative control without seawater), organic silicon film group (group II, the negative control with seawater), OHA/HA-ADH hydrogel group (group III with seawater), OHA/HA-ADH/O-HACC hydrogel group (group IV with seawater), and OHA/HA-ADH/N-HACC hydrogel group (group V with seawater). Prior to surgery, each rat was anesthetized with 3% pentobarbital (45 mg/kg), and the dorsal surface of the rats was shaved and disinfected with iodine. Four full-thickness skin wounds (diameter = 12 mm) were then created on the right and left sides of the backbone of each rat (see **Figure S1A**). Later, the wounded rats were soaked in seawater at a constant temperature of 28°C for 1 h. After 1 h of seawater immersion of the full-thickness skin wounds, the wounds were sewed up with their corresponding hydrogels using silicon film (see **Figure S1B**).

Wound Closure Measurement

The wounds were photographed at the different time points on day 1, 3, 7, 10, 14, and 21 post-surgery. The wound margin was traced, and the wound size was quantified using IPP 6.0 analysis software. The wound area and wound healing rate were calculated using the formulas

$$\text{Wound area} = S_t/S_0 \times 100\%$$

$$\text{Wound healing rate} = (S_0 - S_t)/S_0 \times 100\%$$

where S_0 and S_t were the area of the original wound and the area of the wound at the testing time, respectively. Rats were sacrificed on postoperative days 3, 7, 10, 14, and 21, and the tissue including

the wound site and surrounding healthy skin was excised and fixed for immunohistochemical and histological evaluations.

In vivo Evaluation of the Antimicrobial Efficacy of Hydrogels

The antimicrobial efficacy of the hydrogels was explored by homogenizing skin tissue excised on day 3 for 3 min in a 5 mL centrifuge tube containing 3 mL saline. Ten-fold serial dilutions of sample solutions were prepared, and then 100 μ L samples of the diluted solution were spread onto VRBA-MUG selection medium, Mannitol salt agar, and *P. aeruginosa* selection medium, respectively. VRBA-MUG selection medium was used to selectively culture *E. coli* (Red colony morphology), Mannitol salt agar was used to selectively culture *S. aureus* (yellow-gold colony morphology), and *P. aeruginosa* selection medium was used to selectively culture *P. aeruginosa* (green-yellow colony morphology). The plates were incubated for 24 h at 37°C, and the number of colonies with 5–300 CFU was counted.

Histology and Collagen Staining

The excised skin tissue was fixed by immersion in 4% paraformaldehyde solution for at least 12 h. The fixed skin grafts were dehydrated with a graded series of ethanol and then dimethyl benzene and embedded in paraffin. The paraffin-embedded wounds were cut into sections with a thickness of 4 μ m using a microtome (RM2016, Leica, Shanghai, China). Sections were collected and stained with haematoxylin and eosin (H&E) for histological studies and with Sirius Red for collagen detection according to routine procedures. Finally, the skin sections were photographed by a light microscope (Vectra 3, PerkinElmer, Waltham, MA). The quantifications from Sirius Red staining was performed using IPP 6.0 software. Collagen deposition in the wound sites was calculated using the formula:

$$\text{Collagen deposition} = (\text{red} - \text{stained area of collagen}) / (\text{tissue area}).$$

Immunohistochemistry

For immunofluorescence staining, paraffin sections were stained using primary antibodies to TNF- α , TGF- β 1, IL-1 β , and IL-6 (Abcam, Cambridge, UK; 1:200 dilution). Subsequently, the sections were incubated with the universal secondary antibody (Abcam, ab205719, 1: 500 dilution) and VECTASTAIN Elite ABC reagent, washed in PBS, and reacted with DAB solution (Agilent Dako, Santa Clara, CA, USA). Finally, the nuclei were counterstained with hematoxylin. Images of the stained samples were photographed under a light microscope (Vectra 3, PerkinElmer, Waltham, MA). The positive marker percentage was quantified using IPP 6.0 software.

Western Blot Analysis

Tissue samples were completely homogenized in 10 times tissue volume protease inhibitors. Subsequently, the homogenates were centrifuged at 12,000 rpm for 10 min and loaded on 10–12% sodium dodecyl sulfate (SDS)-polyacrylamide gels. After being transferred to PVDF Western blot membranes, the proteins were incubated with different primary antibodies, specifically

mouse anti- TGF- β 1 (Abcam, ab92486, 1:1,000 dilution), rabbit anti- IL-1 β (Abcam, ab108499, 1:1,000 dilution), rabbit anti- TNF- α (Abcam, ab6671, 1:1,000 dilution), and mouse anti-IL-6 (Abcam, ab9324, 1:1,000 dilution), overnight at 4°C. The membrane was further incubated with goat anti-mouse IgG H&L (HRP) conjugated secondary antibody (Abcam, ab205719, 1:5,000 dilution) for 1 h at room temperature, and was visualized via enhanced chemiluminescent reagent (Beyotime, Jiangsu, China) on X-ray film.

Assessment of Endotoxin and Inflammatory Mediators

Endotoxin was measured in blood serum. Blood was also obtained from each rat. The blood obtained was centrifuged at 5,000 rpm at 4°C for 10 min, and the upper serum was collected and stored at –80°C for subsequent evaluation. The serum was diluted 1:10 in sterile pyrogen-free water. The concentration of endotoxin (EU/mL) was measured by enzyme-linked immunosorbent assay (ELISA) techniques according to the manufacturer's protocol (Shanghai Biotechnology Co., Ltd., Shanghai, China). In this test, the detection limit of the endotoxin assay was 0–80 pg/mL (1 EU/mL = 100 pg/mL). The absorbance of each well was determined to be 450 nm using a microplate reader. The standard curve of endotoxin was constructed, and the corresponding concentration for the unknown sample was calculated. All determinations were performed in triplicate.

Statistical Analysis

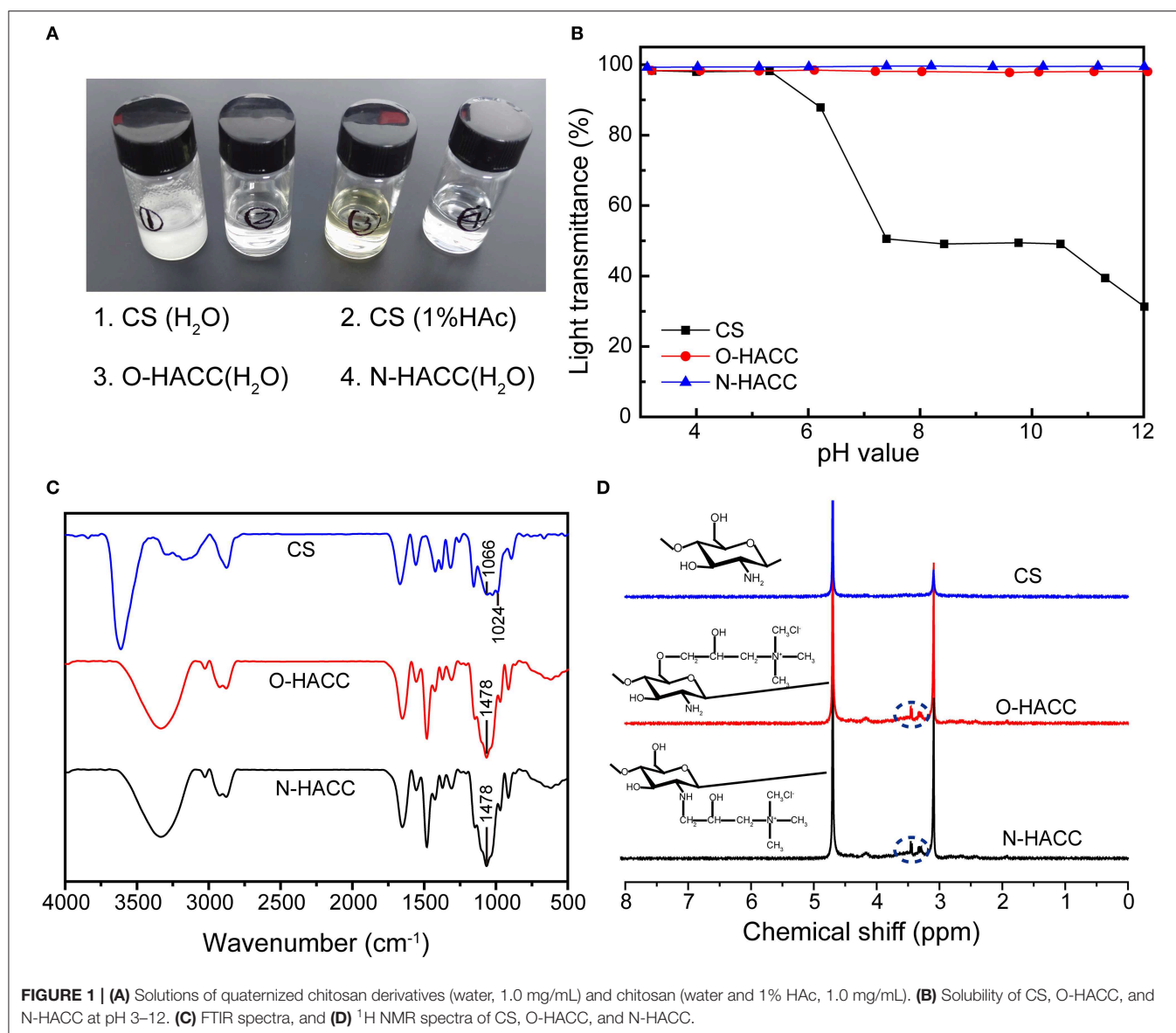
Data were plotted using Origin 9.1 (OriginLab Corporation, Northampton, MA, USA). Error bars represent standard deviations (SDs). The statistical trends were analyzed by one-way analysis of variance (ANOVA). * $p < 0.05$, ** $p < 0.01$, and *** $p < 0.001$ were considered to be significantly different.

RESULTS AND DISCUSSION

Synthesis of O-HACC and N-HACC

Limited solubility at pH 5.5–7.4 is one of the main disadvantages of chitosan, which restricts its application in biomedicine. The CS (water and 1% HAc, 1.0 mg/mL) and O-HACC and N-HACC derivatives (water, 1.0 mg/mL) all had the appearance of solubility (Figure 1A). The dependence of the solubility of CS, O-HACC, and N-HACC on pH was further investigated (Figure 1B). CS was completely soluble in the pH range from 3 to 5, and as the pH value reached 5.0, its solubility decreased. However, O-HACC and N-HACC were almost completely soluble in the pH range from 3 to 12. The results indicated that O-HACC and N-HACC increased solubility under different pH conditions.

The FT-IR spectra of CS, O-HACC, and N-HACC are shown in Figure 1C. The main bands of chitosan included a peak at 3,303 cm^{-1} , corresponding to the stretching of the O–H and N–H bonds, and the band at 1,024 cm^{-1} corresponded to the C=O bending vibration. The peak at 1,478 cm^{-1} , corresponding to the C–H bending vibration of CH₃, is presented in the infrared spectra of O-HACC and N-HACC but not that of CS (Ye et al., 2014; Xin et al., 2015).



This was indicative of the quaternary ammonium salt side-chain grafted onto the CS chain. In order to further determine whether the quaternary amino bond was conjugated to CS, ^1H NMR measurement was carried out (Figure 1D). Prior to the reaction with the quaternary amino group, the spectra of CS samples were determined. Compared to the spectra of the initial chitosan, a characteristic new peak in the strong-field region at $\delta = 3.2\text{--}3.5$ ppm (d, $-\text{N}^+(\text{CH}_3)_3$) indicates the presence of a trimethyl ammonium fragment in the structure of the macromolecules.

Physical and Mechanical Properties of Hydrogels

In this study, we designed a kind of hydrogel formed by dynamic Schiff's base linkage that has an appropriate swelling ratio, good compressive properties, and a comparable modulus to human soft tissue (Chen, 2017). Following the synthesis routes shown

in Schemes 1A,B, OHA and HA-ADH macromolecules were successfully obtained.

The OHA/HA-ADH and OHA/HA-ADH/N-HACC hydrogels had a white color, while OHA/HA-ADH/O-HACC had a yellow color (Figure 2A). The swelling properties of the hydrogels were investigated to illustrate their water sorption capacity (Zhou et al., 2018). The results revealed that the swelling ratios of the OHA/HA-ADH, OHA/HA-ADH/O-HACC, and OHA/HA-ADH/N-HACC hydrogels in PBS reached 44.47, 6.03, and 10.96, respectively, in the first 2 h (Figure 2B). Compared to OHA/HA-ADH hydrogels, OHA/HA-ADH/O-HACC, and OHA/HA-ADH/N-HACC hydrogels showed a lower swelling ratio, which may be related to their higher crosslink density. The hydrogels had almost reached equilibrium swelling in 4 h, with a swelling ratio in PBS of 62.31, 14.11, and 28.84, respectively. A lower swelling ratio will not have a negative impact on the organization of the material.

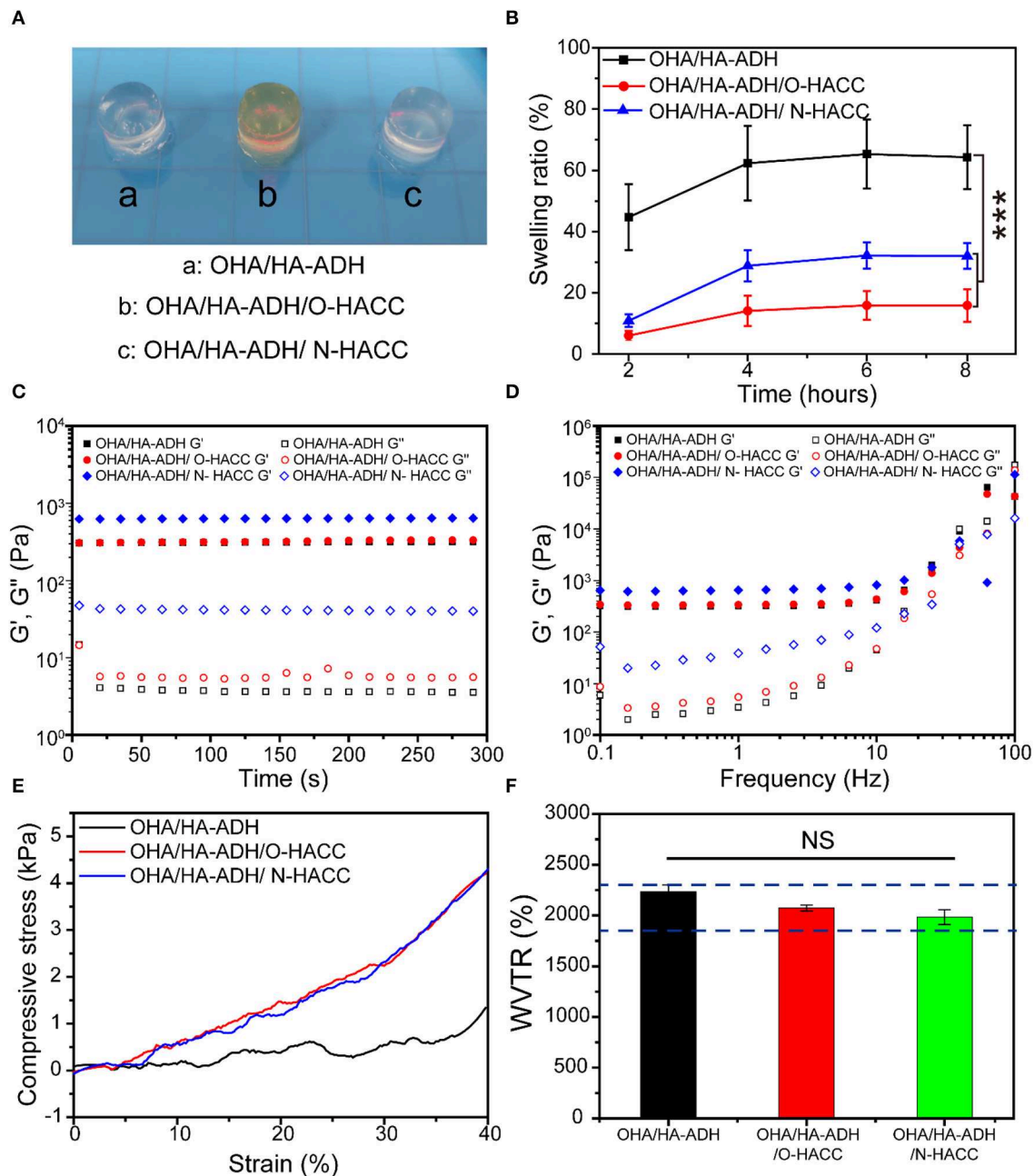


FIGURE 2 | Physical and mechanical properties of the hydrogels. **(A)** Photograph of typical hydrogels. **(B)** Swelling ratio. **(C)** Rheological properties. **(D)** Gel viscosity with frequency ranging from 0.1 to 100 Hz. **(E)** Compression modulus. **(F)** Water vapor transmission rate (WVTR); the blue dotted line represents the optimal WVTR range. *** $p < 0.001$.

The gelation behavior of the hydrogels was monitored by rheological analysis. As presented in **Figure 2C**, G' surpassed G'' immediately after the addition of OHA to the HA-ADH solution due to the rapid formation of the hydrogel. This could provide hydrogel formation through diffusion of the polymer solution to the surrounding tissues when injected into the body. The final G' of OHA/HA-ADH hydrogel can reach a plateau of 10^2 – 10^3 Pa,

which would be able to maintain a structurally robust 3D network shape. Meanwhile, the storage modulus (G') of OHA/HA-ADH/O-HACC and OHA/HA-ADH/N-HACC hydrogels was increased due to an increase in hydrogel concentration and dynamic Schiff's base bonding. As shown in **Figure 2D**, G' surpassed G'' with a shear frequency from 0.1 to 100 rad/s due to the Schiff's base, which indicated that the hydrogel was stable.

An ideal hydrogel should have mechanical properties that enable it to maintain its integrity during use. The compression moduli of the hydrogels are presented in **Figure 2E**. The results showed the OHA/HA-ADH/O-HACC and OHA/HA-ADH/N-HACC hydrogels had a higher modulus (~ 4 kPa) than did OHA/HA-ADH hydrogel, comparable to that of human skin (Chen, 2017). This mechanical property was related to the structure of the hydrogels, i.e., the pore size of OHA/HA-ADH/O-HACC and OHA/HA-ADH/N-HACC hydrogels, which had a higher crosslinking density, was smaller than that of OHA/HA-ADH hydrogel, leading to a more compact structure. Our results showed that the compression modulus of the hydrogel could be improved by adding O-HACC or N-HACC.

Moisture control is a critical parameter in evaluating the healing process in wounds. A higher WVTR will result in dehydration of wound tissue and scarring, while a lower WVTR will cause wound maceration and harm to surrounding tissues. The WVTR values of the OHA/HA-ADH/O-HACC and OHA/HA-ADH/N-HACC hydrogels were tested to be lower than that of OHA/HA-ADH hydrogel due to their denser network structure (**Figure 2F**). This may be because the addition of quaternary ammonia chitosan leads to an increase in hydrogel concentration, resulting in a denser network structure. It is reported that the WVTR of normal skin ranges from 240 to 1,920 $\text{g/m}^2 \cdot 24\text{h}$, while that of an uncovered wound is in the order of $5,138 \pm 202 \text{ g/m}^2 \cdot 24\text{h}$ (Xu et al., 2015; Yang et al., 2017). Previous studies have reported that an ideal wound dressing with a WVTR of $2,028.3 \pm 237.8 \text{ g/m}^2 \cdot 24\text{h}$ was able to maintain a moist environment and promote exudate adsorption and that cells can also migrate more easily, promoting tissue regeneration (Xu et al., 2016). The WVTR value of the prepared hydrogels is close to that of the intact skin and ideal range, a value that avoids the risk of wound dehydration and is suitable for wound healing applications.

The weight loss curve of the prepared hydrogels when in PBS (either in the presence or absence of 100 U/mL hyaluronidase) decreased gradually as the incubation time

increased (**Figures 3A,B**). All of the hydrogels degraded by 20–33% after 7 days, 50–63% after 14 days, 54–68% after 21 days, and 66–78% after 28 days (**Figure 3A**). When the hydrogels were submerged in PBS in the presence of hyaluronidase, the weight loss by degradation was significantly higher than that in PBS solution (**Figure 3B**). All of the hydrogels degraded by 82–93% after 28 days; this fast degradation rate was related to the β -elimination caused by hyaluronidase (Zhu et al., 2018b). Compared with OHA/HA-ADH, the OHA/HA-ADH/O-HACC and OHA/HA-ADH/N-HACC hydrogels shown a lower weight loss ratio. The results indicated that the addition of O-HACC and N-HACC effectively improves the enzymatic stability of the hydrogels by increasing the formation of dynamic chemical bonds (Schiff base linkage between $-\text{NH}_2$ and $-\text{CHO}$) (Qu et al., 2018). Therefore, the developed hydrogels could prolong the usage period and reduce replacement frequency. The MIC values of the O-HACC and N-HACC obtained were tested and are shown in **Table S1**. The results showed that the MIC values of O-HACC and N-HACC against gram-negative bacteria *E. coli* were 6.25 and 0.039 mg/mL and against gram-positive bacteria *S. aureus* were 24.2 and 0.078 mg/mL, respectively. In addition, the antibacterial effect of the O-HACC and N-HACC series against *E. coli* was stronger than that against *S. aureus*.

In vitro Biocompatibility of the Hydrogels

On the basis that the developed hydrogels had good physical properties and antibacterial activity, it was necessary to determine their biocompatibility, which is a prerequisite for well-designed biomedical materials (Wu et al., 2016; Cai et al., 2018). The cell viability ratio was evaluated by culturing murine-derived cell line L929 fibroblast cells with the leach liquor of the hydrogels. TCP and OHA/HA-ADH hydrogel without O-HACC and N-HACC were used as the control groups. It was clear that continuous increases in cell intensity from days 1 to 3 were observed for all groups, which indicated continuous proliferation of L929 fibroblast cells (**Figure 4A**). There were a large number of alive cells (green) and few dead cells (red) in all hydrogel groups,

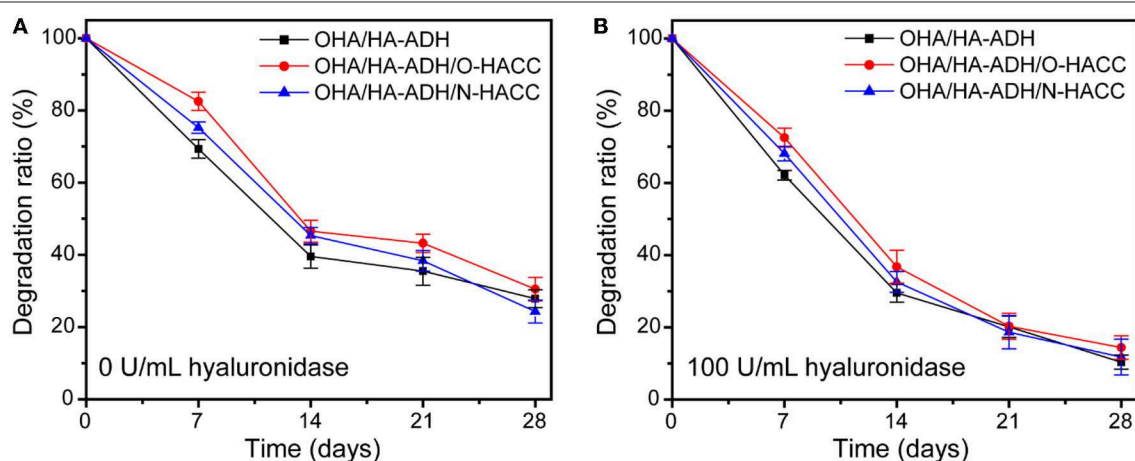


FIGURE 3 | Weight loss rate of the hydrogels in pure PBS solution (A) and PBS solution containing 100 U/mL hyaluronidase (B).

and they showed no obvious difference from the control groups, which indicated the innate biocompatibility of the hydrogels. It is worth noting that the cell densities of the OHA/HA-ADH/O-HACC and HA/HA-ADH/N-HACC groups at predetermined time points were slightly lower than those of the OHA/HA-ADH hydrogel A and TCP groups.

The cell viability rate of L929 fibroblast cells on the hydrogel groups was further quantitatively examined in accordance with the CCK-8 assay, as shown in **Figure 4B**. For the first and second days, the cell viability of all of the hydrogel groups

was comparable to the control groups. On the third day, the OHA/HA-ADH/N-HACC and OHA/HA-ADH/O-HACC groups exhibited slightly lower cell viability than the OHA/HA-ADH hydrogel and TCP groups because of the interaction between N-HACC and O-HACC, which have a positive charge, and the cells, but it still comparable with the control group (Kowapradit et al., 2011). This excellent biocompatibility can be related to the dynamic chemical bond (Schiff base linkage) of the hydrogels. All of the results confirmed that the addition of N-HACC or O-HACC to an OHA/HA-ADH hydrogel resulted

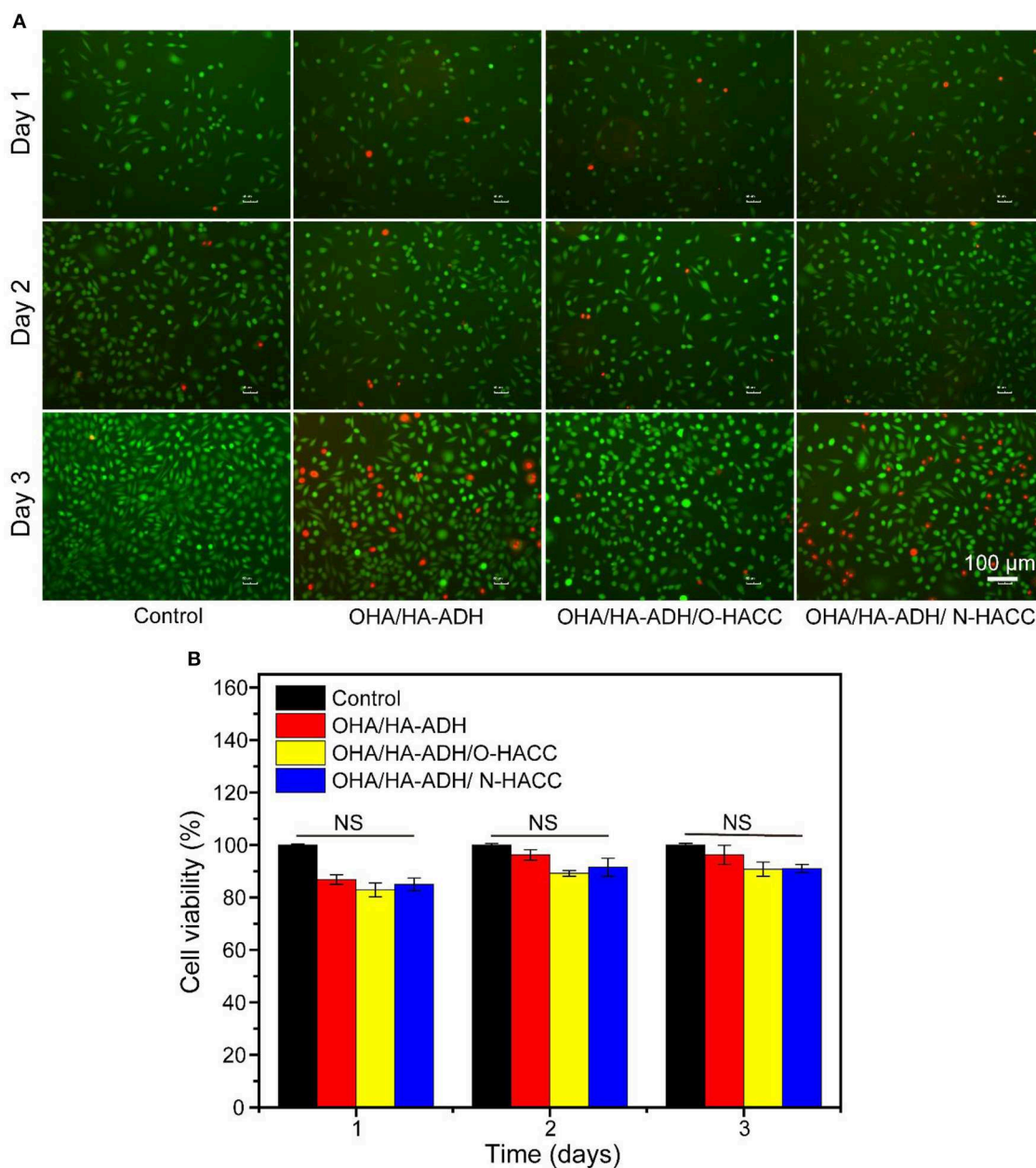


FIGURE 4 | *In vitro* biocompatibility evaluation of the hydrogels. **(A)** Fluorescence images of L929 cells after live/dead staining at day 1, day 2, and day 3. Green fluorescence indicates living cells, and red fluorescence indicates dead cells. **(B)** Cell viability of L929 cells at different culture times according to CCK-8 assay.

in satisfactory biocompatibility that was favorable for L929 cell growth and proliferation.

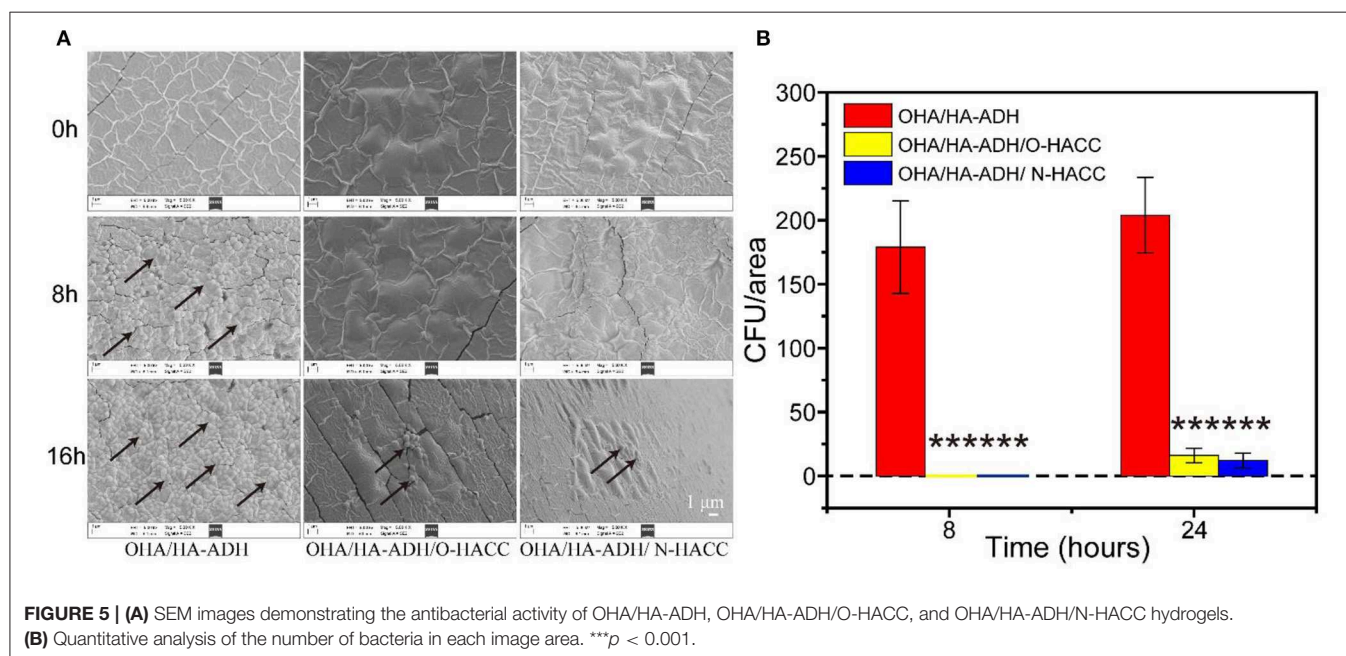
Bacterial Growth on the Hydrogel Surface and SEM Imaging

Besides serving as a barrier to protect wound tissues from external bacterial infections, hydrogels with inherent antimicrobial properties will be particularly attractive because they can prevent wound infections and promote the healing process (Gopinath et al., 2004). *S. aureus* was selected as a representative bacterium to evaluate the antimicrobial effect of the developed hydrogels. The inhibition of the growth of *S. aureus* by the developed hydrogels was assessed by measuring the number of *S. aureus* on the surface of the hydrogels. Bacterial growth on the hydrogels was observed using an SEM. It was clear that the OHA/HA-ADH hydrogel, which lacked antimicrobial material, had a large number of *S. aureus* attached to it, whereas *S. aureus* had significantly inhibited growth and was killed by OHA/HA-ADH/O-HACC and HA/HA-ADH/N-HACC hydrogels (Figure 5A). In addition, at 8 h, the number of *S. aureus* on OHA/HA-ADH was calculated to be about 179 CFU/area. However, the number of bacteria on OHA/HA-ADH/O-HACC and HA/HA-ADH/N-HACC hydrogels was 0 CFU/area for *S. aureus* (Figure 5B). At 24 h, the bacterial growth in the OHA/HA-ADH hydrogel increased significantly, with the bacteria number calculated to be 204 CFU/area, whereas the number of bacteria in OHA/HA-ADH/O-HACC and HA/HA-ADH/N-HACC hydrogels was only 16 and 12 CFU/area, respectively. The results indicated that *S. aureus* on the surface of the hydrogels were significantly inhibited or killed by the antimicrobial hydrogels (Peng et al., 2010).

The Hydrogels Promote Seawater-Immersion Wound Healing

The effect of the hydrogels on wound healing was further evaluated *in vivo* by using an animal wound model with seawater immersion. Figure 6A shows representative images of the wound surface on days 0, 3, 7, 10, 14, and 21 for each group. The wound area in all five groups became larger before 3 days, and obvious inflammation was observed in the control and OHA/HA-ADH groups with seawater immersion at day 3. Though the wound bed was infected, the wound area in the OHA/HA-ADH, OHA/HA-ADH/O-HACC, and OHA/HA-ADH/N-HACC groups became smaller with increasing time after 3 days, scab formation was observed in all groups at day 7. At day 14, the wounds of the control and OHA/HA-ADH groups had not healed well, whereas the wounds of the OHA/HA-ADH/O-HACC and OHA/HA-ADH/N-HACC groups had healed significantly. It was found that the OHA/HA-ADH/O-HACC and OHA/HA-ADH/N-HACC hydrogels significantly promoted wound healing, which could be ascribed to the combined effects of the inherent antibacterial performance of O-HACC and N-HACC and the moist wound bed provided by the OHA/HA-ADH hydrogel dressing.

The wound area percentage of the different groups at days 0, 3, 7, 10, 14, and 21 is shown in Figure 6B. The control group without seawater immersion showed the lowest wound area percentage of the groups. At days 3, 7, 10, and 14, the wound area percentages of the OHA/HA-ADH/O-HACC and OHA/HA-ADH/N-HACC groups were significantly lower than those of the control group and OHA/HA-ADH group with seawater immersion, which indicated that the addition of the antibacterial material (O-HACC and N-HACC) could induce bacterial death and prevent further infection. The same trend is presented through a more intuitive three-dimensional view of the wound



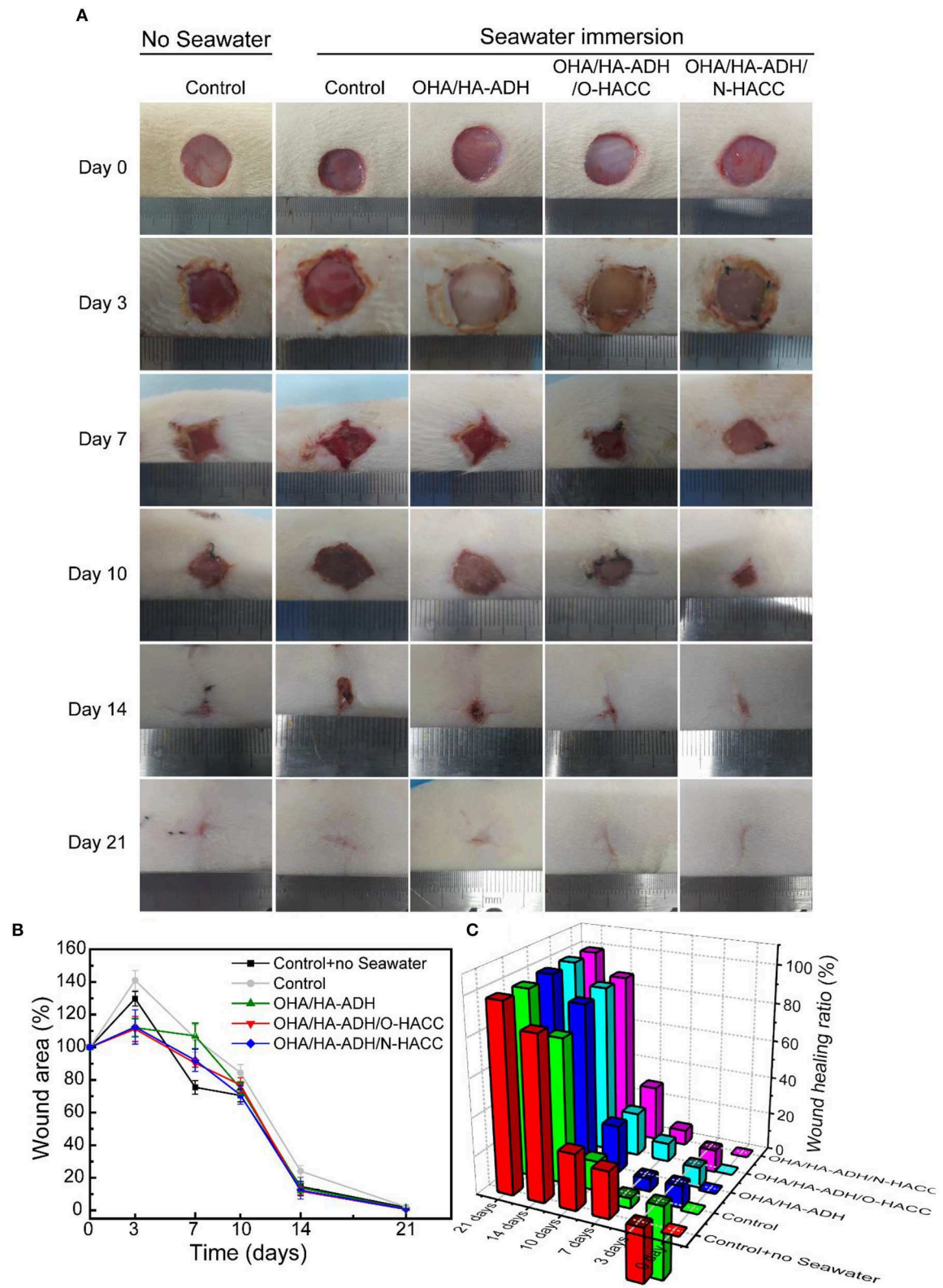


FIGURE 6 | (A) Photographs of wounds caused in the control group with or without seawater immersion and OHA/HA-ADH, OHA/HA-ADH/O-HACC, and OHA/HA-ADH/N-HACC groups with seawater immersion. **(B)** Percentage change in wound area, presented as mean \pm SD. **(C)** Wound healing ratio over a 21-day period.

healing rate in **Figure 6C**. In the results, OHA/HA-ADH/O-HACC and OHA/HA-ADH/N-HACC hydrogels can be seen to accelerate and promote wound closure and re-epithelialization on the seawater-immersed wound infection of full-thickness skin wounds. Moreover, the wound-healing effect of the OHA/HA-ADH/N-HACC group was better than that of OHA/HA-ADH/O-HACC, which might be attributable to the antibacterial effect of N-HACC being stronger than that of O-HACC.

Number of Bacteria on Wound

The bacterial count on seawater-immersed wound infections of full-thickness wounds was determined at day 3. The bacteria from the wound site tissues were cultured on three selected agar media for 24 h and were then counted for further

analysis (**Figure 7**). The results demonstrated that the number of bacteria on the seawater immersed wounds in the control group were approximately 6.2×10^8 CFU/wound for *E. coli*, 6.8×10^8 CFU/wound for *S. aureus*, and 2.3×10^8 CFU/wound for *P. aeruginosa*. However, the number of bacteria was significantly reduced in the OHA/HA-ADH/O-HACC group ($\sim 10^6$ CFU/wound for *E. coli*, 1.3×10^6 CFU/wound for *S. aureus*, and 2.7×10^6 CFU/wound for *P. aeruginosa*) and the OHA/HA-ADH/N-HACC group (3.0×10^6 CFU/wound for *E. coli*, 3.9×10^6 CFU/wound for *S. aureus*, and 1.6×10^6 CFU/wound for *P. aeruginosa*) at day 3. The results demonstrated that the bacteria in the wound site were inhibited or killed by the antimicrobial hydrogels. In addition, the antimicrobial hydrogels could accelerate skin wound closure and healing by

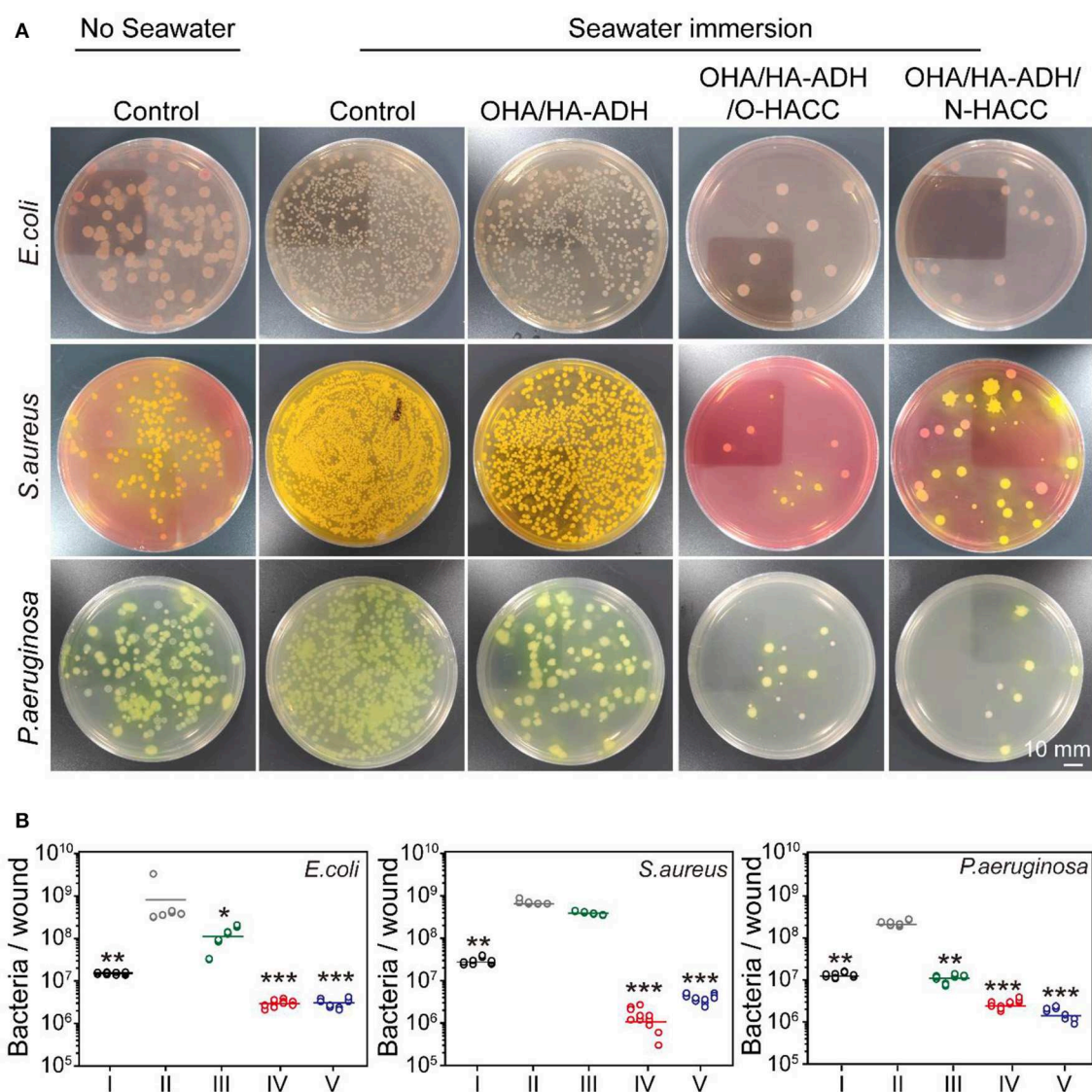


FIGURE 7 | (A) *E. coli*, *S. aureus*, and *P. aeruginosa* colonies from tissues formed on agar plates. A red ring-like morphology precipitating on VRBA-MUG selection medium means *E. coli*, a yellow-gold colony morphology on Mannitol salt agar indicates *S. aureus*, and a green-yellow colony morphology on *P. aeruginosa* selection medium represents *P. aeruginosa*. **(B)** Quantitative analysis of the number of bacteria remaining in the wound area. * $p < 0.05$, ** $p < 0.01$, *** $p < 0.001$.

reducing the bacterial counts in seawater-immersed wounds of rats.

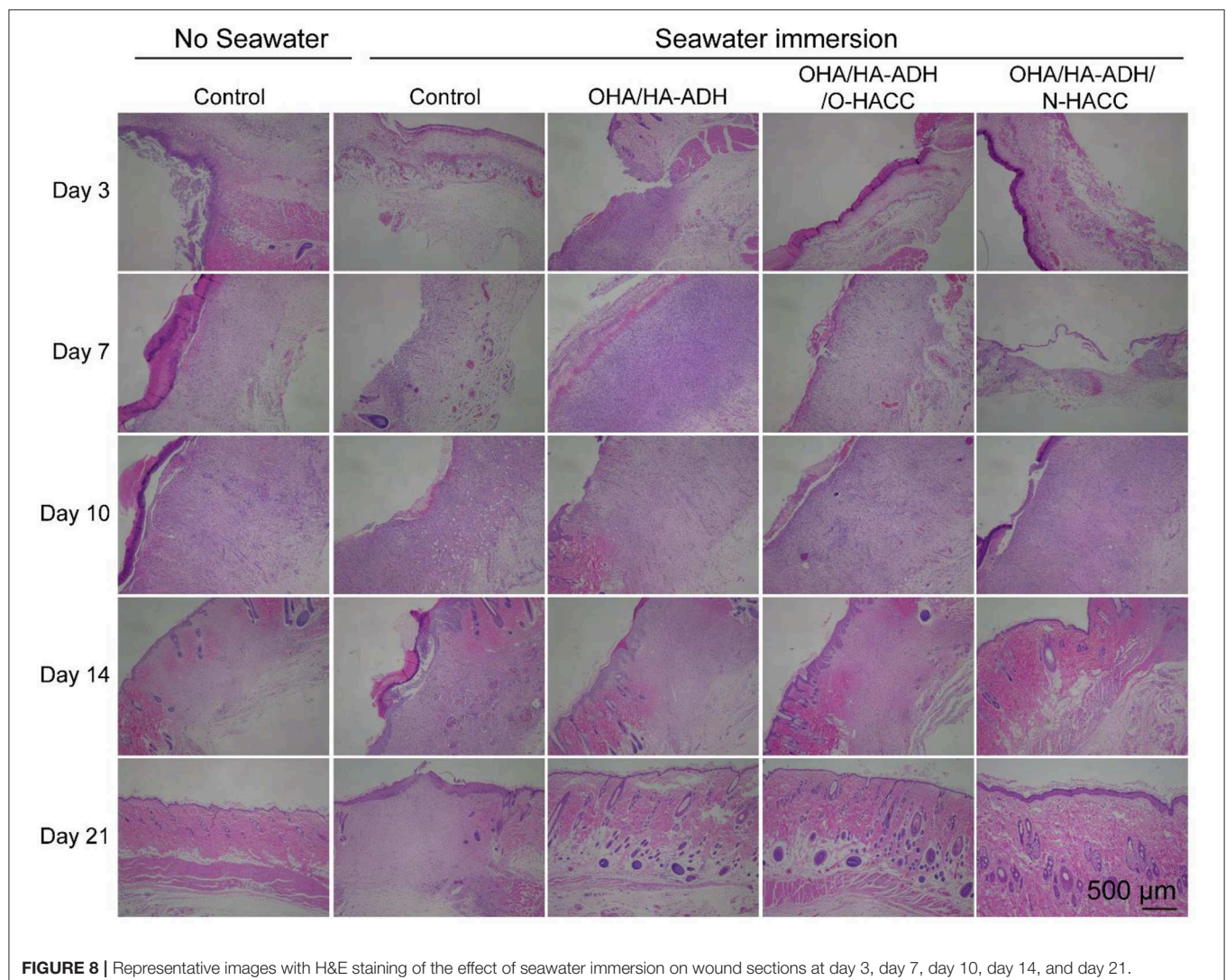
Histological Observations

The histologic structures of the regenerated dermis were stained with H&E to evaluate wound healing progress. The degrees of epithelial closure and granulation tissue formation in the different treatment groups were very pronounced (**Figure 8**). At day 3, a clear newly formed squamous epithelial layer was observed in OHA/HA-ADH/O-HACC and OHA/HA-ADH/N-HACC hydrogels, whereas the OHA/HA-ADH hydrogels and the control groups with seawater immersion showed an incomplete epidermal structure and a thinner dermal layer. In addition, obvious inflammatory cell infiltration was present in the wounds of the control group with seawater immersion on day 7, whereas the number of inflammatory cells on the OHA/HA-ADH/O-HACC and OHA/HA-ADH/N-HACC hydrogel groups was negligible (locally enlarged images of the tissue sections are shown in **Figure S2**). Remarkably, thick and well-formed

granulation tissue was apparent in the OHA/HA-ADH/O-HACC and OHA/HA-ADH/N-HACC hydrogel-treated group on day 10, indicating that the antimicrobial hydrogels could promote rapid wound healing. At day 14, the epidermis of the new granulation tissue was integrated and thick in both the OHA/HA-ADH/O-HACC and OHA/HA-ADH/N-HACC hydrogel groups. At day 21, the OHA/HA-ADH/O-HACC and OHA/HA-ADH/N-HACC hydrogel groups developed some newly formed hair follicles in the center of the wound, which were not seen in the control group with seawater immersion. However, with respect to the microstructure of regenerated tissues, a more complete re-epithelialization and tight junction between epidermis and dermis was found in the antimicrobial hydrogel groups, which were significant for functional and scar-free tissue recovery.

Collagen Deposition

In order to gain more insight into the granulation tissue, collagen deposition and maturation were further assessed in each group by Picrosirius red staining (**Figure 9A**). Ipp 6.0 software was used to



quantify the collagen deposition in the wound sites by calculating the intensity of the red areas in tissue area (**Figure 9B**). After 14 days of treatment, it can be seen that the OHA/HA-ADH/O-HACC and OHA/HA-ADH/N-HACC hydrogel groups not only had nearly twice as much collagen deposition as the other groups, as reflected by the Picrosirius red staining, but also had the most organized fibrous structure (local enlarged images of the wound sections are shown in **Figure S3**). In addition, at day 21, more mature fibers with regular orientation and distribution

were seen in the wound sites treated with OHA/HA-ADH/O-HACC and OHA/HA-ADH/N-HACC as compared to those treated with the control with seawater immersion. With further quantitative analysis, the collagen contents in the wounds treated with OHA/HA-ADH/O-HACC and OHA/HA-ADH/N-HACC hydrogel were significantly higher than those of the OHA/HA-ADH hydrogel and control group without seawater ($p < 0.01$) and the control group with seawater ($p < 0.001$) at day 14. The enhanced collagen deposition could be attributed to the

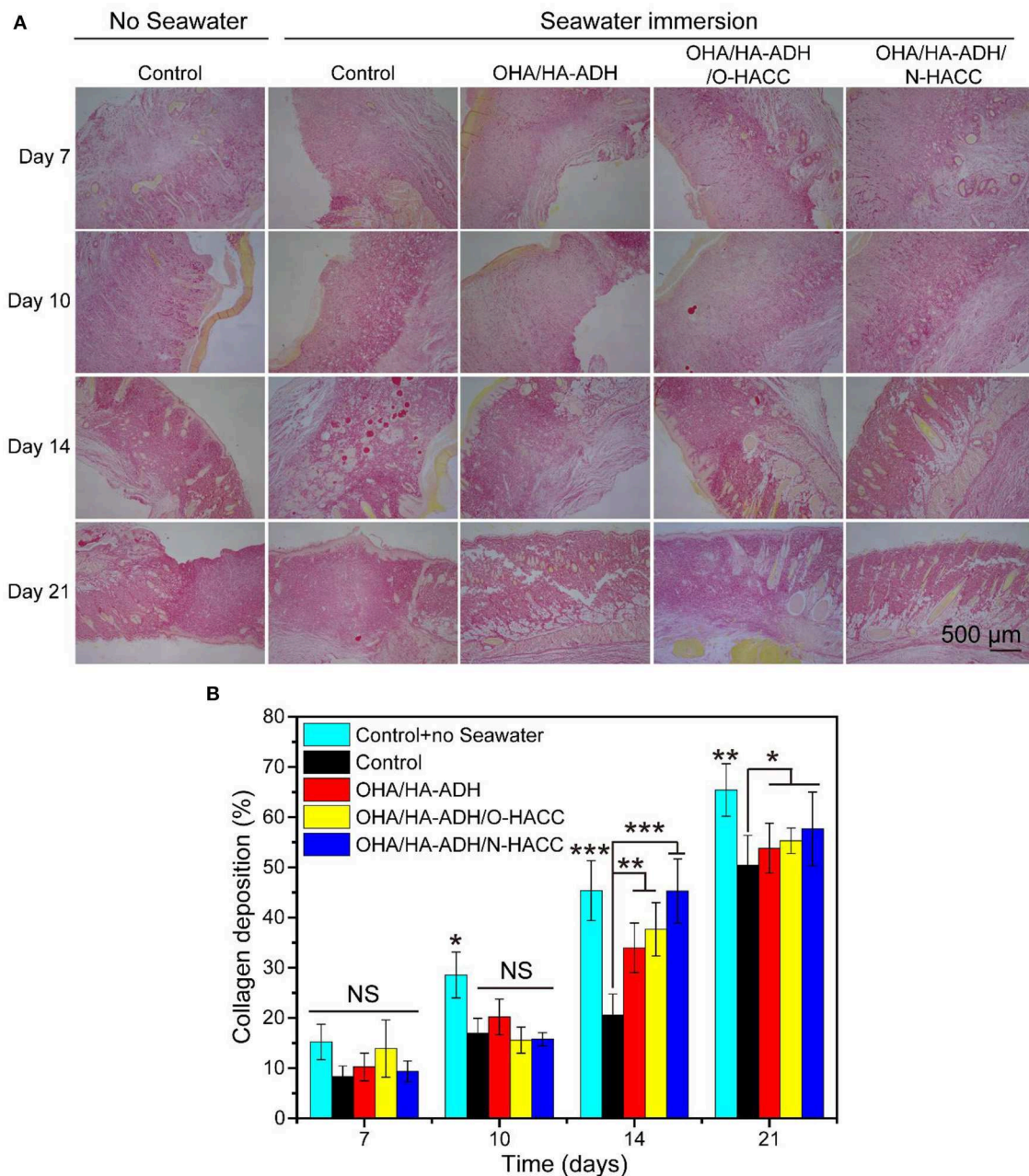


FIGURE 9 | Collagen deposition in wound sites. **(A)** Representative images of Sirius red staining in the control group with or without seawater immersion and the OHA/HA-ADH, OHA/HA-ADH/O-HACC, and OHA/HA-ADH/N-HACC groups with seawater immersion. **(B)** Quantitative analysis of collagen deposition in wound tissue. * $p < 0.05$, ** $p < 0.01$, *** $p < 0.001$.

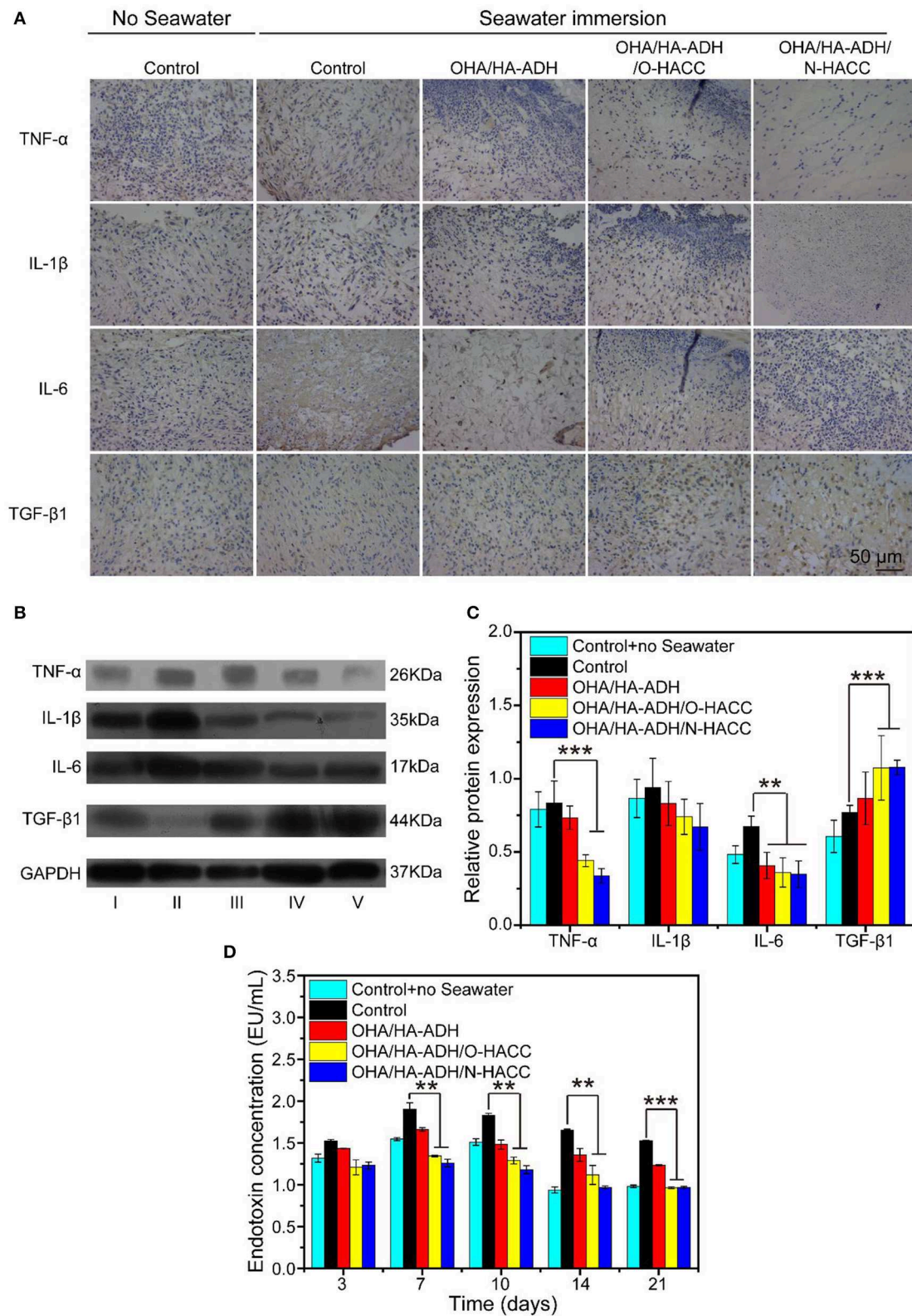


FIGURE 10 | (A) Representative images of immunohistochemistry pro-inflammatory factors (TNF- α , IL-1 β , and IL-6) and anti-inflammatory factors (TGF- β 1) of wound sections. **(B)** Western blot analyses were performed for TNF- α , IL-1 β , IL-6, and TGF- β 1. **(C)** Quantitative analysis of inflammatory factor. **(D)** Comparison of serum endotoxin concentration (EU/mL) in the different groups. ** p < 0.01, *** p < 0.001.

HA (which promotes collagen synthesis in fibroblasts) and the antibacterial properties of O-HACC or N-HACC (Kisiel et al., 2013; Hu et al., 2019).

Immunohistochemistry

The mechanism of the prepared hydrogel-promoted wound healing in the rat wound with seawater immersion model was explored by performing immunohistochemistry with pro-inflammatory factors (TNF- α , IL-1 β , and IL-6) and anti-inflammatory factors (TGF- β 1) in the wound (**Figure 10A**). The OHA/HA-ADH/O-HACC and OHA/HA-ADH/N-HACC hydrogel treatment decreased the expression level of pro-inflammatory factors (TNF- α , IL-1 β , and IL-6) at day 7. On the other hand, the expression level of the anti-inflammatory factors (TGF- β 1) was enhanced much more in the OHA/HA-ADH/O-HACC and OHA/HA-ADH/N-HACC hydrogel groups than in the OHA/HA-ADH hydrogel and control groups. The results indicated that OHA/HA-ADH/O-HACC and OHA/HA-ADH/N-HACC hydrogels reduced the expression of pro-inflammatory factors and increased that of anti-inflammatory factors in a wound with seawater immersion, which was important for the wound healing process. The Western blot analysis of TGF- β 1, TNF- α , IL-1 β , and IL-6 further supports these results, as less pro-inflammatory factors and more anti-inflammatory factors occurred in the antimicrobial hydrogel-treated wounds compared to the other groups (**Figures 10B,C**), which could be attributed to O-HACC and N-HACC being efficient inherently antibacterial materials capable of reducing infection (Qu et al., 2019).

Endotoxin Concentration

More specifically, the serum endotoxin levels of five groups were substantially elevated in the OHA/HA-ADH/O-HACC and OHA/HA-ADH/N-HACC groups compared to the control group with seawater (**Figure 10D**). The endotoxin concentration of the control group without seawater was about 1.0–1.5 EU/mL. However, the highest endotoxin concentration of the control group with seawater was about 1.5 EU/mL at day 3, 1.9 EU/mL at day 7, 1.8 EU/mL at day 10, 1.6 EU/mL at day 14, and 1.5 EU/mL at day 21. In addition, there was a significant decrease in endotoxin concentration in the OHA/HA-ADH/O-HACC and OHA/HA-ADH/N-HACC group compared to the control group with seawater ($P < 0.05$ at days 7, 10, and 14 and $P < 0.001$ at day 21), which was related to the bacteria numbers of their corresponding groups.

CONCLUSION

The aim of the present work was to develop biocompatible hydrogel wound dressings with inherent antibacterial properties. OHA/HA-ADH hydrogels with the addition of quaternized chitosan, OHA/HA-ADH/O-HACC and OHA/HA-ADH/N-HACC, were successfully prepared by dynamic Schiff base linkage. These hydrogels exhibited stable rheological properties, appropriate swelling properties, water vapor transmission rate, and biodegradability, inherent antibacterial properties, and good biocompatibility, meaning that they could effectively

promote the wound healing process. Furthermore, the hydrogels accelerated the healing process in a seawater-immersed full-thickness skin defect model *in vivo*, as well as exhibiting excellent reepithelialization and greater granulation tissue thickness, higher-density collagen deposition, a smaller number of bacteria, a lower endotoxin level, and more balanced inflammatory infiltration than control. In particular, by reducing wound healing process-related pro-inflammatory factors (TNF- α , IL-1 β , and IL-6) and upregulating anti-inflammatory factors (TGF- β 1) in wound, the OHA/HA-ADH/O-HACC and OHA/HA-ADH/N-HACC antibacterial hydrogels presented the best wound healing effect among all groups. All results demonstrated that OHA/HA-ADH/O-HACC and OHA/HA-ADH/N-HACC represent promising antimicrobial hydrogel wound dressings for wound healing application, especially for open and infected traumas, due to their good bioactivity and inherent antibacterial properties.

DATA AVAILABILITY STATEMENT

All datasets generated for this study are included in the article/**Supplementary Material**.

ETHICS STATEMENT

This animal study was reviewed and approved by the Institutional Animal Care and Use Committee (IACUC) of the General Hospital of the Southern Theater Command of the PLA.

AUTHOR CONTRIBUTIONS

RG and BC designed the experiments. XW and PX conducted most of the experiments and analyzed the data. ZY helped with cell experiments. QF and LF helped with animal experiments and *in vivo* characterization. XW, PX, RG, and BC wrote the manuscript.

FUNDING

This study was supported financially by the Natural Science Foundation of China (Nos. 81671924, 81571733, and 81272105), the National Key Research and Development Program of China (2017YFC1103301), the Science and Technology Program of Guangzhou (201508020253, 201508020115, 201604020094, 201601010270, 2017010160489, 201704030083, 201907010032, 201907010037), the Science and Technology Project of Guangdong Province (2014B020212010, 2015B020233012, 2017A010103009, 2017B020227009, 2015A010101313, 2017A050506011, 2017B090911012, 2018A050506021, 2018A050506019, 2018A050506040), the Military Medical Innovation Special Projects (18CXZ029), and the Joint Logistic Support Force Project (CWH17J023).

SUPPLEMENTARY MATERIAL

The Supplementary Material for this article can be found online at: <https://www.frontiersin.org/articles/10.3389/fbioe.2019.00360/full#supplementary-material>

REFERENCES

- Blacklow, S. O., Li, J., Freedman, B. R., Zeidi, M., Chen, C., and Mooney, D. J. (2019). Bioinspired mechanically active adhesive dressings to accelerate wound closure. *Sci. Adv.* 5:eaw3963. doi: 10.1126/sciadv.aaw3963
- Cai, X., Hu, S., Yu, B., Cai, Y., Yang, J., Li, F., et al. (2018). Transglutaminase-catalyzed preparation of crosslinked carboxymethyl chitosan/carboxymethyl cellulose/collagen composite membrane for postsurgical peritoneal adhesion prevention. *Carbohydr. Polym.* 201, 201–210. doi: 10.1016/j.carbpol.2018.08.065
- Chen, X. (2017). Making electrodes stretchable. *Small Methods* 1:1600029. doi: 10.1002/smt.201600029
- Chen, Y., Qiu, H., Dong, M., Cheng, B., Jin, Y., Tong, Z., et al. (2019). Preparation of hydroxylated lecithin complexed iodine/carboxymethyl chitosan/sodium alginate composite membrane by microwave drying and its applications in infected burn wound treatment. *Carbohydr. Polym.* 206, 435–445. doi: 10.1016/j.carbpol.2018.10.068
- Chin, W. G., Zhong, Q., Pu, C., Yang, W., Lou, P. F. D., Sessions, B., et al. (2018). A macromolecular approach to eradicate multidrug resistant bacterial infections while mitigating drug resistance onset. *Nat. Commun.* 9:917. doi: 10.1038/s41467-018-03325-6
- Chung, E. M. C., Dean, S. N., Propst, C. N., Bishop, B. M., and Hoek, M. L. V. (2017). Komodo dragon-inspired synthetic peptide DRGN-1 promotes wound-healing of a mixed-biofilm infected wound. *NPJ Biofilms Microbiomes* 3:9. doi: 10.1038/s41522-017-0017-2
- Gonzálezhenriquez, C. M., Sarabiavallejos, M. A., and Rodríguezhernandez, J. (2017). Advances in the fabrication of antimicrobial hydrogels for biomedical applications. *Materials* 10:232. doi: 10.3390/ma10030232
- Gopinath, D. M., Rafiuddin, A., Gomathi, K., Chitra, K., Sehgal, P. K., and Jayakumar, R. (2004). Dermal wound healing processes with curcumin incorporated collagen films. *Biomaterials* 25, 1911–1917. doi: 10.1016/S0142-9612(03)00625-2
- Hu, H., Yu, L., Tan, S., Tu, K., and Wang, L. Q. (2010). Novel complex hydrogels based on N-carboxyethyl chitosan and quaternized chitosan and their controlled *in vitro* protein release property. *Carbohydr. Res.* 345, 462–468. doi: 10.1016/j.carres.2009.11.029
- Hu, S., Cai, X., Qu, X., Yu, B., Yan, C., Yang, J., et al. (2019). Preparation of biocompatible wound dressings with long-term antimicrobial activity through covalent bonding of antibiotic agents to natural polymers. *Int. J. Biol. Macromol.* 123, 1320–1330. doi: 10.1016/j.ijbiomac.2018.09.122
- Jia, X., Colombo, G. R., Langer, R., and Kohane, D. S. (2004). Prolongation of sciatic nerve blockade by *in situ* cross-linked hyaluronic acid. *Biomaterials* 25, 4797–4804. doi: 10.1016/j.biomaterials.2003.12.012
- Julia, D., Andreas, K., Lena, M. L., George, K., Markus, M. W., Astrid, D., et al. (2013). Fully defined *in situ* cross-linkable alginate and hyaluronic acid hydrogels for myocardial tissue engineering. *Biomaterials* 34, 940–951. doi: 10.1016/j.biomaterials.2012.10.008
- Kaoru, M., Hiroshi, A., Shingo, N., Shin-Ichiro, N., Megumi, T., Motoaki, H., et al. (2010). Hydrogel blends of chitin/chitosan, fucoidan and alginate as healing-impaired wound dressings. *Biomaterials* 31, 83–90. doi: 10.1016/j.biomaterials.2009.09.031
- Kisiel, M., Martino, M. M., Ventura, M., Hubbell, J. A., Hilborn, J., and Ossipov, D. A. (2013). Improving the osteogenic potential of BMP-2 with hyaluronic acid hydrogel modified with integrin-specific fibronectin fragment. *Biomaterials* 34, 704–712. doi: 10.1016/j.biomaterials.2012.10.015
- Kowapradit, J., Opanasopit, P., Ngawhirunpat, T., Rojanarata, T., and Sajomsang, W. (2011). Structure–activity relationships of methylated -aryl chitosan derivatives for enhancing paracellular permeability across Caco-2 cells. *Carbohydr. Polym.* 83, 430–437. doi: 10.1016/j.carbpol.2010.08.005
- Kumar, A., Boyer, C., Nebhani, L., and Wong, E. H. H. (2018). Highly bactericidal macroporous antimicrobial polymeric gel for point-of-use water disinfection. *Sci. Rep.* 8:7965. doi: 10.1038/s41598-018-26202-0
- Li, M., Chen, J., Shi, M., Zhang, H., Ma, P. X., and Guo, B. (2019). Electroactive anti-oxidant polyurethane elastomers with shape memory property as non-adherent wound dressing to enhance wound healing. *Chem. Eng. J.* 375:121999. doi: 10.1016/j.cej.2019.121999
- Li, S., Dong, S., Xu, W., Tu, S., Yan, L., Zhao, C., et al. (2018). Antibacterial hydrogels. *Adv. Sci.* 5:1700527. doi: 10.1002/adv.201700527
- Li, Y., Han, M., Liu, T., Cun, D., Fang, L., and Yang, M. (2017). Inhaled hyaluronic acid microparticles extended pulmonary retention and suppressed systemic exposure of a short-acting bronchodilator. *Carbohydr. Polym.* 172:197. doi: 10.1016/j.carbpol.2017.09.038
- Li, Z., He, C., Yuan, B., Dong, X., and Chen, X. (2016). Injectable polysaccharide hydrogels as biocompatible platforms for localized and sustained delivery of antibiotics for preventing local infections. *Macromol. Biosci.* 17:1600347. doi: 10.1002/mabi.201600347
- Liang, Y., Zhao, X., Hu, T., Chen, B., Yin, Z., Ma, P. X., Guo, B. (2019b). Adhesive hemostatic conducting injectable composite hydrogels with sustained drug release and photothermal antibacterial activity to promote full-thickness skin regeneration during wound healing. *Small* 15:e1900046. doi: 10.1002/smll.201900046
- Liang, Y., Zhao, X., Ma, P. X., Guo, B., Du, Y., Han, X. (2019a). pH-responsive injectable hydrogels with mucosal adhesiveness based on chitosan-grafted-dihydrocaffeic acid and oxidized pullulan for localized drug delivery. *J. Colloid Interface Sci.* 536:224–234. doi: 10.1016/j.jcis.2018.10.056
- Lin, Z., Wu, T., Wang, W., Li, B., Wang, M., Chen, L., et al. (2019). Biofunctions of antimicrobial peptide-conjugated alginate/hyaluronic acid/collagen wound dressings promote wound healing of a mixed-bacteria-infected wound. *Int. J. Biol. Macromol.* 140, 330–342. doi: 10.1016/j.ijbiomac.2019.08.087
- Mohamed, R. R., Elella, M. H., and Sabaa, M. W. (2017). Cytotoxicity and metal ions removal using antibacterial biodegradable hydrogels based on N-quaternized chitosan/poly(acrylic acid). *Int. J. Biol. Macromol.* 98:302. doi: 10.1016/j.ijbiomac.2017.01.107
- Park, T. Y., Jeon, E. Y., Kim, H. J., Choi, B. H., and Cha, H. J. (2019). Prolonged cell persistence with enhanced multipotency and rapid angiogenesis of hypoxia pre-conditioned stem cells encapsulated in marine-inspired adhesive and immiscible liquid micro-droplets. *Acta Biomater.* 86, 257–268. doi: 10.1016/j.actbio.2019.01.007
- Peng, Z. X., Wang, L., Du, L., Guo, S. R., Wang, X. Q., and Tang, T. T. (2010). Adjustment of the antibacterial activity and biocompatibility of hydroxypropyltrimethyl ammonium chloride chitosan by varying the degree of substitution of quaternary ammonium. *Carbohydr. Polym.* 81, 275–283. doi: 10.1016/j.carbpol.2010.02.008
- Pires, N. R., Cunha, P. L. R., Maciel, J. S., Angelim, A. L., Melo, V. M. M., Paula, R. C. M. D., et al. (2013). Sulfated chitosan as tear substitute with no antimicrobial activity. *Carbohydr. Polym.* 91, 92–99. doi: 10.1016/j.carbpol.2012.08.011
- Purcell, B. P., Elser, J. A., Anbin, M., Margulies, K. B., and Burdick, J. A. (2012). Synergistic effects of SDF-1 α chemokine and hyaluronic acid release from degradable hydrogels on directing bone marrow derived cell homing to the myocardium. *Biomaterials* 33, 7849–7857. doi: 10.1016/j.biomaterials.2012.07.005
- Qu, J., Zhao, X., Liang, Y., Xu, Y., Ma, P. X., and Guo, B. (2019). Degradable conductive injectable hydrogels as novel antibacterial, anti-oxidant wound dressings for wound healing. *Chem. Eng. J.* 362:548–560. doi: 10.1016/j.cej.2019.01.028
- Qu, J., Zhao, X., Liang, Y., Zhang, T., Ma, P. X., and Guo, B. (2018). Antibacterial adhesive injectable hydrogels with rapid self-healing, extensibility and compressibility as wound dressing for joints skin wound healing. *Biomaterials* 183, 185–199. doi: 10.1016/j.biomaterials.2018.08.044
- Rakhshaei, R., and Namazi, H. (2017). A potential bioactive wound dressing based on carboxymethyl cellulose/ZnO impregnated MCM-41 nanocomposite hydrogel. *Mater. Sci. Eng. C Mater. Biol. Appl.* 73:456. doi: 10.1016/j.msec.2016.12.097
- Sarhan, W. A., Azzazy, H. M., and El-Sherbiny, I. M. (2016). Honey/chitosan nanofiber wound dressing enriched with allium sativum and cleome droserifolia: enhanced antimicrobial and wound healing activity. *ACS Appl. Mater. Interfaces* 8, 6379–6390. doi: 10.1021/acsami.6b00739
- Taichi, I., Yoon, Y., Highley, C. B., Evangelia, B., Benitez, C. A., and Kohane, D. S. (2007). The prevention of peritoneal adhesions by *in situ* cross-linking hydrogels of hyaluronic acid and cellulose derivatives. *Biomaterials* 28, 975–983. doi: 10.1016/j.biomaterials.2006.10.021
- Thanou, M., Florea, B. I., Geldof, M., Junginger, H. E., and Borchard, G. (2002). Quaternized chitosan oligomers as novel gene delivery vectors in epithelial cell lines. *Biomaterials* 23, 153–159. doi: 10.1016/S0142-9612(01)00090-4
- Thattaruparambil, R. N., Baranwal, G., Mavila, C. B., Biswas, R., and Jayakumar, R. (2016). Anti-staphylococcal activity of injectable nano

- tigecycline/chitosan-PRP composite hydrogel using drosophila melanogaster model for infectious wounds. *ACS Appl. Mater. Interfaces* 8, 22074–22083. doi: 10.1021/acsami.6b07463
- Travan, A., Scognamiglio, F., Borgogna, M., Marsich, E., Donati, I., Tarusha, L., et al. (2016). Hyaluronan delivery by polymer demixing in polysaccharide-based hydrogels and membranes for biomedical applications. *Carbohydr. Polym.* 150, 408–418. doi: 10.1016/j.carbpol.2016.03.088
- Wang, W., Liu, S., Chen, B., Yan, X., Li, S., Ma, X., et al. (2019). DNA-inspired adhesive hydrogels based on the biodegradable polyphosphoesters tackified by nucleobase. *Biomacromolecules* 20, 3672–3683. doi: 10.1021/acs.biomac.9b01446
- Wu, Y., Ling, W., Guo, B., Shao, Y., and Ma, P. X. (2016). Electroactive biodegradable polyurethane significantly enhanced Schwann cells myelin gene expression and neurotrophin secretion for peripheral nerve tissue engineering. *Biomaterials* 87, 18–31. doi: 10.1016/j.biomaterials.2016.02.010
- Xin, Z., Peng, L., Guo, B., and Ma, P. X. (2015). Antibacterial and conductive injectable hydrogels based on quaternized chitosan-graft polyaniline/oxidized dextran for tissue engineering. *Acta Biomater.* 26, 236–248. doi: 10.1016/j.actbio.2015.08.006
- Xu, R., Xia, H., He, W., Li, Z., Zhao, J., Liu, B., et al. (2016). Controlled water vapor transmission rate promotes wound-healing via wound re-epithelialization and contraction enhancement. *Sci. Rep.* 6:24596. doi: 10.1038/srep24596
- Xu, Z., Shi, L., Yang, M., Zhang, H., and Zhu, L. (2015). Fabrication of a novel blended membrane with chitosan and silk microfibers for wound healing: characterization, *in vitro* and *in vivo* studies. *J. Mater. Chem. B* 3, 3634–3642. doi: 10.1039/C5TB00226E
- Yang, Y., Bechtold, T., Redl, B., Caven, B., and Hong, H. (2017). A novel silver-containing absorbent wound dressing based on spacer fabric. *J. Mater. Chem. B* 5, 6786–6793. doi: 10.1039/C7TB01286A
- Yang, Z., Hideyoshi, S., Jiang, H., Matsumura, Y., Dziki, J. L., Lopresti, S. T., et al. (2018). Injectable, porous, biohybrid hydrogels incorporating decellularized tissue components for soft tissue applications. *Acta Biomater.* 73:112–126. doi: 10.1016/j.actbio.2018.04.003
- Ye, W., Yi, D., Wen, X., Ling, Y., Li, H., Wang, X., et al. (2014). Interface behavior of quaternized chitosan on cellulosic substrates. *Fibers Polym.* 15, 1450–1455. doi: 10.1007/s12221-014-1450-y
- Yi, X., He, J., Wang, X., Zhang, Y., Tan, G., Zhou, Z., et al. (2018). Tunable mechanical, antibacterial, and cytocompatible hydrogels based on a functionalized dual network of metal coordination bonds and covalent crosslinking. *ACS Appl. Mater. Interfaces* 10, 6190–6198. doi: 10.1021/acsami.7b18821
- Yildirim-Aksoy, M., and Beck, B. H. (2017). Antimicrobial activity of chitosan and a chitosan oligomer against bacterial pathogens of warmwater fish. *J. Appl. Microbiol.* 122:1570. doi: 10.1111/jam.13460
- You, J., Xie, S., Cao, J., Hao, G., Min, X., Zhang, L., et al. (2016). Quaternized chitosan/poly(acrylic acid) polyelectrolyte complex hydrogels with tough, self-recovery, and tunable mechanical properties. *Macromolecules* 49, 1049–1059. doi: 10.1021/acs.macromol.5b02231
- Zhang, J., Ma, Y., Liang, X., and Bing, S. (2017). Applications of vacuum sealing drainage in treating seawater-immersed sulfur mustard injury. *Toxicol. Env. Chem.* 99, 975–986. doi: 10.1080/02772248.2017.1338702
- Zhao, X., Wu, H., Guo, B., Dong, R., Qiu, Y., and Ma, P. X. (2017). Antibacterial anti-oxidant electroactive injectable hydrogel as self-healing wound dressing with hemostasis and adhesiveness for cutaneous wound healing. *Biomaterials* 122, 34–47. doi: 10.1016/j.biomaterials.2017.01.011
- Zhou, F., Hong, Y., Zhang, X., Yang, L., and Zhang, S. (2018). Tough hydrogel with enhanced tissue integration and *in situ* forming capability for osteochondral defect repair. *Appl. Mater. Today* 13, 32–44. doi: 10.1016/j.apmt.2018.08.005
- Zhu, H., Li, X., and Zheng, X. (2017). A descriptive study of open fractures contaminated by seawater: infection, pathogens, and antibiotic resistance. *Biomed Res. Int.* 2017:2796054. doi: 10.1155/2017/2796054
- Zhu, J., Li, F., Wang, X., Yu, J., and Wu, D. (2018a). Hyaluronic acid and polyethylene glycol hybrid hydrogel encapsulating nanogel with hemostasis and sustainable antibacterial property for wound healing. *ACS Appl. Mater. Interfaces* 10, 13304–13316. doi: 10.1021/acsami.7b18927
- Zhu, Q., Ming, J., Qiang, L., Yan, S., and Rui, G. (2018b). Enhanced healing activity of burn wound infection by dextran-HA hydrogel enriched with sanguinarine. *Biomater. Sci.* 6, 2472–2486. doi: 10.1039/C8BM00478A

Conflict of Interest: LF was employed by company Beogene Biotech Co.

The remaining authors declare that the research was conducted in the absence of any commercial or financial relationships that could be construed as a potential conflict of interest.

Copyright © 2019 Wang, Xu, Yao, Fang, Feng, Guo and Cheng. This is an open-access article distributed under the terms of the Creative Commons Attribution License (CC BY). The use, distribution or reproduction in other forums is permitted, provided the original author(s) and the copyright owner(s) are credited and that the original publication in this journal is cited, in accordance with accepted academic practice. No use, distribution or reproduction is permitted which does not comply with these terms.



Electrospun Nanofibrous Poly (Lactic Acid)/Titanium Dioxide Nanocomposite Membranes for Cutaneous Scar Minimization

Teresa C. O. Marsi^{1†}, Ritchelli Ricci^{1†}, Tatiane V. Toniato¹, Luana M. R. Vasconcellos², Conceição de Maria Vaz Elias³, Andre D. R. Silva⁴, Andre S. A. Furtado⁵, Leila S. S. M. Magalhães⁵, Edson C. Silva-Filho⁵, Fernanda R. Marciano⁶, Andrea Zille⁷, Thomas J. Webster⁸ and Anderson O. Lobo^{5*}

OPEN ACCESS

Edited by:

Ubaldo Armato,
University of Verona, Italy

Reviewed by:

Saeid Kargozar,
Mashhad University of Medical
Sciences, Iran
Ahmed El-Fiqi,
Dankook University, South Korea

*Correspondence:

Anderson O. Lobo
lobo@ufpi.edu.br

[†]These authors have contributed
equally to this work

Specialty section:

This article was submitted to
Biomaterials,
a section of the journal
Frontiers in Bioengineering and
Biotechnology

Received: 06 August 2019

Accepted: 29 November 2019

Published: 20 December 2019

Citation:

Marsi TCO, Ricci R, Toniato TV, Vasconcellos LMR, Elias CdMV, Silva ADR, Furtado ASA, Magalhães LSSM, Silva-Filho EC, Marciano FR, Zille A, Webster TJ and Lobo AO (2019) Electrospun Nanofibrous Poly (Lactic Acid)/Titanium Dioxide Nanocomposite Membranes for Cutaneous Scar Minimization. *Front. Bioeng. Biotechnol.* 7:421. doi: 10.3389/fbioe.2019.00421

¹ Institute of Research and Development, University of Vale Do Paraiba, São José dos Campos, Brazil, ² Department of Bioscience and Oral Diagnosis, Institute of Science and Technology, São Paulo State University, São Paulo, Brazil, ³ Scientific and Technological Institute, Brasil University, São Paulo, Brazil, ⁴ Air Force Academy, Brazilian Air Force, Pirassununga, Brazil, ⁵ LIMAV - Interdisciplinary Laboratory for Advanced Materials, Materials Science & Engineering Graduate Program, UFPI-Federal University of Piauí, Teresina, Brazil, ⁶ Department of Physics, Federal University of Piauí, Teresina, Brazil, ⁷ Department of Textile Engineering, Centre for Textile Science and Technology, University of Minho, Guimarães, Portugal, ⁸ Department of Chemical Engineering, Northeastern University, Boston, MA, United States

Poly (lactic acid) (PLA) has been increasingly used in cutaneous tissue engineering due to its low cost, ease of handling, biodegradability, and biocompatibility, as well as its ability to form composites. However, these polymers possess a structure with nanoporous that mimic the cellular environment. In this study, nanocomposites are prepared using PLA and titanium dioxide (TiO₂) (10 and 35%—w/w) nanoparticles that also function as an active anti-scarring agent. The nanocomposites were prepared using an electrospinning technique. Three different solutions were prepared as follows: PLA, 10% PLA/TiO₂, and 35% PLA/TiO₂ (w/w%). Electrospun PLA and PLA/TiO₂ nanocomposites were characterized morphologically, structurally, and chemically using electron scanning microscopy, transmission electron microscopy, goniometry, and X-ray diffraction. L929 fibroblast cells were used for *in vitro* tests. The cytotoxic effect was evaluated using 3-(4,5-dimethylthiazol-2-yl)-2,5-diphenyltetrazolium bromide assays. Versican (VCAN), biglican (BIG), interleukin-6 (IL6), interleukin-10 (IL-10), and type-1 collagen (COL1A1) genes were evaluated by RT-qPCR. *In vivo* tests using Wistar rats were conducted for up to 15 days. Nanofibrous fibers were obtained for all groups that did not contain residual solvents. No cytotoxic effects were observed for up to 168 h. The genes expressed showed the highest values of versican and collagen-1 ($p < 0.05$) for PLA/TiO₂ nanocomposite scaffolds when compared to the control group (cells). Histological images showed that PLA at 10 and 35% w/w led to a discrete inflammatory infiltration and expression of many newly formed vessels, indicating increased metabolic activity of this tissue. To summarize, this study supported the potential of PLA/TiO₂ nanocomposites ability to reduce cutaneous scarring in scaffolds.

Keywords: PLA, nanocomposites, electrospinning, cutaneous scarring, gene expression, *in vivo*

INTRODUCTION

The standard treatment for skin lesions uses dressings that come in direct contact with the injured region. By replacing these dressings with scaffolds, this treatment becomes non-invasive to minimally invasive along with other positive outcomes such as a reduction in patient recovery times, medical costs and consumption of scarce and valuable health-care resources around the world for treatment of large-scale musculoskeletal injuries with traumatic lesions, birth defects and surgical excisions (Bardosova and Wagner, 2015; Beyth et al., 2015; Walmsley et al., 2015; Ghannadian et al., 2018). Bioabsorbable and biodegradable polymers have been shown enough mechanical properties that accelerate the cell proliferation process while providing antimicrobial protection. This makes them promising materials for biomedical applications as they have been shown to optimize the tissue repair process which in turn speeds up patient recovery times (Simoes, 2011; Wang et al., 2014; Fonseca et al., 2015). Among the various polymers, poly (lactic acid) (PLA) has proven to be an ideal candidate material due to its mechanical properties, good biocompatibility, low cost, and the adjustable degradation profile with CO₂, H₂O (Hidalgo et al., 2013; Tawakkal et al., 2014; Annunziata et al., 2015; Toniatto et al., 2017) and polyester as by-products, either from the esterification of lactic acid and its fermentation (Toniatto et al., 2017).

PLA-based nanofibrous fibers have large surface areas, allowing them to interact with large volumes of other substances in their environment. This is a distinguishing feature of this material (Bayon et al., 2016; Toniatto et al., 2017; Salles et al., 2018). The fiber surfaces have several characteristics that make them similar to the extracellular matrices (ECMs) used in biomedical applications. In addition, the interaction of the cells and the substrate influences their morphology, proliferation, and viability (Braunger et al., 2017). ECMs have been assumed to be inert structures that consist of proteins and polysaccharides that are synthesized and secreted by cells. Their sole purpose was once considered to fill up extracellular space. However, recent research indicates that ECMs perform other key roles. They function as scaffolds, aid in cell binding, allow for tissue formation, and play an important role in the control of cell growth, differentiation, adhesion, migration, proliferation, and angiogenesis (Villarreal-Gómez et al., 2016; Saldin et al., 2017).

Studies have shown that titanium dioxide (TiO₂) nanoparticles are highly biocompatible and have good physical, chemical, mechanical, and biological properties. These nanoparticles have a variety of uses in many biomedical applications. One study found that they help increase protein absorption and reduce infections caused by both Gram-positive and Gram-negative bacteria (Roy et al., 2007; Liou and Chang, 2012; Kandiah et al., 2014; Wu et al., 2014; Toniatto et al., 2017).

Electrospinning of polymers can be used to generate three-dimensional fibrous structures and is therefore used to produce mats with these polymers. The electrospun mats closely resemble natural ECM (Villarreal-Gómez et al., 2016; Toniatto et al., 2017) and are capable of supporting cell adhesion and proliferation. Due to their inherent material properties, these mats not only

provide a three-dimensional structure but are also biocompatible, bioabsorbable, and have antibacterial properties, making them extremely desirable for use in scaffolds and medical devices (Roux et al., 2013; Stocco et al., 2018). PLA/TiO₂-nanofibrous fibers produced by electrospinning are being studied in order to evaluate their potential in dressing and wound healing applications (Bayon et al., 2016; Toniatto et al., 2017; Ghosal et al., 2018; Salles et al., 2018).

In prior studies, we have shown that PLA/TiO₂-based scaffolds have bactericidal properties and do not exhibit cytotoxicity (Toniatto et al., 2017). Here, we further evaluated the toxicity of electrospun PLA in fibroblast cells and rats (skin model) and compare the results when the material is embedded two different concentrations of TiO₂ nanoparticles PLA/TiO₂-10% w/w (PLA-A) and PLA/TiO₂-35% w/w (PLA-B). We also investigated their potential to upregulate specific genes related to the regenerative process. These electrospun scaffolds are biocompatible and showed no inflammations in rats. They were also found to have upregulated the versicam and type-1 collagen genes. These results provide a strong rationale to use PLA/TiO₂ scaffolds as dressings for skin lesion applications.

MATERIALS AND METHODS

Materials

Chloroform, N, N-diethylformamide (DMF), ethyl alcohol, Dulbecco's MEM (DMEM), Fetal Bovine Serum (FBS), 3-4,5-dimethylthiazol-2-yl-2,5-diphenyltetrazolol bromide, neutral buffered Formalin, Hematoxylin and Eosin were purchased from Sigma-Aldrich® (USA). PLA (2003D, with 4.30% of D-lactic acid monomer) was donated by NatureWorks (Minnetonka, Minnesota, United States). TiO₂ nanoparticles were donated by Evonik Degussa (AEROXIDE® TiO₂ P25, Essen, North Rhine-Westphalia, Germany). NCTC clone 929 (L CELL, L-929) cells were purchased from a bank cell in Rio de Janeiro, Brazil. 24-wells plates were purchased from Ciencor®. RNAeasy™ mini kit was purchased from Qiagen (São Paulo, Brazil). Versicam, biglicam, interleukins-6, interleukins-10, collagen-1 genes, complementary DNA (cDNA), RNA, and GoTaq® qPCR Master Mix amplifier kit were purchased from Promega (São Paulo, Brazil).

Electrospinning of PLA/TiO₂ Nanocomposite Membranes

Three types of solutions were prepared: PLA, PLA with 10% TiO₂ by weight, and PLA with 35% TiO₂ by weight. In the first step, 0.09 g of PLA was dissolved in 0.6 mL of chloroform at room temperature for about 150 min in closed system. Three sets of these PLA solution compositions were prepared. Afterwards in two separate containers, TiO₂ nanoparticles (0.01 and 0.05 g, respectively) were dispersed in 0.4 mL DMF using a tip ultrasound (Sonics, VCX 500) for ~90 min. A third container with 0.4 mL DMF was also prepared without the addition of TiO₂. Subsequently, each of the three DMF solutions (two of them containing TiO₂ of different concentrations, and one without TiO₂) was added to each of the three PLA solutions in chloroform and then stirred magnetically for 20 h in an enclosed system at

TABLE 1 | Description of produced solutions prior electrospinning process.

Scaffolds	PLA (g)	TiO ₂ (g)	Chloroform (mL)	DMF (mL)
PLA	0.09	–	0.6	0.4
PLA–A	0.09	0.01	0.6	0.4
PLA–B	0.09	0.05	0.6	0.4

room temperature. **Table 1** summarizes the masses and volumes of three prepared solutions. The electrospinning process was performed under a temperature and humidity-controlled exhaust hood (at a temperature of $25 \pm 2^\circ\text{C}$ and relative humidity of 30–40%). The electrospinning parameters/apparatus used were: 12 kV (Bertan 203R), syringe (5 mL, BD®), metal needle (23G, Inbras), infusion rate (0.05 mL/h), on a collector covered with aluminum foil ($100 \times 100 \times 1$ mm, at a distance of 10 cm) and total time of 30 min.

Characterization of Structural, Physical, and Chemical Properties

The samples were characterized after 24 h under vacuum. Scanning electron microscope (SEM, Zeiss EVO MA10) was used to analyze the morphology and determine the diameters of the fibers. To aid the analysis, a thin layer of gold (~ 10 nm thickness) was deposited using sputtering under an Argon plasma at a pressure of 0.2 mbar under an applied current of 30 mA for 2 min. The micrographs were obtained using magnifications of 500x, 1,000x, and 5,000x. Images were obtained using the SEM and analyzed using ImageJ software to establish the mean diameters for the fibers, and the mean and standard deviations of the data were calculated. Transmission electron microscopy (TEM, Philips CM120) was used to evaluate the homogeneity of the TiO₂ nanoparticles incorporated into the fibers. To perform the analysis, the fibers were collected for 5 s onto a copper transmission grid of 3.05 mm in diameter. The grid was positioned at a working distance of 10 cm, and the material was deposited for a few seconds, until a thin layer was formed on the grid.

A goniometer (Krüss DSA 100) operating in dynamic mode was used to measure the angle between the scaffolds and air using water and diiodomethane. Two microliters of deionized water was dropped on each scaffold and images were recorded after 1 min. This test was performed on 5 samples, and the mean and standard deviations for the results were calculated.

TGA measurements were carried out in a STA 7200 Hitachi (Tokyo, Japan). TGA plots were obtained within the range of 25 – 900°C under nitrogen atmosphere ($200 \text{ mL}\cdot\text{min}^{-1}$) at $10^\circ\text{C}\cdot\text{min}^{-1}$. Specimens were left at room temperature (25°C) until equilibrium was reached and placed in an aluminum pan. Data was plotted as weight loss percentage vs. temperature, and the mass of dried residues was calculated for each case. The derivative thermogravimetric (DTG) analysis was also performed to identify the maximum peaks of the thermal transformation events.

DSC analyses were carried out in a Mettler-Toledo DSC822 instrument (Giessen, Germany). Analyses were carried out in an aluminum sample pan under nitrogen atmosphere with a flow

rate of $20 \text{ mL}\cdot\text{min}^{-1}$ and heating rate of $10^\circ\text{C}\cdot\text{min}^{-1}$. In order to eliminate the thermal history of the material, the first heating cycle was obtained in the range of 0 – 110°C , afterwards it was cooled down to 0°C and heated again up to 500°C . The graph was plotted as heat flow vs. temperature.

The tensile strength, elongation at break and fracture strain of the nanofibers were measured using a texture analyzer (TA.XT plus, Stable Micro Systems Ltd., Vienna, UK). Rectangular samples of the polymeric scaffolds were specifically cut to have dimensions of $10.00 \times 30.00 \times 0.10$ mm and fixed with the probe provided by instrumentation attached to a 5 kg load cell. Measurements were recorded at 25°C with a strain rate of $1 \text{ mm}\cdot\text{min}^{-1}$ ($N = 3$).

X-ray diffraction (XRD) (PANalytical X'Pert Pro diffractometer) using a monochromatic X-Ray CuK α radiation, was used to study the crystalline structure of the samples. Data were collected over a range of 10 – 80° using a scanning speed of 0.08 degrees per minute. Data was analyzed using HighScore 3.0a software (PaNalytical, Almelo, Netherlands) for phase identification. The crystalline index was calculated as the ratio of the crystalline scattering fraction to the total crystalline and amorphous scattering.

Biomedical Characterizations of PLA/TiO₂ Nanocomposite Membranes

Prior to performing any biological assay, the samples were vacuum dried. For the biological assays, L929 fibroblasts cells were cultured in Dulbecco's Modified Eagle's Medium supplemented with fetal bovine serum (90:10 v/v) and kept in a 5% CO₂ atmosphere at 37°C for 7 days to obtain a confluence layer. The polymer sheets were sterilized in ultraviolet radiation and then placed in 70% ethyl alcohol, washed with phosphate-buffered saline, and hydrated with the DMEM/FBS medium prior to use in the biological assays (Lobo et al., 2008).

A 3-(4,5-dimethylthiazol-2-yl)-2,5-diphenyltetrazolium bromide (MTT) assay was used to analyze the scaffold (PLA only, PLA–A, and PLA–B) scaffolds for cytotoxicity. Twenty thousand cells were plated in a 24-well plate. After 24 h, a 10×10 mm square piece of each of the scaffold types was placed on separate plates. After both 24 and 168 h, $100 \mu\text{L}$ MTT (1 mg/mL) was added to the culture medium in each well. The plate was then covered with an aluminum foil and incubated for 2 h in an oven with a consistent a 5% CO₂ atmosphere and 37°C temperature (Lobo et al., 2008). The MTT was then removed and $100 \mu\text{L}$ of dimethyl sulfoxide (DMSO) was added in each sample. The absorbance was then measured using a spectrophotometer (570 nm wavelength; instrumentation by AsysHitech GmbH, Eugendorf, Austria). Cells were used as negative controls and latex fragments (10×10 mm) as positive controls for cytotoxicity tests. To normalize the results, the absorbance of a blank sample and DMSO were also measured. Gene expression analysis by RT-qPCR, and extraction of total RNA from adhered cells on scaffolds were performed after 7, 14, and 21 days. Versicam, Biglicam, interleukins-6, interleukins-10, and collagen-1 (COL1A1) genes were expressed upon performing RT-qPCR. The integrity of the RNA was evaluated using agarose

TABLE 2 | Description of the gene used in RT-qPCR.

Gene	Gene name	Primer sequences	Ref. Fast Pubmed
VCAN	Versicam	5'-CAAACCTGCCTCAACGGAGG-3' 5'-CCTTCAGCAGCATCCCATGTGCGT-3'	NM_001101
BGN	Biglycan	5'-GATGGCCTGAAGCTCAA-3' 5'-GGTTGTTGAAGAGGCTG-3'	NM_199173
COL1A1	Type I Collagen alpha 1	5'-CCCTGGAAAGAATGGAGATGAT-3' 5'-ACTGAAACCTCTGTGTCCTTCA-3'	NM_000088.3
IL6	Interleukin 6	5'-AGCCAGAGCTGTGCAGATGA-3' 5'-GCAGGCTGGCATTGTGGTT-3'	NM_031168.2
IL-10	Interleukin 10	5'-AGCCAGCAGCTCTCAAGTC-3' 5'-GTGTTCACTGTGGTCTGGAT-3'	NM_010548.2

gel electrophoresis (1.5%) and analyzed using the 18S and 28S bands. Thereafter, the outer diameter was measured (at 260 and 280 nm wavelengths using Nano Drop 2000 manufactured by Thermo Fisher) and the concentration and purity of the RNA sample was determined. Values A260/A280 between 1.8 and 2.0 were accepted. For the synthesis of deoxyribonucleic acid (cDNA), 2.0 µg of RNA obtained via reverse transcription was used following the manufacturer's instructions. The cDNA was amplified and an ABI PRISM 7500 sequence detector (Applied Biosystems, USA) was used for quantitative analysis of the gene expression. The primers analyzed are listed in **Table 2**. The conditions/parameters applied during this analysis were 95°C (for 5 min), 40 cycles of 15 min each at 95°C, 60°C (for 1 min), and a final cycle of 5 min at 72°C. Each experiment was repeated three times and the data was normalized according to the expression of the reference gene using the selection of the most appropriate endogenous control. Three reference genes were used: Glyceraldehyde 3-phosphate dehydrogenase (GAPDH), ribosomal 18S RNA (18SrRNA), and beta-actin (β-actin); β-actin was the preferred reference gene. The $\Delta\Delta C_t$ method acquires average cycle limit values (Cts) of the target genes and compares them with the Cts of the average reference gene. Relative gene expression was calculated using the $2^{-\Delta\Delta C_t}$ method (Livak and Schmittgen, 2001).

The RNA samples were analyzed using the NanoDrop ND-1000 spectrophotometer (Thermo Fisher Scientific, USA) at wavelengths of 260 nm for RNA and 280 nm for the protein.

The primers were designed with the aid of the RTD program (Integrated DNA Technologies, www.idtdna.com) and Primer 3 software (frodo.wi.mit.edu/cgi-bin/primer3/primer3_www.cgi).

Experimental Model—*in-vivo*

All *in-vivo* procedures were performed in accordance with ethical standards. The testing protocol was approved by the Brazilian committee (10/2015-CEUA/ICT/CJSC-UNESP). Six male Wistar rats (*Rattus norvegicus*) aged 90 days and weighing between 350 and 400 g were used. The animals were provided with food and water *ad libitum*. The PLA, PLA—A, and PLA—B samples were implanted in the rat dorsal subcutaneous tissue ($n = 2$). The apparatus was cleaned using 70% ethanol and sterilized for

2 h using UV radiation and surgically inserted using procedures described in Camargo et al. (2010). The rats were euthanized 15 days after the surgery.

For histological analysis, a 10% neutral buffered formalin was applied on the surgical sites. After 48 h, the specimens were processed using paraffin embedding. The paraffin block was oriented parallel to the long axis of the material, and serial sections of 5 µm thickness were cut. These sections were then stained with hematoxylin and eosin. Histological qualitative evaluation was conducted using microscopic analysis.

Statistical Analysis

A sample size of 5 has been used in this study. The data was analyzed using two-way analysis of variance (ANOVA) followed by a Tukey's test (GraphPad Prism software, v. 5.01). A value of $p < 0.05$ was considered statistically significant.

RESULTS

Characterization of the Electrospun Scaffolds

Figures 1A–C shows SEM micrographs of PLA, PLA—A, and PLA—B nanofibrous scaffolds, respectively. The homogeneity of the nanofibers can be observed; the diameters of the nanofibers appear to be similar and they no obvious deformation and free of beads. The mean values of the diameters of the nanofibers in the samples of PLA with 10 and 35% TiO₂ were 332 ± 108 and 332 ± 95 nm, respectively—slightly larger than that observed in the PLA sample without TiO₂ (315 ± 87 nm). The images obtained by TEM showed that TiO₂ nanoparticles were homogeneously dispersed within the PLA fibers at both the concentration levels of 10 and 35%—w/w (**Figures 1B.1,C.1**). **Figure 1D** shows contact angle measurement using water. It can be observed that incorporation of TiO₂ nanoparticles causes an observable decrease in the contact angle. The PLA, PLA—A, and PLA—B samples had contact angles of 160.0 ± 3.0 , 140.0 ± 2.1 , $130.0 \pm 2.2^\circ$, respectively. XRD measurements showed that TiO₂ has a different growth process in the single crystalline phase corresponding to the anatase phase (**Figure 1E**). The preferred orientation plane is the crystalline plane (101) around of $2\theta = 25^\circ$, which is typical of the anatase phase and the rutile phase, indicating a high purity of the material. This is confirmed by the peaks, $2\theta = 37, 49, 54, 56, 63, 70$, and 76° at the corresponding crystallographic planes (1 0 3), (2 0 0), (2 1 1), (2 1 1), (2 0 4), (1 1 6), and (2 1 5) (Dinari and Haghighi, 2017; Pava-Gómez et al., 2018). The peaks at 25, 37, and 49° are characteristic of TiO₂ and are clearly observed when they are part in the fibers. The intensity of the XRD peaks was lower in the samples that contained the TiO₂ than in those without TiO₂ (**Figures 2A.1–A.3**). The measured crystalline index was 89, 87, and 82% for PLA, PLA—A, and PLA—B samples, respectively.

Figure 2 shows deconvolutions obtained from XRD, as shown in **Figure 1E**. The amplitude of the peak found between 16.45 and 16.80° was used to determine the proportion of pure PLA scaffold area. It was found that for the PLA membranes (**Figure 2A.1**), PLA—A membranes (**Figure 2A.2**), and PLA—B membranes (**Figure 2A.3**) had 60.2, 51.45, and 44.38% of

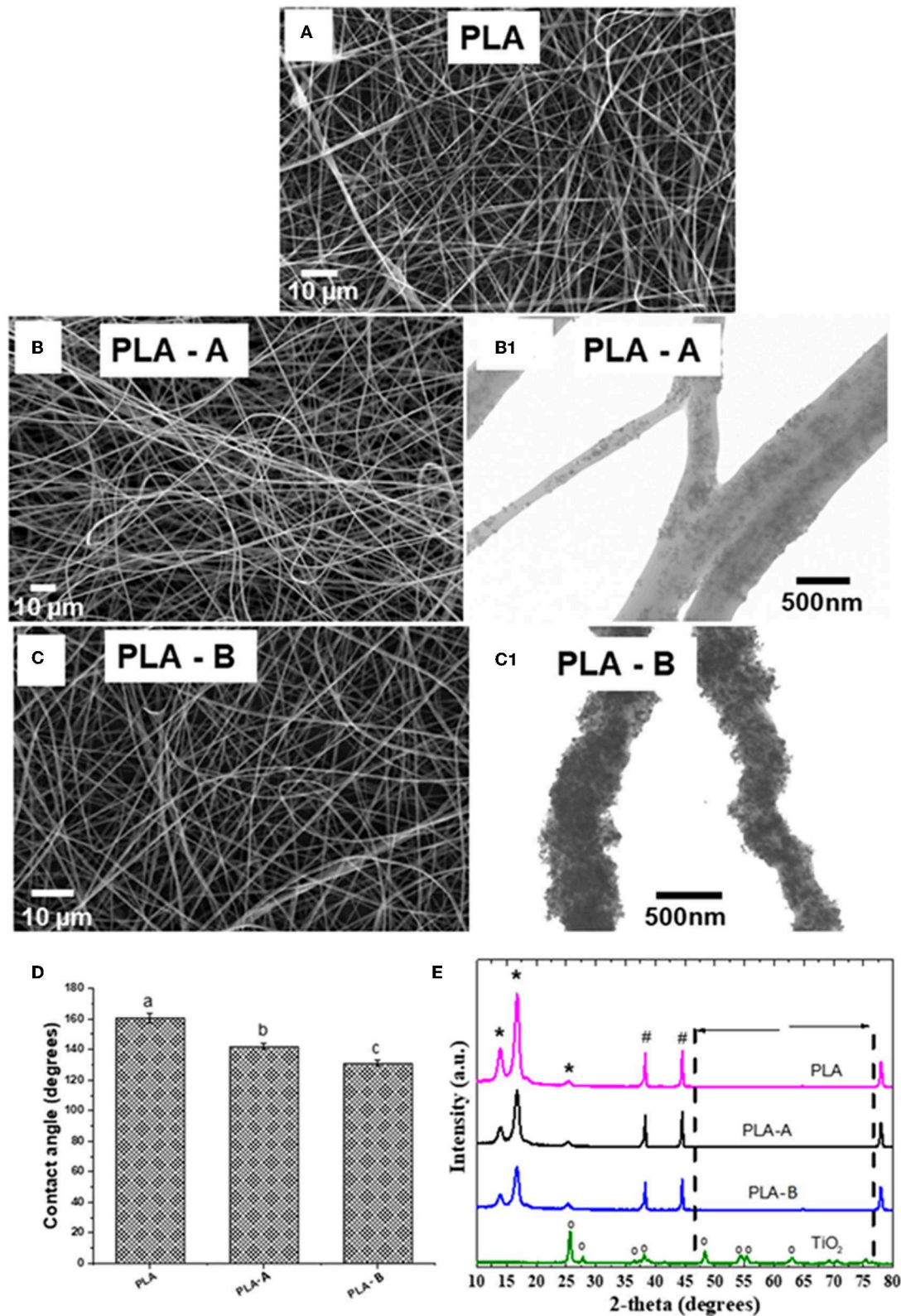


FIGURE 1 | (A) Micrograph for PLA fiber without TiO₂ addition; micrographs of polymer solutions with **(B)** PLA-A; **(C)** PLA-B. **(D)** Contact angles measured. **(E)** XRD of the developed membrane. Images obtained by TEM **(B.1)** PLA-A, **(C.1)** PLA-B. * and # referred to typical PLA crystalline planes. ° referred to typical TiO₂ crystalline planes.

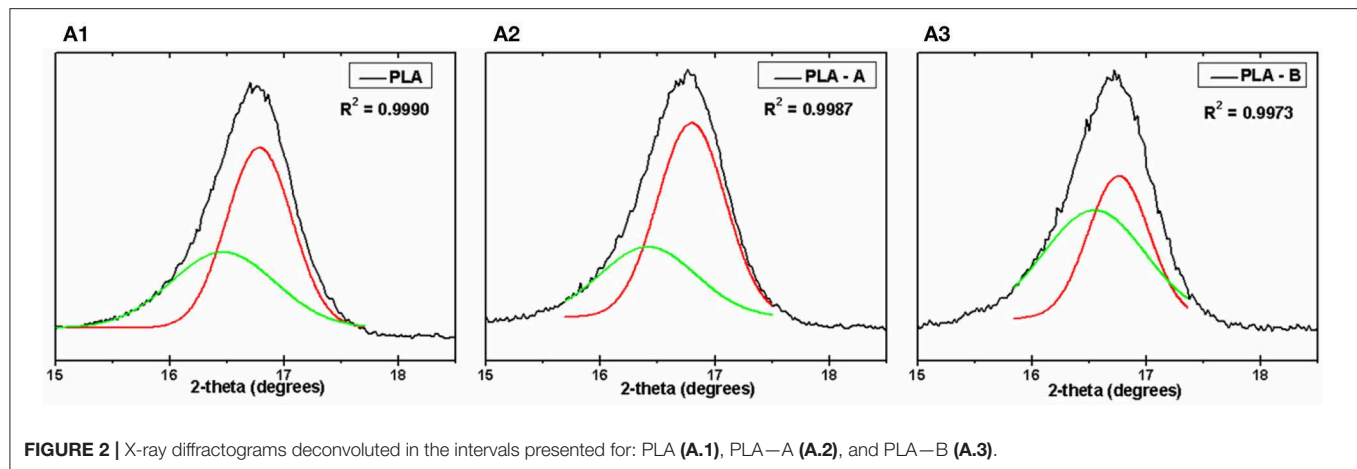


FIGURE 2 | X-ray diffractograms deconvoluted in the intervals presented for: PLA (A.1), PLA-A (A.2), and PLA-B (A.3).

TABLE 3 | Main DSC thermal transitions ($n = 3$; S.D. < 1%), TGA mass loss temperature peaks and residual weight (R_w) at 900°C of samples ($n = 3$; \pm S.D.).

Sample	T_{Onset} (°C)	T_{Peak} (°C)	T_{Endset} (°C)	ΔH (J g ⁻¹)	T_g (°C)	DTG T_{Max} (°C)	R_w 900°C (%)	R_w 900°C (mg/mg)
PLA	132.8	154.9	170.1	57.7	55.3	326.6 \pm 2.6	0	7.2/0
PLA-A (1st peak)	146.6	157.4	163.3	44.8	61.8	354.8 \pm 5.6	5.0 \pm 0.6	8.95/0.45
PLA-A (2nd peak)	308.1	350.5	364.4	638.8				
PLA-B (1st peak)	148.6	157.6	162.9	35.6	65.8	354.9 \pm 2.2	28.2 \pm 0.4	8.15/2.30
PLA-B (2nd peak)	330.8	356.8	368.8	540.2				

pure PLA membranes area respectively. Diffractogram fitting was performed in order to quantify the percentage of area formed under the curve where the characteristic PLA peaks are identified. For this, the deconvolution method with Gaussian function was used in a software Origin 8.0, obtaining curves with $R^2 = 0.99$. The study of this device has been used as a tool in several works of our research group (Silva et al., 2018, 2019a,b).

Table 3 and **Figure 3** display the result of the thermal characterization of the sample containing TiO₂ nanoparticles. The TGA result shows that the degradation temperature of the composite nanofiber (peak around 355°C against the peak at 326.6°C of the pure PLA) is significantly affected by the presence of TiO₂ but not by its concentrations in the polymer matrix (Laske et al., 2015; Wacharawichanant et al., 2017; Anžlovar et al., 2018). It is clear from **Table 3** that the residual weight expressed in mg/mg is proportional to the TiO₂ content on the PLA electrospun nanofibers.

The DSC results display a glass transition temperature (T_g) and two endothermic peaks in the second heating cycle. The T_g (**Figure 3B** inset) increase with the amount of TiO₂ in the PLA matrix from the 55.4°C of pure PLA to the 61.8°C of PLA-A and 65.8°C of PLA-B. The first peak, attributed to the melting point of PLA, is slightly affected by the presence of the nanoparticles (peak around 157.5°C against the peak at 154.9°C of the pure PLA). The second one, attributed to the PLA degradation, has sharper peaks and shifts to a higher temperature in the presence of TiO₂. The introduction of higher concentration of TiO₂ in the PLA structure significantly decreases the melting enthalpy of both peaks.

The **Figure 4** illustrates the mechanical properties (FS, EM, and TS) of PLA/TiO₂ nanofibers with different TiO₂ contents. As can be seen, the mechanical properties of the scaffolds were affected by the addition of TiO₂. There is an increase in the value of these properties for PLA-A and subsequently a reduction for PLA-B. The changes in evaluated values are summarized in **Table 4**.

Cytotoxicity and Gene Expression Analyses

Cytotoxicity studies were performed at two different time points (24 and 168 h) and the analyzed groups were compared to a positive control (latex, **Figure 5A**). The expression of the genes of interest was studied using RT-qPCR from cDNA obtained by the reverse transcription of mRNA obtained from the fibroblast lineage. Before initiating the RT-qPCR reactions, expression of these genes was analyzed by semi-quantitative or end-point RT-PCR to ensure they were expressed (data not shown). The expression of extracellular matrix Versicam, Biglicam type 1 collagen, interleukins-6, and interleukins-10 were analyzed. It was observed that the expression of Versicam increased when L929 fibroblast cells were cultivated on PLA and PLA-A and PLA-B when compared to the control (only cells, $p < 0.05$, **Figure 5B**). Meanwhile, over expression of type I collagen (COL-1) occurred in the fibroblastic cells in contact when cultivated on PLA and PLA-A and PLA-B ($p < 0.05$, **Figure 5C**). No statistical differences were observed when the expressions of interleukins-6 and -10 were analyzed (**Figure 5D**).

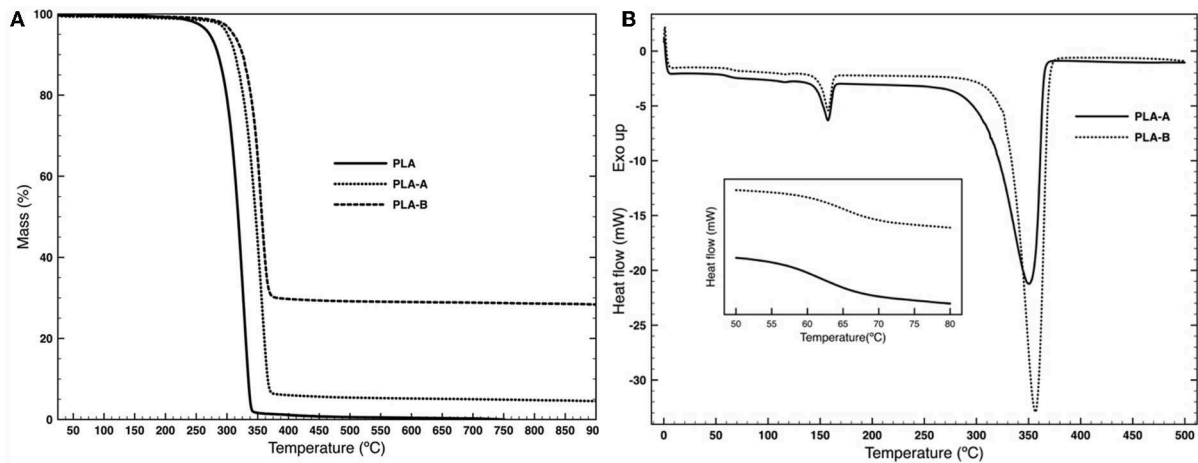


FIGURE 3 | (A) TGA curves from 25 to 900°C performed at a heating rate of 10°C min⁻¹ under nitrogen atmosphere with a flow rate of 20 mL min⁻¹ and **(B)** DSC thermogram from 0 to 500°C and the glass transition region between 40 and 80°C (inset) performed at a heating rate of 10°C min⁻¹ under nitrogen atmosphere with a flow rate of 20 mL min⁻¹ of the PLA/TiO₂ samples.

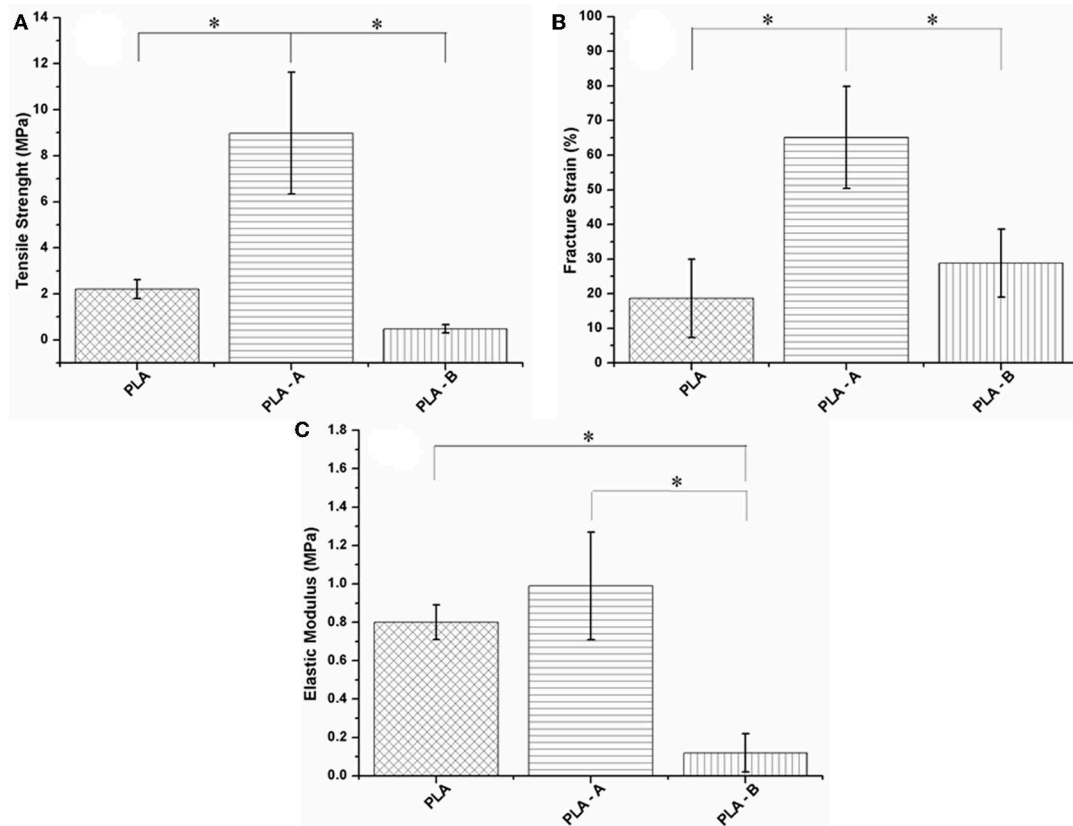


FIGURE 4 | (A) Variation in tensile strength (TS), **(B)** fracture strain (FS), and **(C)** elastic modulus (EM) of PLA nanofibers. Statistical test: One-way ANOVA followed by post-test multiple Tukey comparisons **P* < 0.05.

Histological Analysis

The groups were compared qualitatively to check for similar histological aspects. The figures show an overview of the control material and nanocomposites.

Clinically, the animals showed no signs of infection, and no foreign body reaction was observed under a microscope (**Figures 6–8**). A capsule of connective tissue was observed around the membranes of all the three types, indicating a close

TABLE 4 | Mechanical properties analysis of PLA—A and PLA—B over neat PLA scaffolds.

Scaffolds	Fracture strain (%)	Elastic modulus (MPa)	Tensile strength (MPa)
PLA	18.59	0.80	2.20
PLA—A	+250%	+23%	+308%
PLA—B	+55%	−85%	−78%

contact between the material and the surrounding connective tissue. The presence of discrete inflammatory infiltrate was also observed. However, the histological sections of PLA—A (**Figure 7**) and PLA—B (**Figure 8**) showed the newly formed vessels, suggesting a higher rate of metabolic activity in this tissue (compared to control, **Figure 6**). These observed differences are positive events that occurred in the regenerative process, influenced by presence of PLA/TiO₂ membranes.

DISCUSSION

None of the electrospun membranes showed beads formation, indicating that the work distances and applied voltage were appropriately chosen (Schuster et al., 2003). It was also observed that the solvents had completely evaporated during the electrospinning process, resulting in fiber diameters with little variation (Schuster et al., 2003; Efron and Moldawer, 2004; Zhang and An, 2007). The decision to keep the membranes for 15 h in a vacuum chamber resulted in the elimination of any residual liquid present in the nanofibers (Efron and Moldawer, 2004; Zhang and An, 2007). The incorporation of TiO₂ nanoparticles also did not promote bead formation, as seen in **Figures 1A–C**, indicating that our strategy to disperse these particles using ultrasound resulted in homogeneous dispersion of TiO₂ nanoparticles inside PLA fibers—as seen in **Figures 1B.1,C.1**—without inhibiting the PLA behavior—as shown by the XRD images (**Figure 1E**). A discrete reduction in contact angle was observed while using water when TiO₂ nanoparticles were incorporated into the PLA (**Figure 1D**). The XRD deconvolution analysis showed that the addition of TiO₂ interrupted the arrangement in the PLA polymer backbone by modifying its crystallinity (Baskaran et al., 2006). This intensity was assessed by deconvolutions of the XRD of **Figure 2A**. Crystallinity plays a very important role in the physical properties of biodegradable polymers—especially the thermal and mechanical behavior—and also affects their biodegradability (D'amico et al., 2016). The addition of 10 and 35% w/w of TiO₂ on the PLA matrix resulted in a significant decrease of crystallinity index of about 2 and 8%, respectively. Electrospun PLA exhibited two α crystal reflection peaks at 14.0 and 16.8° and a small phase peak at 25.0° due to the high degree of deformation that the electrospinning process causes to the material (**Figure 1E**). The positive shift of higher values of 2θ and the high degree of crystallinity of the of the electrospun nanofibers of PLA compared to the PLA films can be ascribed to the higher stretching of the polymer chains resulting in higher

degree of molecular organization (Oliveira et al., 2013; Farid et al., 2018).

Thermogravimetric analysis (**Figure 3A**) showed that the degradation of PLA containing TiO₂ nanoparticles takes place in a well-defined single step with a derivative thermogravimetric (DTG) temperature peak at around 355°C (**Table 3**) with significant differences between nanoparticles content and pure PLA that showed a lower degradation peak at around 327°C in accordance with the DSC results (Mofokeng and Luyt, 2015; Zhang et al., 2015). After degradation, the weight remained constant until 900°C and leading to a residue content in function of the TiO₂ concentration (**Table 3**). PLA lead to a 0% residue at this temperature as previously observed (Virovska et al., 2014). With an increase of TiO₂ on the PLA nanofibers, there was an increase in residue produced which supports the presence of the nanoparticles in the nanospun fibers structure (Costa et al., 2013).

During the cooling cycle in the DSC analysis, no crystalline structures or other transitions appeared (data not shown). The DSC thermogram during the second heating shows two endothermic peaks at 157 and 350°C, indicating the melting and degradation peaks of PLA, respectively (Gupta et al., 2007). The inclusion of TiO₂ showed small differences in the melting peak (157°C) compared to the pure PLA (155°C). However, comparing the 10 and 35% TiO₂ containing PLA nanofibers, the degradation peak displayed a slight increase (from 351 to 357°C) and a large positive shift of around 20°C in the onset temperature (from 308 to 331°C). The Tg of PLA nanofibers showed a significant increase with the addition of TiO₂ in the polymer matrix (**Table 3**). This suggests an interaction between TiO₂ and PLA matrix (Zdraveva et al., 2018; Kaseem et al., 2019). These interactions restrict the mobility of the molecular chains in the PLA amorphous segments enhancing the cooperative motions of the chains which require much more activation energy to occur (Gasmi et al., 2019).

Moreover, the significant increase in decomposition onset temperature and the decrease in both enthalpy and crystallinity of the PLA composite with higher TiO₂ nanoparticles reinforce the hypothesis that there was an efficient inclusion of intermolecular bonding with the PLA matrix due to the anti-plasticizing effect of TiO₂ nanoparticles (El-Sayed et al., 2011; Amin et al., 2019).

Several researches have studied how addition of nanoparticles can improve mechanical properties in ultra-thin polymeric fibers. It has been proven that, the improvement in mechanical properties of PLA—A over neat PLA in this study was attributed to the favorable interactions between the polymer matrix and the homogeneous distribution of TiO₂ nanoparticles (as augmented in the internal friction) within the fibers as a filler, showed in the **Figure 1C.1**, making it toughest and most flexible (Ramier et al., 2014; Sadeghi and Shahedi, 2016; Feng et al., 2019). The reduction of TS, FS, and EM in PLA—B (**Figure 4** and **Table 4**) can be attributed to an anti-plasticizing effect, in which nano-TiO₂ might play the part of an anti-plasticizer due to increased interaction, a decreased the free volume between chains, a reduction in film flexibility and reduction in crystallinity, showed in **Figure 1E**, making it less tough (Shaili et al., 2015; Feng et al., 2019).

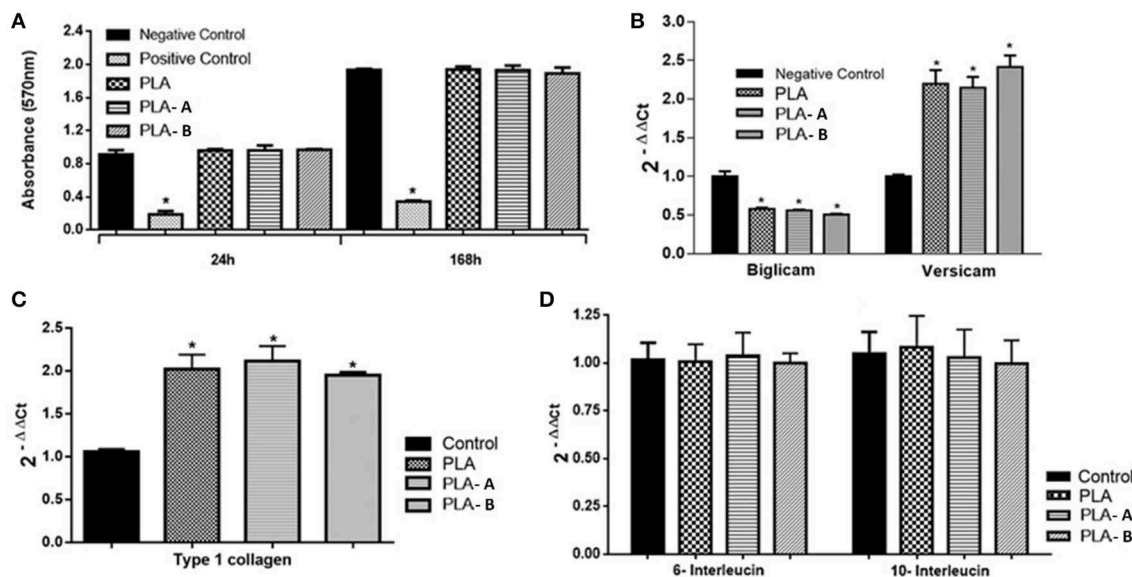


FIGURE 5 | (A) Cell viability assay performed by the MTT assay (PLA, PLA—A, and PLA—B). One-way statistical analysis ANOVA and post-test of Tukey Multiple Comparison * $P < 0.05$ (compared to cells); **(B)** mRNA expression of the versicam and biglicam genes in L929 cells in the control groups and in the PLA, PLA—A, and PLA—B groups. **(C)** mRNA expression of the versicam and biglicam genes in the L929 cells in the control groups and in the PLA, PLA—A, and PLA—B groups. All groups were compared to the control group (cells only). **(D)** Expression of the interleukin-6 and—10 mRNA in L929 cells in the control groups and in the PLA, PLA—A, and PLA—B groups. Statistical test: One-way ANOVA followed by post-test multiple Tukey comparisons * $P < 0.05$ (compared to control).

The membranes did not cause any decrease in the number of cells when compared to the control group in the cytotoxicity assay (**Figure 5A**). Cytotoxicity or evaluation of toxicity in cell culture is a complex *in-vivo* phenomenon that manifests a broad spectrum of effects, from cell death to metabolic aberrations—i.e., no cell death but functional changes (Kao et al., 2007). All groups of materials (PLA—A, and PLA—B) caused an over expression of the versicam mRNA in fibroblasts when compared to the control group. On the other hand, the biglicam showed a decrease in expression in the fibroblasts (down expression) when in contact with the studied nanocomposites in all three groups (**Figure 5B**). Type-I collagen was upregulated in all the membranes (**Figure 5C**). The electrospun membranes, however, did not show differences from control when analyzed for 6- and 10-interleukins (**Figure 5D**).

Type-I collagen plays an important role in maintaining the integrity of the extracellular matrix. Type-I collagen has a fibrillar type structure and is the most investigated type of collagen due to its abundance and the fact that it is the main structural element of several tissues. It is expressed in almost all connective tissues and plays a key role in the skin repair processes (Wong et al., 2013). Versicam is present in the dermis (Ruoslahti, 1989) and has important biological functions in the regulation of skin behavior (Bianco et al., 1990; Kinsella et al., 2004). Recent studies have shown that versicam interacts with leukocytes, promoting their adhesion. In addition, the incorporation of versicam into the ECM blocks monocyte adhesion and attenuates the inflammatory response. When binding to hyaluronic acid, versicam influences the T lymphocytes, aiding these cells to

synthesize and secrete cytokines that assist the immune response. Versicam is emerging as a potential target in the treatment of inflammation, promising broad therapeutic benefits in the future due to the fact that it is an ECM molecule that plays a central role in the inflammatory process (Wight et al., 2014). The upregulation of versicam and type-1 collagen can be attributed to the activation of connective tissue formation, presumed to be related to repair of wounds and fibrotic diseases of the skin (Wahab et al., 1996).

A study conducted in 2001 compared down regulation of the decorin gene mRNA expression in post-surgical regenerated fibroblast cells in comparison to healthy human gingiva. The expression of mRNA for the versicam presented increased expression (upregulation) in this study (Ivanovski et al., 2001). In this study, the expression of versicam and biglicam genes corroborate with observations by Ivanovski. In our study, it was observed that all of the three groups of membranes (PLA, PLA—A, and PLA—B) caused over expression of the versicam in the fibroblasts when compared to the control group (**Figure 5B**). These findings are also in agreement with previous studies where the downregulation of decorin mRNA and upregulation of versicam in gingival cells and periodontal ligament cells were also observed (Haase et al., 1998). Other studies also report the correlation between exposure of growth factors, rates of cell proliferation, and synthesis of proteoglycans in other cell lines (Kähäri et al., 1991; Mauviel et al., 1995).

The gene expression findings of interleukins in the present study demonstrate that there is no change between the control and nanomaterials groups. The cited references support the idea that the developed membranes do not cause an inflammatory

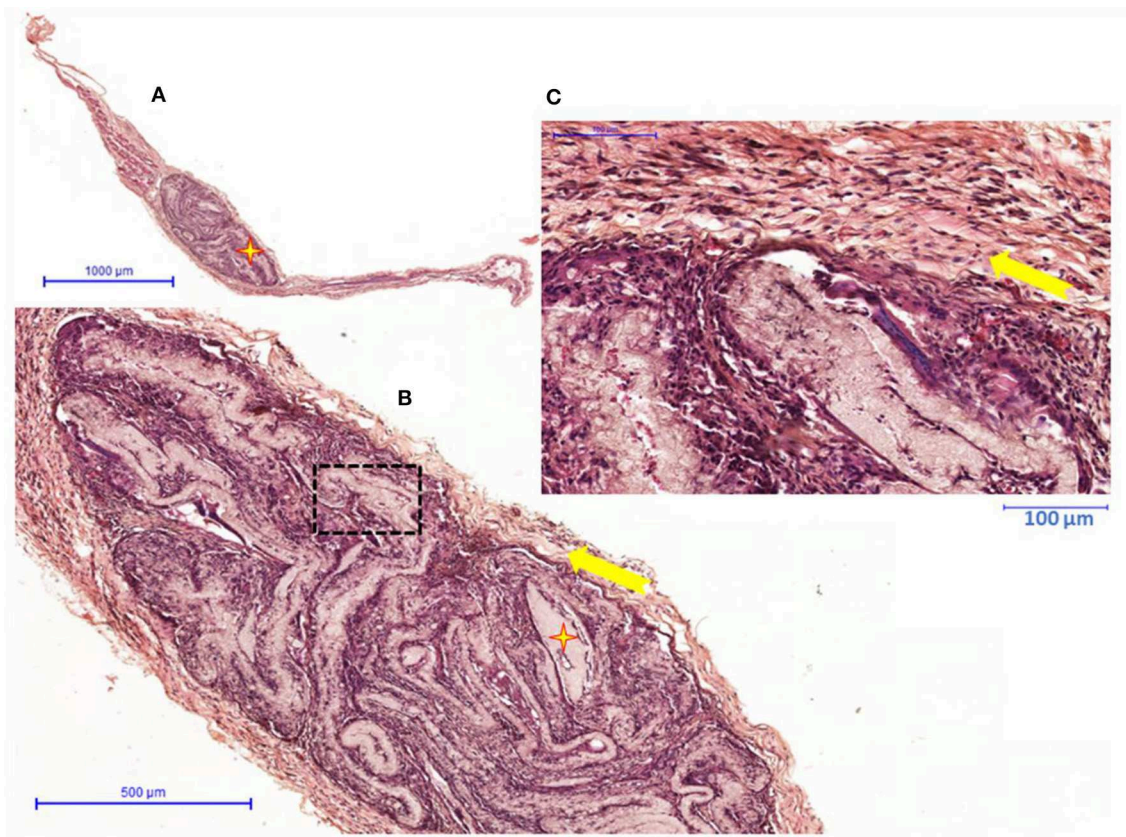


FIGURE 6 | PLA—(A) Overview hematoxylin and eosin staining histological image of connective tissue with biomaterial (✦) implanted; **(B)** Detail of representative histologic section of connective tissue (➡) forming the capsule around of biomaterial (✦); **(C)** Capsule detail with inflammatory infiltrate discrete (➡).

response in the cells of the fibroblast line used. This is an important property of a material that can be used in dressings in the future, since it would avoid problems related to scarring—such as excessive inflammatory response—that would delay the regenerative process (Kopf et al., 2010; Scheller et al., 2011).

TiO₂ has been proven to be a nanoparticle that can modulate the immune functions, it is dependent to concentration, dose or route of administration (Lappas, 2015). The ability of TiO₂ nanoparticles to produce reactive oxygen species (ROS) and increase membrane permeability maximize antibacterial activity and improve the wound healing as was observed previously (Sankar et al., 2014). Moreover, the TiO₂ nanoparticles could cause enhanced blood coagulation, which is an important first step in the wound healing process (Seisenbaeva et al., 2017). Our *in vivo* results were (Figures 4–6) similar to Seisenbaeva et al. (2017) and in the study, it was observed that TiO₂ improved wound healing. We confirmed that the electrospun membranes with TiO₂ can stimulate and modulate inflammation, which is very important for human health, since there is bigger formation of blood vessels (Babelova et al., 2009; Moreth et al., 2014).

Various biological and synthetic skin replacements are available commercially available. Although there are over 3,000 types of dressings on the market, there is no product that is effective for treatment of chronic wounds such as venous leg ulcers, diabetic wounds, and pressure ulcers and burns. The membranes discussed in this study are ideal candidates for curative materials in the care of difficult-to-treat wounds and aiding the healing process and helping patients and health care professionals (Dhivya et al., 2015).

SUMMARY AND CONCLUSIONS

Three different membranes types were evaluated: One with PLA nanofibers but without TiO₂ content, and two with PLA and varying concentrations of TiO₂ (10% and 35% w/w). A higher concentration of TiO₂ in the PLA structure significantly decreases the melting enthalpy of PLA. PLA with 10% of TiO₂ improved in more than 300% the tensile strain compared to PLA. All three membranes were found to be non-toxic against fibroblast L929 cells. The membranes also increased mRNA expression in Versican and type-1 collagen, which are both important for the tissue repair

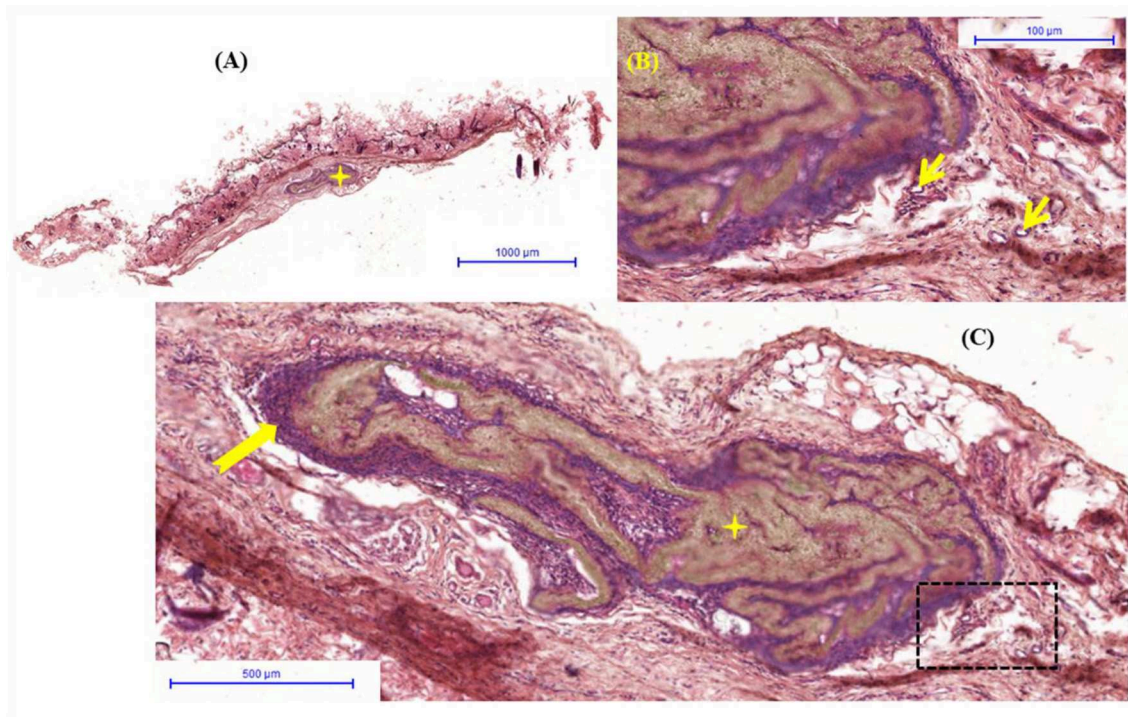


FIGURE 7 | PLA—(A) Overview hematoxylin and eosin staining histological image of connective tissue with biomaterial (★) implanted; (B) Detail of representative histologic section of connective tissue (→) forming the capsule around of biomaterial (★) with inflammatory infiltrate discrete; (C) Capsule reveals details of neoformed blood vessels (→).

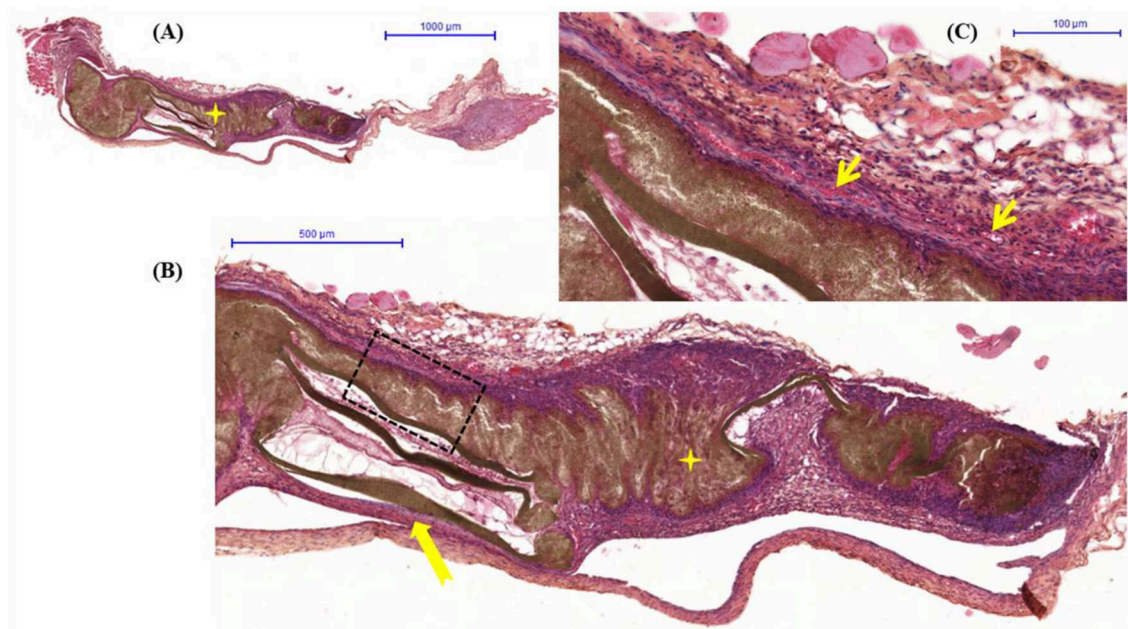


FIGURE 8 | PLA—(A) Overview hematoxylin and eosin staining histological image of connective tissue with biomaterial (★) implanted; (B) Detail of representative histologic section of connective tissue (→) forming the capsule around of biomaterial (★) with inflammatory infiltrate discrete; (C) Capsule reveals details of neoformed blood vessels (→).

process. It was also observed that the membranes did cause inflammations as demonstrated by the absence of alterations in the expression of interleukins-6 and -10. *In vivo* analysis indicated that our membranes can be used as materials for wound healing applications, as there were no inflammations observed, and the formation of blood vessels was identified.

DATA AVAILABILITY STATEMENT

The datasets generated for this study are available on request to the corresponding author.

ETHICS STATEMENT

The animal study was reviewed and approved by 10/2015-CEUA/ICT/CJSC-UNESP.

REFERENCES

- Amin, M. R., Chowdhury, M. A., and Kowser, M. A. (2019). Characterization and performance analysis of composite bioplastics synthesized using titanium dioxide nanoparticles with corn starch. *Heliyon* 5:e02009. doi: 10.1016/j.heliyon.2019.e02009
- Annunziata, M., Natri, L., Borgonovo, A., Benigni, M., and Poli, P. P. (2015). Poly-DL-lactic acid membranes for bone regeneration. *J. Craniofacial Surg.* 26, 1691–1696. doi: 10.1097/SCS.0000000000001786
- Anžlovar, A., Kržan, A., and Žagar, E. (2018). Degradation of PLA/ZnO and PHBV/ZnO composites prepared by melt processing. *Arab. J. Chem.* 11, 343–352. doi: 10.1016/j.arabjc.2017.07.001
- Babelova, A., Moreth, K., Tsalastra-Greul, W., Zeng-Brouwers, J., Eickelberg, O., Young, M. F., et al. (2009). Biglycan, a danger signal that activates the NLRP3 inflammasome via toll-like and P2X receptors. *J. Biol. Chem.* 284, 24035–24048. doi: 10.1074/jbc.M109.014266
- Bardosova, M., and Wagner, T. (2015). *Nanomaterials and Nanoarchitectures: A Complex Review of Current Hot Topics and their Applications*. Springer. doi: 10.1007/978-94-017-9921-8
- Baskaran, R., Selvasekarapandian, S., Kuwata, N., Kawamura, J., and Hattori, T. (2006). Conductivity and thermal studies of blend polymer electrolytes based on PVAc-PMMA. *Solid State Ionics* 177, 2679–2682. doi: 10.1016/j.ssi.2006.04.013
- Bayon, Y., Bohner, M., Eglin, D., Procter, P., Richards, R., Weber, J., et al. (2016). Innovating in the medical device industry – challenges & opportunities ESB 2015 translational research symposium. *J. Mater. Sci.: Mater. Med.* 27, 144. doi: 10.1007/s10856-016-5759-5
- Beyth, N., Hourri-Haddad, Y., Domb, A., Khan, W., and Hazan, R. (2015). Alternative antimicrobial approach: nano-antimicrobial materials. *Evid Based Complement Alternat Med.* 2015:246012. doi: 10.1155/2015/246012
- Bianco, P., Fisher, L. W., Young, M. F., Termine, J. D., and Robey, P. G. (1990). Expression and localization of the two small proteoglycans biglycan and decorin in developing human skeletal and non-skeletal tissues. *J. Histochem. Cytochem.* 38, 1549–1563. doi: 10.1177/38.11.2212616
- Braunger, J. A., Björnmalm, M., Isles, N. A., Cui, J., Henderson, T. M., O'Connor, A. J., et al. (2017). Interactions between circulating nanoengineered polymer particles and extracellular matrix components *in vitro*. *Biomater. Sci.* 5, 267–273. doi: 10.1039/C6BM00726K
- Camargo, S. E., Rode Sde, M., do Prado, R. F., Carvalho, Y. R., and Camargo, C. H. (2010). Subcutaneous tissue reaction to castor oil bean and calcium hydroxide in rats. *J. Appl. Oral Sci.* 18, 273–278. doi: 10.1590/S1678-77572010000300014

AUTHOR CONTRIBUTIONS

All authors contributed to the design of the study, writing of the manuscript, and read and approved the final manuscript. TM and RR performed the biological *in vitro* and *in vivo* tests. TT, CE, AS, AF, AZ, and LM produced and characterized all membranes. LV, ES-F, FM, TW, and AL supervised all students.

FUNDING

This work was supported by the National Council for Scientific and Technological Development (CNPq, #303752/2017-3 and #404683/2018-5 to AL and #304133/2017-5 and #424163/2016-0 to FM). AZ acknowledges financial support of the FCT through UID/CTM/00264/2019 and Investigator FCT Research contract (IF/00071/2015) and the project PTDC/CTM—TEX/28295/2017 financed by FCT, FEDER, and POCI.

- Costa, R. G., Ribeiro, C., and Mattoso, L. H. (2013). Study of the effect of rutile/anatase TiO₂ nanoparticles synthesized by hydrothermal route in electrospun PVA/TiO₂ nanocomposites. *J. Appl. Polymer Sci.* 127, 4463–4469. doi: 10.1002/app.38031
- D'amico, D. A., Montes, M. I., Manfredi, L. B., and Cyran, V. P. (2016). Fully bio-based and biodegradable polylactic acid/poly (3-hydroxybutyrate) blends: use of a common plasticizer as performance improvement strategy. *Polymer Testing* 49, 22–28. doi: 10.1016/j.polymertesting.2015.11.004
- Dhivya, S., Padma, V. V., and Santhini, E. (2015). Wound dressings—a review. *BioMedicine* 5:22. doi: 10.7603/s40681-015-0022-9
- Dinari, M., and Haghighi, A. J. P. C. (2017). Surface modification of TiO₂ nanoparticle by three dimensional silane coupling agent and preparation of polyamide/modified-TiO₂ nanocomposites for removal of Cr (VI) from aqueous solutions. *Prog. Organ. Coatings* 110, 24–34. doi: 10.1016/j.porgcoat.2017.04.044
- Efron, P. A., and Moldawer, L. L. (2004). Cytokines and wound healing: the role of cytokine and anticytokine therapy in the repair response. *J. Burn Care Rehabil.* 25, 149–160. doi: 10.1097/01.BCR.0000111766.97335.34
- El-Sayed, S., Mahmoud, K., Fatah, A., and Hassen, A. (2011). DSC, TGA and dielectric properties of carboxymethyl cellulose/polyvinyl alcohol blends. *Phys. B Condens. Matter* 406, 4068–4076. doi: 10.1016/j.physb.2011.07.050
- Farid, T., Herrera, V., and Kristiina, O. (2018). “Investigation of crystalline structure of plasticized poly (lactic acid)/Banana nanofibers composites,” in *IOP Conference Series: Materials Science and Engineering* (Kitakyushu: IOP Publishing), 012031. doi: 10.1088/1757-899X/369/1/012031
- Feng, S., Zhang, F., Ahmed, S., and Liu, Y. (2019). Physico-mechanical and antibacterial properties of PLA/TiO₂ composite materials synthesized via electrospinning and solution casting processes. *Coatings* 9:525. doi: 10.3390/coatings9080525
- Fonseca, C., Ochoa, A., Ulloa, M. T., Alvarez, E., Canales, D., and Zapata, P. A. (2015). Poly (lactic acid)/TiO₂ nanocomposites as alternative biocidal and antifungal materials. *Mater. Sci. Eng.* 57, 314–320. doi: 10.1016/j.msec.2015.07.069
- Gasmi, S., Hassan, M. K., and Luyt, A. S. (2019). Crystallization and dielectric behaviour of PLA and PHBV in PLA/PHBV blends and PLA/PHBV/TiO₂ nanocomposites. *Express Polymer Lett.* 13, 199–212. doi: 10.3144/expresspolymlett.2019.16
- Ghannadian, P., Moxley Jr, J. W., Machado de Paula, M. M., Lobo, A. O., and Webster, T. J. (2018). Micro-nanofibrillar polycaprolactone scaffolds as translatable osteoconductive grafts for the treatment of musculoskeletal defects without infection. *ACS Appl. Bio Mater.* 1, 1566–1578. doi: 10.1021/acsabm.8b00453

- Ghosal, K., Agatemor, C., Špitálský, Z., Thomas, S., and Kny, E. (2018). Electrospinning tissue engineering and wound dressing scaffolds from polymer–titanium dioxide nanocomposites. *Chem. Eng. J.* 358, 1262–1278. doi: 10.1016/j.cej.2018.10.117
- Gupta, B., Revagade, N., and Hilborn, J. (2007). Poly (lactic acid) fiber: an overview. *Prog. Polym. Sci.* 32, 455–482. doi: 10.1016/j.progpolymsci.2007.01.005
- Haase, H. R., Clarkson, R. W., Waters, M. J., and Bartold, P. M. (1998). Growth factor modulation of mitogenic responses and proteoglycan synthesis by human periodontal fibroblasts. *J. Cell. Physiol.* 174, 353–361.
- Hidalgo, I., Sojot, F., Arvelo, F., Sabino, M. A. (2013). Functional electrospun poly (lactic acid) scaffolds for biomedical applications: experimental conditions, degradation and biocompatibility study. *Mol. Cell Biomech.* 10, 85–105. doi: 10.3970/mcb.2013.010.085
- Ivanovski, S., Haase, H., and Bartold, P. (2001). Isolation and characterization of fibroblasts derived from regenerating human periodontal defects. *Arch. Oral Biol.* 46, 679–688. doi: 10.1016/S0003-9969(01)00036-X
- Kähäri, V., Larjava, H., and Uitto, J. (1991). Differential regulation of extracellular matrix proteoglycan (PG) gene expression. Transforming growth factor- β 1 up-regulates biglycan (PGI), and versican (large fibroblast PG) but down-regulates decorin (PGII) mRNA levels in human fibroblasts in culture. *J. Biol. Chem.* 266, 10608–10615.
- Kandiah, K., Muthusamy, P., Mohan, S., and Venkatachalam, R. (2014). TiO₂–graphene nanocomposites for enhanced osteocalcin induction. *Mater. Sci. Eng.* 38, 252–262. doi: 10.1016/j.msec.2014.02.010
- Kao, C.-T., Ding, S.-J., Min, Y., Hsu, T. C., Chou, M.-Y., and Huang, T.-H. (2007). The cytotoxicity of orthodontic metal bracket immersion media. *Eur. J. Orthodontics* 29, 198–203. doi: 10.1093/ejo/cjl083
- Kaseem, M., Hamad, K., and Ur Rehman, Z. (2019). Review of recent advances in poly(lactic acid)/TiO₂ composites. *Materials* 12:3659. doi: 10.3390/ma12223659
- Kinsella, M. G., Bressler, S. L., and Wight, T. N. (2004). The regulated synthesis of versican, decorin, and biglycan: extracellular matrix proteoglycans that influence cellular phenotype. *Crit. Rev. Eukaryot. Gene Expr.* 14, 32. doi: 10.1615/CritRevEukaryotGeneExpr.v14.i3.40
- Kopf, M., Bachmann, M. F., and Marsland, B. J. (2010). Averting inflammation by targeting the cytokine environment. *Nat. Rev. Drug Discov.* 9:703. doi: 10.1038/nrd2805
- Lappas, C. M. (2015). The immunomodulatory effects of titanium dioxide and silver nanoparticles. *Food Chem. Toxicol.* 85, 78–83. doi: 10.1016/j.fct.2015.05.015
- Laske, S., Ziegler, W., Kainer, M., Wuerfel, J., and Holzer, C. (2015). Enhancing the temperature stability of PLA by compounding strategies. *Polymer Eng. Sci.* 55, 2849–2858. doi: 10.1002/pen.24176
- Liou, J.-W., and Chang, H.-H. (2012). Bactericidal effects and mechanisms of visible light-responsive titanium dioxide photocatalysts on pathogenic bacteria. *Arch. Immunol. Ther. Exp.* 60, 267–275. doi: 10.1007/s00005-012-0178-x
- Livak, K. J., and Schmittgen, T. D. (2001). Analysis of relative gene expression data using real-time quantitative PCR and the 2⁻ $\Delta\Delta$ CT method. *Methods* 25, 402–408. doi: 10.1006/meth.2001.1262
- Lobo, A. O., Antunes, E. F., Machado, A. H. A., Pacheco-Souares, C., Trava-Airoldi, V. J., and Corat, E. J. (2008). Cell viability and adhesion on as grown multi-wall carbon nanotube films. *Mater. Sci. Eng.* 28, 264–269. doi: 10.1016/j.msec.2007.01.003
- Mauviel, A., Santra, M., Chen, Y. Q., Uitto, J., and Iozzo, R. V. (1995). Transcriptional regulation of decorin gene expression. Induction by quiescence and repression by tumor necrosis factor- α . *J. Biol. Chem.* 270, 11692–11700. doi: 10.1074/jbc.270.19.11692
- Mofokeng, J., and Luyt, A. (2015). Morphology and thermal degradation studies of melt-mixed poly (lactic acid)(PLA)/poly (ϵ -caprolactone)(PCL) biodegradable polymer blend nanocomposites with TiO₂ as filler. *Polymer Testing* 45, 93–100. doi: 10.1016/j.polymertesting.2015.05.007
- Moreth, K., Frey, H., Hubo, M., Zeng-Brouwers, J., Nastase, M.-V., Hsieh, L. T.-H., et al. (2014). Biglycan-triggered TLR-2-and TLR-4-signaling exacerbates the pathophysiology of ischemic acute kidney injury. *Matrix Biol.* 35, 143–151. doi: 10.1016/j.matbio.2014.01.010
- Oliveira, J. E., Mattoso, L. H., Orts, W. J., and Medeiros, E. S. (2013). Structural and morphological characterization of micro and nanofibers produced by electrospinning and solution blow spinning: a comparative study. *Adv. Mater. Sci. Eng.* 2013:409572. doi: 10.1155/2013/409572
- Pava-Gómez, B., Vargas-Ramírez, X., Díaz-Urbe, C. J. J., and Chemistry, P. A. (2018). Physicochemical study of adsorption and photodegradation processes of methylene blue on copper-doped TiO₂ films. *J. Photochem. Photobiol. Chem.* 360, 13–25. doi: 10.1016/j.jphotochem.2018.04.022
- Ramier, J., Boudierlique, T., Stoilova, O., Manolova, N., Rashkov, I., Langlois, V., et al. (2014). Biocomposite scaffolds based on electrospun poly (3-hydroxybutyrate) nanofibers and electrosprayed hydroxyapatite nanoparticles for bone tissue engineering applications. *Mater. Sci. Eng.* 38, 161–169. doi: 10.1016/j.msec.2014.01.046
- Roux, R., Ladavière, C., Montembault, A., and Delair, T. (2013). Particle assemblies: toward new tools for regenerative medicine. *Mater. Sci. Eng.* 33, 997–1007. doi: 10.1016/j.msec.2012.12.002
- Roy, S. C., Paulose, M., and Grimes, C. A. J. B. (2007). The effect of TiO₂ nanotubes in the enhancement of blood clotting for the control of hemorrhage. *Biomaterials* 28, 4667–4672. doi: 10.1016/j.biomaterials.2007.07.045
- Ruoslathi, E. (1989). Proteoglycans in cell regulation. *J. Biol. Chem.* 264, 13369–13372.
- Sadeghi, K., and Shahedi, M. (2016). Physical, mechanical, and antimicrobial properties of ethylene vinyl alcohol copolymer/chitosan/nano-ZnO (ECNZN) nanocomposite films incorporating glycerol plasticizer. *J. Food Measur. Charact.* 10, 137–147. doi: 10.1007/s11694-015-9287-7
- Saldin, L. T., Cramer, M. C., Velankar, S. S., White, L. J., and Badylak, S. F. (2017). Extracellular matrix hydrogels from decellularized tissues: structure and function. *Acta Biomater.* 49, 1–15. doi: 10.1016/j.actbio.2016.11.068
- Salles, G. N., Calió, M. L., Afewerki, S., Pacheco-Souares, C., Porcionatto, M., and Hölscher, C. (2018). Prolonged drug-releasing fibers attenuate Alzheimer's Disease-like pathogenesis. *Appl. Mater. Interfaces* 10, 36693–36702. doi: 10.1021/acsami.8b12649
- Sankar, R., Dhivya, R., Shivashangari, K. S., and Ravikumar, V. (2014). Wound healing activity of *Origanum vulgare* engineered titanium dioxide nanoparticles in Wistar Albino rats. *J. Mater. Sci.* 25, 1701–1708. doi: 10.1007/s10856-014-5193-5
- Scheller, J., Chalaris, A., Schmidt-Arras, D., and Rose-John, S. (2011). The pro-and anti-inflammatory properties of the cytokine interleukin-6. *Biochim. Biophys. Acta.* 1813, 878–888. doi: 10.1016/j.bbamcr.2011.01.034
- Schuster, B., Kovaleva, M., Sun, Y., Regenhart, P., Matthews, V., Grötzinger, J., et al. (2003). Signaling of human ciliary neurotrophic factor (CNTF) revisited: the interleukin-6 receptor can serve as an α -receptor for CNTF. *J. Biol. Chem.* 278, 9528–9535. doi: 10.1074/jbc.M210044200
- Seisenbaeva, G. A., Fromell, K., Vinogradov, V. V., Terekhov, A. N., Pakhomov, A. V., Nilsson, B., et al. (2017). Dispersion of TiO₂ nanoparticles improves burn wound healing and tissue regeneration through specific interaction with blood serum proteins. *Sci. Rep.* 7:15448. doi: 10.1038/s41598-017-15792-w
- Shaili, T., Abdorreza, M. N., and Fariborz, N. (2015). Functional, thermal, and antimicrobial properties of soluble soybean polysaccharide biocomposites reinforced by nano TiO₂. *Carbohydr. Polymers* 134, 726–731. doi: 10.1016/j.carbpol.2015.08.073
- Silva, A. D. R., Pallone, E. M. J. A., and Lobo, A. O. (2019a). Modification of surfaces of alumina-zirconia porous ceramics with Sr²⁺ after SBF. *J. Austr. Ceramic Soc.* 55, 1–8. doi: 10.1007/s41779-019-00360-4
- Silva, A. D. R., Rigoli, W. R., Mello, D. C. R., Vasconcellos, L. M. R., Pallone, E. M. J. A., and Lobo, A. O. (2019b). Porous alumina scaffolds chemically modified by calcium phosphate minerals and their application in bone grafts. *Appl. Ceramic Technol.* 16, 562–573. doi: 10.1111/ijac.13153
- Silva, A. D. R., Rigoli, W. R., Osiro, D., Mello, D. C. R., Vasconcellos, L. M. R., Lobo, A. O., et al. (2018). Surface modification using the biomimetic method in alumina-zirconia porous ceramics obtained by the replica method. *J. Biomed. Mater. Res. Part B.* 106, 2615–2624. doi: 10.1002/jbm.b.34078
- Simoes, M. (2011). Antimicrobial strategies effective against infectious bacterial biofilms. *Curr. Med. Chem.* 18, 2129–2145. doi: 10.2174/092986711795656216
- Stocco, T. D., Bassous, N. J., Zhao, S., Granato, A. E., Webster, T. J., and Lobo, A. O. (2018). Nanofibrous scaffolds for biomedical applications. *Nanoscale* 10, 12228–12255. doi: 10.1039/C8NR02002G
- Tawakkal, I. S., Cran, M. J., Miltz, J., and Bigger, S. W. J. J. (2014). A review of poly (lactic acid)-based materials for antimicrobial packaging. *Food Sci.* 79, R1477–R1490. doi: 10.1111/1750-3841.12534

- Toniatto, T., Rodrigues, B., Marsi, T., Ricci, R., Marciano, F., Webster, T., et al. (2017). Nanostructured poly (lactic acid) electrospun fiber with high loadings of TiO₂ nanoparticles: insights into bactericidal activity and cell viability. *Mater. Sci. Eng.* 71, 381–385. doi: 10.1016/j.msec.2016.10.026
- Villarreal-Gómez, L. J., Cornejo-Bravo, J. M., Vera-Graziano, R., and Grande, D. (2016). Electrospinning as a powerful technique for biomedical applications: a critically selected survey. *J. Biomater. Sci. Polymer* 27, 157–176. doi: 10.1080/09205063.2015.1116885
- Virovska, D., Paneva, D., Manolova, N., Rashkov, I., and Karashanova, D. (2014). Electrospinning/electrospraying vs. electrospinning: a comparative study on the design of poly (l-lactide)/zinc oxide non-woven textile. *Appl. Surface Sci.* 311, 842–850. doi: 10.1016/j.apsusc.2014.05.192
- Wacharawichanant, S., Ounyai, C., and Rassamee, P. (2017). Effects of organoclay to miscibility, mechanical and thermal properties of poly(lactic acid) and propylene-ethylene copolymer blends. *IOP Conf. Series Mater. Sci. Eng.* 223:012016. doi: 10.1088/1757-899X/223/1/012016
- Wahab, N. A., Harper, K., and Mason, R. M. (1996). Expression of extracellular matrix molecules in human mesangial cells in response to prolonged hyperglycaemia. *Biochem. J.* 316, 985–992. doi: 10.1042/bj3160985
- Walmsley, G. G., McArdle, A., Tevlin, R., Momeni, A., Atashroo, D., Hu, M. S., et al. (2015). Nanotechnology in bone tissue engineering. *Nanomedicine* 11, 1253–1263. doi: 10.1016/j.nano.2015.02.013
- Wang, B., Lilja, M., Ma, T., Sörensen, J., Steckel, H., Ahuja, R., et al. (2014). Theoretical and experimental study of the incorporation of tobramycin and strontium-ions into hydroxyapatite by means of co-precipitation. *Appl. Surface Sci.* 314, 376–383. doi: 10.1016/j.apsusc.2014.06.193
- Wight, T. N., Kang, I., and Merrilees, M. J. (2014). Versican and the control of inflammation. *Matrix Biol.* 35, 152–161. doi: 10.1016/j.matbio.2014.01.015
- Wong, V. W., Gurtner, G. C., and Longaker, M. T. (2013). “Wound healing: a paradigm for regeneration,” in *Mayo Clinic Proceedings* (Elsevier), 1022–1031. doi: 10.1016/j.mayocp.2013.04.012
- Wu, S., Weng, Z., Liu, X., Yeung, K., and Chu, P. K. (2014). Functionalized TiO₂ based nanomaterials for biomedical applications. *Adv. Funct. Mater.* 24, 5464–5481. doi: 10.1002/adfm.201400706
- Zdraveva, E., Mijovic, B., Govorcin Bajsic, E., and Grozdanic, V. (2018). The efficacy of electrospun polyurethane fibers with TiO₂ in a real time weathering condition. *Textile Res. J.* 88, 2445–2453. doi: 10.1177/0040517517723025
- Zhang, H., Huang, J., Yang, L., Chen, R., Zou, W., Lin, X., et al. (2015). Preparation, characterization and properties of PLA/TiO₂ nanocomposites based on a novel vane extruder. *RSC Adv.* 5, 4639–4647. doi: 10.1039/C4RA14538K
- Zhang, J.-M., and An, J. (2007). Cytokines, inflammation and pain. *Int. Anesthesiol. Clin.* 45:27. doi: 10.1097/AIA.0b013e318034194e

Conflict of Interest: The authors declare that the research was conducted in the absence of any commercial or financial relationships that could be construed as a potential conflict of interest.

Copyright © 2019 Marsi, Ricci, Toniato, Vasconcellos, Elias, Silva, Furtado, Magalhães, Silva-Filho, Marciano, Zille, Webster and Lobo. This is an open-access article distributed under the terms of the Creative Commons Attribution License (CC BY). The use, distribution or reproduction in other forums is permitted, provided the original author(s) and the copyright owner(s) are credited and that the original publication in this journal is cited, in accordance with accepted academic practice. No use, distribution or reproduction is permitted which does not comply with these terms.



Application of 3D Printed Models of Complex Hypertrophic Scars for Preoperative Evaluation and Surgical Planning

Peng Liu^{1,2†}, Zhicheng Hu^{1†}, Shaobin Huang^{1†}, Peng Wang¹, Yunxian Dong¹, Pu Cheng¹, Hailin Xu¹, Bing Tang^{1*} and Jiayuan Zhu^{1*}

¹ Department of Burn Surgery, The First Affiliated Hospital of Sun Yat-sen University, Guangzhou, China, ² Department of Burn and Plastic Surgery, Guangzhou Red Cross Hospital, Medical College, Jinan University, Guangzhou, China

OPEN ACCESS

Edited by:

Malcolm Xing,
University of Manitoba, Canada

Reviewed by:

Narendra Pal Singh Chauhan,
Bhopal Nobles University, India
Fateme Kabirian,
Materials and Energy Research
Center, Iran

*Correspondence:

Bing Tang
tangbing@mail.sysu.edu.cn
Jiayuan Zhu
zhujay@mail.sysu.edu.cn

[†] These authors have contributed
equally to this work

Specialty section:

This article was submitted to
Biomaterials,
a section of the journal
Frontiers in Bioengineering and
Biotechnology

Received: 01 October 2019

Accepted: 05 February 2020

Published: 03 March 2020

Citation:

Liu P, Hu Z, Huang S, Wang P,
Dong Y, Cheng P, Xu H, Tang B and
Zhu J (2020) Application of 3D Printed
Models of Complex Hypertrophic
Scars for Preoperative Evaluation
and Surgical Planning.
Front. Bioeng. Biotechnol. 8:115.
doi: 10.3389/fbioe.2020.00115

Background: Complex hypertrophic scar is a condition that causes multiple joint contractures and deformities after trauma or burn injuries. Three-dimensional (3D) printing technology provides a new evaluation method for this condition. The objective of this study was to print individualized 3D models of complex hypertrophic scars and to assess the accuracy of these models.

Methods: Twelve patients with complex hypertrophic scars were included in this study. Before surgery, each patient underwent a computed tomography (CT) scan to obtain cross-sectional information for 3D printing. Mimics software was used to process the CT data and create 3D printed models. The length, width, height, and volume measurements of the physical scars and 3D printed models were compared. Experienced surgeons used the 3D models to plan the operation and simulate the surgical procedure. The hypertrophic scar was completely removed for each patient and covered with skin autografts. The surgical time, bleeding, complications, and skin autograft take rate were recorded. All patients were followed up at 12 months. The surgeons, young doctors, medical students, and patients involved in the study completed questionnaires to assess the use of the 3D printed models.

Results: The 3D models of the hypertrophic scars were printed successfully. The length, width, height, and volume measurements were significantly smaller for the 3D printed models than for the physical hypertrophic scars. Based on preoperative simulations with the 3D printed models, the surgeries were performed successfully and each hypertrophic scar was completely removed. The surgery time was shortened and the bleeding was decreased. On postoperative day 7, there were two cases of subcutaneous hemorrhage, one case of infection and one case of necrosis. On postoperative day 12, the average take rate of the skin autografts was 97.75%. At the 12-month follow-up, all patients were satisfied with the appearance and function.

Conclusion: Accurate 3D printed models can help surgeons plan and perform successful operations, help young doctors and medical students learn surgical methods, and enhance patient comprehension and confidence in their surgeons.

Keywords: 3D printed models, hypertrophic scars, preoperative evaluation, surgical planning, wound scarring prevention

INTRODUCTION

Complex hypertrophic scar is a condition caused by trauma or burn injuries that may cause multiple joint contractures and deformities (Butzelaar et al., 2015; Anthonissen et al., 2016; Seo and Jung, 2016). The treatment of complex hypertrophic scars can dramatically improve a patient's quality of life. At present, many conservative methods are used to treat complex hypertrophic scars; however, the outcomes are poor for patients with multiple skeletal deformities and scar contractures. Therefore, surgery is often the first treatment choice for patients with complex hypertrophic scars. When there are abnormal anatomical structures around the complex hypertrophic scar caused by skeletal deformities and soft tissue contractures, it is difficult for doctors to identify and assess the size of the scar clearly. Preoperative evaluation of complex hypertrophic scars is important for effective surgical treatment.

Currently, preoperative evaluation of complex hypertrophic scars depends exclusively on traditional, two-dimensional (2D) images, namely X-rays, computed tomography (CT), and magnetic resonance imaging (MRI). These types of imaging are used to evaluate the limits of complex hypertrophic scars and bone deformities; however, it is difficult to establish precise limits with 2D images (Ploch et al., 2016; Pfeil et al., 2017). Furthermore, it is also difficult to provide spatial anatomical information and tactile feedback for surgeons using these techniques.

Recently, 3D printing has been widely applied in orthopedic surgery, stomatology, and other medical fields because it has advantages in terms of individualization, tactility, and visualization (Cutroneo et al., 2016; Fitzhugh et al., 2016; Gu et al., 2016; Rashaan et al., 2016; Schepers et al., 2016). In this study, we made 3D models of complex hypertrophic scars to measure their dimensions preoperatively. We evaluated the accuracy of the 3D printed models. In addition, we assessed whether the 3D printed models were useful to surgeons in planning the operation, if they were helpful in the training of young doctors and medical students, and if they were useful tools for explaining the disease and operation to patients. Lastly, we assessed the clinical effect after surgery.

MATERIALS AND METHODS

Patients

Twelve patients who were hospitalized with complex hypertrophic scars from 1 December 2014 to 1 December 2015 were enrolled in this study. All patients experienced a loss of joint function and activity and exhibited severe deformity due to a complex hypertrophic scar (Figures 1, 2A,B). The study protocol was approved by the Institutional Review Board of The First Affiliated Hospital of Sun Yat-sen University, and informed consent was obtained from all participants.

Image Processing and 3D Printing

A 64-slice spiral CT (Toshiba-Aquilion Corporation, Japan) was utilized to acquire serial cross-sectional data for each

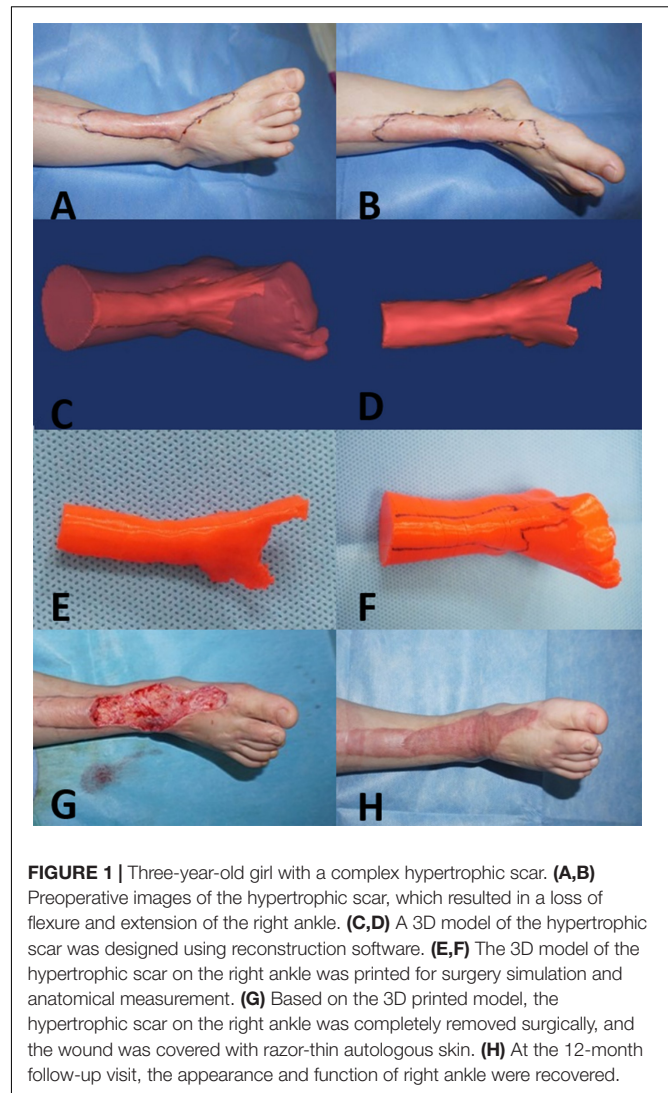


FIGURE 1 | Three-year-old girl with a complex hypertrophic scar. (A,B) Preoperative images of the hypertrophic scar, which resulted in a loss of flexure and extension of the right ankle. (C,D) A 3D model of the hypertrophic scar was designed using reconstruction software. (E,F) The 3D model of the hypertrophic scar on the right ankle was printed for surgery simulation and anatomical measurement. (G) Based on the 3D printed model, the hypertrophic scar on the right ankle was completely removed surgically, and the wound was covered with razor-thin autologous skin. (H) At the 12-month follow-up visit, the appearance and function of right ankle were recovered.

hypertrophic scar. Hypertrophic scar tissues were segmented from the optimal cross-sectional images with a thresholding tool using reconstruction software. Next, the 3D geometric models of the hypertrophic scar were exported as stereolithography (STL) format files for 3D printing (Figures 1, 2C,D). The STL format files were imported to PST-ZB (PST Photon Technology Co., Ltd., China), a rapid prototyping 3D printer with fused deposition modeling (FDM) principles. The printing material is polylactic acid (PLA), which is obtained by extracting starch from plants such as corn and cassava through multiple processes, fermenting it into lactic acid by microorganisms, and then polymerizing it. PLA is safer, lower in carbon, and greener compared with traditional materials. The printing parameters: printing speed 150 mm/s, temperature 200°C, and layer thickness 0.1 mm. The 3D scar models produced by the 3D printer were used preoperatively by experienced surgeons to simulate the surgical procedure to remove the hypertrophic scar. The printing process is shown in Figure 3.

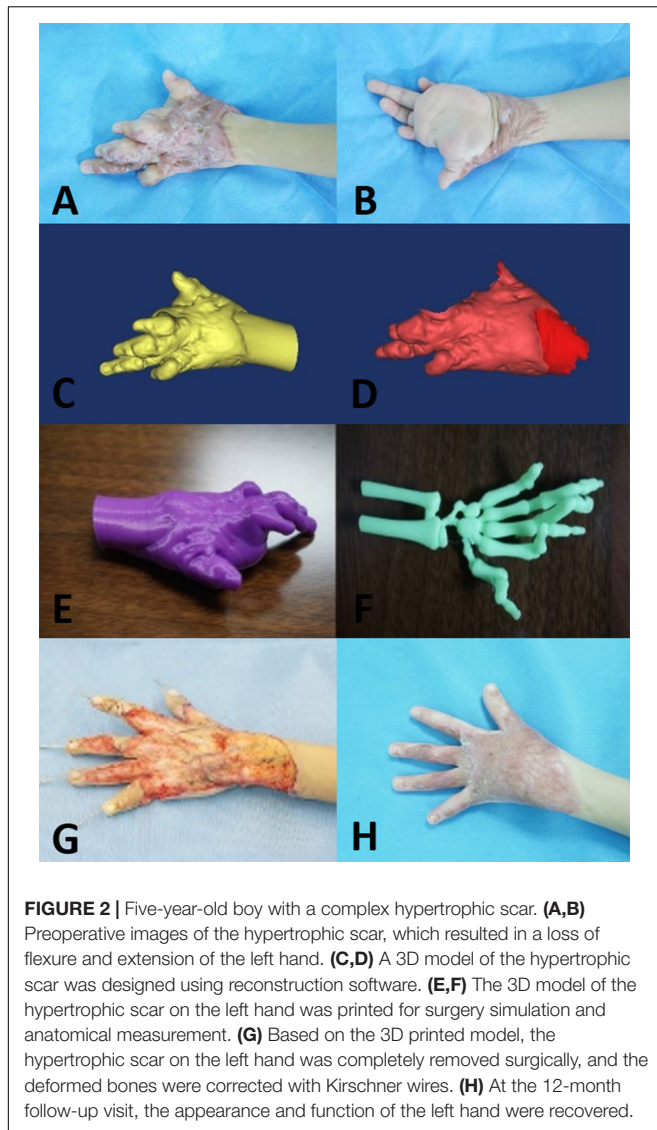


FIGURE 2 | Five-year-old boy with a complex hypertrophic scar. (A,B) Preoperative images of the hypertrophic scar, which resulted in a loss of flexure and extension of the left hand. (C,D) A 3D model of the hypertrophic scar was designed using reconstruction software. (E,F) The 3D model of the hypertrophic scar on the left hand was printed for surgery simulation and anatomical measurement. (G) Based on the 3D printed model, the hypertrophic scar on the left hand was completely removed surgically, and the deformed bones were corrected with Kirschner wires. (H) At the 12-month follow-up visit, the appearance and function of the left hand were recovered.

Validating Accuracy of the 3D Printed Models

The length, width, and height of each hypertrophic scar were measured manually using rulers for the physical scar and with reconstructive software for the 3D printed model. Then the measurements of the physical scar and 3D printed model were compared as shown in **Figure 4** (Olszewski et al., 2014; Yong et al., 2014; Lee et al., 2015; Wu et al., 2015; Yin et al., 2015). The volume of each 3D printed model was calculated automatically by Gemagic Quality software, and the volume of each 3D printed model was measured using the drainage method. These parameters were statistically analyzed by SPSS 13.0.

Surgical Procedure and Postoperative Visits

Hypertrophic scar resection was performed for all 12 patients by the same group of experienced surgeons. Each hypertrophic

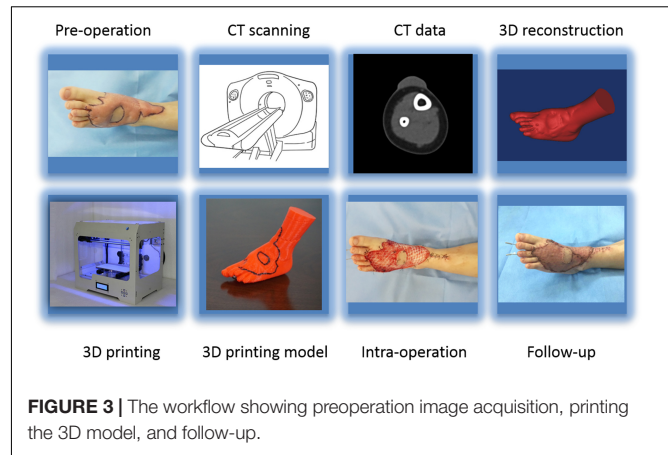


FIGURE 3 | The workflow showing preoperation image acquisition, printing the 3D model, and follow-up.

scar was completely removed according to the measurement data and preoperative surgical simulation on the 3D printed models. A nurse recorded the surgery time and bleeding for each patient. Razor-thin skin autografts were harvested from the inner thigh to cover the scar area. The autografts were placed over human acellular dermal matrix scaffold (Jie-Ya Life Tissue Engineering, Beijing, China) intraoperatively and sutured to the graft area. Pressure was applied on the graft area. The 12 patients were followed up for 12 months after they were discharged from the hospital. At the 12-month follow-up visit, the skin autografts were assessed for skin color, appearance, elasticity, and texture at the suture.

Evaluation of the 3D Models

The surgeons, young doctors, medical students, and patients evaluated the 3D printed models with specially designed feedback questionnaires. The responses to the questions were made on a 5-point Likert scale where 1 represents strongly disagree, 2 represents disagree, 3 represents neither agree nor disagree, 4 represents agree, and 5 represents strongly agree. The surgeons assessed the use of the models as surgical aids in terms of their visual appearance, quality, size, and surgical anatomy. The young doctors and medical students evaluated the use of the models for surgery simulation and training as well as the quality and size of the models. The patients assessed whether the use of the 3D printed models helped illustrate and explain the disease and helped them understand the surgical process and risks.

Statistical Analysis

Statistical significance between groups was determined by paired *t*-test. All data were analyzed using SPSS version 16.0 software (IBM, Armonk, NY, United States).

RESULTS

Before surgery, individualized 3D models of the hypertrophic scars and deformed bones were successfully printed (**Figures 1, 2E,F**). The size and depth of the hypertrophic scar could be measured accurately on the 3D printed models.

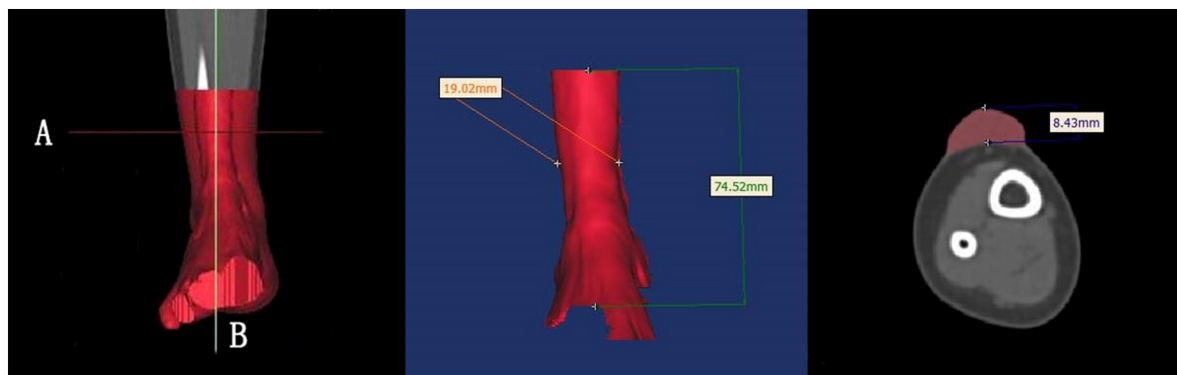


FIGURE 4 | The length, width, and height of each hypertrophic scar were measured manually with rulers. These dimensions were measured with reconstruction software on the 3D printed models.

The average length, width, height, and volume of the physical hypertrophic scars and 3D printed models are presented in **Table 1**. The average length, width, and height of the 3D printed models were significantly smaller than the measurements of the physical scars. The average volume of the 3D scar models was significantly smaller than the average volume of the physical scars.

For each patient, surgery was completed according to the planned simulation by the same group of experienced surgeons, and the results were satisfactory. The medical students indicated that they had an improved comprehension of many surgical skills for resecting hypertrophic scars because of the simulated operations using the 3D printed models. The patients indicated that the explanations using the 3D printed models improved their understanding of the surgery and increased their trust of the surgeons. The average score of the evaluation about 3D printed models in each group on was greater than 3 points, which indicated that all of the groups were satisfied with the surgical simulations using the 3D printed models (**Figure 5**).

All patients successfully underwent hypertrophic scar resection according to the surgical simulations using the 3D printed models. The hypertrophic scar tissue was completely removed, and deformed bones were corrected according to the preoperative surgical plan (**Figures 1, 2G**). The surgical time was shortened and the bleeding was decreased. On postoperative day

7, there were two cases of subcutaneous hemorrhage, one case of infection and one case of necrosis, which may have been caused by excessive postoperative activity. On postoperative day 12, the average take rate of the skin autografts was 97.75% (**Table 2**). At the 12-month follow-up visit, all patients had satisfactory appearance and function (**Figures 1, 2H**).

DISCUSSION

Surgery is generally recommended for the treatment of hypertrophic scars. For surgery to be successful, it is important to identify the precise size of the hypertrophic scar (So et al., 2011; Amici, 2014; Lim et al., 2014; Orgill and Ogawa, 2014). The present study applied 3D printing to produce personalized models and observe the spatial position of the hypertrophic scar and bone deformity (Srougi et al., 2016). Using the models, anatomical measurements were made of the hypertrophic scar, including its length, width, and height (Silberstein et al., 2014). Our results suggest that 3D printed models of hypertrophic scars may guide surgeons to identify the surgical cutting plane that marks the limit between scar tissue and normal tissue. Knowledge of the surgical cutting plane can influence surgical effectiveness and potentially reduce complications (**Figure 6**).

Although 3D printing technology has been applied in many fields, it is necessary to evaluate its accuracy to meet clinical requirements. In the present study, the 3D printed models had a significantly smaller average length, width, height, and volume compared with the physical scars. These differences were caused by shrinkage of the material during printing, which affected the accuracy of the 3D models. The results of our study were similar to those of Lee et al. (2015; Wu et al., 2015). Although these differences were statistically significant, they were regarded as clinically insignificant. The 3D models served as valuable references for measuring anatomical parameters of the hypertrophic scar preoperatively, for planning the surgery, and for guiding the intraoperative manipulations.

The preoperative method for surgical resection of hypertrophic scar was direct measurement mainly to measure the size of hypertrophic scar, and the flap covered the wound

TABLE 1 | Measurements of the patient scars and 3D printed models.

Parameter	Physical hypertrophic scar	3D printed model	p-value
Length (cm)	7.16 ± 2.17	7.10 ± 2.16	0.001*
Width (cm)	4.68 ± 1.40	4.57 ± 1.32	0.002*
Height (cm)	1.14 ± 0.37	1.10 ± 0.36	0.000*
Volume (ml)	38.22 ± 19.94	38.08 ± 19.94	0.001*

The maximum length, width, and height of the hypertrophic scar were measured with rulers and reconstruction software. The volume of the hypertrophic scar was measured using the water displacement method with a 5 L container. $n = 12$. * $p < 0.05$; paired t-test.

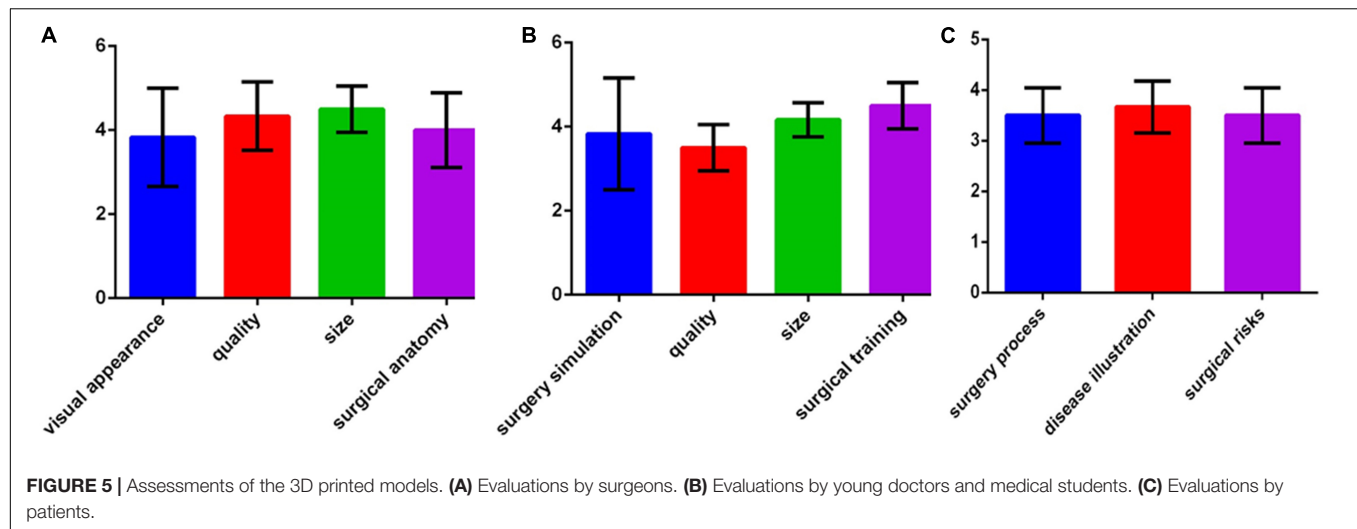
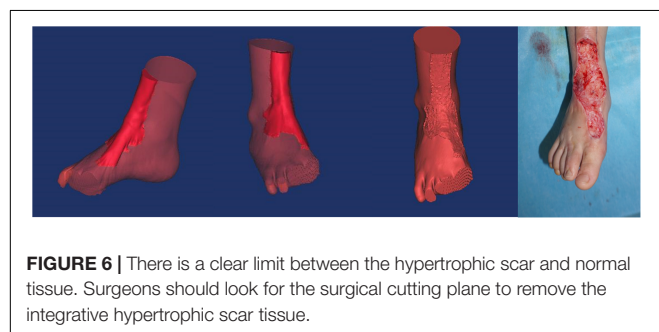


TABLE 2 | Patient characteristics and the take rate after surgery.

Patient	Sex	Age (years)	Cause of injury	Location	Injury time (years)	Take rate (%)*	Complication
1	Male	5	Hot water	Left hand	4	98	None
2	Female	19	Hot water	Left foot	10	97	Hematoma
3	Female	3	Flame	Right foot	2	99	None
4	Male	2	Hot water	Right hand	1	98	Hematoma
5	Male	16	Hot water	Left elbow joint	11	97	None
6	Female	4	Hot water	Right foot	2	98	Infection
7	Male	18	Hot water	Left hand	15	97	None
8	Female	3	Hot water	Right foot	2	97	Necrosis
9	Male	22	Flame	Left foot	14	98	None
10	Female	5	Hot water	Left hand	3	99	None
11	Female	26	Hot water	Left foot	18	97	None
12	Male	18	Flame	Right foot	9	99	None

*The take rates of skin autografts were recorded on postoperative day 12.

after scar removal (Alali et al., 2015; Hwang et al., 2015; Martelli et al., 2016). However, this method lacked important parameters such as scar depth and volume, and cannot assess the anatomical relationship between scars and important anatomical structures such as nerves, blood vessels, and tendons, which in turn affects preoperative planning. Furthermore, we also successfully printed 3D models of deformed bones before surgery in the present study, measured the angle of the skeletal deformity,



and corrected the angle of the deformity, which would be more helpful for surgeons to preoperative surgical evaluation and surgical planning (Figure 2F).

Many studies reported that 3D printed models were used in clinical practice and achieved good clinical results (Matsumoto et al., 2015; Rose et al., 2015; Powers et al., 2016; Youssef et al., 2016). Valverde et al. (2015) also used a Likert scale to assess the effect of 3D printed models by two experts for treatment of aortic hypoplasia and that it could reduce complications and operative time. Liu et al. (2014) demonstrated that the use of 3D printed models led to a 20% reduction in operating time. In this study, preparation of such 3D models for each hypertrophic scar patient can be feasible for surgeons. Preparation of 3D models has the following advantages. First, 3D printing can provide physiologically, anatomically, and tactilely realistic models before surgery. Second, individualized 3D models can be used for preoperative evaluation to reduce the operation time and bleeding, which can shorten hospital stay and reduce hospitalization costs. Third, individualized 3D models provide an effective way to improve communication and build trust between patients and doctors. Fourth, individualized 3D models may be

used to simulate surgery and to teach new doctors (Alali et al., 2015; Hwang et al., 2015; Matsumoto et al., 2015; Rose et al., 2015; Martelli et al., 2016; Powers et al., 2016).

CONCLUSION

Preoperative 3D printing technology can provide accurate 3D models to help surgeons plan operations to resect hypertrophic scars, help young doctors and medical students learn surgical methods, enhance communication and trust between patients and surgeons, and achieve good clinical effects.

DATA AVAILABILITY STATEMENT

All datasets generated for this study are included in the article/supplementary material.

ETHICS STATEMENT

The studies involving human participants were reviewed and approved by the Institutional Review Board of The First Affiliated Hospital of Sun Yat-sen University. Written informed

consent to participate in this study was provided by the participants' legal guardian/next of kin.

AUTHOR CONTRIBUTIONS

JZ and BT designed the research, and reviewed and edited the manuscript. PL, ZH, SH, BT, JZ, PW, YD, PC, and HX performed the experiment. PL, ZH, and SH wrote the manuscript. BT, JZ, ZH, and PL researched the data.

FUNDING

This work was supported by research grant 81471875 (JZ), 81571908 (BT), 81871565 (BT), and 81501675 (ZH) from the National Natural Science Foundation of China, research grant 2016B090916001 (JZ) from the Science and Technology Planning Project of Guangdong Province, research grant 2019A1515012208 (ZH) from the Guangdong Provincial Natural Science Foundation of China, research grant 19ykpy66 (ZH) from the Fundamental Research Funds for the Central Universities of Sun Yat-sen University, and research grant 2013001 (JZ) and 2018003 (BT) from the Sun Yat-sen University Clinical Research 5010 Program.

REFERENCES

- Alali, A. B., Griffin, M. F., and Butler, P. E. (2015). Three-dimensional printing surgical applications. *Eplasty* 15:e37.
- Amici, J. M. (2014). Early hypertrophic scar after surgery on the nasal region: value of long-acting corticosteroid injections. *Ann. Dermatol. Venereol.* 141, 7–13. doi: 10.1016/j.annder.2013.09.167
- Anthonissen, M., Daly, D., Janssens, T., and Kerckhove, E. (2016). The effects of conservative treatments on burn scars: a systematic review. *Burns* 42, 508–518. doi: 10.1016/j.burns.2015.12.006
- Butzelaar, L., Ulrich, M. M., Mink, V. D. M. A., Niessen, F. B., and Beelen, R. H. J. (2015). Currently known risk factors for hypertrophic skin scarring: a review. *J. Plast. Reconstr. Aesthet. Surg.* 69, 163–169. doi: 10.1016/j.bjps.2015.11.015
- Cutroneo, G., Bruschetta, D., Trimarchi, F., Alberto, C., Maria, C., Antonio, D., et al. (2016). In Vivo CT direct volume rendering: a three-dimensional anatomical description of the heart. *Pol. J. Radiol.* 81, 21–28. doi: 10.12659/PJR.895476
- Fitzhugh, A., Naveed, H., Davagnanam, I., and Ashraf, M. (2016). Proposed three-dimensional model of the orbit and relevance to orbital fracture repair. *Surg. Radiol. Anat.* 38, 557–561. doi: 10.1007/s00276-015-1561-1
- Gu, X., Yeoh, G. H., and Timchenko, V. (2016). Three-dimensional modeling of flow and deformation in idealized mild and moderate arterial vessels. *Comput. Methods Biomech. Biomed. Eng.* 19, 1395–1408. doi: 10.1080/10255842.2016.1145211
- Hwang, T. J., Kiang, C., and Paul, M. (2015). Surgical applications of 3-dimensional printing and precision medicine. *JAMA Otolaryngol. Head Neck Surg.* 141, 305–306.
- Lee, K. Y., Cho, J. W., Chang, N. Y., Chae, J. M., Kang, K. H., Kim, S. C., et al. (2015). Accuracy of three-dimensional printing for manufacturing replica teeth. *Korean J. Orthod.* 45, 217–225. doi: 10.4041/kjod.2015.45.5.217
- Lim, A. F., Weintraub, J., Kaplan, E. N., Januszyk, M., Cowley, C., McLaughlin, P., et al. (2014). The embrace device significantly decreases scarring following scar revision surgery in a randomized controlled trial. *Plast. Reconstr. Surg.* 133, 398–405. doi: 10.1097/01.prs.0000436526.64046.d0
- Liu, Y. F., Xu, L. W., Zhu, H. Y., and Liu, S. S. (2014). Technical procedures for template-guided surgery for mandibular reconstruction based on digital design and manufacturing. *Biomed. Eng. Online* 23:63. doi: 10.1186/1475-925X-13-63
- Martelli, N., Serrano, C., van den Brink, H., Pineau, J., Prognon, P., Borget, I., et al. (2016). Advantages and disadvantages of 3-dimensional printing in surgery: a systematic review. *Surgery* 159, 1485–1500. doi: 10.1016/j.surg.2015.12.017
- Matsumoto, J. S., Morris, J. M., Foley, T. A., Williamson, E. E., Leng, S., McGee, K. P., et al. (2015). Three-dimensional physical modeling: applications and experience at mayo clinic. *Radiographics* 35, 1989–2006. doi: 10.1148/rg.2015140260
- Olzowski, R., Szymor, P., and Kozakiewicz, M. (2014). Accuracy of three-dimensional, paper-based models generated using a low-cost, three-dimensional printer. *J. Craniomaxillofac. Surg.* 42, 1847–1852. doi: 10.1016/j.jcms.2014.07.002
- Orgill, D. P., and Ogawa, R. (2014). Discussion: the embrace device significantly decreases scarring following scar revision surgery in a randomized controlled trial. *Plast. Reconstr. Surg.* 133, 406–407. doi: 10.1097/01.prs.0000436812.73412.a4
- Pfeil, A., Haugeberg, G., Renz, D. M., Li, R., Christian, J., Marcus, F., et al. (2017). Digital X-ray radiogrammetry and its sensitivity and specificity for the identification of rheumatoid arthritis-related cortical hand bone loss. *J. Bone Miner. Metab.* 35, 192–198. doi: 10.1007/s00774-016-0741-3
- Ploch, C. C., Mansi, C. S., Jayamohan, J., and Ellen, K. (2016). Using 3D printing to create personalized brain models for neurosurgical training and preoperative planning. *World Neurosurg.* 90, 668–674. doi: 10.1016/j.wneu.2016.02.081
- Powers, M. K., Lee, B. R., and Silberstein, J. (2016). Three-dimensional printing of surgical anatomy. *Curr. Opin. Urol.* 26, 283–288. doi: 10.1097/MOU.0000000000000274
- Rashan, Z. M., Stekelenburg, C., van der Wal, M. B., Euser, A. M., Hagendoorn, B. J. M., Zuijlen, P., et al. (2016). Three-dimensional imaging: a novel, valid, and reliable technique for measuring wound surface area. *Skin Res. Technol.* 22, 443–450. doi: 10.1111/srt.12285
- Rose, A. S., Webster, C. E., Harrysson, O. L., Formeister, E. J., Rawal, R. B., and Iseli, C. E. (2015). Pre-operative simulation of pediatric mastoid surgery

- with 3D-printed temporal bone models. *Int. J. Pediatr. Otorhinolaryngol.* 79, 740–744. doi: 10.1016/j.ijporl.2015.03.004
- Schepers, R. H., Kraeima, J., Vissink, A., Lahoda, L. U., Roodenburg, J. L. N., Reintsema, H., et al. (2016). Accuracy of secondary maxillofacial reconstruction with prefabricated fibula grafts using 3D planning and guided reconstruction. *J. Craniomaxillofac. Surg.* 44, 392–399. doi: 10.1016/j.jcms.2015.12.008
- Seo, B. F., and Jung, S. N. (2016). The immunomodulatory effects of mesenchymal stem cells in prevention or treatment of excessive scars. *Stem Cells Int.* 2016:6937976. doi: 10.1155/2016/6937976
- Silberstein, J. L., Maddox, M. M., Dorsey, P., Feibus, A., Thomas, R., and Lee, B. R. (2014). Physical models of renal malignancies using standard cross-sectional imaging and 3-dimensional printers: a pilot study. *Urology* 84, 268–272. doi: 10.1016/j.urology.2014.03.042
- So, K., McGrouther, D. A., Bush, J. A., Durani, P., Taylor, L., Skotny, G., et al. (2011). Avotermin for scar improvement following scar revision surgery: a randomized, double-blind, within-patient, placebo-controlled, phase II clinical trial. *Plast. Reconstr. Surg.* 128, 163–172. doi: 10.1097/PRS.0b013e318217429b
- Srougi, V., Rocha, B. A., Tanno, F. Y., Almeida, M., Baroni, B., Mendonça, B., et al. (2016). The use of three-dimensional printers for partial adrenalectomy: estimating the resection limits. *Urology* 90, 217–221. doi: 10.1016/j.urology.2015.11.043
- Valverde, I., Gomez, G., Coserria, J. F., Suarez-Mejias, C., Uribe, S., Sotelo, J., et al. (2015). 3D printed models for planning endovascular stenting intransverse aortic arch hypoplasia. *Catheter. Cardiovasc. Interv.* 85, 1006–1012. doi: 10.1002/ccd.25810
- Wu, A. M., Shao, Z. X., Wang, J. S., Yang, X. D., Weng, W. Q., Wang, X. Y., et al. (2015). The accuracy of a method for printing three-dimensional spinal models. *PLoS One* 10:124291. doi: 10.1371/journal.pone.0124291
- Yin, H., Dong, X., and Yang, B. (2015). A new three-dimensional measurement in evaluating the cranial asymmetry caused by craniosynostosis. *Surg. Radiol. Anat.* 37, 989–995. doi: 10.1007/s00276-015-1430-y
- Yong, W. J., Tan, J., Adikrishna, A., Lee, H. Y., Jung, J. W., Cho, D. W., et al. (2014). Morphometric analysis of the proximal ulna using three-dimensional computed tomography and computer-aided design: varus, dorsal, and torsion angulation. *Surg. Radiol. Anat.* 36, 763–768. doi: 10.1007/s00276-014-1260-3
- Youssef, R. F., Spradling, K., Yoon, R., Dolan, B., Chamberlin, J., Okhunov, Z., et al. (2016). Applications of three-dimensional printing technology in urological practice. *BJU Int.* 116, 697–702. doi: 10.1111/bju.13183

Conflict of Interest: The authors declare that the research was conducted in the absence of any commercial or financial relationships that could be construed as a potential conflict of interest.

Copyright © 2020 Liu, Hu, Huang, Wang, Dong, Cheng, Xu, Tang and Zhu. This is an open-access article distributed under the terms of the Creative Commons Attribution License (CC BY). The use, distribution or reproduction in other forums is permitted, provided the original author(s) and the copyright owner(s) are credited and that the original publication in this journal is cited, in accordance with accepted academic practice. No use, distribution or reproduction is permitted which does not comply with these terms.



Selection of Appropriate Wound Dressing for Various Wounds

Chenyu Shi^{1,2}, Chenyu Wang³, He Liu², Qiuju Li², Ronghang Li², Yan Zhang², Yuzhe Liu², Ying Shao^{2,3*} and Jincheng Wang^{1,2*}

¹ School of Nursing, Jilin University, Changchun, China, ² Orthopaedic Medical Center, The Second Hospital of Jilin University, Changchun, China, ³ Department of Plastic and Reconstructive Surgery, The First Hospital of Jilin University, Changchun, China

OPEN ACCESS

Edited by:

Bing Tang,
First Affiliated Hospital of Sun Yat-sen
University, China

Reviewed by:

Wuyu Zhang,
University of Louisville, United States
Kun Zhou,
Boston Children's Hospital,
United States
Tianjiao Ji,
Boston Children's Hospital and
Harvard Medical School,
United States
Lesan Yan,
Wuhan University of
Technology, China

*Correspondence:

Ying Shao
13844880131@163.com
Jincheng Wang
jinchengwang@hotmail.com

Specialty section:

This article was submitted to
Biomaterials,
a section of the journal
Frontiers in Bioengineering and
Biotechnology

Received: 12 November 2019

Accepted: 24 February 2020

Published: 19 March 2020

Citation:

Shi C, Wang C, Liu H, Li Q, Li R,
Zhang Y, Liu Y, Shao Y and Wang J
(2020) Selection of Appropriate
Wound Dressing for Various Wounds.
Front. Bioeng. Biotechnol. 8:182.
doi: 10.3389/fbioe.2020.00182

There are many factors involved in wound healing, and the healing process is not static. The therapeutic effect of modern wound dressings in the clinical management of wounds is documented. However, there are few reports regarding the reasonable selection of dressings for certain types of wounds in the clinic. In this article, we retrospect the history of wound dressing development and the classification of modern wound dressings. In addition, the pros and cons of mainstream modern wound dressings for the healing of different wounds, such as diabetic foot ulcers, pressure ulcers, burns and scalds, and chronic leg ulcers, as well as the physiological mechanisms involved in wound healing are summarized. This article provides a clinical guideline for selecting suitable wound dressings according to the types of wounds.

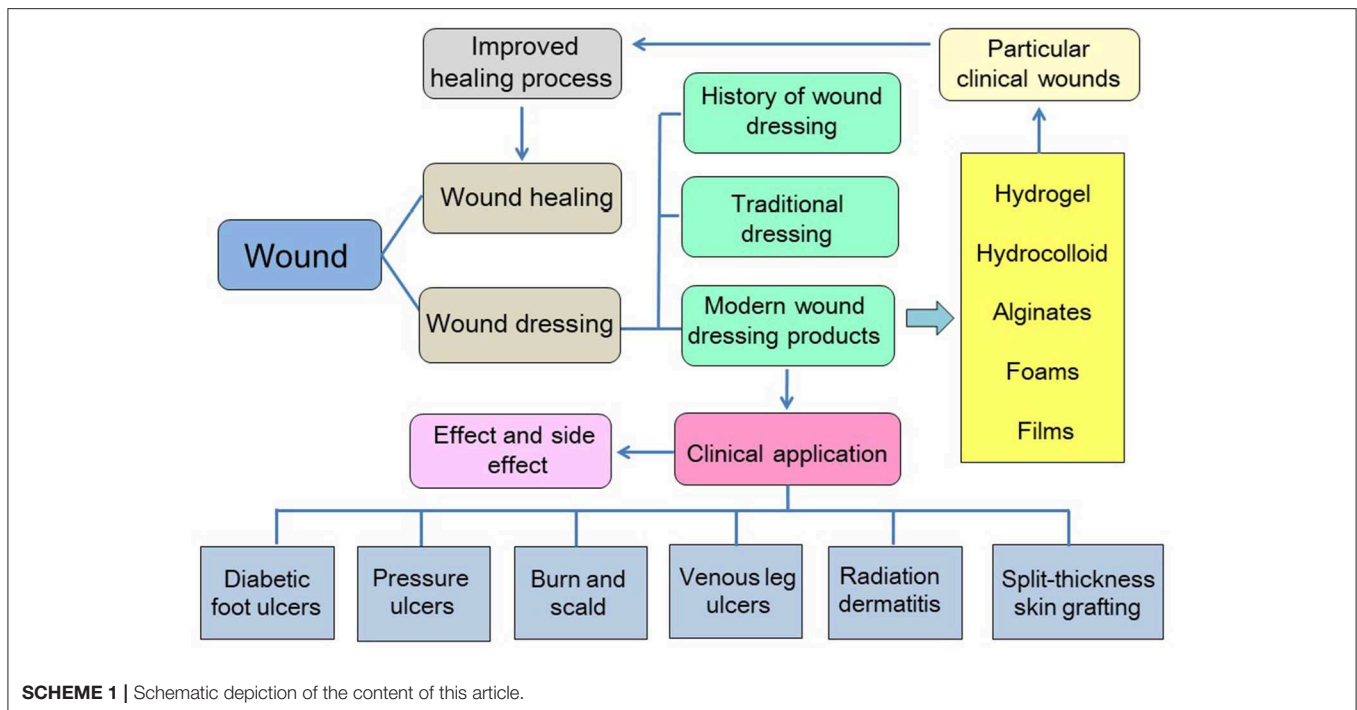
Keywords: wound, wound healing, wound dressing, clinical application, physiological mechanism

INTRODUCTION

Physical or thermal damage can cause defects or interruptions in the epidermis of the skin or mucous membranes, forming a wound (Singh et al., 2013). Wounds are classified as acute or chronic wounds. Acute wounds can recover in a short period of time. The size, depth, and degree of injury of the wound are factors that influence the healing process. However, the healing process of chronic wounds is longer and different from that of acute wounds (Schreml et al., 2010). The healing of acute wounds occurs in a normal, orderly and timely manner throughout the entire process. However, the repair of chronic trauma in this fashion is challenging, and it is difficult to restore normal anatomical structure and function (Tarnuzzer and Schultz, 1996; Borda et al., 2016).

There are many factors involved in wound healing (Guo and Dipietro, 2010). The healing process is not static and growth involves four different phases, namely coagulation and hemostasis, inflammatory, proliferation, and remodeling. These phases are not independent but partially overlap on the basis of a sequence by hemostasis, inflammatory, proliferation, and remodeling (Kasuya and Tokura, 2014; Wilhelm et al., 2017). After skin injury, the wound or tissue fracture is filled with blood clots, followed by acute inflammation of the surrounding tissue. The release of inflammatory mediators and infiltration of inflammatory cells cause tissue swelling and pain. Proliferative fibroblasts, endothelial cells, and newly formed capillaries interact to form granulation tissue filling the crevices. During the shaping period, the scars are softened without affecting the tensile strength through the action of various enzymes and stress, thereby adapting to physiological functions (Jeffcoate, 2012; Harper et al., 2014; Nuutila et al., 2016; Ascione et al., 2017a,b).

Medical dressings are essential devices in healthcare. According to the types and stages of wounds, dressings can be applied to their surface and promote healing. The therapeutic effects



of traditional dry dressings and modern wet dressings in the clinical management of wounds are documented. Although dressings commonly used in clinical practice (gauze, sterilized absorbent cotton, and bandages) are economical, they can only offer physical protection and have limited benefit on wound healing and prevention of infection. Adherence of the dressing to the wound will cause secondary damage when the two are eventually separated. The generation and development of modern dressings are based on the healing theory of the moist environment and have numerous advantages compared with traditional dressings (Skorkowska-Telichowska et al., 2013; Vowden and Vowden, 2014). For example, modern dressings are conducive to the dissolution and absorption of necrotic tissue and fibrin, as well as play a role in autolysis and debridement. Moreover, they are beneficial in maintaining a relatively constant local temperature and humidity of the wound, providing the wound with conditions similar to those of the body's internal environment (Richetta et al., 2011; Heyer et al., 2013). Furthermore, modern dressings avoid re-injury of new granulation tissue due to scarring and promote cell proliferation, differentiation, and epithelial cell migration. Particularly, they may play a role in avoiding wound contact with external bacteria and effectively prevent cross-infection (Murakami et al., 2010; Horn, 2012). Although various advanced wound dressings have been developed and applied in the clinical setting, there is no relevant study investigating the reasonable selection of dressing for a certain type of wound (Powers et al., 2016).

In this review, we summarized the mechanisms of wound healing, traditional and modern wound dressings, and the advantages and disadvantages of both types of dressings. In particular, the clinical application of commercialized modern

dressing products in various pathological wounds (diabetic foot ulcers [DFUs], pressure ulcers, burns and scalds, chronic leg ulcers, radiation dermatitis, and skin grafts) is described in detail to provide insight into the care of wounds. The content of this article is shown in **Scheme 1**.

WOUND DRESSINGS

With the gradual acknowledgment of wound healing theories, the development of wound dressings also evolved considerably. At present, wound dressings are expected to cover the wound and accelerate the healing process (Vowden and Vowden, 2014). Traditional dressings, also termed inert dressings (gauze, cotton pads, and bandages), are the most widely used clinical dressings owing to their low cost and simple manufacturing process (Broughton et al., 2006). However, several shortcomings limit their application, such as difficulty to maintain the wound bed moist and proneness to adhesion to granulation tissue (Moore and Webster, 2013). Modern dressings may be more suitable candidates owing to their properties providing a moist environment for wound healing (Heyer et al., 2013; Moura et al., 2013). Compared with traditional dressings, modern dressings are characterized by better biocompatibility, degradability, and moisture retention. These advantages of modern dressings relieve pain and improve the hypoxic or anaerobic environment (Hopper et al., 2012; Thu et al., 2012; Okuma et al., 2015). The most commonly used modern dressings in clinical practice are hydrogels, hydrocolloid, alginates, foams, and films (**Table 1**).

Hydrogels have a three-dimensional structure composed of hydrophilic substances (Tsang and Bhatia, 2004). They are insoluble in water and subsequently absorb water from 10%

TABLE 1 | Modern dressings used in clinical practice.

Variety	Description	Characteristics	Suitable conditions
Hydrogel	Three-dimensional network of hydrophilic polymers	Moisturizing, removal of necrotic tissue, and monitoring of the wound without removing the dressing	Pressure ulcers, surgical wounds, burns, radiation dermatitis
Hydrocolloid	Hydrogel mixed with synthetic rubber and sticky materials	Excellent exudate absorption properties	Severe exudative wound
Alginate	Consists of polysaccharides derived from brown seaweed	Excellent exudate absorption properties, hemostasis	Infected and non-infected wounds with a large amount of exudate
Foam	Consists of polyurethane or is silicone-based	Semipermeability, thermal insulation, antimicrobial activity	Infected wounds
Film	Consists of adhesive, porous, and thin transparent polyurethane	Autolytic debridement properties, impermeable to liquids and bacteria	Epithelializing wounds and superficial wounds with limited exudate

to thousands fold their equivalent weight (Goodwin et al., 2016). Owing to their excellent moisturizing ability, hydrogels maintain the wound moist and play a positive role in the cleansing of necrotic tissue. In addition, a wound covered with a dressing can be monitored, as the hydrogels are typically transparent (Hunt, 2003; Scanlon, 2003; Kamoun et al., 2017). Based on these characteristics, hydrogels are primarily used on pressure ulcers, surgical wounds, burns, radiation dermatitis, etc. (Francesco et al., 2017; Shamloo et al., 2018). They are suitable for wounds with minimal-to-moderate exudate. The degradation rate of the hydrogel can also be adjusted, which renders this material appropriate for use as a drug carrier and biologically active substance (Gil et al., 2017). For example, silver nanoparticles (Ag NPs) and ZnO NPs loaded hydrogels can maintain antibacterial activity for a long period of time (Li S. et al., 2018). Recently, a study prepared a multifunctional hydrogel for diabetic wounds. This hydrogel can be used on wounds to collect wound photos via mobile phone and transformed into RGB signals to monitor the pH and glucose levels of diabetic wounds in real time (Zhu et al., 2019). Hydrocolloid and hydrofiber dressings are composed of the same materials in nature. Notably, the latter type is a variant of hydrocolloid dressing appropriate for use as a secondary dressing, which can absorb >25-fold its own weight in fluid while maintaining its integrity (Hobot et al., 2008; Richetta et al., 2011).

Sodium alginate (SA) dressings are fibrous products derived from brown seaweed, which can form a gel after binding to wound exudate (Dumville et al., 2013c; O'Meara and Martyn-St James, 2013). The SA dressings used in the clinic are generally made into sheet fibers, which can be freely cut according to the shape of the wound. SA is also often used to synthesize hydrogels. The SA dressings also possess excellent exudate absorption properties; hence, they can be used in infected and non-infected wounds with a large amount of exudate (Hess, 2000). Owing to the strong absorption property of alginates, their use in the treatment of dry wounds or wounds with minimal exudate should be avoided. Meanwhile, A study developed an alginate hydrogel contained both bioglass and desferrioxamine, which better facilitated diabetic skin wound healing. The results demonstrated that combination use of BG and DFO improved

the migration and tube formation of HUVECs as compared with the use of either BG or DFO alone as BG and DFO could synergistically upregulate VEGF expression (Kong et al., 2018).

Foam dressings are semipermeable and either hydrophilic or hydrophobic with a bacterial barrier (Sedlarik, 1994). They are composed of polyurethane or silicone-based, rendering them suitable for handling moderate-to-high volumes of wound exudate (Marks and Ribeiro, 1983). Foam dressings provide thermal insulation and maintain moisture to the wound, and prevent damage to the wound at the time of removal. These dressings may also be used as secondary dressings with hydrogel or alginate dressings, in conjunction with a topical antimicrobial agent for infected wounds (Davies et al., 2017). Moreover, polyaniline/polyurethane foam dressing carried an anti-biofilm lichen metabolite usnic acid indicated an improved antibiofilm activity of conducting polymer (dos Santos et al., 2018).

Film dressings are composed of adhesive, porous, and thin transparent polyurethane. Oxygen, carbon dioxide, and water vapor from the wound pass through the dressing, whereas liquids and bacteria are well-isolated. Furthermore, film dressings possess autolytic debridement properties (Thomas, 1990; Fletcher, 2003), and are suitable for use on epithelializing wounds and superficial wounds with few exudates (Imran et al., 2004). The various types of dressings described above have their own characteristics; thus, the selection of the dressing should be based on the specific conditions of the wound.

CLINICAL APPLICATIONS OF MODERN WOUND DRESSING PRODUCTS

Wound healing involves four different phases, namely coagulation and hemostasis, inflammatory, proliferation, and remodeling (Amini-Nik et al., 2018). Different types of dressings have different characteristics; different pathological types of wounds also have their own characteristics (Table 2). For example, DFUs are prone to infection and cause unsatisfactory wound healing. The prevention of pressure ulcers is focused on the reduction of the shear force and pressure in the hazardous area. Following the formation of the ulcer, it is equally important to prevent further pressure on the ulcer and apply the dressing.

TABLE 2 | Overview of various wounds and appropriate clinical dressings.

Variety	Description	Characteristics	Appropriate dressing
Diabetic foot ulcer	Caused by neuropathy and lower extremity vascular disease	Lack of supply of oxygen and blood in the wound bed; long-term stagnation in the inflammatory phase	Silver ion foam dressing, hydrofiber dressing, UrgoStart Contact dressing, Mepilex® Lite Dressing, hyaluronic acid, Biatain® Non-adhesive Dressing
Pressure injury	Caused by stress and tissue tolerance	A local injury to the skin or subcutaneous soft tissue occurring at the site of the bone prominence or the compression of the medical device	Foam dressing, hydrocolloids dressing, multi-layered soft silicone foam dressings, polyurethane film, Mepilex® Ag dressing, polyurethane foam dressing
Burn and scald	Tissue damage caused by heat	A large amount of exudate; prone to infection; severe cases can injure subcutaneous and submucosal tissues	Moist occlusive dressing (AQUACEL® Ag), ACTICOAT™ with nano silver
Chronic venous leg ulcer	Caused by high pressure of the blood in the leg veins	Lack of blood supply to the wound; a large amount of necrotic tissue and abnormal exudate on the surface of the ulcer, accompanied by multiple bacterial infections	Alginate dressing, AQUACEL® Ag dressing, Urgotul® Silver dressing, ALLEVYN® Hydrocellular foam dressings, Mepilex® foam dressing
Radiation dermatitis	Local skin lesions caused by radiation	Slow cell proliferation; decreased cytokine activity; decreased collagen content	Film dressing (Airwall), silver-containing hydrofiber, film dressing (3M™ Cavilon® No Sting Barrier Film), Mepilex® Lite dressing
Split-thickness skin grafting	None	Hypertrophic scars; hypopigmentation; hyperpigmentation	Polyurethane foam (ALLEVYN™), calcium alginate (Kaltostat®), AQUACEL® Ag (Convatec), Alginate Silver (Coloplast)

Lower extremity chronic ulcers are associated with exudation from wounds due to lower limb edema. Acute wounds, such as burns and scalds, also have their own characteristics. The application of different dressings to different pathological types of wounds in the clinical setting is illustrated in **Table 2**.

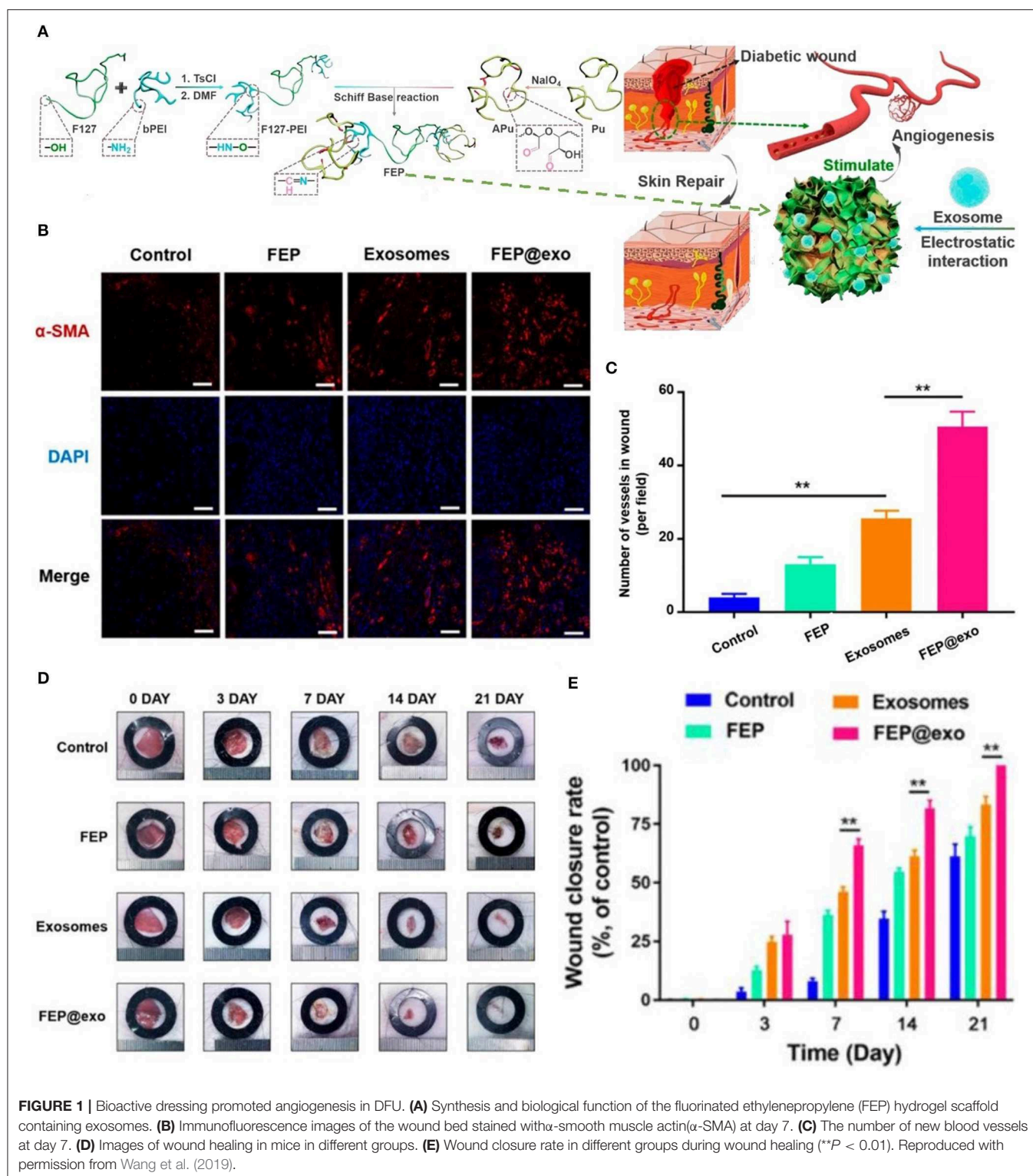
DFUs

In diabetics, the incidence of DFUs is approximately 5–10%. It is one of the most common chronic complications and the cause of lower extremity amputation in patients with diabetes mellitus (Brennan et al., 2017). DFUs as a common type of non-healing or chronic wounds are attracting considerable attention in the medical field (Khanolkar et al., 2008). Currently, the selection of the most appropriate treatment is challenging. During this process, multiple types of dressings are applied to the treatment of DFUs (Saco et al., 2016). One such method is the application of various kinds of modern dressings. Treatment with suitable dressings is an important part of the management of DFUs.

DFU is defined as foot pain, foot ulcer, and foot gangrene caused by neuropathy and lower extremity vascular disease. The pathogenesis of DFU is very complicated, and its clinical manifestations are heterogeneous (Acosta et al., 2008; Blakytyn and Jude, 2009). Therefore, the treatment strategy for DFU is a multi-disciplinary, long-term combination therapy process. Application of dressings is an integral part of long-term treatment options. In the diabetic state, multiple factors cause stagnation in one or more stages of the normal healing process. Microvascular disease results in a reduced supply of oxygen and blood in the wound bed, which delays healing and increases the risk of infection (Rathur and Boulton, 2005; Snyder and Waldman, 2009). Bioactive dressings are a good choice for the

repair of diabetic wounds. As shown in **Figure 1**, researchers have prepared an injectable adhesive thermosensitive multifunctional polysaccharide-based dressing (fluorinated ethylenepropylene) that can continuously release exosomes to promote angiogenesis at the wound site and accelerate the healing process (Khanolkar et al., 2008; Wang et al., 2019). The silver ion foam dressing used in patients with diabetic foot maintains the wound moist. Studies have shown that a better extracellular matrix environment is a vital factor in promoting the migration of keratinocytes and fibroblasts, and synthesis of collagen (Alvarez, 1988; Morton and Phillips, 2012). In addition, silver ions prevent wound infection, thereby avoiding long-term stagnation in the inflammatory phase due to recurrent infections (Barnea et al., 2010).

Several studies have applied modern dressings containing silver ions to the treatment of DFUs. Jude et al. reported the effect of AQUACEL® Hydrofiber® (E. R. Squibb & Sons, L.L.C., Princeton, NJ, USA) dressings containing ionic silver and Algosteril® (Les Laboratoires Brothier, S.A., Nanterre, France) calcium alginate (CA) dressings in patients with diabetes mellitus and non-ischemic Wagner Grade 1 or 2 DFUs. The study found that the clinical effect of ionic silver dressings was better compared with that of CA dressings, especially for the reduction of ulcer depth and healing of infected ulcers. Ionic silver-treated ulcers reduced in depth nearly twice as much as CA-treated ulcers (Jude et al., 2007). Another study used Contreet Foam (Coloplast A/S, Humlebaek, Denmark), a foam dressing containing silver ions to manage patients with diabetic foot. The study showed that Contreet Foam is safe and easy to use, and effectively accelerates the wound healing process (Rayman et al., 2005). A study evaluated the efficacy of hydrofiber dressings and wound healing in DFUs, comparing the safety, final outcome, and patient



compliance. Following treatment, hydrofiber dressing showed better healing of the foot ulcer vs. the povidone dressing (Suvarna et al., 2016). Richard et al. studied the effect, tolerance, and acceptability of UrgoStart Contact dressing (Laboratoires Urgo,

Chenove, France) in diabetic patients with a neuropathic foot ulcer. The results indicated that the UrgoStart Contact dressing is linked to good tolerance and acceptability, which can effectively promote the healing of neuropathic DFU (Richard et al., 2012).

Zhang et al. compared the efficacy of Mepilex® Lite Dressings (Mölnlycke Health Care, Gothenburg, Sweden) with Vaseline Gauze in the treatment of DFU. The results showed that the study group (Mepilex® Lite) was significantly different from the control group in terms of the mean healing time and wound area. The investigators concluded that the Mepilex® Lite dressing provides a better alternative for the treatment of DFU and warrants further research (Zhang and Xing, 2014). In one study, pure hyaluronic acid was applied to the treatment of DFUs. The results showed that pure hyaluronic acid without other ingredients significantly promotes the healing of DFU without the occurrence of adverse reactions (Lee M. et al., 2016). Lohmann et al. investigated the effect and safety of Biatain® Non-adhesive Dressing (Coloplast A/S, Humlebaek, Denmark) in the treatment of patients with DFU. The results indicated that the average wound area was reduced by more than half in patients treated with the Biatain® dressing (Lohmann et al., 2004). In addition to the common dressings mentioned above, there are other dressings that promote the healing of DFU. A study used sucrose octasulfate dressing treating neuroischemic DFU for 20 weeks, result indicated this dressing significantly improved wound closure without affecting safety (Edmonds et al., 2018). Other study compared bioimplant dressing, a tissue-engineered form of wound dressing containing acellular human amniotic collagen membrane (Life Patch, International Bioimplant Company, Tehran, Iran) with wet dressing in treating DFU. The results show that bio-implantable dressings promote wound healing in DFU better than wet dressings (Edmonds et al., 2018).

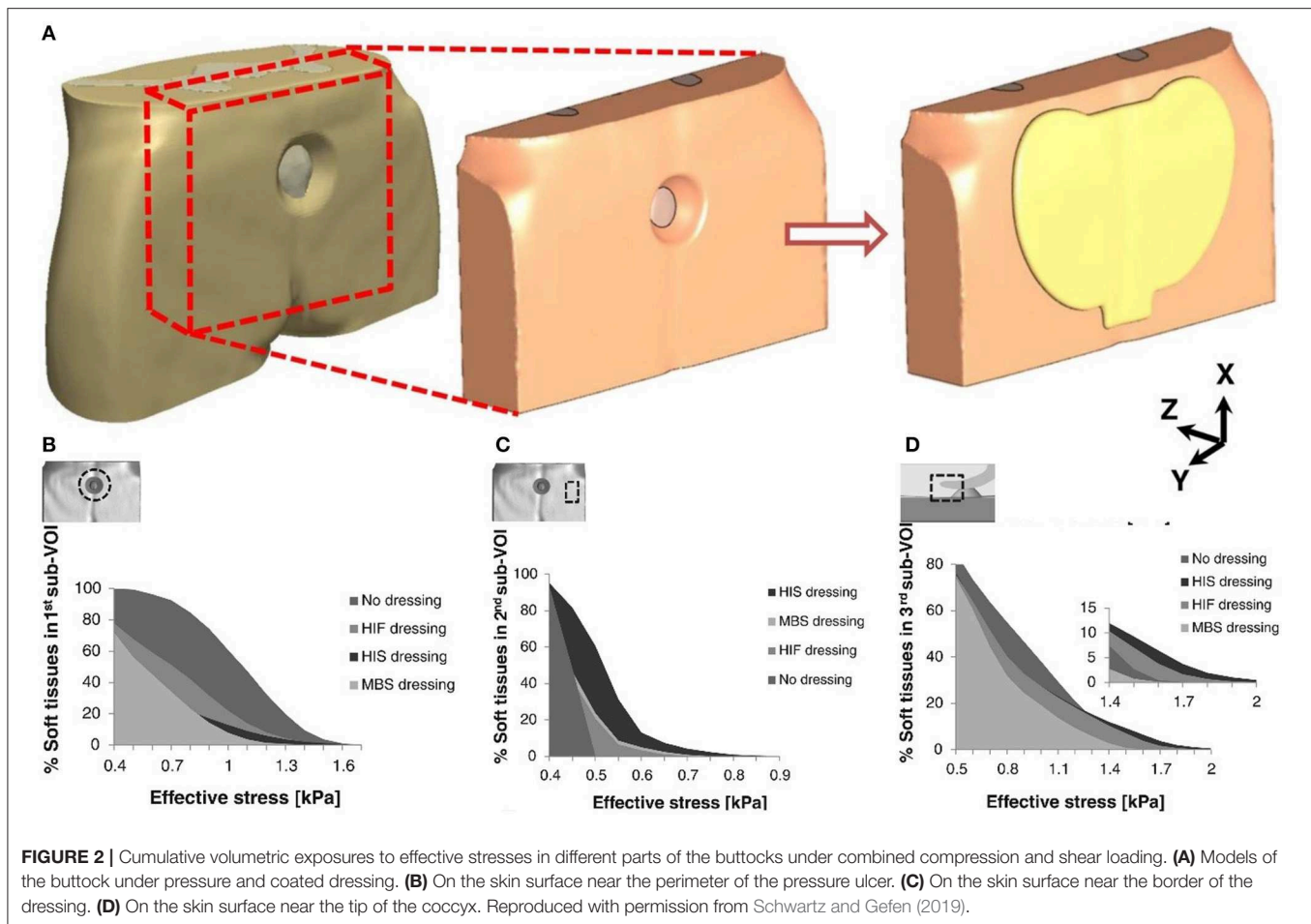
DFU is a prevalent and serious global health issue. Wound dressings are regarded as important components of treatment system, with clinicians and patients having many different dressing types to choose from, including hydrogel, foam, hydrocolloid, alginate. The effectiveness of these dressings in DFU has been systematically evaluated, but the conclusions indicated only hydrogels are superior to other types of dressings in healing of DFU (Dumville et al., 2013a,b,c,d). It is worth noting that these systematic reviews included a very small number of studies and were performed several years ago. Decision makers can consider aspects such as the cost of the dressing and the wound management features provided by each type of dressing to determine its use (Wu L. et al., 2015). The effectiveness of these dressings in DFU has been systematically evaluated, but only conclusions are that only hydrogels are superior to other types of dressings in healing of DFU. It is worth noting that these systematic reviews included a very small number of studies and were performed several years ago. Decision makers can consider aspects such as the cost of the dressing and the wound management features provided by each type of dressing to determine its use. It is suggested that more higher quality clinical dressing studies and more comprehensive systematic reviews of the effects of dressings will be conducted in the future.

Pressure Injury

Pressure injury is local injury to the skin or subcutaneous soft tissue, manifested as intact skin or an open ulcer, possibly accompanied by pain. It usually occurs at the site of bone

prominence or compression of the medical device (Webb, 2017). Stress injuries often occur in patients who are unable to change their position (Pancorbo-Hidalgo et al., 2006; Pieper et al., 2009). The application of dressings is one of the preventive strategies employed in such cases; however, this approach also increases the total cost of treatment. Therefore, it is necessary to determine whether the use of these dressings provides potential benefit to patients (Sebern, 1986). The main factors in the occurrence of injury are stress and tissue tolerance. Stress factors include compressive strength and duration; tissue tolerance is usually affected by the patient's condition and the external microenvironment (Tirgari et al., 2018; Weller et al., 2018). Since the formation of stress injuries can be avoided, prevention is the main task in the clinic. Foam dressings help to reduce the vertical pressure, shear, and friction of the skin, effectively preventing the occurrence of pressure damage (Bolton, 2016; Truong et al., 2016). As shown in **Figure 2**, researchers have evaluated the effects of the structural and mechanical properties of different dressings to the soft tissue around the wound. These three dressings were Mepilex® Border Sacrum, hypothetical isotropic stiff dressing, and hypothetical isotropic flexible dressing. The anisotropic stiffness feature of the Mepilex® Border Sacrum dressing is essential in wound healing (Schwartz and Gefen, 2019). Studies have shown that excessive skin moisture leads to excessive hydration and damage to the normal barrier function of the skin, hence increasing the risk of ulceration (Demarre et al., 2015). Hydrocolloids or foam dressings for patients with incontinence protect the skin of the appendix from infestation, maintain the skin dry, provide a good microenvironment, and improve tissue tolerance (Williams, 2000). A study assessed the pressure-reducing effect of 10 dressing products, consisting of five types of material (polyurethane foam, hydropolymeric, hydrofiber, hydrocolloid, and low-adherent absorbent). ALLEVYN Non-Adhesive (Smith & Nephew Healthcare, London, UK) exhibited the lowest pressure, while DuoDERM® Extra Thin CGF (ConvaTec Inc., Princeton, NJ, USA) showed the highest pressure (Matsuzaki and Kishi, 2015). Interestingly, a study investigated the modes of action preventing the occurrence of pressure ulcer, such as shear and friction force redistribution, and pressure distribution. The results revealed that the use of Mepilex® and ALLEVYN® dressings reduced frictional forces and shear forces at high-risk areas. In addition, dressings with horizontal fabric structures transferred load over a greater area (Call et al., 2015).

Many clinical studies show that foam dressings can reduce the incidence of pressure ulcers. A randomized controlled trial investigated the role of Mepilex® Border Sacrum and Mepilex® Heel dressings in preventing stress injuries in critically ill patients prior to transfer to the intensive care unit (ICU). The results showed significant differences in the incidence of pressure injuries between the two groups ($\leq 10\%$). Thus, the study concluded that the application of multi-layered soft silicone foam dressings reduces the incidence in patients prior to transfer to the ICU (Santamaria et al., 2015). A study reported the preventive effect of a five-layer soft silicone border dressing in patients undergoing cardiac surgery in the ICU. The results indicated that there are differences in the occurrence of pressure



injury; however, the difference was not significant (Brindle and Wegelin, 2012). Chaiken et al. applied a silicone border foam dressing to the appendix of patients in the ICU to examine whether the dressing reduces sacral pressure injury. The results showed that the incidence of pressure ulcers decreased from 13.6 to 1.8% after application of the dressing, indicating that this type of dressing effectively reduces the incidence of sacral pressure injury in the ICU (Chaiken, 2012). Furthermore, Walsh et al. applied a silicone border foam dressing to the tibia region of patients in the ICU. The results showed that the incidence of hospital-acquired pressure injury in the ICU decreased from 12.5% in 2009 to 7% in 2010, and the number of sacral pressure injury cases decreased from 50 to 13, respectively (Walsh et al., 2012). Nakagami et al. reported a new dressing containing ceramide 2, which can improve the water-holding capacity. The results indicated that the incidence of persistent erythema was significantly lower in the intervention area compared with the control area. The study concluded that the dressing may be applied to patients with thin and dry skin for the prevention of pressure injury (Nakagami et al., 2007). Another study reported the effect of a polyurethane film in preventing postoperative pressure ulcers. The study found that the polyurethane film patch effectively prevented the occurrence of erythema in the sacral area immediately after surgery (Imanishi et al.,

2006). A retrospective study investigated the effectiveness of Mepilex® Ag dressings in decreasing post tracheotomy pressure injury. Another retrospective study reported the effectiveness of Mepilex® Ag dressings in preventing stress injuries in children after thoracotomy. Prior to the application of Mepilex® Ag, the incidence of skin rupture during replacement of the first tracheostomy tube was 11.8%. When Mepilex® Ag was applied, there was no occurrence of skin rupture around the stoma. The study concluded that use of Mepilex® Ag reduces the occurrence of postoperative peristomal pressure injury (Kuo et al., 2013). A systematic review evaluated the effectiveness of dressings and topical preparations in preventing pressure ulcers. Nine dressing studies were included in the 18 included studies. It is concluded that silicone dressings can reduce the incidence of pressure ulcers, but the certainty of the evidence is still low and further research is needed to confirm it. At the same time, the role of polyurethane foam dressings and conventional treatments or hydrocolloids in the prevention of pressure ulcers was also compared. Although the results showed no significant difference, the level of evidence in these studies was very low, and more high-quality studies are needed in the future (Moore and Webster, 2018).

Dressings are widely used to treat pressure ulcers and promote healing, and there are many options, including alginates,

hydrocolloids, etc. In 2017, a network meta-analysis of dressings and topical medications for pressure ulcers has been performed. This work concluded that there is currently insufficient evidence to determine whether any dressing or topical treatment promotes the healing of pressure ulcers over other methods. However, it is worth noting that many of the trials in this review are small and carry a high risk of bias (Westby et al., 2017). Only one of these studies had a low risk of bias, which compared the effects of local collagen and hydrocolloids on pressure ulcer healing. Although the results showed no significant difference in healing results between collagen and hydrocolloids, the cost of using collagen was more than double that of hydrocolloids (Graumlich et al., 2003).

Although some research results have demonstrated the role of dressings in the prevention and treatment of pressure ulcers. At the same time, the network meta-analysis also revealed generally poor quality of randomized controlled trials of pressure ulcer dressings, which indicates that the trial plan in this field needs to be improved and perfected. Given the uncertainty of the effectiveness of dressing interventions, any investment in future research must maximize its value to decision makers. Any evaluation of future interventions for the healing of compression ulcers should focus on the dressings most widely used by health professionals. In addition, for people with pressure ulcers, faster recovery is as important as whether recovery occurs, so future research should consider the time to recover from pressure ulcers.

Burns

Burns, generally caused by heat (i.e., hydrothermal fluids, vapors, hot gases, flames, hot metal liquids or solids) cause tissue damage, mainly on the skin and mucous membranes. Severe cases may also injure subcutaneous and submucosal tissues, such as muscles, bones, joints, and even internal organs (Park, 1978). Acute burns are divided into surface, partial, and full thickness burns (Stavrou et al., 2014). Full-thickness burns involve the entire structure of the skin, and even affect the muscles and bones in severe cases. Despite causing considerable pain and suffering, these types of burns heal easily without surgical intervention. Accurate assessment of the depth of burns is crucial for treatment decision-making. In the presence of infection, superficial and partial thickness wounds can deteriorate into deeper burns. A large amount of exudate causes the patient to lose water and nutrients, and provides the appropriate conditions for bacterial growth. Exudation continues to increase in the inflammatory phase, eventually leading to delayed wound healing. Therefore, most of the dressings (e.g., Ag foam dressings) have the ability of osmotic absorption and prevention of infection. Modern dressings used in the remodeling stage reduce the formation of scars and maximize functional recovery at the wound area. Researchers have prepared a new type of hydrogel, termed HA-az-F127 hydrogel. It is formed by the reaction of a hydrazide-modified hyaluronic acid with a F127 triblock copolymer terminated with a benzaldehyde, as shown in **Figure 3**. The excellent physical properties of this hydrogel and the action of

aspiration drainage promote healing of burn wounds (Li Z. et al., 2018).

Mabrouk et al. compared the effects of two moist wound management methods, AQUACEL® Ag (ConvaTec Inc., Princeton, NJ, USA), a moist occlusive dressing, and MEBO® (Beijing, China), a moist open dressing, in children with facial partial thickness burns. The results showed that the AQUACEL® Ag group had a faster re-epithelialization rate, a lower frequency of dressing change, and less pain, compared with the MEBO® group. The study concluded that the healing rate and long-term outcomes of the moist occlusive wound dressing was better than those of the moist open dressing for the repair of facial partial thickness burns (Mabrouk et al., 2012). A study reported the effectiveness of two commonly used silver dressings, ACTICOAT™ (Smith & Nephew, Hull, UK) and AQUACEL® Ag, in the treatment of partial burns. The results showed that the healing time and bacterial control of the two silver dressings was similar. However, AQUACEL® Ag dressings have advantages over ACTICOAT™ dressings in terms of patient comfort and cost-effectiveness (Verbelen et al., 2014). Bugmann conducted a study to compare the effects of Mepitel® (Mölnlycke Health Care, Gothenburg, Sweden) and silver sulfadiazine for the treatment of pediatric burns. The results indicated that the Mepitel® group achieved a faster healing process (Bugmann et al., 1998). Huang et al. reported the efficacy and safety of the ACTICOAT™ Ag dressing and silver sulfadiazine for the treatment of burn wounds. The study concluded that ACTICOAT™ with nano silver effectively promoted the healing process of residual wounds after burns without the occurrence of adverse effects (Huang et al., 2007).

A study investigated the degree of pain experienced by the patient when using two different dressings: ACTICOAT™ dressing and silver sulfadiazine. The results demonstrated that the use of the ACTICOAT™ dressing for burn wound care is less painful than the use of silver sulfadiazine in patients with partial thickness burns (Varas et al., 2005). A study reported the pain-reducing function of a silver dressing (AQUACEL® Ag) in patients with partial thickness burns. The results indicated that the wound healing time in the AQUACEL® Ag group was significantly shorter compared with that observed in the silver sulfadiazine group. In addition, the patient's pain was also significantly reduced (Muangman et al., 2010). Another study reported the efficacy of an alginate silver dressing, Askina Calgitrol Ag® (B. Braun Hospicare Ltd, Collooney Co. Sligo, Ireland), and 1% silver sulfadiazine in the management of partial-thickness burn wounds. The results indicated that the average pain score and wound healing time in the Askina Calgitrol Ag® group was significantly lower/shorter than those reported in the silver sulfadiazine group (Opasanon et al., 2010).

Similar to DFUs, burns and scalds are generally larger and prone to infection. Therefore, some antibacterial dressings are often used. Silver sulfadiazine is a commonly used wound management method for burns; however, it can easily cause pain in patients. A recent systematic review evaluated the effectiveness of silver-containing foam dressings and traditional SDD dressings in treating partial thickness burns. This work concluded that there is no significant difference in wound healing

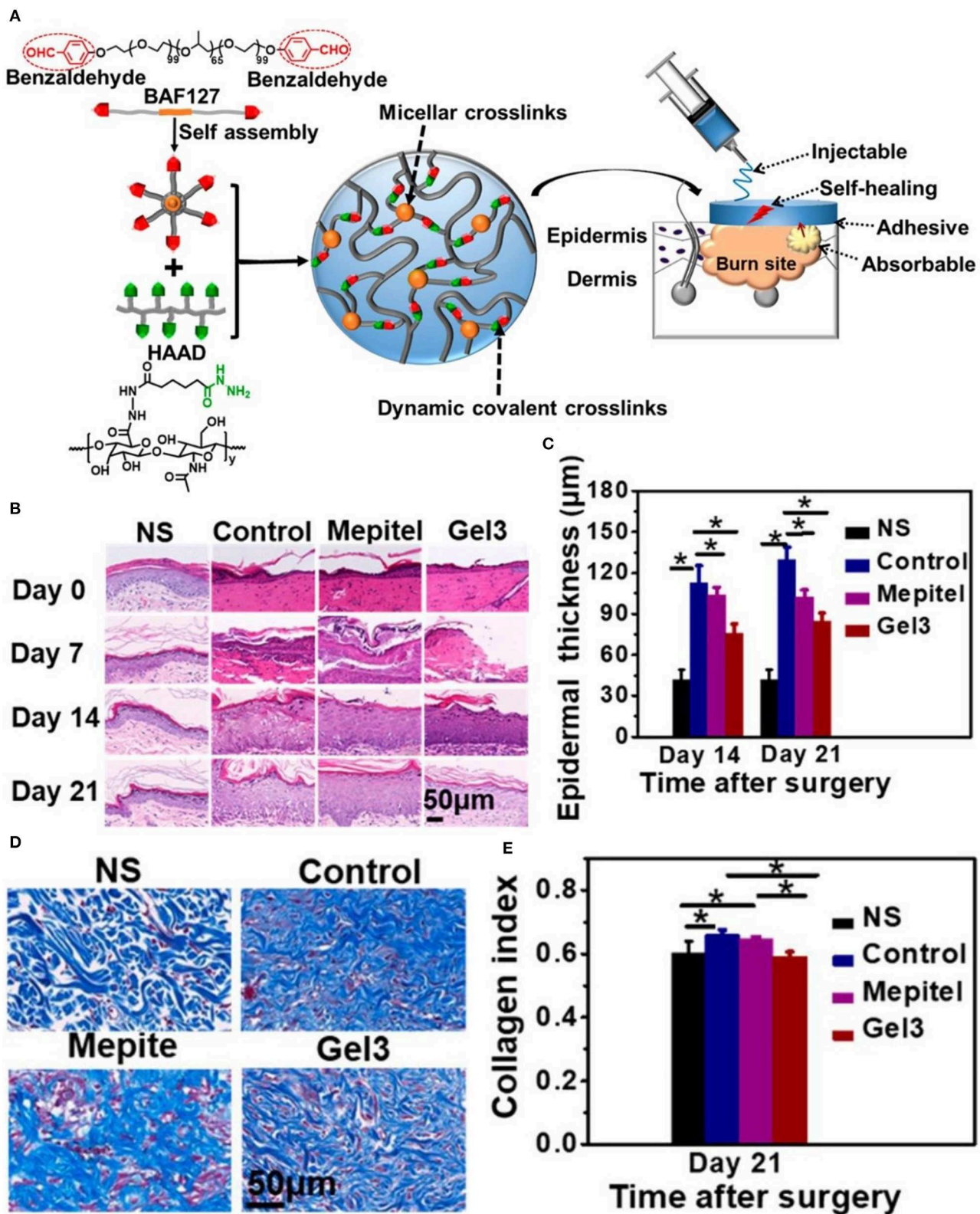


FIGURE 3 | HA-az-F127 hydrogel promotes healing of burn wounds. **(A)** Synthesis and physical characteristics of the HA-az-F127 hydrogel. **(B)** H&E staining at different days after treatment. **(C)** Epidermal thickness in different treatment groups at days 14 and 21. **(D)** Masson's trichrome staining of wounds at day 21. **(E)** Quantification of collagen content in different treatment groups at day 21 (* $P < 0.05$). Reproduced with permission from Li Z. et al. (2018).

between silver-containing foam dressing and SSD dressing, but silver-containing foam dressing reduced pain during the early treatment phase and potentially decreased infection rates. Excessive pain may severely affect the patient's mental and physiological state. Therefore, most studies select the severity of pain as one of the outcome variables to compare these two dressings. Rapid healing of wounds and the prevention of hyperplasia of scars in advanced stages of healing are important aspects for patients with burns. Scar hyperplasia in key areas will seriously affect the patient's physiological function and quality of life. Nevertheless, very few studies have focused on this aspect. Future studies including larger sample sizes and follow-up of patients with wound scar hyperplasia are warranted.

Chronic Venous Leg Ulcers (VLU)

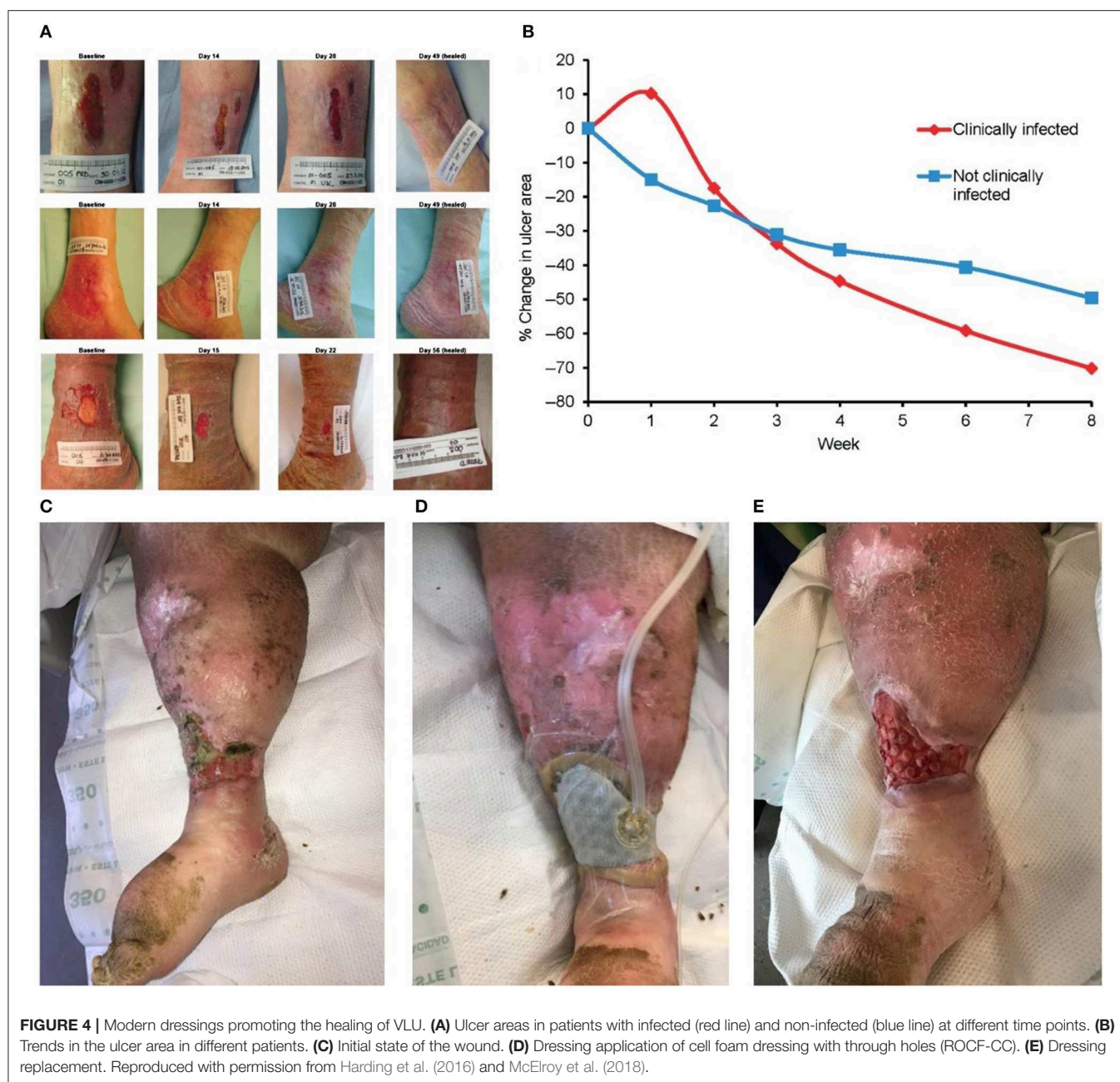
Venous leg ulcers (VLU) are chronic ulcers caused by excessive venous pressure in the lower extremities and abnormal venous blood flow, eventually leading to the formation of an ulcer on the skin of the lower leg (Palfreyman et al., 2007; Chapman, 2017). It is one of the clinical manifestations of chronic venous insufficiency at the most severe stage. The underlying causes of the disease are venous valve incompetence and calf muscle pump insufficiency, leading to venous stasis and hypertension (Gianfaldoni et al., 2017). In this case, the local blood circulation is altered, and the blood supply to the local tissue is insufficient (Serra et al., 2016). Prolonged care leads to high treatment costs. Moreover, the quality of life of patients with chronic VLU is severely affected (Salome et al., 2016).

The venous regurgitation disorder, insufficiency of the vascular function, weak venous wall, and incomplete systolic muscle pump function are considered to be the main causes of VLU formation (Lozano Sanchez et al., 2014). The inflammatory response of leukocytes and endothelial cells is important in the development of VLU (Raffetto, 2009). Based on the above, skin capillary damage, local microcirculation and tissue absorption disorders, fibrin exudation, accumulation of metabolites, lower extremity edema, and skin nutrition changes, followed by bacterial and other microbial infections, eventually lead to the development of ulcers (Dawkins, 2017). Compression therapy is the main conservative treatment of VLU. The treatment mainly includes bandages, elastic stockings, and inflation and compression devices (Rajendran et al., 2007). Moreover, there is substantial necrotic tissue and abnormal exudate on the surface of the ulcer, often accompanied by multiple bacterial infections. Thus, treatment of the wound surface is also necessary. The Ag foam dressing absorbs a large amount of exudate, and it can be used for the prevention of infection. The dressing can be combined with compression therapy to promote wound healing. The alginate dressing absorbs large amounts of exudate and is also suitable for the treatment of VLU. As shown in **Figures 4A,B**, silver ion dressing plays a positive role in wound healing (Harding et al., 2016). Of course, debridement is inevitable. A new type of porous mesh foam dressing, cell foam dressing with through holes (ROCF-CC), was introduced into negative pressure wound therapy with instillation and dwell. As shown

in **Figures 4C–E**, this dressing is highly effective on debridement (McElroy et al., 2018).

A study evaluated the effectiveness of knitted viscose and hydrocolloid dressings for venous ulceration. The results indicated that there are no significant differences in these two dressings (Nelson et al., 2007). Maggio et al. tested the effectiveness and safety of Vulnamin[®] gel (Errekappa, Milan, Italy) and compressive bandages in patients with lower limb chronic venous ulcers. The results indicated that the use of Vulnamin[®] together with elastic compressive bandages is safe and more effective than standard dressing (Maggio et al., 2012). Another study compared the wound healing efficacy of AQUACEL[®] Ag dressing and Urgotul[®] (Laboratoires Urgo, Chenove, France) Silver dressing for the treatment of venous ulcers at risk of infection. The results showed that both silver dressings were effective in the healing of venous ulcers (Harding et al., 2012). Lammoglia et al. reported the effectiveness and safety of *M. tenuiflora* cortex extract (MTC-2G) in patients with VLU. The results indicated that there was no significant difference between hydrogel containing MTC-2G and hydrogel alone for the treatment of VLU (Lammoglia-Ordiales et al., 2012). A study evaluated LyphoDermTM (XCELLentis, Belgium) gel containing allogeneic epidermal keratinocytes in the treatment of patients with venous ulcers, which are difficult to heal. The results indicated that, in the subgroup with enlarging ulcers, there were significantly more healed ulcers in the LyphoDermTM group vs. the control group (Harding et al., 2005). Franks et al. compared the effectiveness of ALLEVYN[®] Hydrocellular and Mepilex[®], two commonly used foam dressings, in the treatment of chronic VLU. Although the results did not reveal significant differences in the number of patients achieving complete repair of ulcers between the two groups, both dressings reduced pain after treatment (Franks et al., 2007). Another study compared the treatment effect and cost-effectiveness of silver-containing and non-silver low-adherence dressings in the management of VLU. The results indicated that there were no significant differences between the silver-containing dressing group and the control group (Michaels et al., 2009). A study evaluated the effectiveness and safety of Contreet Foam, a dressing with sustained release of silver, in the management of chronic VLU with moderate and high exudation. The results indicated that Contreet Foam combined with silver achieved excellent exudate management in patients with hard-to-heal chronic VLU (Karlsmark et al., 2003).

Unlike the aforementioned types of wounds, VLU in the lower extremities requires treatment of lower extremity edema to promote wound healing. Tissue edema can stress the arteries and affect the blood circulation in the lower extremities, resulting in insufficient blood supply to the wound. The combination of wound dressings and multiple lamination treatments may exert the best therapeutic effect. At the meantime, a network meta-analysis show that silver-containing dressings can increase the likelihood of VLU healing, but because of the small number of related studies and high risk of bias, the most effective treatment is still not determined (Norman et al., 2018). This results of this network meta-analysis focus exclusively on complete healing, did not take other important outcomes into consideration.



Therefore, decision makers can appropriately draw on the results of the above studies according to the actual situation of the wound when choosing a dressing. At the same time, more high-quality research is needed in order to obtain more definitive evidence-based evidence in order to provide reliable decision-making basis for decision makers.

Radiation Dermatitis

Radiation therapy is a common method for the treatment of cancer. It is used to treat cancer that is not suitable for surgery or assist surgery (Terasawa et al., 2009). Radiation-related skin lesions are most common in radioactive local lesions

and can be classified as acute radiation-induced skin injury, chronic radiation-induced skin injury, and radiation skin cancer (Kirkwood et al., 2014). Skin side effects of radiation therapy occasionally limit its application (Wickline, 2004; Hird et al., 2008). Severe adverse skin reactions may affect further treatment. At present, the prevention and management of radiation-induced skin injury remains a challenge. Modern wound dressing can be used as a prevention and management method.

Radiation increases the expression of apoptosis-related genes, retards cell proliferation, and decreases cytokine activity and collagen content, resulting in delayed wound healing (Zhang et al., 2012, 2014). A transparent film dressing can be used to

protect the skin in the illuminated area. The film dressing using Airwall exhibited a satisfactory prophylactic effect (Arimura et al., 2016).

Radiation dermatitis severity was reduced in patients with breast cancer radiotherapy after prophylactic use of Hydrofilm (Paul Hartmann AG, Heidenheim, Germany) compared with control (Schmeel et al., 2019). A study examined the effect of a film dressing (Airwall) in the management of acute radiation dermatitis induced by proton beam therapy. The results indicated that the Airwall group experienced less severe acute radiation dermatitis compared with the standard management group (Arimura et al., 2016). Perea et al. evaluated the effectiveness of silver-containing Hydrofiber® dressings in minimizing or preventing radiation-induced dermatitis. They suggested that silver-containing Hydrofiber® dressings are effective in reducing radiation dermatitis and arresting its progression, consequently leading to shorter healing time (Whaley et al., 2013). A clinical study investigated the effects of film dressings 3M™ Cavilon® No Sting Barrier Film (3M, Minneapolis, MN, USA), and topical corticosteroids on skin exposed to radiotherapy and compared the effects of the two methods in preventing radiation dermatitis. The results showed that although 3M™ film dressings and corticosteroids were not significantly different vs. control in all respects, 3M™ film dressings may reduce skin itching, while corticosteroids may delay the onset of severe skin inflammation (Shaw et al., 2015). In a single-blind, randomized controlled trial for the prophylactic use of a silicone-based film forming gel dressing (StrataXRT® Stratapharma AG, Basel, Switzerland) in patients with head and neck cancer undergoing radiation therapy, the results show that it is effective for preventing, and delaying the development of grade 2 and 3 skin toxicity (Chan et al., 2019).

For skin already suffering from radiation dermatitis, the use of a suitable dressing can promote healing. Lee et al. studied the effects of a foam dressing combined with recombinant human epidermal growth factor on the treatment of seven patients with head and neck cancer experiencing radiation-induced dermatitis. The wounds of these seven patients with radiation-induced dermatitis healed within 14 days (Lee J. et al., 2016). A study compared the effects of Mepilex® Lite dressing on wound healing and the quality of life in patients with nasopharyngeal carcinoma. The results indicated that the patients in the Mepilex® group had significantly shorter wound healing time and improved sleep quality compared with those in the control group (Zhong et al., 2013).

The onset time of chronic dermatitis usually occurs after radiotherapy for a prolonged period of time (Spalek, 2016). Therefore, the application of modern dressings in radiation dermatitis is mostly focused on acute dermatitis. Although the above studies have concluded that the use of modern dressings and growth factors can improve radiation dermatitis, there is a lack of evidence-based, randomized, controlled trials comparing different types of these dressings. Importantly, future studies should examine skin-specific quality of life and cost-effectiveness. Medical staff should focus on the prevention of radiation dermatitis. They can comprehensively evaluate the skin in the

radiotherapy area prior to radiotherapy and use film dressings or liquid dressings to protect the skin.

Split-Thickness Skin Grafting (SSG)

SSG is a common reconstructive technique used to repair orthopedic wounds and burns. However, the repair and regeneration of the donor site is overlooked, causing unnecessary pain to the patient (Shoemaker, 1982; Kirsner et al., 1997; Coruh and Yontar, 2012). In recent years, the application of new dressings is one of the common methods used to promote the repair of the donor site (Malakar and Malakar, 2001). Studies have shown that as many as half of donor sites show signs of infection, and patients often experience pain at these sites. Leakage of blood and fluid is also common. Infections, pain, and leakage are factors that complicate and retard the healing process, as well as cause hypertrophic scars and hypopigmentation or hyperpigmentation. Therefore, appropriate management of the donor site after the collection of SSG is essential. The application of the dressing is a key part of this process. The ideal dressing should assist rapid epithelialization, prevent infection and leakage, and feel comfortable and painless for the patients. It is also adjustable according to different parts, easy to use, and cost-effective.

The skin graft donor site is a type of surgical wound; therefore, it is less likely to be infected than the aforementioned types of wounds. Dressings used in this condition provide a good healing environment to prevent wound infection and reduce the formation of scars. Researchers have combined antimicrobial-impregnated dressing with negative-pressure wound therapy to greatly improve the survival rate of skin grafts (Wu C. C. et al., 2015). Alginate dressings, hydrocolloid dressings, and foam dressings are used in this setting. A study compared the effectiveness of two types of advanced dressings, namely polyurethane foam (ALLEVYN™) and CA (Kaltostat®), in the management of the donor site after SSG. The results indicated that, although there were no significant differences in wound healing time, pain intensity, length of stay, and staff and patient satisfaction between the ALLEVYN™ group and Kaltostat® group, the former dressing was more cost effective than the latter (Higgins et al., 2012). A study compared the effectiveness of two silver dressings, AQUACEL® Ag (Convatec) and Alginate Silver (Coloplast), in the management of donor site wounds. The results showed that Alginate Silver exhibited superior performance in terms of pain and re-epithelialization time (Ding et al., 2013). A trial compared the effectiveness of six wound dressings, including semipermeable film, alginate, hydrocolloid, gauze dressing, hydrofiber, and silicon, in the management of donor-site wounds. The results showed that the hydrocolloid group had the fastest epithelialization rate, and the wound infection rate in the gauze group was 2-fold higher than that reported in the other five groups (Brolmann et al., 2013). A study compared the effectiveness of banded dressings and not banded dressings in patients who underwent skin grafting. Studies showed that the use of polyurethane foams and elastic tape was a simpler but effective method of trimming and may be associated with a shorter operating time than conventional fixation methods using bonded pads (Yuki et al., 2017).

SSG, as a reconstructive technique, is used in burn patients with larger wound bed. The goal of donor site management is to achieve a faster healing speed without pain. Treatment of donor site wounds after SSG is an important clinical issue because patients generally report greater pain at the donor site than at the graft receiving site (Voineskos et al., 2009). Acute wound pain has been shown to increase patient stress and subsequently negatively affect quality of life and lead to delayed wound healing (Broadbent et al., 2003). An evidence-based review summarizes the current evidence that wet wound healing dressing products have clear clinical advantages over non-wet dressing products in treating SSG donor site wounds (Brown and Holloway, 2018). However, no clear trend was detected regarding the performance of each dressing type. So far, there has been limited discussion about the influence of secondary dressings as well as methods/techniques of primary dressing use on donor site wounds. Further research is clearly needed in this area. Especially should explore the role of secondary dressing use, and using more than one primary dressing product throughout the donor site wound-healing process should be taken into consideration.

PROSPECT

With the increase in the incidence of diabetes and chronic vascular diseases, wound management (especially for certain chronic wounds) has gradually attracted the attention of clinicians. The poor healing of wounds results in pain to patients and causes a heavy medical burden. For example, DFU can cause severe and persistent infections and, in extreme cases, lead to amputation. The use of dressings is a common treatment for the management of wounds. In particular, modern dressings are superior to traditional dressings in preventing infection, accelerating wound healing, and reducing pain in patients. The selection of the most appropriate modern dressing product is a challenge for clinicians. An ideal dressing should have the ability to maintain moisture balance in the wound, promote oxygen exchange, isolate proteases, stimulate growth factors, prevent infection, facilitate autolytic debridement, and promote the production of granulation tissue and re-epithelialization (Moura et al., 2013).

Although these modern dressing products are superior to traditional dressings in some respects, their cost is higher than that of traditional dressings. The use of modern dressings in countries and regions where health insurance systems are not well-established involves a significant cost, especially for those with low- or average-income levels. Therefore, dressing manufacturers improve production efficiency, optimize production processes, and reduce costs to ensure that more patients benefit from the use of these new dressings. At the same time, research on a variety of new materials for wounds has emerged, but few have been applied to the clinic in the end. Therefore, promoting the industrialization of scientific research results and providing patients with more alternative dressings is a problem that needs to be solved. Most of the studies discussed above were conducted in hospitals and the subjects

were hospitalized patients. Nevertheless, chronic wounds (e.g., DFUs and PUs) were treated at home or nursing home in most cases. It is suggested that how to promote wound healing in a home and nursing home should be studied in the future. In particular, most studies have only evaluated the effect of a single dressing on the wound, but it may have better results when combined with other treatments, such as light therapy and topical drugs. It is suggested that this research direction can be considered in the future. At the same time, additional multi-center, high-quality, randomized, controlled clinical trials are warranted to prove the advantages of modern dressing products in wound healing. Last, systematic review and meta-analysis of DFU and pressure ulcers is slightly lagging, and it is recommended to include research in recent years for timely updates to provide reliable evidence for decision.

CONCLUSION

In summary, the process of wound healing is not static. It requires an appropriate environment at each stage of the healing process, and a reasonable approach to the selection of dressing for certain types of wounds should be clarified for clinical professionals. In the opinion of the author, an ideal dressing is expected to possess the capacity of moisture balance, promote oxygen exchange, isolate proteases, stimulate growth factors, prevent infection, facilitate autolytic debridement, and promote the production of granulation tissue and re-epithelialization. However, currently, there are no dressings that can achieve all these functions. Hence, the specific selection of modern wound dressings for different wounds should be based on the particular conditions, such as the patient's primary disease, the characteristics of the dressing, and especially the physiological mechanisms of wounds. This article summarized the advantages of various wound dressings and their applications in different wounds, aiming to provide a clinical guideline for the selection of suitable wound dressings for effective wound healing.

AUTHOR CONTRIBUTIONS

JW and YS conceived and coordinated this project. CS and CW wrote this paper. RL and YZ collected and summarized literatures. QL and YL edited pictures in this paper. HL revised this paper.

FUNDING

This work was supported by the National Natural Science Foundation of China (grant nos. 51861145311, 21174048, 81671804, and 81772456); Scientific Development Program of Jilin Province (grant nos. 20190304123YY, 20180623050TC, and 20180201041SF); Program of Jilin Provincial Health Department (grant nos. 2019SCZT001 and 2019SRCJ001); Cultivation Program from the Second Hospital of Jilin University for National Natural Science Foundation (grant no. KYPY2018-01); and Youth Talents Promotion Project of Jilin Province (grant no. 192004).

REFERENCES

- Acosta, J. B., del Barco, D. G., Vera D. C., Savigne, W., Lopez-Saura, P., Guillen Nieto, G., et al. (2008). The pro-inflammatory environment in recalcitrant diabetic foot wounds. *Int. Wound J.* 5, 530–539. doi: 10.1111/j.1742-481X.2008.00457.x
- Alvarez, O. (1988). Moist environment for healing: matching the dressing to the wound. *Ostomy Wound Manage.* 21, 64–83.
- Amini-Nik, S., Yousuf, Y., and Jeschke, M. G. (2018). Scar management in burn injuries using drug delivery and molecular signaling: current treatments and future directions. *Adv. Drug Deliv. Rev.* 123, 135–154. doi: 10.1016/j.addr.2017.07.017
- Arimura, T., Ogino, T., Yoshiura, T., Toi, Y., Kawabata, M., Chuman, I., et al. (2016). Effect of film dressing on acute radiation dermatitis secondary to proton beam therapy. *Int. J. Radiat. Oncol. Biol. Phys.* 95, 472–476. doi: 10.1016/j.ijrobp.2015.10.053
- Ascione, F., Caserta, S., and Guido, S. (2017a). The wound healing assay revisited: a transport phenomena approach. *Chem. Eng. Sci.* 160, 200–209. doi: 10.1016/j.ces.2016.11.014
- Ascione, F., Guarino, A. M., Calabro, V., Guido, S., and Caserta, S. (2017b). A novel approach to quantify the wound closure dynamic. *Exp. Cell Res.* 352, 175–183. doi: 10.1016/j.yexcr.2017.01.005
- Barnea, Y., Weiss, J., and Gur, E. (2010). A review of the applications of the hydrofiber dressing with silver (Aquacel Ag) in wound care. *Ther. Clin. Risk Manage.* 6, 21–27. doi: 10.2147/TCRM.S3462
- Blakytyn, R., and Jude, E. B. (2009). Altered molecular mechanisms of diabetic foot ulcers. *Int. J. Low. Extrem. Wounds* 8, 95–104. doi: 10.1177/1534734609337151
- Bolton, L. (2016). Evidence corner: dressings can prevent pressure injury. *Wounds* 28, 376–378.
- Borda, L. J., Macquhae, F., and E., Kirsner, R. S. (2016). Wound dressings: a comprehensive review. *Curr. Dermatol. Rep.* 5, 287–297. doi: 10.1007/s13671-016-0162-5
- Brennan, M. B., Hess, T. M., Bartle, B., Cooper, J. M., Kang, J., Huang, E. S. (2017). Diabetic foot ulcer severity predicts mortality among veterans with type 2 diabetes. *J. Diabetes Complicat.* 31, 556–561. doi: 10.1016/j.jdiacomp.2016.11.020
- Brindle, C. T., and Wegelin, J. A. (2012). Prophylactic dressing application to reduce pressure ulcer formation in cardiac surgery patients. *J. Wound Ostomy Continence Nurs.* 39, 133–142. doi: 10.1097/WON.0b013e318247cb82
- Broadbent, E., Petrie, K. J., Alley, P. G., and Booth, R. (2003). Psychological stress impairs early wound repair following surgery. *Psychosom. Med.* 65, 865–869. doi: 10.1097/01.PSY.0000088589.92699.30
- Brolmann, F. E., Eskes, A. M., Goslings, J. C., Niessen, F. B., de Bree, R., Vahl, A. C., et al. (2013). Randomized clinical trial of donor-site wound dressings after split-skin grafting. *Br. J. Surg.* 100, 619–627. doi: 10.1002/bjs.9045
- Broughton, G., II, Janis, J., and Attinger, C. E. (2006). A brief history of wound care. *Plast. Reconstr. Surg.* 117, 6S–11S. doi: 10.1097/01.prs.0000225429.76355.dd
- Brown, J. E., and Holloway, S. L. (2018). An evidence-based review of split-thickness skin graft donor site dressings. *Int. Wound J.* 15, 1000–1009. doi: 10.1111/iwj.12967
- Bugmann, P., Taylor, S., Gyger, D., Lironi, A., Genin, B., Vunda, A., et al. (1998). A silicone-coated nylon dressing reduces healing time in burned paediatric patients in comparison with standard sulfadiazine treatment: a prospective randomized trial. *Burns* 24, 609–612. doi: 10.1016/S0305-4179(98)00095-3
- Call, E., Pedersen, J., Bill, B., Black, J., Alves, P., Brindle, C., et al. (2015). Enhancing pressure ulcer prevention using wound dressings: what are the modes of action? *Int. Wound J.* 12, 408–413. doi: 10.1111/iwj.12123
- Chaiken, N. (2012). Reduction of sacral pressure ulcers in the intensive care unit using a silicone border foam dressing. *J. Wound Ostomy Continence Nurs.* 39, 143–145. doi: 10.1097/WON.0b013e318246400c
- Chan, R. J., Blades, R., Jones, L., Downer, T. R., Peet, S. C., Button, E., et al. (2019). A single-blind, randomised controlled trial of StrataXRT(R) - a silicone-based film-forming gel dressing for prophylaxis and management of radiation dermatitis in patients with head and neck cancer. *Radiother. Oncol.* 139, 72–78. doi: 10.1016/j.radonc.2019.07.014
- Chapman, S. (2017). Venous leg ulcers: an evidence review. *Br. J. Community Nurs.* 22, S6–S9. doi: 10.12968/bjcn.2017.22.Sup9.S6
- Coruh, A., and Yontar, Y. (2012). Application of split-thickness dermal grafts in deep partial- and full-thickness burns: a new source of auto-skin grafting. *J. Burn Care Res.* 33, e94–e100. doi: 10.1097/BCR.0b013e31823499e9
- Davies, P., McCarty, S., and Hamberg, K. (2017). Silver-containing foam dressings with Safetac: a review of the scientific and clinical data. *J. Wound Care* 26, S1–S32. doi: 10.12968/jowc.2017.26.Sup6a.S1
- Dawkins, H. (2017). Non-healing venous leg ulcer. *Br. J. Nurs.* 26, S26–S27. doi: 10.12968/bjon.2017.26.Sup20a.S26
- Demarre, L., Verhaeghe, S., Van Hecke, A., Clays, E., Grypdonck, M., and Beeckman, D. (2015). Factors predicting the development of pressure ulcers in an at-risk population who receive standardized preventive care: secondary analyses of a multicentre randomised controlled trial. *J. Adv. Nurs.* 71, 391–403. doi: 10.1111/jan.12497
- Ding, X., Shi, L., Liu, C., and Sun, B. (2013). A randomized comparison study of Aquacel Ag and Alginate Silver as skin graft donor site dressings. *Burns* 39, 1547–1550. doi: 10.1016/j.burns.2013.04.017
- dos Santos, M. R., Alcaraz-Espinoza, J. J., da Costa, M. M., and de Oliveira, H. (2018). Usnic acid-loaded polyaniline/polyurethane foam wound dressing: preparation and bactericidal activity. *Mater. Sci. Eng. C Mater. Biol. Appl.* 89, 33–40. doi: 10.1016/j.msec.2018.03.019
- Dumville, J. C., Deshpande, S., O'Meara, S., and Speak, K. (2013a). Foam dressings for healing diabetic foot ulcers. *Cochrane Database Syst. Rev.* 6:CD009111. doi: 10.1002/14651858.CD009111.pub3
- Dumville, J. C., Deshpande, S., O'Meara, S., and Speak, K. (2013b). Hydrocolloid dressings for healing diabetic foot ulcers. *Cochrane Database Syst. Rev.* 2:CD009099. doi: 10.1002/14651858.CD009099.pub3
- Dumville, J. C., O'Meara, S., Deshpande, S., and Speak, K. (2013c). Alginate dressings for healing diabetic foot ulcers. *Cochrane Database Syst. Rev.* 2:CD009110. doi: 10.1002/14651858.CD009110.pub3
- Dumville, J. C., O'Meara, S., Deshpande, S., and Speak, K. (2013d). Hydrogel dressings for healing diabetic foot ulcers. *Cochrane Database Syst. Rev.* 9:CD009101. doi: 10.1002/14651858.CD009101.pub3
- Edmonds, M., Lazaro-Martinez, J. L., Alfayate-Garcia, J. M., and Martini, J. (2018). Sucrose octasulfate dressing versus control dressing in patients with neuroischaemic diabetic foot ulcers (Explorer): an international, multicentre, double-blind, randomised, controlled trial. *Lancet Diabetes Endocrinol.* 6, 186–196. doi: 10.1016/S2213-8587(17)30438-2
- Fletcher, J. (2003). Using film dressings. *Nurs. Times* 99:57.
- Francesco, A., Petkova, P., and Tzanov, T. (2017). Hydrogel dressings for advanced wound management. *Curr. Med. Chem.* 25, 5782–5797. doi: 10.2174/0929867324666170920161246.
- Franks, P. J., Moody, M., Moffatt, C. J., Hiskett, G., Gatto, P., Davies, C., et al. (2007). Randomized trial of two foam dressings in the management of chronic venous ulceration. *Wound Repair Regen.* 15, 197–202. doi: 10.1111/j.1524-475X.2007.00205.x
- Gianfaldoni, S., Wollina, U., Lotti, J., Gianfaldoni, R., Lotti, T., Fioranelli, M., et al. (2017). History of venous leg ulcers. *J. Biol. Regul. Homeost. Agents* 31(2 Suppl. 2), 107–120.
- Gil, J., Natesan, S., Li, J., Valdes, J., Harding, A., Solis, M., et al. (2017). A PEGylated fibrin hydrogel-based antimicrobial wound dressing controls infection without impeding wound healing. *Int. Wound J.* 14, 1248–1257. doi: 10.1111/iwj.12791
- Goodwin, N. S., Spinks, A., and Wasia, J. (2016). The efficacy of hydrogel dressings as a first aid measure for burn wound management in the pre-hospital setting: a systematic review of the literature. *Int. Wound J.* 13, 519–525. doi: 10.1111/iwj.12469
- Graumlich, J. F., Blough, L. S., McLaughlin, R. G., and Milbrandt, J. (2003). Healing pressure ulcers with collagen or hydrocolloid: a randomized, controlled trial. *J. Am. Geriatr. Soc.* 51, 147–154. doi: 10.1046/j.1532-5415.2003.51051.x
- Guo, S., and Dipietro, L. A. (2010). Factors affecting wound healing. *J. Dent. Res.* 89, 219–229. doi: 10.1177/0022034509359125
- Harding, K., Gotttrup, F., Jawien, A., Mikosinski, J., Twardowska-Sauch, K., Kaczmarek, S., et al. (2012). A prospective, multi-centre, randomised, open label, parallel, comparative study to evaluate effects of AQUACEL(R) Ag and Urgotul(R) Silver dressing on healing of chronic venous leg ulcers. *Int. Wound J.* 9, 285–294. doi: 10.1111/j.1742-481X.2011.00881.x
- Harding, K. G., Krieg, T., Eming, S. A., and Flour, M. L. (2005). Efficacy and safety of the freeze-dried cultured human keratinocyte lysate, LyphoDerm 0.9%, in

- the treatment of hard-to-heal venous leg ulcers. *Wound Repair Regen.* 13, 138–147. doi: 10.1111/j.1067-1927.2005.130204.x
- Harding, K. G., Szczepkowski, M., Mikosinski, J., Twardowska-Sauchka, K., Blair, S., Ivins, N., et al. (2016). Safety and performance evaluation of a next-generation antimicrobial dressing in patients with chronic venous leg ulcers. *Int. Wound J.* 13, 442–448. doi: 10.1111/iwj.12450
- Harper, D., Young, A., and McNaught, C.-E. (2014). The physiology of wound healing. *Surgery* 32, 445–450. doi: 10.1016/j.mpsur.2014.06.010
- Hess, C. T. (2000). When to use alginate dressings. *Adv. Skin Wound Care* 13:131.
- Heyer, K., Augustin, M., Protz, K., Herberger, K., Spehr, C., Rustenbach, S., et al. (2013). Effectiveness of advanced versus conventional wound dressings on healing of chronic wounds: systematic review and meta-analysis. *Dermatology* 226, 172–184. doi: 10.1159/000348331
- Higgins, L., Wasiak, J., Spinks, A., and Cleland, H. (2012). Split-thickness skin graft donor site management: a randomized controlled trial comparing polyurethane with calcium alginate dressings. *Int. Wound J.* 9, 126–131. doi: 10.1111/j.1742-481X.2011.00867.x
- Hird, A. E., Wilson, J., Symons, S., Sinclair, E., Davis, M., and Chow, E. (2008). Radiation recall dermatitis: case report and review of the literature. *Curr. Oncol.* 15, 53–62. doi: 10.3747/co.2008.201
- Hobot, J., Walker, M., Newman, G., and Bowler, P. (2008). Effect of hydrofiber wound dressings on bacterial ultrastructure. *J. Electron Microsc.* 57, 67–75. doi: 10.1093/jmicro/dfn002
- Hopper, G. P., Deakin, A. H., Crane, E. O., and Clarke, J. (2012). Enhancing patient recovery following lower limb arthroplasty with a modern wound dressing: a prospective, comparative audit. *J. Wound Care* 21, 200–203. doi: 10.12968/jowc.2012.21.4.200
- Horn, T. (2012). [Wound dressings. Overview and classification]. *Unfallchirurg* 115, 774–782. doi: 10.1007/s00113-012-2209-9
- Huang, Y., Li, X., Liao, Z., Zhang, G., Liu, Q., Tang, J., et al. (2007). A randomized comparative trial between Acticoat and SD-Ag in the treatment of residual burn wounds, including safety analysis. *Burns* 33, 161–166. doi: 10.1016/j.burns.2006.06.020
- Hunt, D. L. (2003). Review: debridement using hydrogel seems to be better than standard wound care for healing diabetic foot ulcer. *ACP J. Club* 139:16.
- Imanishi, K., Morita, K., Matsuoka, M., Hayashi, H., Furukawa, S., Terashita, F., et al. (2006). Prevention of postoperative pressure ulcers by a polyurethane film patch. *J. Dermatol.* 33, 236–237. doi: 10.1111/j.1346-8138.2006.00057.x
- Imran, D., Sassoon, E., and Lewis, D. (2004). Protection of dressings and wounds by cling film. *Plast. Reconstr. Surg.* 113, 1093–1094. doi: 10.1097/01.PRS.0000107737.67371.D7
- Jeffcoate, W. J. (2012). Wound healing—a practical algorithm. *Diabetes Metab. Res. Rev.* 28(Suppl. 1), 85–88. doi: 10.1002/dmrr.2235
- Jude, E. B., Apelqvist, J., Spraul, M., Martini, J., and Silver Dressing Study Group. (2007). Prospective randomized controlled study of Hydrofiber dressing containing ionic silver or calcium alginate dressings in non-ischaemic diabetic foot ulcers. *Diabet. Med.* 24, 280–288. doi: 10.1111/j.1464-5491.2007.02079.x
- Kamoun, E. A., Kenawy, E. S., and Chen, X. (2017). A review on polymeric hydrogel membranes for wound dressing applications: PVA-based hydrogel dressings. *J. Adv. Res.* 8, 217–233. doi: 10.1016/j.jare.2017.01.005
- Karlsmark, T., Agerslev, R. H., Bendz, S. H., and Larsen, J. (2003). Clinical performance of a new silver dressing, Contreet Foam, for chronic exuding venous leg ulcers. *J. Wound Care* 12, 351–354. doi: 10.12968/jowc.2003.12.9.26534
- Kasuya, A., and Tokura, Y. (2014). Attempts to accelerate wound healing. *J. Dermatol. Sci.* 76, 169–172. doi: 10.1016/j.jdermsci.2014.11.001
- Khanolkar, M. P., Bain, S. C., and Stephens, J. W. (2008). The diabetic foot. *QJM* 101, 685–695. doi: 10.1093/qjmed/hcn027
- Kirkwood, M. L., Arbiq, G. M., Guild, J. B., and Timaran, C. (2014). Radiation-induced skin injury after complex endovascular procedures. *J. Vasc. Surg.* 60, 742–748. doi: 10.1016/j.jvs.2014.03.236
- Kirsner, R. S., Eaglstein, W. H., and Kerdell, F. A. (1997). Split-thickness skin grafting for lower extremity ulcerations. *Dermatol. Surg.* 23, 85–91. doi: 10.1111/j.1524-4725.1997.tb00666.x
- Kong, L. Z., Wu, Z., Zhao, H., Cui, H., Shen, J., Chang, J., et al. (2018). Bioactive injectable hydrogels containing desferrioxamine and bioglass for diabetic wound healing. *ACS Appl. Mater. Interfaces* 10, 30103–30114. doi: 10.1021/acsami.8b09191
- Kuo, C. Y., Wootten, C. T., Tylor, D. A., and Werkhaven, J. A., Huffman, K. F., and Goudy, S. L. (2013). Prevention of pressure ulcers after pediatric tracheotomy using a mepilex ag dressing. *Laryngoscope* 123, 3201–3205. doi: 10.1002/lary.24094
- Lammoglia-Ordiales, L., Vega-Memije, M. E., Herrera-Arellano, A., Rivera-Arce, E., Aguero, J., Vargas-Martinez, F., et al. (2012). A randomised comparative trial on the use of a hydrogel with tepescahuete extract (*Mimosa tenuiflora* cortex extract-2G) in the treatment of venous leg ulcers. *Int. Wound J.* 9, 412–418. doi: 10.1111/j.1742-481X.2011.00900.x
- Lee, J., Lee, S. W., Hong, J. P., Shon, M., Ryu, S. H., and Ahn, S. D. (2016). Foam dressing with epidermal growth factor for severe radiation dermatitis in head and neck cancer patients. *Int. Wound J.* 13, 390–393. doi: 10.1111/iwj.12317
- Lee, M., Han, S. H., Choi, W. J., Chung, K., and Lee, J. W. (2016). Hyaluronic acid dressing (*Healoderm*) in the treatment of diabetic foot ulcer: a prospective, randomized, placebo-controlled, single-center study. *Wound Repair Regen.* 24, 581–588. doi: 10.1111/wrr.12428
- Li, S., Dong, S. J., Xu, W. G., Tu, S. C., Yan, L., Zhao, C. W., et al. (2018). Antibacterial hydrogels. *Adv. Sci.* 5:1700527. doi: 10.1002/adv.201700527
- Li, Z., Zhou, F., Li, Z., Lin, S., Chen, L., Liu, L., et al. (2018). Hydrogel cross-linked with dynamic covalent bonding and micellization for promoting burn wound healing. *ACS Appl. Mater. Interfaces* 10, 25194–25202. doi: 10.1021/acsami.8b08165
- Lohmann, M., Thomsen, J. K., Edmonds, M. E., Harding, K. G., Apelqvist, J., Gottrup, F., et al. (2004). Safety and performance of a new non-adhesive foam dressing for the treatment of diabetic foot ulcers. *J. Wound Care* 13, 118–120. doi: 10.12968/jowc.2004.13.3.26591
- Lozano Sanchez, F. S., Marinello Roura, J., Carrasco Carrasco, E., Gonzalez-Porras, J. R., Escudero Rodriguez, J. R., Sanchez Nevarez, I., et al. (2014). Venous leg ulcer in the context of chronic venous disease. *Phlebology* 29, 220–226. doi: 10.1177/0268355513480489
- Mabrouk, A., Boughdadi, N. S., Helal, H. A., Zaki, B. M., and Maher, A. (2012). Moist occlusive dressing (Aquacel® Ag) versus moist open dressing (MEBO®) in the management of partial-thickness facial burns: a comparative study in Ain Shams University. *Burns* 38, 396–403. doi: 10.1016/j.burns.2011.09.022
- Maggio, G., Armenio, A., Ruccia, F., Giglietto, D., Pascone, M., and Ribatti, D. (2012). A new protocol for the treatment of the chronic venous ulcers of the lower limb. *Clin. Exp. Med.* 12, 55–60. doi: 10.1007/s10238-011-0136-7
- Malakar, S., and Malakar, R. S. (2001). Surgical pearl: composite film and graft unit for the recipient area dressing after split-thickness skin grafting in vitiligo. *J. Am. Acad. Dermatol.* 44, 856–858. doi: 10.1067/mjd.2001.111334
- Marks, J., and Ribeiro, D. (1983). Silicone foam dressings. *Nurs. Times* 79, 58–60.
- Matsuzaki, K., and Kishi, K. (2015). Investigating the pressure-reducing effect of wound dressings. *J. Wound Care* 24, 514–517. doi: 10.12968/jowc.2015.24.11.512
- McElroy, E., Lemay, S., Reider, K., and Behnam, A. B. (2018). A case review of wound bed preparation in an infected venous leg ulcer utilizing novel reticulated open cell foam dressing with through holes during negative pressure wound therapy with instillation. *Cureus* 10:e3504. doi: 10.7759/cureus.3504
- Michaels, J. A., Campbell, B., King, B., Palfreyman, S. J., Shackley, P., Stevenson, M., et al. (2009). Randomized controlled trial and cost-effectiveness analysis of silver-donating antimicrobial dressings for venous leg ulcers (VULCAN trial). *Br. J. Surg.* 96, 1147–1156. doi: 10.1002/bjs.6786
- Moore, Z. E., and Webster, J. (2013). Dressings and topical agents for preventing pressure ulcers. *Cochrane Database Syst. Rev.* 8:CD009362. doi: 10.1002/14651858.CD009362.pub2
- Moore, Z. E., and Webster, J. (2018). Dressings and topical agents for preventing pressure ulcers. *Cochrane Database Syst. Rev.* 12:CD009362. doi: 10.1002/14651858.CD009362.pub3
- Morton, L. M., and Phillips, T. J. (2012). Wound healing update. *Semin. Cutan. Med. Surg.* 31, 33–37. doi: 10.1016/j.sder.2011.11.007
- Moura, L. I., Dias, A. M., Carvalho, E., and de Sousa, H. C. (2013). Recent advances on the development of wound dressings for diabetic foot ulcer treatment—a review. *Acta Biomater.* 9, 7093–7114. doi: 10.1016/j.actbio.2013.03.033
- Muangman, P., Pundee, C., Opasanon, S., and Muangman, S. (2010). A prospective, randomized trial of silver containing hydrofiber dressing versus 1% silver sulfadiazine for the treatment of partial thickness burns. *Int. Wound J.* 7, 271–276. doi: 10.1111/j.1742-481X.2010.00690.x

- Murakami, K., Aoki, H., Nakamura, S., Nakamura, S., Takikawa, M., Hanzawa, M., et al. (2010). Hydrogel blends of chitin/chitosan, fucoidan and alginate as healing-impaired wound dressings. *Biomaterials* 31, 83–90. doi: 10.1016/j.biomaterials.2009.09.031
- Nakagami, G., Sanada, H., Konya, C., Kitagawa, A., Tadaka, E., and Matsuyama, Y. (2007). Evaluation of a new pressure ulcer preventive dressing containing ceramide 2 with low frictional outer layer. *J. Adv. Nurs.* 59, 520–529. doi: 10.1111/j.1365-2648.2007.04334.x
- Nelson, E. A., Prescott, R. J., Harper, D. R., Gibson, B., Brown, D., Ruckley, C. V., et al. (2007). A factorial, randomized trial of pentoxifylline or placebo, four-layer or single-layer compression, and knitted viscose or hydrocolloid dressings for venous ulcers. *J. Vasc. Surg.* 45, 134–141. doi: 10.1016/j.jvs.2006.09.043
- Norman, G., Westby, M. J., Rithalia, A. D., Stubbs, N., Soares, M. O., and Dumville, J. C. (2018). Dressings and topical agents for treating venous leg ulcers. *Cochrane Database Syst. Rev.* 6:CD012583. doi: 10.1002/14651858.CD012583.pub2
- Nuutila, K., Singh, M., Kruse, C., Philip, J., Caterson, E. J., and Eriksson, E. (2016). Titanium wound chambers for wound healing research. *Wound Repair Regen.* 24, 1097–1102. doi: 10.1111/wrr.12472
- Okuma, C. H., Andrade, T. A., Caetano, G. F., Finci, L. I., Maciel, N. R., Topan, J. F., et al. (2015). Development of lamellar gel phase emulsion containing marigold oil (*Calendula officinalis*) as a potential modern wound dressing. *Eur. J. Pharm. Sci.* 71, 62–72. doi: 10.1016/j.ejps.2015.01.016
- O'Meara, S., and Martyn-St James, M. (2013). Alginate dressings for venous leg ulcers. *Cochrane Database Syst. Rev.* 4:CD010182. doi: 10.1002/14651858.CD010182.pub2
- Opasanon, S., Muangman, P., and Namviriyachote, N. (2010). Clinical effectiveness of alginate silver dressing in outpatient management of partial-thickness burns. *Int. Wound J.* 7, 467–471. doi: 10.1111/j.1742-481X.2010.00718.x
- Palfreyman, S., King, B., and Walsh, B. (2007). A review of the treatment for venous leg ulcers. *Br. J. Nurs.* 16, S6–14. doi: 10.12968/bjon.2007.16.8.23412
- Pancorbo-Hidalgo, P. L., Garcia-Fernandez, F. P., Lopez-Medina, I. M., and Alvarez-Nieto, C. (2006). Risk assessment scales for pressure ulcer prevention: a systematic review. *J. Adv. Nurs.* 54, 94–110. doi: 10.1111/j.1365-2648.2006.03794.x
- Park, G. B. (1978). Burn wound coverings - a review. *Biomater. Med. Devices Artif. Organs* 6, 1–35. doi: 10.3109/10731197809118690
- Pieper, B., Langemo, D., and Cuddigan, J. (2009). Pressure ulcer pain: a systematic literature review and national pressure ulcer advisory panel white paper. *Ostomy Wound Manage.* 55, 16–31.
- Powers, J. G., Higham, C., Broussard, K., and Phillips, T. J. (2016). Wound healing and treating wounds: Chronic wound care and management. *J. Am. Acad. Dermatol.* 74, 607–25. doi: 10.1016/j.jaad.2015.08.070
- Raffetto, J. D. (2009). Dermal pathology, cellular biology, and inflammation in chronic venous disease. *Thromb. Res.* 123(Suppl. 4), S66–S71. doi: 10.1016/S0049-3848(09)70147-1
- Rajendran, S., Rigby, A. J., and Anand, S. C. (2007). Venous leg ulcer treatment and practice-Part 3: the use of compression therapy systems. *J. Wound Care* 16, 107–109. doi: 10.12968/jowc.2007.16.3.27016
- Rathur, H. M., and Boulton, A. J. (2005). Recent advances in the diagnosis and management of diabetic neuropathy. *J. Bone Joint Surg. Br.* 87, 1605–1610. doi: 10.1302/0301-620X.87B12.16710
- Rayman, G., Rayman, A., Baker, N., R., Jurgevicene, N., Dargis, V., Sulcaite, R., et al. (2005). Sustained silver-releasing dressing in the treatment of diabetic foot ulcers. *Br. J. Nurs.* 14, 109–114. doi: 10.12968/bjon.2005.14.2.17441
- Richard, J. L., Martini, J., Bonello Farail, M. M., Bemba, J. M., Lepeut, M., Truchetet, F., et al. (2012). Management of diabetic foot ulcers with a TLC-NOSF wound dressing. *J. Wound Care* 21, 142–147. doi: 10.12968/jowc.2012.21.3.142
- Richetta, A. G., Cantisani, C., Li, V. W., Mattozzi, C., Melis, L., De Gado, F., et al. (2011). Hydrofiber dressing and wound repair: review of the literature and new patents. *Recent Pat. Inflamm. Allergy Drug Discov.* 5, 150–154. doi: 10.2174/187221311795399264
- Saco, M., Howe, N., Nathoo, R., and Cherpelis, B. (2016). Comparing the efficacies of alginate, foam, hydrocolloid, hydrofiber, and hydrogel dressings in the management of diabetic foot ulcers and venous leg ulcers: a systematic review and meta-analysis examining how to dress for success. *Dermatol. Online J.* 22, 1087–2108. doi: 10.1016/j.jaad.2016.02.1129
- Salome, G. M., de Almeida, S. A., de Jesus Pereira, M. T., Massahud, M. R. Jr., de Oliveira Moreira, C. N., de Brito, M. J. et al. (2016). The impact of venous leg ulcers on body image and self-esteem. *Adv. Skin Wound Care* 29, 316–321. doi: 10.1097/01.ASW.0000484243.32091.0c
- Santamaria, N., Gerditz, M., Sage, S., McCann, J., Freeman, A., Vassiliou, T., et al. (2015). A randomised controlled trial of the effectiveness of soft silicone multi-layered foam dressings in the prevention of sacral and heel pressure ulcers in trauma and critically ill patients: the border trial. *Int. Wound J.* 12, 302–308. doi: 10.1111/iwj.12101
- Scanlon, L. (2003). Review: debridement using hydrogel appears to be more effective than standard wound care for healing diabetic foot ulcers. *Evid. Based Nurs.* 6:83. doi: 10.1136/ebn.6.3.83
- Schmeel, L. C., Koch, D., Schmeel, F. C., Bucheler, B., Leitzen, C., Mahlmann, B., et al. (2019). Hydrofilm polyurethane films reduce radiation dermatitis severity in hypofractionated whole-breast irradiation: an objective, intra-patient randomized dual-center assessment. *Polymers* 11:2112. doi: 10.3390/polym11122112
- Schreml, S., Szeimies, R. M., Prantl, L., Karrer, S., Landthaler, M., and Babilas, P. (2010). Oxygen in acute and chronic wound healing. *Br. J. Dermatol.* 163, 257–268. doi: 10.1111/j.1365-2133.2010.09804.x
- Schwartz, D., and Gefen, A. (2019). The biomechanical protective effects of a treatment dressing on the soft tissues surrounding a non-offloaded sacral pressure ulcer. *Int. Wound J.* 16, 684–695. doi: 10.1111/iwj.13082
- Sebern, M. D. (1986). Pressure ulcer management in home health care: efficacy and cost effectiveness of moisture vapor permeable dressing. *Arch. Phys. Med. Rehabil.* 67, 726–729. doi: 10.1016/0003-9993(86)90004-3
- Sedlarik, K. M. (1994). [Modern wound dressings. 5: foam dressings]. *Z. Arztl. Fortbild.* 88, 141–143.
- Serra, R., Grande, R., Buffone, G., Molinari, V., Perri, P., Perri, A., et al. (2016). Extracellular matrix assessment of infected chronic venous leg ulcers: role of metalloproteinases and inflammatory cytokines. *Int. Wound J.* 13, 53–58. doi: 10.1111/iwj.12225
- Shamloo, A., Sarmadi, M., Aghababaei, Z., and Vossoughi, M. (2018). Accelerated full-thickness wound healing via sustained bFGF delivery based on a PVA/chitosan/gelatin hydrogel incorporating PCL microspheres. *Int. J. Pharm.* 537, 278–289. doi: 10.1016/j.ijpharm.2017.12.045
- Shaw, S. Z., Nien, H. H., Wu, C. J., Lui, L., Su, J. F., and Lang, C. H. (2015). 3M cavilon no-sting barrier film or topical corticosteroid (*mometasone furoate*) for protection against radiation dermatitis: a clinical trial. *J. Formos. Med. Assoc.* 114, 407–414. doi: 10.1016/j.jfma.2013.04.003
- Shoemaker, P. J. (1982). Split thickness skin grafting. *Can. Fam. Physician* 28, 1145–1147.
- Singh, M. R., Saraf, S., Vyas, A., Jain, V., and Singh, D. (2013). Innovative approaches in wound healing: trajectory and advances. *Artif. Cells Nanomed. Biotechnol.* 41, 202–212. doi: 10.3109/21691401.2012.716065
- Skorkowska-Telichowska, K., Czemplik, M., Kulma, A., and Szopa, J. (2013). The local treatment and available dressings designed for chronic wounds. *J. Am. Acad. Dermatol.* 68, e117–e126. doi: 10.1016/j.jaad.2011.06.028
- Snyder, B. J., and Waldman, B. J. (2009). Venous thromboembolism prophylaxis and wound healing in patients undergoing major orthopedic surgery. *Adv. Skin Wound Care* 22, 311–315. doi: 10.1097/01.ASW.0000305485.98734.1f
- Spalek, M. (2016). Chronic radiation-induced dermatitis: challenges and solutions. *Clin. Cosmet. Investig. Dermatol.* 9, 473–482. doi: 10.2147/CCID.S94320
- Stavrou, D., Weissman, O., Tessone, A., Zilinsky, I., Holloway, S., Boyd, J., et al. (2014). Health related quality of life in burn patients—a review of the literature. *Burns* 40, 788–796. doi: 10.1016/j.burns.2013.11.014
- Suvarna, R., Viswanadh, K., Hanumanthappa, M. B., and Devidas Shetty, N. (2016). A comparative study between hydrofiber dressing, povidone dressing in diabetic foot ulcers. *J. Evid. Based Med. Healthc.* 3, 986–991. doi: 10.18410/jebmh/2016/226
- Tarnuzzer, R. W., and Schultz, G. S. (1996). Biochemical analysis of acute and chronic wound environments. *Wound Repair Regen.* 4, 321–325. doi: 10.1046/j.1524-475X.1996.40307.x
- Terasawa, T., Dvorak, T., Ip, S., Raman, G., Lau, J., Trikalinos, T., et al. (2009). Systematic review: charged-particle radiation therapy for cancer. *Ann. Intern. Med.* 151, 556–565. doi: 10.7326/0003-4819-151-8-200910200-00145

- Thomas, S. (1990). Semi-permeable film dressings. *Nurs. Times* 86, 49–51.
- Thu, H. E., Zulfakar, M. H., and Ng, S. F. (2012). Alginate based bilayer hydrocolloid films as potential slow-release modern wound dressing. *Int. J. Pharm.* 434, 375–383. doi: 10.1016/j.ijpharm.2012.05.044
- Tirgari, B., Mirshekari, L., and Forouzi, M. A. (2018). Pressure injury prevention: knowledge and attitudes of Iranian intensive care nurses. *Adv. Skin Wound Care* 31, 1–8. doi: 10.1097/01.ASW.0000530848.50085.ef
- Truong, B., Grigson, E., Patel, M., and Liu, X. (2016). Pressure ulcer prevention in the hospital setting using silicone foam dressings. *Cureus* 8:e730. doi: 10.7759/cureus.730
- Tsang, V. L., and Bhatia, S. N. (2004). Three-dimensional tissue fabrication. *Adv. Drug Deliv. Rev.* 56, 1635–1647. doi: 10.1016/j.addr.2004.05.001
- Varas, R. P., O'Keeffe, T., Namias, N., Pizano, L. R., Quintana, O. D., Herrero Tellachea, M., et al. (2005). A prospective, randomized trial of acticoat versus silver sulfadiazine in the treatment of partial-thickness burns: which method is less painful? *J. Burn Care Rehabil.* 26, 344–347. doi: 10.1097/01.BCR.0000170119.87879.CA
- Verbelen, J., Hoeksema, H., Heyneman, A., Pirayesh, A., and Monstrey, S. (2014). Aquacel(R) ag dressing versus acticoat dressing in partial thickness burns: a prospective, randomized, controlled study in 100 patients. part I: burn wound healing. *Burns* 40, 416–427. doi: 10.1016/j.burns.2013.07.008
- Voineskos, S. H., Ayeni, O. A., McKnight, L., and Thoma, A. (2009). Systematic review of skin graft donor-site dressings. *Plast. Reconstr. Surg.* 124, 298–306. doi: 10.1097/PRS.0b013e3181a8072f
- Vowden, K., and Vowden, P. (2014). Wound dressings: principles and practice. *Surgery* 32, 462–467. doi: 10.1016/j.mpsur.2014.07.001
- Walsh, N. S., Blanck, A. W., Smith, L., Cross, M., Andersson, L., Polito, C. (2012). Use of a sacral silicone border foam dressing as one component of a pressure ulcer prevention program in an intensive care unit setting. *J. Wound Ostomy Continence Nurs.* 39, 146–149. doi: 10.1097/WON.0b013e3182435579
- Wang, M., Wang, C., Chen, M., Xi, Y., Cheng, W., Mao, C., et al. (2019). Efficient angiogenesis-based diabetic wound healing/skin reconstruction through bioactive antibacterial adhesive ultraviolet shielding nanodressing with exosome release. *ACS Nano*. 13, 10279–10293. doi: 10.1021/acsnano.9b03656
- Webb, R. (2017). Pressure ulcer over pressure injury. *Br. J. Nurs.* 26:S4. doi: 10.12968/bjon.2017.26.6.S4
- Weller, C. D., Gershenson, E. R., Evans, S. M., Team, V., McNeil, J. J. (2018). Pressure injury identification, measurement, coding, and reporting: key challenges and opportunities. *Int. Wound J.* 15, 417–423. doi: 10.1111/iwj.12879
- Westby, M. J., Dumville, J. C., Soares, M. O., Stubbs, N., Norman, G. (2017). Dressings and topical agents for treating pressure ulcers. *Cochrane Database Syst. Rev.* 6:CD011947. doi: 10.1002/14651858.CD011947.pub2
- Whaley, J. T., Kirk, M., Cengel, K., McDonough, J., Bekelman, J., Christodouleas, J., et al. (2013). Protective effect of transparent film dressing on proton therapy induced skin reactions. *Radiat. Oncol.* 8:19. doi: 10.1186/1748-717X-8-19
- Wickline, M. M. (2004). Prevention and treatment of acute radiation dermatitis: a literature review. *Oncol. Nurs. Forum* 31, 237–247. doi: 10.1188/04.ONF.237-247
- Wilhelm, K. P., Wilhelm, D., and Bielfeldt, S. (2017). Models of wound healing: an emphasis on clinical studies. *Skin Res. Technol.* 23, 3–12. doi: 10.1111/srt.12317
- Williams, C. (2000). 3M tegasorb thin: a hydrocolloid dressing for chronic wounds. *Br. J. Nurs.* 9, 720–723. doi: 10.12968/bjon.2000.9.11.6263
- Wu, C. C., Chew, K. Y., Chen, C. C., Kuo, Y. R. (2015a). Antimicrobial-impregnated dressing combined with negative-pressure wound therapy increases split-thickness skin graft engraftment: a simple effective technique. *Adv. Skin Wound Care* 28, 21–27. doi: 10.1097/01.ASW.0000459038.81701.fb
- Wu, L., Norman, G., Dumville, J. C., O'Meara, S., Bell-Syer, S. E. (2015). Dressings for treating foot ulcers in people with diabetes: an overview of systematic reviews. *Cochrane Database Syst. Rev.* 7:CD010471. doi: 10.1002/14651858.CD010471.pub2
- Yuki, A., Takenouchi, T., Takatsuka, S., Fujikawa, H., and Abe, R. (2017). Investigating the use of tie-over dressing after skin grafting. *J. Dermatol.* 44, 1317–1319. doi: 10.1111/1346-8138.13916
- Zhang, S., Song, C., Zhou, J., Xie, L., Meng, X., Liu, P., et al. (2012). Amelioration of radiation-induced skin injury by adenovirus-mediated heme oxygenase-1 (HO-1) overexpression in rats. *Radiat. Oncol.* 7:4. doi: 10.1186/1748-717X-7-4
- Zhang, S., Wang, W., Gu, Q., Xue, J., Cao, H., Tang, Y., et al. (2014). Protein and miRNA profiling of radiation-induced skin injury in rats: the protective role of peroxiredoxin-6 against ionizing radiation. *Free Radic. Biol. Med.* 69, 96–107. doi: 10.1016/j.freeradbiomed.2014.01.019
- Zhang, Y., and Xing, S. Z. (2014). Treatment of diabetic foot ulcers using Mepilex Lite Dressings: a pilot study. *Exp. Clin. Endocrinol. Diabetes* 122, 227–230. doi: 10.1055/s-0034-1370918
- Zhong, W. H., Tang, Q. F., Hu, L. Y., and Feng, H. X. (2013). Mepilex lite dressings for managing acute radiation dermatitis in nasopharyngeal carcinoma patients: a systematic controlled clinical trial. *Med. Oncol.* 30:761. doi: 10.1007/s12032-013-0761-y
- Zhu, Y. N., Zhang, J. M., Song, J. Y., Yang, J., Du, Z., Zhao, W. Q., et al. (2019). A multifunctional pro-healing zwitterionic hydrogel for simultaneous optical monitoring of pH and glucose in diabetic wound treatment. *Adv. Func. Mater.* 30:1905493. doi: 10.1002/adfm.201905493

Conflict of Interest: The authors declare that the research was conducted in the absence of any commercial or financial relationships that could be construed as a potential conflict of interest.

Copyright © 2020 Shi, Wang, Liu, Li, Li, Zhang, Liu, Shao and Wang. This is an open-access article distributed under the terms of the Creative Commons Attribution License (CC BY). The use, distribution or reproduction in other forums is permitted, provided the original author(s) and the copyright owner(s) are credited and that the original publication in this journal is cited, in accordance with accepted academic practice. No use, distribution or reproduction is permitted which does not comply with these terms.



Electrospun Biomaterials in the Treatment and Prevention of Scars in Skin Wound Healing

Eoghan J. Mulholland*

Gastrointestinal Stem Cell Biology Laboratory, Wellcome Trust Centre for Human Genetics, University of Oxford, Oxford, United Kingdom

OPEN ACCESS

Edited by:

Ubaldo Armato,
University of Verona, Italy

Reviewed by:

Lynn Jena,
Queen's University Belfast,
United Kingdom
Peng Hu,
University of Verona, Italy

*Correspondence:

Eoghan J. Mulholland
eoghan.mulholland@well.ox.ac.uk

Specialty section:

This article was submitted to
Biomaterials,
a section of the journal
Frontiers in Bioengineering and
Biotechnology

Received: 27 August 2019

Accepted: 24 April 2020

Published: 04 June 2020

Citation:

Mulholland EJ (2020) Electrospun Biomaterials in the Treatment and Prevention of Scars in Skin Wound Healing. *Front. Bioeng. Biotechnol.* 8:481. doi: 10.3389/fbioe.2020.00481

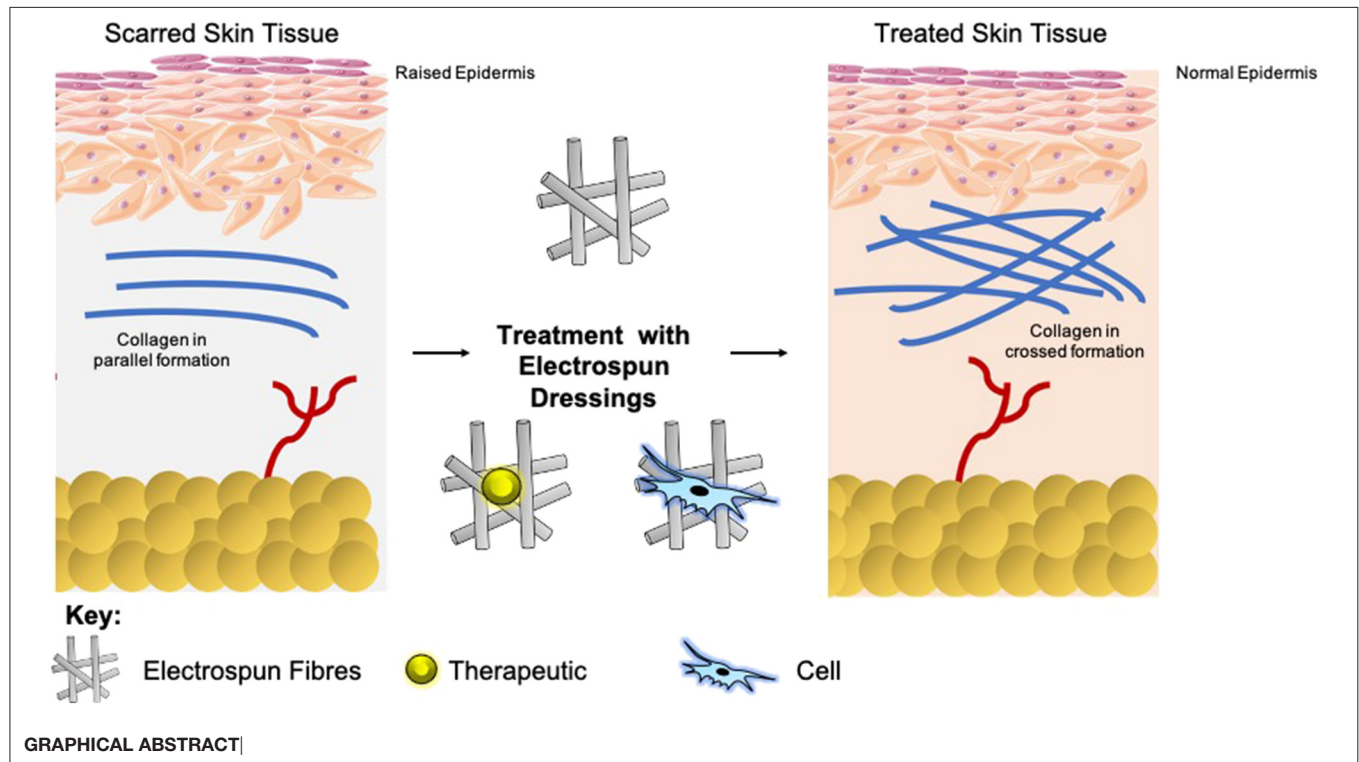
Electrospinning is a promising method for the rapid and cost-effective production of nanofibers from a wide variety of polymers given the high surface area morphology of these nanofibers, they make excellent wound dressings, and so have significant potential in the prevention and treatment of scars. Wound healing and the resulting scar formation are exceptionally well-characterized on a molecular and cellular level. Despite this, novel effective anti-scarring treatments which exploit this knowledge are still clinically absent. As the process of electrospinning can produce fibers from a variety of polymers, the treatment avenues for scars are vast, with therapeutic potential in choice of polymers, drug incorporation, and cell-seeded scaffolds. It is essential to show the new advances in this field; thus, this review will investigate the molecular processes of wound healing and scar tissue formation, the process of electrospinning, and examine how electrospun biomaterials can be utilized and adapted to wound repair in the hope of reducing scar tissue formation and conferring an enhanced tensile strength of the skin. Future directions of the research will explore potential novel electrospun treatments, such as gene therapies, as targets for enhanced tissue repair applications. With this class of biomaterial gaining such momentum and having such promise, it is necessary to refine our understanding of its process to be able to combine this technology with cutting-edge therapies to relieve the burden scars place on world healthcare systems.

Keywords: nanofibers, nanotechnology, electrospinning, polymer, drug delivery, tissue engineering, wound healing, scars

INTRODUCTION

Pathological scar formation is the physiological conclusion of wound healing, and so it is important to understand its underlying cellular and molecular processes in order to apprehend how a scar is formed, but also for the exploration of potential therapeutic targets. Currently, scarring is a huge burden on world healthcare, and the global scar treatment market is projected to represent as much as \$34.9 billion by the year 2023¹. Indeed, scarring can lead to many adverse side effects such as reduced mobility, compromised function in organs such as the liver or kidney, and the development of functional disabilities such as the psychological stress (Krafts, 2010; Sarrazy et al., 2011). A plethora of treatment options are available for scarring including topical treatments and

¹<https://www.prnewswire.com/news-releases/global-scar-treatment-market-2013-2018--2023---rise-in-online-retailing-of-scar-treatment-products-300698219.html>



dressings but are met with many limitations and are proving ineffective. This review will explore the use of electrospun nanofibers as novel instruments for efficient wound healing and reducing scar formation. The large surface area to volume ratio make electrospun fibers attractive options as they offer therapeutic incorporation capabilities whilst also being absorptive. A key focus of this review will be how these nanofibers can be applied alone, but also in conjunction with pharmacotherapies and cells for effective skin repair.

WOUND HEALING

Wound healing is a highly complex process which stems from three well-defined phases: inflammation, proliferation, and remodeling. Inflammation is the immediate response phase, commencing with the contact of platelets from blood with exposed collagen at the site of injury (Qin, 2016). This contact initiates the formation of a fibrin clot, comprised of the platelets, thrombin, and fibronectin. The fibrin clot acts as a reservoir of cytokines and growth factors, stimulating inflammatory mediators to migrate to the wound, while also providing an architecture for infiltrating cells (Hsieh et al., 2017). For example, transforming growth factors (TGF- α , TGF- β) is a highly significant signaling pathway initiated by platelets within the fibrin clot (Ramirez et al., 2014). TGFs draw leukocytes to the injury site and initiate the inflammatory stage (Kryczka and Boncela, 2015). These leukocytes support the secretion of additional cytokines, e.g., platelet-derived growth factor (PDGF), interleukin-1 (IL-1), and fibroblast growth factor (FGF) (Grove and Kligman, 1983). During proliferation, the secondary stage

of wound healing, TGF signaling becomes increasingly crucial, especially in cell types such as keratinocytes, macrophages, and fibroblasts, essential for the transcription of collagen, fibronectin, and proteoglycan. Additionally, TGFs prevent the release of protease enzymes responsible for the degradation of the matrix and activates inhibitors of protease production (Broughton et al., 2006). As proliferation progresses, fibroblasts are the principal cell type. Fibroblasts are of mesenchymal origin and are accountable for new matrix production, resulting in the restoration of tissue homeostasis (Darby et al., 2014). Remodeling, the final stage, can last up to 1-year after injury. Collagenase enzymes secreted from fibroblasts, macrophages, and neutrophils, cleave the molecules of collagen, thereby breaking it down (Caley et al., 2015). This results in Type I collagen gradually replacing Type III collagen, which in time increases the tensile strength of the new tissue (Longaker et al., 2008). The collagen fibers in the wound tissue are thinner than that of normal dermal collagen. These thinner fibers will gradually thicken over time and organize along the stress lines of the injury. This resulting scar tissue, however, will never be as strong as the preceding normal tissue (White et al., 1971; Schilling, 1976; Corr et al., 2009). Many studies suggest that variations in inflammation during the wound healing process are directly related to the extent of scar tissue formation (Lim et al., 2006). For example, fetal wound healing presents with a lack of typical inflammatory markers and is “scarless” up to a certain age (Longaker et al., 2008). In adult wound healing, polymorphonuclear leukocytes are recruited to the site of injury, followed by macrophages and lymphocytes. Contrastingly, fetal wounds are void of polymorphonuclear leukocytes, and as

healing progresses, fetal macrophages enter the wound site but in lesser numbers than that of an adult (Mackool et al., 1998). This characteristic lack of an inflammatory response may be credited to a dearth in appropriate signaling in fetal wounds, and the fundamentally immature condition of fetal inflammatory cell populations. Many non-healing wounds fail to switch from the inflammatory phase into the proliferative phase, thus resulting in abnormal wound repair.

SCAR FORMATION

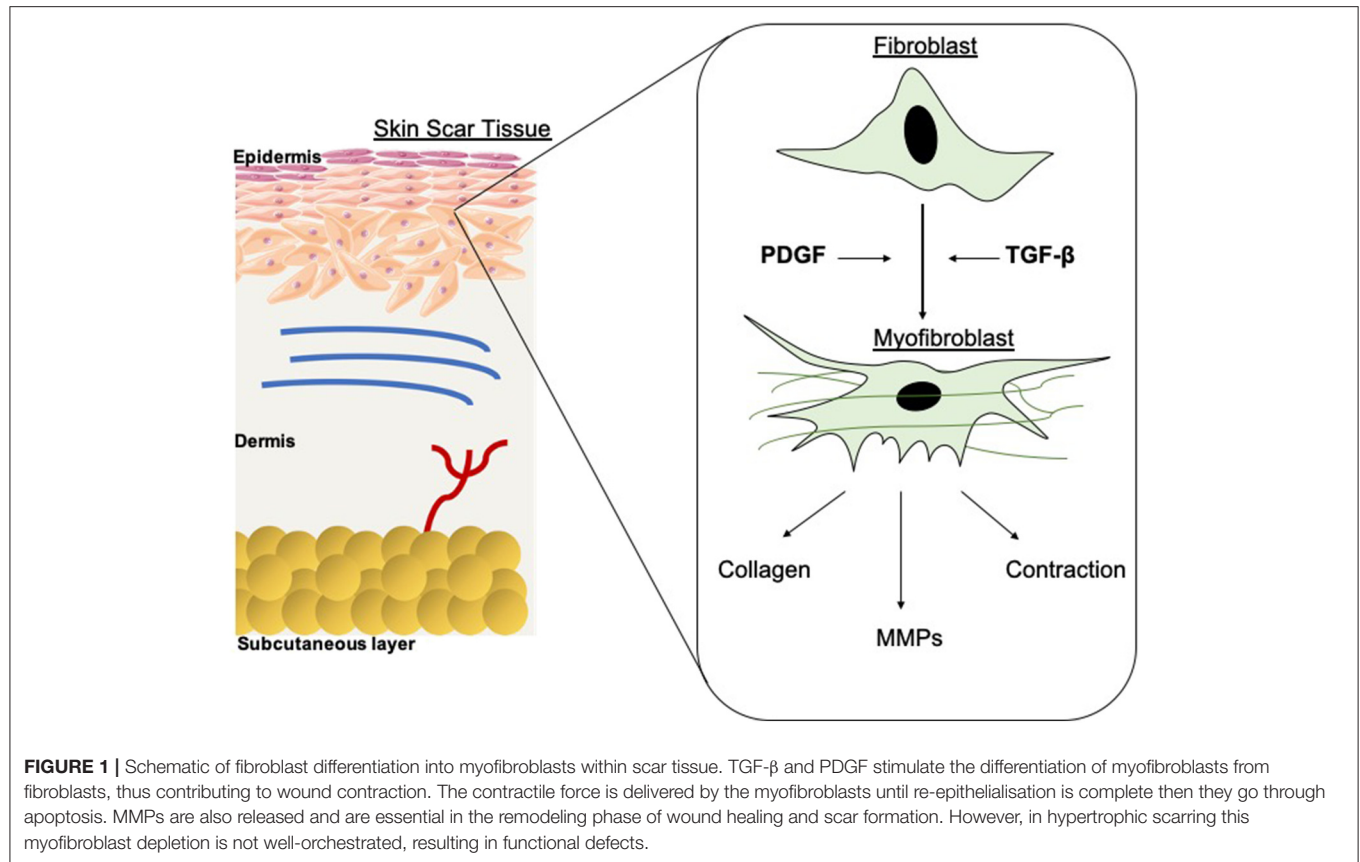
Scars present as a significant burden to healthcare systems, and so are a catalyst for global research for prevention and reduction (Mirastschijski et al., 2015; Barnes et al., 2018). A mature scar consists predominantly of Type I collagen (Marshall et al., 2018). Within scar tissue, this collagen is arranged in bundles parallel to the skin surface, as opposed to a non-parallel conformation in normal skin. This parallel configuration in scar tissue equates to an overall reduction in tensile strength (van Zuijlen et al., 2003). The epidermal basement membrane presents with a more flattened nature as opposed to normal skin, as it does not contain the rete pegs which typically infiltrate the dermis (Monaco and Lawrence, 2003). Furthermore, scar tissue is void of other classic dermal adjuncts such as hair follicles or sweat glands (Fu et al., 2005; Kiani et al., 2018). Upon maturation, the concentration of fibroblasts with the scar tissue depletes, which in combination with the lack of dermal adjuncts results in a dermal layer comprising of few cells. The extracellular matrix (ECM) of this tissue has less elastin than healthy tissue, which contributes to the loss in tensile strength, and means that re-injury is more probable (Kordestani, 2019).

The extent of fibrosis post-injury varies between organs and tissues. When the molecular regulation of the remodeling phase of wound healing is inefficient or disturbed, more problematic scars occur: hypertrophic scars and keloids. Hypertrophic scars typically develop post-surgery or from other trauma such as burns (Carswell and Borger, 2019). Keloids contrast from hypertrophic scars in that they grow beyond the natural margins of the initial damaged tissue (Berman et al., 2017). These keloidal scars do not naturally revert, as opposed to hypertrophic scars which typically regress to a degree within 6 months. Histologically speaking, keloid, and hypertrophic scars are distinguishable by a difference in collagen fiber architecture, presence of myofibroblasts which are alpha-smooth muscle actin-positive, and the degree of angiogenesis (Carswell and Borger, 2019). Keloids are characterized by thick fibers of collagen, while hypertrophic scars encompass thin fibers organized in nodules. The dysregulation to normal collagen maturation is a central influencer on excessive scar formation. Hypertrophic scars contain high concentrations of microvessels, attributed to excess proliferation and loss of functionality of endothelial cells. This phenomenon can be traced back to myofibroblast hyperactivity and the resulting excess collagen fabrication. Myofibroblasts are the principal cell type responsible for scar contraction (Li and Wang, 2011), and are derived from fibroblasts ~2 weeks post-wounding (Singer and Clark, 1999). PDGF and TGF- β stimulate

this cellular differentiation and the resultant contractile force exerted by the myofibroblasts enables wound edges in humans to come together, at a rate of ~0.75 mm a day (**Figure 1**) (Werner and Grose, 2003; Storch and Rice, 2005). Of course, in normal scars this wound contraction is an essential process; however, myofibroblasts typically go through apoptosis post-epithelialization, thus halting contractive pathways (Desmoulière et al., 2005). In hypertrophic scars, these myofibroblasts do not apoptose beyond epithelialization and so cause persistent contraction, resulting in functional implications to the skin (Ehrlich et al., 1994). Keloid scars, however, are smooth muscle actin negative (Ehrlich et al., 1994). This can be attributed to the presence of protomyofibroblasts in keloids, which can manufacture large quantities of ECM but not the force to contract lesions. This explains why functional defects resulting from contraction are only observed in hypertrophic scarring. Typically, the granulation tissue continues to expand and secrete growth factors, while lacking molecules essential for apoptosis or ECM remodeling such as cleaved-caspase 3, -8, and -9 (Yang et al., 2016). Indeed, upregulation of p53 expression has been reported in scarring phenotypes, a protein important for the inhibition of apoptosis (Tanaka et al., 2004).

Most lab-based *in vivo* assessment of wound closure and development is performed in rodents. This is mainly due to the high-throughput and low costs of these systems. However, it is important to understand that rodent wounds close differently to that of human's, primarily due to the process of contraction. This is mainly owed to an extensive subcutaneous striated muscle layer known as the panniculus carnosus that is virtually non-existent in humans. In rodents however, the panniculus carnosus allows the skin to move independently of the deeper muscles and is accountable for the rapid contraction of skin following injury. This physiological difference therefore creates difficulties to replicate the wound closure processes of human skin. This is a universal problem, one that is noted in much recent literature (Wang et al., 2013; Hu et al., 2018). Wang et al. discussed this problem, proposing an alternative model which involved splinting rodent wounds to inhibit contraction and force re-epithelialization. Nevertheless, this model also encountered limitations including inflammation induced from sutures used to anchor the splint to the mouse skin which could influence any molecular changes (Dunn et al., 2013). Formerly published reports utilizing the splinted wound model lack descriptive details of splint management and exclusion criteria for removing animals from analysis in cases where splints might have been incompletely secured due to suture rupture or damage to the splint by the animal.

Another alternative method is the direct suturing of a scaffold to the edges of the experimental wounds. Anjum et al. conducted wounding experiments of this nature with (Nu/Nu) mice and found that contraction is still observed in all wounds, however a more reepithelialization route was observed in the central wound regions (Anjum et al., 2017). However, limitations of this method again point to the provoking of an inflammatory response and coincidentally with an increased risk of surgical site infections (He et al.,



2009). Suture knots, for example, can act as platforms for bacterial colonization and reproduction (Mashhadi and Loh, 2011).

To overcome these limitations, porcine models of wound healing are often used. Pigs are anatomically and physiologically similar to humans, and therefore can be considered excellent models of human diseases (Seaton et al., 2015; Acevedo et al., 2019). Indeed, the skin of pigs and humans are similar in that they have a relatively thick epidermis and dermal papillae (Montagna and Yun, 1964).

CURRENT SCAR TREATMENTS

There is a vast array of current treatments for scars which come in a variety of forms. Topical treatments such as Mederma® Skin Care gel (Merz Pharmaceuticals, Greensboro, NC, USA)² is available over the counter. The active ingredients of Mederma® gel include onion extract; however, this product displayed no benefit when tested in a trial involving patients subjected to Mohs microsurgery (Jackson and Shelton, 1999).

Surgical revision is sometimes utilized for hypertrophic or normal scars. It is common practice in the clinic to wait several months before surgically excising scars, allowing them to become fully mature (Thomas and Somenek, 2012). The most direct

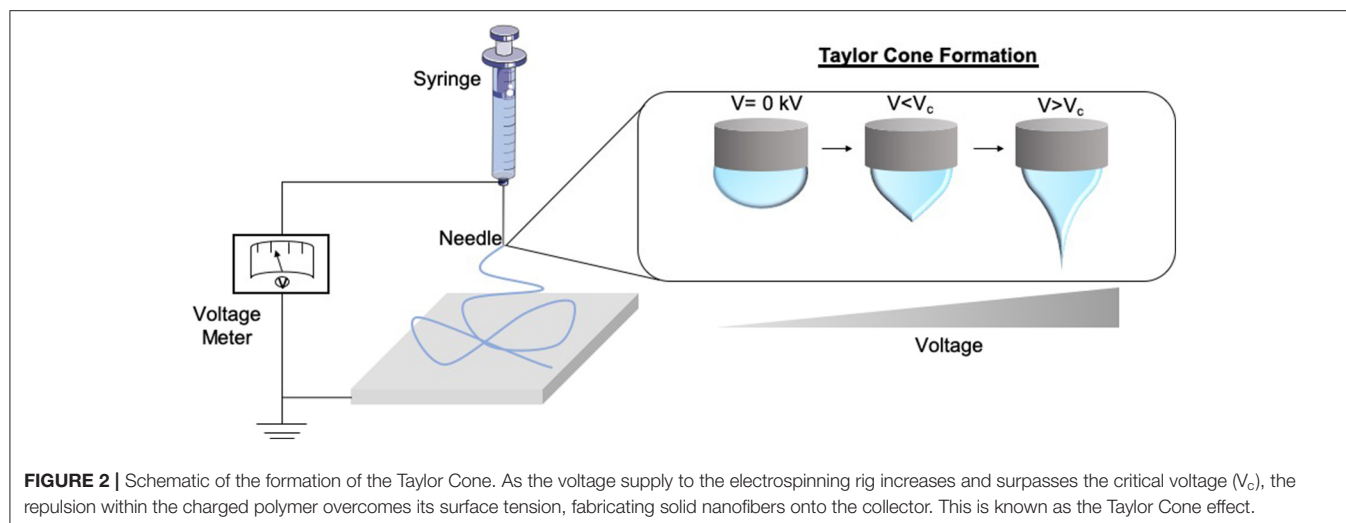
excision technique for scar removal is surgical removal followed by linear closure of the skin. Surgery as a treatment, however, can result in excessive tension across the wound area or infection (Marshall et al., 2018). There are also many injectable treatments which can be used for scar treatment, including corticosteroids which is common therapy for keloid and hypertrophic scars (Thomas and Somenek, 2012).

A further example is Botulinum toxin [BOTOX® Cosmetic (onabotulinumtoxinA)³, Allergan, Irvine, CA], which is linked with improving scar appearance (Gassner et al., 2000). However, in a clinical trial in humans who presented with forehead wounds in an emergency department and were treated with botox or placebo, there was no difference in scar appearance in 3 of 4 visual scales upon suturing (Ziade et al., 2013).

Dressings are the traditional treatment mode for wound healing and scar reduction as a means of protecting the wounds, keeping a moist microenvironment, and offloading tension from the skin (Commander et al., 2016). Indeed, the use of simple paper tape alone has shown promise. When paper tape was applied to patients with cesarean section wounds for 12 weeks post-surgery, there was a reduction in scar formation, and it decreased the probability of the patient developing hypertrophic scars (Atkinson et al., 2005).

²<https://www.mederma.com/>

³<https://hcp.botoxcosmetic.com/Contact>



With current treatments offering varying degrees of efficacy it is imperative to develop novel modalities of treatment. The electrospinning of polymers holds potential in this regard.

ELECTROSPINNING

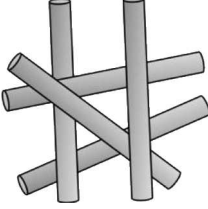
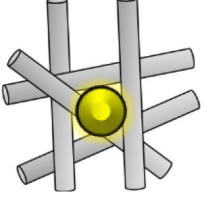
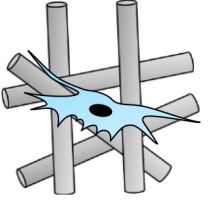
Electrospinning forms fibres through the application of an electrostatic field to a polymer solution (Cui et al., 2007; Bhardwaj and Kundu, 2010; Lagaron et al., 2017). The process of electrospinning can produce fibers right down to nanoscale and have applications in various fields, for example, wound dressings, drug delivery, and tissue engineering devices. The process itself is rapid and can be scaled to meet industrial demands to continuously produce fibers. This technique involves the use of a high voltage field strength from as low as 1 kV cm^{-1} , to charge the surface of a polymer solution droplet, subsequently inducing the ejection of a liquid jet toward a grounded surface. When the voltage reaches the optimal threshold [critical voltage (V_c)] by radial charge repulsion, the single jet will divide into multiple filaments; this is recognized as the Taylor cone effect (Figure 2). This cone formation results in the construction of solidified fibers as the solvent evaporates. The V_c value varies between polymers due to alterations in chemical properties (Quinn et al., 2018). Solution properties such as viscosity, concentration, and dielectric constant, and operational parameters including the strength of the applied voltage, jet to collector distance, and flux, will all affect the morphology of the resulting fibers (Sencadas et al., 2012; Haider et al., 2015). Electrospun fibers possess high surface area to volume ratios, meaning they exhibit many of the desirable properties of an effective wound dressing such as protection from mechanical stimuli and providence of excellent gaseous exchange, and as such a lot of research has gone into optimizing them for this application. The following sections, therefore, explore the use of electrospun fibers in the treatment of scars and the potential future applications this technology could hold as a therapeutic (Table 1).

Electrospinning is a versatile process which encompasses many different modes of fabrication for the incorporation of

therapeutics (Figure 3). Blending is the predominant method for drug incorporation into electrospun nanofibers. The process of blending consists of drug or drug precursors encapsulated by means of dissolving or dispersing it into the polymer solution, before subsequent electrospinning. As the drug itself is in direct contact with the polymer, the drug-polymer interaction must be analyzed to ensure functionality is retained and that the drug can be adequately released from the product fibers. For example, Yang et al. investigated the use of gold nanoparticles modified with an antibacterial intermediate (6-aminopenicillanic acid) for wound healing applications. The gold nanoparticles were assimilated into electrospun nanofibers composed of polycaprolactone (PCL) and gelatin by blending. The nanoparticles release profile was investigated by nanofiber dipping into saline. The results showed that after Day 1 20.4% of the gold had been released, increasing to 65.7% by Day 7. Burst release was apparent within the initial days which can be attributed to a percentage of the gold existing near the surface of the fibers (Yang et al., 2017).

Modification of nanofiber surfaces to allow incorporation of therapeutics is another method for drug and cell loading (Prabhakaran et al., 2008; Ma et al., 2011; Wakuda et al., 2018). This method is advantageous for avoiding burst discharge of therapeutics and results in a more gradual release profile (Im et al., 2010). This technique is particularly beneficial for biomolecular therapeutics such as enzymes as surface conjugation, and slow-release helps to preserve functionality (Zamani et al., 2013). Plasma treatment of polymers is a typical method of surface modification. Nanofiber treatment with plasma in the presence of oxygen, ammonia, or air has resulted in the generation of amine or carboxyl groups on the surface of the fibers (Baker et al., 2006; Yan et al., 2013). This process functionalizes fibers for a variety of applications, such as the adhesion of the collagen or gelatin, which are key proteins found in the extracellular matrix, and so can improve cell adhesion and proliferation (He et al., 2005; Koh et al., 2008). It has been shown that poly(lactic-co-glycolic acid) PLGA nanofibers can be transformed to contain carboxylic acid groups through plasma glow discharge in the presence of oxygen and gaseous

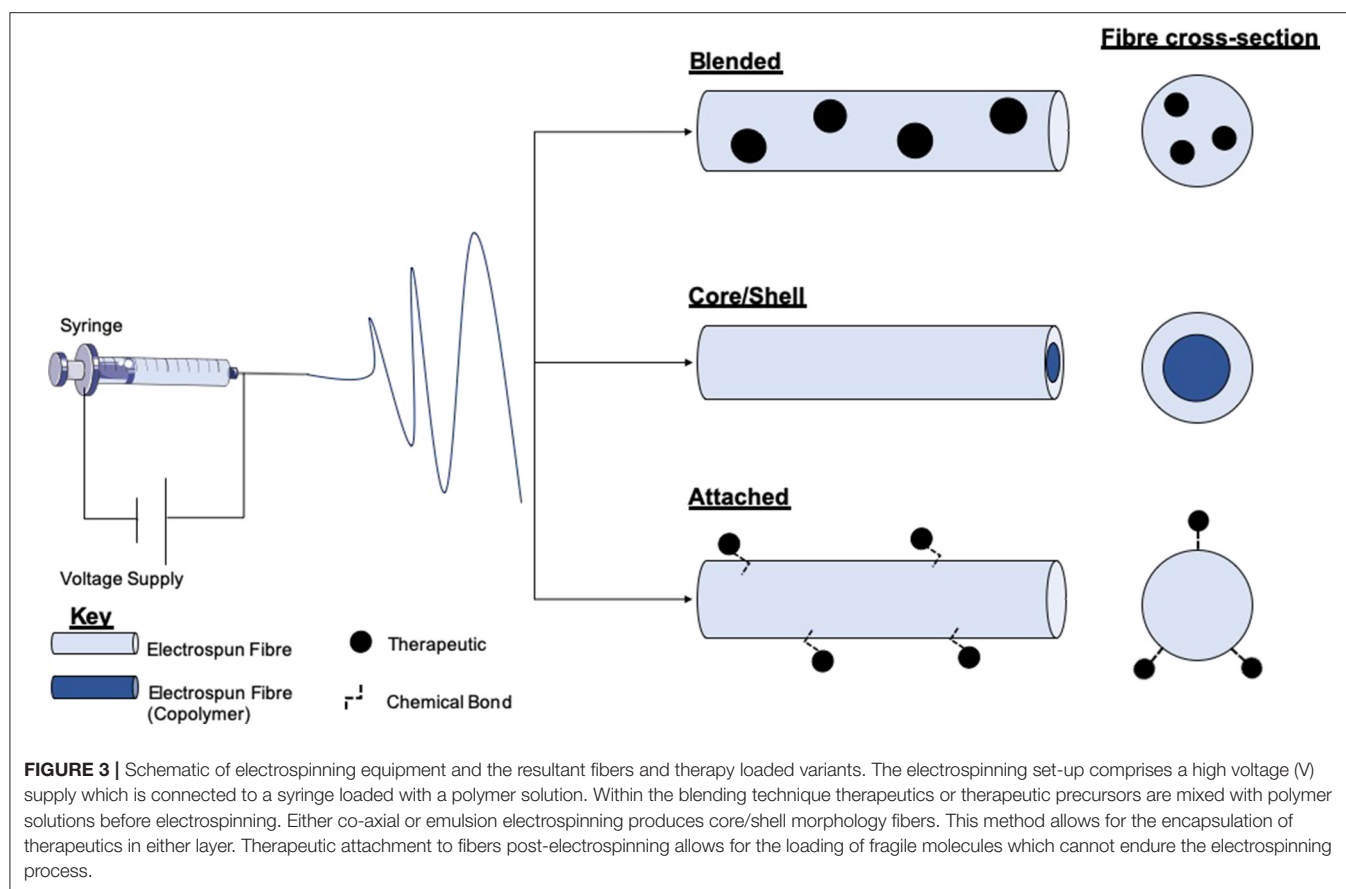
TABLE 1 | Therapeutic potential of various electrospun polymers including therapy loaded nanofibers and tissue engineering options.

Electrospun devices	Electrospun polymers	Incorporated therapeutics	Therapeutic outcomes	References
	Recombinant Human Collagen, Chitosan and PEO	–	This dressing resulted in elevated levels of collagen III <i>in vivo</i> 14 days post-surgery in normal male SD rats compared to control groups, which is indicative of less scar tissue formation.	Deng et al., 2018
	Collagen Type I and PCL	–	Significantly reduced the area of scar tissue formation in back skin wounds of Sprague-Dawley rat compared to controls as determined via H&E staining.	Bonvallet et al., 2014
	Silk fibroin/gelatin	–	This dressing inhibited scar tissue formation <i>in vivo</i> via stimulating wound closure ($p < 0.05$), enhancing angiogenesis, and successfully refining collagen organization.	Shan et al., 2015
	Silk fibroin/PEO	–	This dressing stimulated rapid collagen production with a similar architecture to normal skin.	Ju et al., 2016
	Collagen (Col, mimicking protein), PCL	Bioactive glass nanoparticles	This dressing delivered bioglass nanoparticles resulting in enhanced endothelial cell attachment and proliferation <i>in vitro</i> . This translated to well organized collagen deposition and skin appendages <i>in vivo</i> compared to controls without nanoparticles in specific pathogen-free male Sprague-Dawley rats.	Gao et al., 2017
	PELA and PEG	pbFGF and PEI	This dressing after 4 weeks resulted in fully differentiated epidemic cells, closely arranged basal cells and elevated occurrences of hair and sebum, consistent with the epithelial structure of normal skin.	Yang et al., 2012
	Poly(ϵ -caprolactone) (PCL)/gelatin	TGF- β 1 inhibitor (SB-525334)	This dressing released PGT to effectively inhibit fibroblast proliferation <i>in vitro</i> and this translated to the successful prevention of hypertrophic scar formation <i>in vivo</i> in a full-thickness wound model on the ear of female New Zealand white rabbits.	Wang et al., 2017
	Recombinant Human Tropoelastin	Adipose derived stem cells (ADSC)	This dressing significantly improved wound closure and enhanced epithelial thickness <i>in vivo</i> in a murine excisional wound model compared to controls. It is hypothesized that the device could persist within the skin after healing and improve the overall tensile strength of the resulting scar tissue.	Machula et al., 2014
	Collagen and PCL	Keratinocytes and Fibroblasts	This layered dressing becoming unrecognizable after Day 21 post-implantation, indicative of high grafting efficiency.	Mahjour et al., 2015
	PLGA and Collagen	Bone marrow-derived MSCs (BM-MSCs)	This dressing resulted in faster wound closure times <i>in vivo</i> in full-thickness wound models in rats, with wounds closing 8 days earlier than controls.	Ma et al., 2011

acrylic acid (Park et al., 2007). These fibers exhibited enhanced fibroblast cell adhesion and proliferation, desirable properties for wound healing.

The fabrication of core/shell nanofibers is another attractive method of bioactive incorporation into electrospun nanofibers. The production of electrospun core-shell nanofibers is accomplished through either co-axial or emulsion electrospinning. Co-axial electrospinning is a two-stream process that results in the fabrication of multipolymer fibers with the inner stream being the “core,” and the outer polymer passed stream forms the shell (Jiang et al., 2014). This method is auspicious for the incorporation of fragile cargos (e.g., DNA

or growth factors) as the therapeutic interaction with the shell polymer blend which may be produced with harsh solvents is minimized, therefore preserving the cargo (Ghosh et al., 2008; Xie et al., 2016; Cheng et al., 2019). Wei et al. utilized this technique for the development of a wound dressing, comprising a PCL core and collagen shell nanofibers. The shell was blended with silver nanoparticles to take advantage of the anti-bacterial activity, and the core permeated with vitamin A, which has been shown to help with wound healing by increasing intra- and extracellular hydration (Campos et al., 1999; Wei et al., 2016). Emulsion electrospinning produces nanofibers of core/shell morphology by first introducing an emulsion into an initial



polymer solution before the addition of a surfactant to isolate the different phases from each other (Liao et al., 2009). Castro et al. manufactured nanofibers composed of PCL and PCL/gelatin, which retained and delivered ketoprofen by solution and emulsion electrospinning, respectively. It was reported that using emulsion electrospinning of PCL/gelatin could diminish the burst release of ketoprofen compared with single PCL nanofibers, and sustained drug release for >100 h. Furthermore, the combination of gelatin into the nanofibers resulted in an increase in the cell proliferation of L929 fibroblast cells (murine) (Basar et al., 2017). It should be noted however that emulsion electrospinning can cause damage to molecules such as DNA via interface tension between the organic and aqueous phases within the emulsion (He et al., 2012).

ELECTROSPINNING POLYMERS FOR SCAR TREATMENT

With the process of electrospinning being so versatile, a plethora of both synthetic and natural polymers can be processed to form fibrous structures with the potential to promote scar-free wound healing. Expectedly, not every polymer can be easily electrospun. Many factors influence this ability, including polymer viscosity, concentration, and entanglement. For polymers with inadequate characteristics for electrospinning, a copolymer can be employed

to improve mechanical properties. Alginate is an example of a naturally occurring polymer with a well-noted history for improving wound healing due to its excellent ability to swell and maintain a moist microenvironment, which aids healing (Aderibigbe and Buyana, 2018). However, alginate alone does not possess ideal attributes for electrospinning due to its low chain entanglement (Nie et al., 2008). Poly (vinyl alcohol) (PVA) is a reputable polymer for electrospinning and as a result is frequently selected as a copolymer. Indeed, PVA is extensively used on an industrial scale and is favored in the medical industry due to excellent physical properties, processability, and biocompatibility. Tarun et al. developed an electrospun matrix composed of PVA/ sodium alginate (Tarun and Gobi, 2012). It was demonstrated that the matrix displayed excellent water vapor transmission rates, thus maintaining a moist wound microenvironment. Furthermore, *in vivo* studies using the full-thickness wound model in rats exhibited seemingly new epithelium development, void of any local adverse reactions. Indeed, the movement of epithelial cells across the surface of a wound is enabled in a wound that is kept moist, and in turn, promotes efficient healing (Field and Kerstein, 1994). Wounds that are kept moist typically present with less scar tissue formation (Atiyeh et al., 2003).

A further example of a natural polymer includes chitosan, which has noted antibacterial and antifungal properties, which would be highly beneficial for a wound dressing. It was suggested

by Ignatova et al. that the crosslinking of PVA/Q-chitosan (a chitosan derivative) through the photo-crosslinking electrospinning procedure, would have antimicrobial effects on both Gram-positive and Gram-negative bacteria (Ignatova et al., 2006). The author's results showed that the matrix had exceptional resistance to the growth of bacteria exhibiting activity against *E. coli* and *S. aureus*. However, it is important to note that with polymers like chitosan there are drawbacks. Chitosan, as an example, is poorly soluble (Shete et al., 2012), and so tends to be dissolved in acidic conditions, namely using acetic acid or trifluoroacetic acid for example (Geng et al., 2005; Bazmandeh et al., 2019; Gu et al., 2019). The toxicity and cost associated with such solvents can impede the potential of chitosan in wound and anti-scarring therapies (Mengistu Lemma et al., 2016), however, during the electrospinning process much of the solvent evaporates under ideal conditions, and so could help alleviate these unwanted side effects when harsher solvents are required (Golecki et al., 2014; Haider et al., 2015).

Another natural polymer of noted potency as a wound-healing material is silk fibroin, a protein produced by some insects (e.g., silkworm). Fibroin makes for an excellent wound repair candidate as it is highly biocompatible, contains anti-inflammatory properties, and has notable anti-scarring potential. As such, much attention has turned to the electrospinning of silk to fabricate bioactive wound dressings. For example, Ju et al. developed electrospun silk fibroin nanofibers as a dressing material for the treatment of burn wounds. The authors found that the expression of IL-1 α , which is pro-inflammatory, had significantly lower expression levels in silk fibroin treated skin compared to a gauze control treatment in the skin of male Sprague-Dawley rats where second degree burn wounds were induced on the backs. Further to this, the expression profile of TGF- β 1 peaked at Day 21 post-wounding before declining, compared to at in gauze treated wounds which crested at Day 7. It was also noted that the silk fibroin nanofibers induced rapid collagen formation, which organized within the wound in a similar fashion to that of normal skin as opposed to a scarring composition (Ju et al., 2016).

ELECTROSPUN POLYMERS WITH ADDED THERAPEUTICS FOR SCAR TREATMENT

With the variety of production avenues for electrospinning nanofibers (blending, core/shell, attachment), there lays the opportunity for the incorporation and delivery of a variety of anti-scarring therapeutics. As discussed, alginate offers an excellent polymer choice for wound dressings as it promotes a moist wound environment, and hence reduces the extent of scarring. In a study by Shalumon et al. the use of electrospun sodium alginate/PVA nanofibers loaded with ZnO nanoparticles (via the blending method) as an antibacterial wound dressing was explored. The study concluded that a concentration of between 0.5 and 5% is required for the fibers to have antibacterial activity as tested with *S. aureus* and *E. coli*, with minimal cytotoxic effects (using L929 murine fibroblast cells) (Shalumon et al.,

2011). These nanofibers were tested *in vivo* using C57BL/6J mice, where UVB irradiation was employed to produce visible skin lesions, and scar formation was evident within 48–96 h. When these lesions were treated with the nanofiber dressings it was reported that no burn marks were detectable after 24 h post-injury. This rapid recovery was further confirmed by the downregulation of inflammatory cytokines IL-6, IL-1 β , and TNF- α after 24 h compared to untreated controls. Taken together this electrospun device shows excellent potential for the reduction of scar tissue formation in a burn wound model (Hajiali et al., 2016).

A historic but still pertinent avenue for the treatment of wounds and scars is the use of essential oils (Sequeira et al., 2019). Previous research has developed electrospun nanofibers composed of alginate/polyethylene glycol (PEO) infused with lavender essential oil, for the treatment of UV-induced skin burns. These fibers showed antibacterial efficacy *in vitro* against *S. aureus*, and furthermore reduced the production of pro-inflammatory cytokines both *in vitro* and *in vivo* (Hajiali et al., 2016). The authors found that the burns of mice treated with the lavender-infused nanofibers healed faster compared to the untreated group. Karami et al. developed electrospun fibers of PCL and polylactic acid (PLA) which encapsulated thymol from thyme essential oil for the treatment of skin infections, with a focus on *E. coli* and *S. aureus* (Karami et al., 2013). Application of these nanofibers *in vivo* using a full-thickness wound model in Male Wistar rats resulted in an enhancement in granulation tissue formation and re-epithelialization at 14 days post-wounding (92.3%) compared to gauze (68%) and commercial (Comfeel Plus) (87%) controls. Histologically, the wounds treated with the commercial dressing exhibited some epidermal tissue at day 14, but this was more extensive in the nanofiber treated wounds (Karami et al., 2013). These results demonstrate the power of essential oils as efficient wound healing therapeutics, which could be employed for the reduction in scar tissue formation.

In another study conducted by Gao et al., endothelial progenitor cells were cultured on composite fibers consisting of PCL/collagen and bioactive glass nanoparticles *in vitro* (Gao et al., 2017). *In vivo* wound healing studies using specific pathogen-free male Sprague-Dawley rats revealed evident blood vessel formation, as well as upregulation of angiogenic markers such as hypoxia-inducible factor-1 α (HIF-1 α) and vascular endothelial growth factor (VEGF). Throughout the *in vivo* study, wound healing potential was superior in wounds treated with nanofibers containing the bioglass nanoparticles. These bioglass-loaded nanofibers achieved 60% wound closure in the first week and ~90% closure with 2 weeks, compared to nanofibers containing no bioglass beads which achieved only 50 and 80% closure within week 1 and week 2, respectively. The total area of scar tissue in wounds treated with the bioactive glass-loaded nanofibers was significantly smaller and with highly organized collagen deposition compared to treatment with unloaded nanofibers (Gao et al., 2017).

Many studies have explored the use of electrospun nanomaterials in the treatment of diabetic foot ulcers (DFU). DFU are categorized as a major complication of diabetes mellitus,

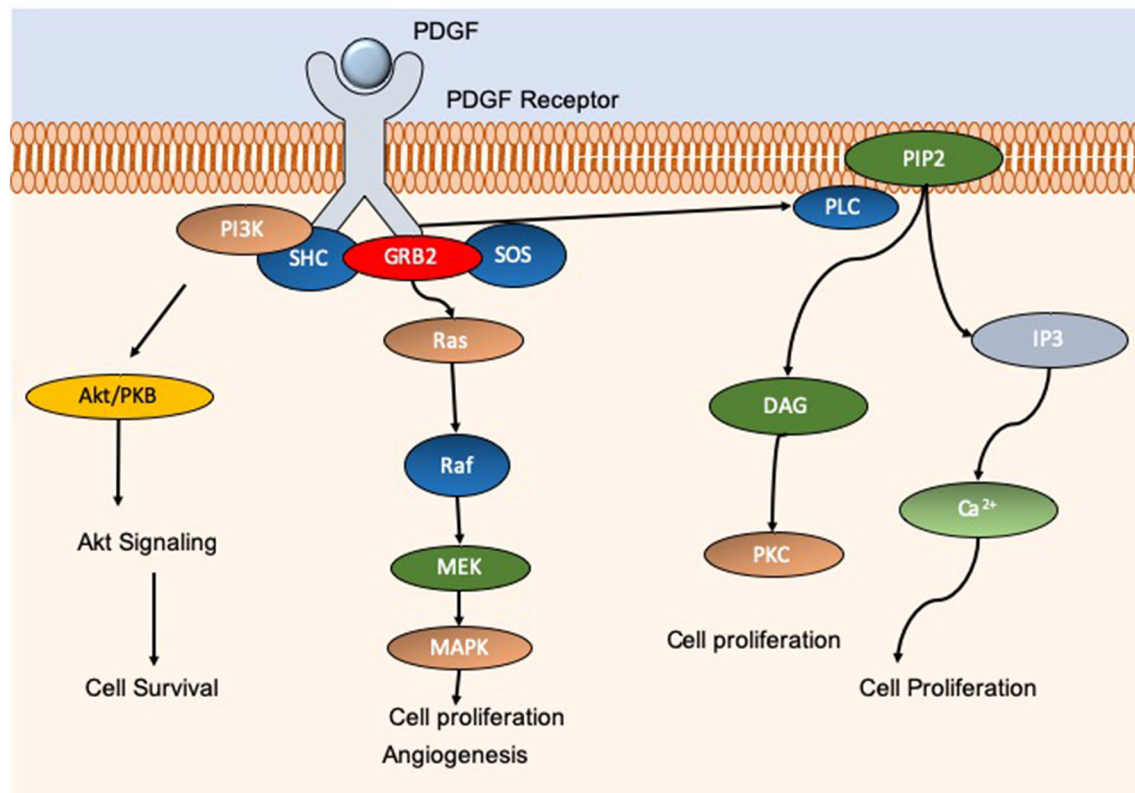


FIGURE 4 | Schematic showing the molecular pathways associated with PDGF. PDGF activation gives rise to an increase in cell proliferation, migration, and angiogenesis through Akt, MAPK, and calcium pathways for example. PDGF is essential for efficient wound repair and minimization of potential scar tissue. Commercial product REGRANEX® utilizes recombinant human PDGF for the treatment of diabetic foot ulcers.

and typically present on the feet, toes, and heels. DFU result from peripheral neuropathy, poor circulation, and impaired immune function, or a combination of these foundations. Of diabetic patients in the USA, 20% of foot ulcer cases displayed insufficiencies in peripheral arterial supply. Moreover, 50% of patients primarily displayed peripheral neuropathy, and ~30% presented with a combination of these conditions (Reiber et al., 1999)⁴ As such, with a wide-reaching cohort of diabetic patients suffering from chronic wounds, there is a continuous need for efficient wound healing options which result in rapid and scar-free results. Indeed, Yang et al. developed an electrospun dressing composed of poly(dl-lactide)-poly(ethylene glycol) (PDLLA-PEG) fibers which had polyethyleneimine (PEI)/pbFGF polyplexes incorporated by the emulsion loading technique, advantageous for the integration of fragile genetic material. PEG was also added to the shell portion of the fibers to aid in smooth release of the cargo. The authors found that the structure was able to sustain release of the polyplexes over a 4-week period, and successful transfection was observed that ensued for over 28 days, enhancing the proliferative capacity of the mouse embryo fibroblast cells *in vitro*. The efficacy of the fibers *in vivo* was tested in skin wounds generated on the dorsal area of diabetic male

Sprague Dawley (SD) rats. The fibers containing PEI/pbFGF complexes resulted in a significantly higher wound recovery rate compared to untreated wounds, exhibiting improved vascularization and completed re-epithelialization (Yang et al., 2012). These are important outcomes as the more rapid and efficient cell migration corresponds to a reduction in scar tissue formation (Hadjizadeh et al., 2017). Yuan et al. also explored the combination of growth factors and electrospun materials for skin regeneration. The authors utilized a dual-spinneret electrospinner to manufacture fibers composed of chitosan- PEO and fibrinogen, loading the polymers with PDGF via blending directly before electrospinning (Yuan et al., 2018). PDGF is a critical player in wound repair initiation and progression, acting as a chemotactic instrument for neutrophils, monocytes, and fibroblasts (Sá et al., 2018). Furthermore, PDGF can block fibroblast differentiation into myofibroblasts thus decreasing scar formation (Yuan et al., 2018). Indeed, a therapy option of wound repair termed Regranex® is the only growth factor wound treatment for diabetic ulcers currently FDA approved, utilizing recombinant human PDGF (Figure 4) (Fang and Galiano, 2008). A single daily application of Regranex® has been shown to enhance wound closure, with a 30% faster healing time observed. It must also be noted that in the case of Regranex® it was previously suggested that it increased the rate of mortality related to malignancy development in patients treated with

⁴<https://www.niddk.nih.gov/about-niddk/strategic-plans-reports/diabetes-in-america-2nd-edition>

>3 tubes of the product, as concluded from a post-marketing retrospective study. However, this warning has since been removed from the product packaging, and many studies have disproved this theory (Ziyadeh et al., 2011; REGRANEX®, 2018). Nevertheless, daily application is considered to be inconvenient for the patient, impacting the quality of life. Thus, the delivery of this growth factor in a controlled manner could be of great benefit. In the instance of Yuan and authors, it was observed that the nanofibers developed exhibited an average fiber diameter of 202.3 ± 113.2 nm, PDGF integrity was retained, and upon release promoted an increase in the migration rate of human dermal fibroblasts. With regards to cytotoxicity, there was a significant decrease in the viability of cells exposed to the nanofibers (unloaded) at 72 h post-incubation compared to a no scaffold control. It is postulated that this decrease is the result of the degree of acetylation of chitosan, which has been shown to elicit strong cellular interactions due to positive charges (Aranaz et al., 2009). Indeed, other groups have observed a decrease in cell viability after 24 h in bladder carcinoma cells exposed to chitosan with a degree of acetylation greater than 50% (Younes et al., 2016). This is an interesting observation, and so should be factored into the rationale for novel wound healing devices. However, it is suggested that this observation may be unique to *in vitro* experimentation, as prior studies using chitosan observed negligible toxic effect *in vivo*, linked with metabolic clearance of biodegradation products (Kean and Thanou, 2010; Jeong et al., 2017).

CELL DELIVERY VIA ELECTROSPUN POLYMERS FOR SCAR TREATMENT

The use of cells in regenerative medicine is widely explored and considered by many to hold great promise⁵. For example, mononuclear umbilical cord cells are easily available and have few associated ethical issues. Furthermore, it has been previously demonstrated that these cell types can be cultured on electrospun nanofibers (Chua et al., 2006).

In light of the advantageous potential of cell therapies for regenerative purposes, they are not without limitations. Therapies of this nature would require a large number of donors, these cells would not survive past low passage numbers, and there is the potential risk of rejection from the host (Venkat et al., 2018). A further example of potential cell therapies includes allogeneic bone marrow cells, which are easily available but carry the risk of rejection and would require specialized techniques for cell harvest and separation. Martinello et al. used allogenic mesenchymal stem cells to treat wounds in a large animal study using female Bergamasca sheep. It was found that at 15 Days post-injury, when compared to a control group, sheep treated with allogeneic bone marrow cells presented with a higher degree of wound closure, reepithelialization, as well as a reduction in inflammation. The latter of which the authors postulate may result in a decreased myofibroblast development and thus scar formation (Martinello et al., 2018).

⁵<https://www.mayoclinic.org/tests-procedures/bone-marrow-transplant/in-depth/stem-cells/art-20048117>

In saying this, autologous cells help mitigate the problem of immune rejection, but nevertheless require the same specialized harvesting and separation expertise (Venkat et al., 2018; Ramotowski et al., 2019).

Many studies have explored the use of cells for wound healing and scar tissue minimization. However, the most typical route for this exploration is the direct injection of cells, which can be highly inefficient, and incurs substantial cell death due to shear forces through the injection needle (Burdick et al., 2016). Electrospun nanofibers may be the solution for the efficient and effective delivery of cells for skin regeneration. Electrospun nanofibers have high surface areas, and therefore have the capacity to retain many cultured cells (Chen et al., 2009). For example, it was shown by Zhao et al. that electrospun nanofibers composed of silk fibroin could successfully host cardiomyocytes (Zhao et al., 2019). This capability of electrospun fibers to host cells is thought by many to be owed to the likeness to the natural ECM, fitting to the fibrous nature of collagen, thereby facilitating the natural proliferation of cells (Ramakrishna et al., 2006).

The disadvantage of using these nanofibers for this purpose, however, is the restricted control over pore structure. The pore size in this instance is proportional to the fiber diameters, with smaller diameters resulting in smaller pore sizes, which consequently can decrease cell infiltration (Wu and Hong, 2016). In some cases, cells only infiltrate the uppermost portion of the nanofibers, which reduces the advantages of three-dimensional cell culture. When nanofibers are compared to microfibers in this regard, it has been shown that larger pore sizes, inherent to macrofibers, promote stem cell differentiation, coupled with improved cellular permeation, however nanofibers are associated with higher cell attachment (Wu and Hong, 2016).

Mahjour et al. developed a skin substitute composed of electrospun PCL/collagen fibers for the treatment of burn wounds. The fibers in question were layered in a composite manner, with different layers infused with keratinocytes (top layer) and fibroblasts (bottom layer). The electrospun fibers were applied in an *in vivo* mouse model of wound healing. Data collected from the study showed that the cell incorporated composite fibers integrated into the wound bed in a highly effective way, becoming unrecognizable after Day 21 post-implantation. This was in comparison to blank fiber scaffolds which received the lowest score of integration. Furthermore, at Day 21, wounds treated with the cell-incorporated composite fibers had 7% remaining non-reepithelialized skin and 45% wound contraction, whereas the blank composite fibers had only 21% re-epithelialization and 56% wound contraction (Mahjour et al., 2015).

Mesenchymal stem cells (MSCs) are multipotent stem cells typically isolated from bone marrow, adipose tissues, and the dermis (Orbay et al., 2012). MSCs have shown avid potential in skin repair, promoting angiogenesis, reducing inflammation, and facilitating the establishment of an ECM (Jackson et al., 2012). When MSCs enter an inflammatory environment a switch to an immunomodulatory phenotype is initiated by Interferon-gamma (IFN γ), Tumor Necrosis Factor-alpha (TNF α) and IL-1 β (Ren et al., 2008). When this phenotype is active; there is evidence suggesting that MSCs can suppress the proliferation of B cells

as well as natural killer cells (Corcione et al., 2006; Sotiropoulou et al., 2006). This suppression enhances the acute immune response to damage and can reduce a pro-fibrotic response that can result from sustained inflammation (Redd et al., 2004). Williams et al. tried to reduce scar sizes in ischemic cardiomyopathy through injection of allogeneic MSCs (Williams et al., 2013). The authors suggested that MSCs could reverse ventricular remodeling, and, indeed, it was shown that MSCs stimulate endogenous cardiac stem cells to proliferate and differentiate. The resulting mature cardiomyocytes exhibited therapeutic effect by secretion of growth factors and cytokines.

Similarly, Li et al. showed that MSCs loaded into a 3D graphene foam decreased scar tissue formation. The foam resulted in upregulation of VEGF as well as bFGF leading to enhanced neovascularization, as well as heightening levels of TGF- β 3, which prevents scarring. The MSC loaded foams were tested *in vivo* in a full-thickness wound model using wild-type rats. The use of MSCs in the foam resulted in a significant closure of the wound from day 3 post-wounding compared to controls of untreated and unloaded foam, this trend was observed consistently until endpoint at 14 Days post-wounding (Li et al., 2015).

With such obvious potential, it is not surprising that many researchers have explored the incorporation of stem cells like MSCs into electrospun nanofibers for wound and scar treatments. For example, Ma et al. integrated bone marrow-derived MSCs (BM-MSCs) into nanofibers comprised of collagen and PLGA. The device demonstrated enhanced healing profiles in a full-thickness wound model *in vivo* using rats. The wounds treated with the BM-MSCs loaded nanofibers resulted in faster closure times compared to the untreated control, closing 8 days earlier (Ma et al., 2011). Furthermore, it was observed that localized treatment with the BM-MSCs resulted in a decrease in myofibroblast numbers. The authors postulated this may be due to MSCs ability to express hepatocyte growth factor 8 which inhibits myofibroblastic differentiation (Ma et al., 2011). These results suggest that this device would reduce scar tissue formation whilst allowing rapid and efficient wound repair.

In another study, Machula et al. electrospun nanofiber membranes of tropoelastin seeded with adipose-derived stem cells for wound healing applications (Machula et al., 2014). The authors found that the stem cells rapidly proliferated on the nanofibers and partook in efficient ECM establishment, covering the entire scaffold *in vitro*. Application of the cell-nanofiber device in an *in vivo* excisional wound model with female SCID mice showed an enhancement in wound closure and restoration of normal epithelium compared to control wounds treated with petrolatum jelly-impregnated gauze. The average thickness of re-epithelized skin tissue for the control and stem cell-nanofiber treated groups was $27.7 \pm 7.8 \mu\text{m}$ and $51.9 \pm 11.27 \mu\text{m}$, respectively ($p = 0.001$). It is postulated by the authors that the electrospun tropoelastin device may persist within the scar tissue of healed skin and in doing so enhance the tensile strength of any resultant scar tissue.

A limitation associated with stem cell culture on electrospun nanofibers is that small pore size may result in a blockage in nutrient diffusion and cellular infiltration. If this

problem can be mitigated, it could lead to a highly potent regenerative device.

CONCLUSIONS AND FUTURE DIRECTIONS

As detailed in this review, the use of electrospun nanofibers for scar treatment has substantial potential. With a plethora of polymers being “*electrospinnable*” alone or in conjunction with therapeutic agents or cells, the problem of scar management could be significantly improved. However, much work is still required to get such therapies into the clinic. Indeed, there are currently 5 clinical trials exploring the use of electrospun nanofibers⁶; yet, none of these are scar tissue-specific, and no current trials are recruiting. Conversely, there are 760 clinical trials listed for skin scarring⁷, 140 of which are recruiting⁸. This suggests that much research is focusing on novel therapies for scar treatment and prevention, which is a favorable scenario, and indeed these therapies if approved could in future be incorporated into electrospun nanofibers. Recent results have been notably discouraging. Metelimumab, for example, a TGF- β 1 targeting antibody, exhibited no improvement in the treatment of systemic sclerosis compared to a placebo control⁹. In saying this, an RNAi-based inhibitor of connective tissue growth factor (CTGF) termed RXI 109 has completed phase I trials and is now in phase II trials for hypertrophic scar treatment¹⁰. With promising therapies in the pipeline, it is exciting to hypothesize the efficiency of their delivery via electrospun nanofibers.

Encouragingly, electrospun nanofibers can be manufactured on an industrial scale, with the production of continuous nanofibers from a variety of polymers already proven (Ramachandran and Gouma, 2008; Zhang et al., 2012; Ma et al., 2015; Wang et al., 2018). Translating nanofiber production from laboratory to commercial scale is readily accommodated through the application of multi-jet nozzle electrospunners, which have been reported to process as much as 6.5 kg/h of polymer to produce fibers (Persano et al., 2013). Current commercial examples include the Zeus Bioweb™ composites, composed of electrospun polytetrafluoroethylene (PTFE). The Bioweb™ exhibits a high surface area and possesses an advantageously minute pore size, typically in the range of 1–4 μm . Zeus boasts a variety of Bioweb™ applications including scaffold potential and implantable structures in the body¹¹. A further commercial example of an electrospinning product is the SpinCare™ system by Nicast. SpinCare™ is a handheld device that fabricates nanofibers from polymers directly for tailored wound healing

⁶<https://clinicaltrials.gov/ct2/results?cond=&term=electrospinning&cntry=&state=&city=&dist=&Search=Search> (Date visited November 15, 2019).

⁷<https://clinicaltrials.gov/ct2/results?cond=Skin+Scarring&term=&cntry=&state=&city=&dist=> (Date visited November 15, 2019).

⁸https://clinicaltrials.gov/ct2/results?cond=Skin+Scarring&Search=Apply&recrs=a&age_v=&gndr=&type=&rslt= (Date visited November 15, 2019).

⁹<https://clinicaltrials.gov/ct2/show/NCT00432328>

¹⁰<https://clinicaltrials.gov/ct2/show/NCT02246465>

¹¹<https://www.zeusinc.com/products/biomaterials/bioweb-composites>

applications. These nanofibers provide a semi-permeable coverage facilitating excellent moisture regulation. The fibers are also comfortable as they are made to fit the shape of the patient's wound¹².

It is well-believed that the combination of gene therapies with biomaterials hold great potential as future generation therapeutic devices (Bleiziffer et al., 2007; Goker et al., 2019). Although promising, gene therapy is not without limitations. For example, therapies of this nature are historically challenging to deliver into cells, due to similarities in charges between nucleic acids and cell membranes. Viral gene delivery is the most common form of gene therapy due to its high efficiency. These vectors, however, are met with numerous trepidations as they can result in mutagenesis and have a restricted capacity for genetic material (Mingozi and High, 2013). Non-viral options for gene therapy also exist and include cationic polymers (Olden et al., 2018), liposomes (Balazs and Godbey, 2011), and peptides (McCarthy et al., 2014; Cole et al., 2019). Indeed, recent literature published by Mulholland et al. explored the delivery of an siRNA complexed with a cell penetrating peptide termed RALA from an electrospun bilayer wound patch. The use of the RALA peptide significantly enhanced the transfection efficient of the nucleic acids *in vitro* using HMEC-1 endothelial cells, downregulating expression anti-angiogenic FK506-binding protein-like FKBP. This high

efficiency translated to significant upsurge in angiogenic activity *in vivo* in wounds on the backs of C57BL/6 mice, resulting in an increase in blood vessel density of 326% compared to untreated wounds (Mulholland et al., 2019). This technology holds excellent potential for scar tissue treatment as a vast array of nucleic acids could be delivered in this manner.

Taken together, with the literature and the state-of-the-art technology discussed in this review, it can be rationalized that electrospinning shows great promise for the development of next generation devices for the treatment and management of scars.

AUTHOR'S NOTE

This manuscript was an invited paper for the article collection on Biomaterials for Skin Wound Repair: Tissue Engineering, Guided Regeneration, and Wound Scarring Prevention.

AUTHOR CONTRIBUTIONS

EM wrote the manuscript and produced all figures and tables with the aid of SMART Servier Medical Art www.smart.servier.com (Attribution 3.0 Unported (CC BY 3.0)).

ACKNOWLEDGMENTS

I would like to thank Dr. James Illingworth for his constant support in the writing of this article.

REFERENCES

- Acevedo, C. A., Sánchez, E., Orellana, N., Morales, P., Olguín, Y., Brown, D. I., et al. (2019). Re-epithelialization appraisal of skin wound in a porcine model using a salmon-gelatin based biomaterial as wound dressing. *Pharmaceutics* 11:196. doi: 10.3390/pharmaceutics11050196
- Aderibigbe, B. A., and Buyana, B. (2018). Alginate in wound dressings. *Pharmaceutics* 10:42. doi: 10.3390/pharmaceutics10020042
- Anjum, F., Agabalyan, N. A., Sparks, H. D., Rosin, N. L., Kallos, M. S., and Biernaskie, J. (2017). Biocomposite nanofiber matrices to support ECM remodeling by human dermal progenitors and enhanced wound closure. *Sci. Rep.* 7:10291. doi: 10.1038/s41598-017-10735-x
- Aranaz, I., Mengibar, M., Harris, R., Panos, I., Miralles, B., Acosta, N., et al. (2009). Functional characterization of chitin and chitosan. *Curr. Chem. Biol.* 3, 203–230. doi: 10.2174/187231309788166415
- Atiyeh, B. S., Amm, C. A., and El Musa, K. A. (2003). Improved scar quality following primary and secondary healing of cutaneous wounds. *Aesthetic Plast. Surg.* 27, 411–417. doi: 10.1007/s00266-003-3049-3
- Atkinson, J.-A. M., McKenna, K. T., Barnett, A. G., McGrath, D. J., and Rudd, M. (2005). A randomized, controlled trial to determine the efficacy of paper tape in preventing hypertrophic scar formation in surgical incisions that traverse Langer's skin tension lines. *Plast. Reconstr. Surg.* 116, 1648–1656; discussion 1657–1658. doi: 10.1097/01.prs.0000187147.73963.a5
- Baker, S. C., Atkin, N., Gunning, P. A., Granville, N., Wilson, K., Wilson, D., et al. (2006). Characterisation of electrospun polystyrene scaffolds for three-dimensional *in vitro* biological studies. *Biomaterials* 27, 3136–3146. doi: 10.1016/j.biomaterials.2006.01.026
- Balazs, D. A., and Godbey, W. (2011). Liposomes for use in gene delivery. *J. Drug Deliv.* 2011, 1–12. doi: 10.1155/2011/326497
- Barnes, L. A., Marshall, C. D., Leavitt, T., Hu, M. S., Moore, A. L., Gonzalez, J. G., et al. (2018). Mechanical forces in cutaneous wound healing: emerging therapies to minimize scar formation. *Adv. Wound Care* 7, 47–56. doi: 10.1089/wound.2016.0709
- Basar, A. O., Castro, S., Torres-Giner, S., Lagaron, J. M., and Turkoglu Sasmazel, H. (2017). Novel poly(ϵ -caprolactone)/gelatin wound dressings prepared by emulsion electrospinning with controlled release capacity of Ketoprofen anti-inflammatory drug. *Mater. Sci. Eng. C* 81, 459–468. doi: 10.1016/j.msec.2017.08.025
- Bazmandeh, A. Z., Mirzaei, E., Ghasemi, Y., and Kouhbanani, M. A. J. (2019). Hyaluronic acid coated electrospun chitosan-based nanofibers prepared by simultaneous stabilizing and coating. *Int. J. Biol. Macromol.* 138, 403–411. doi: 10.1016/j.ijbiomac.2019.07.107
- Berman, B., Maderal, A., and Raphael, B. (2017). Keloids and hypertrophic scars: pathophysiology, classification, and treatment. *Dermatol. Surg.* 43(Suppl. 1), S3–S18. doi: 10.1097/DSS.0000000000000819
- Bhardwaj, N., and Kundu, S. C. (2010). Electrospinning: a fascinating fiber fabrication technique. *Biotechnol. Adv.* 28, 325–347. doi: 10.1016/j.biotechadv.2010.01.004
- Bleiziffer, O., Eriksson, E., Yao, F., Horch, R. E., and Kneser, U. (2007). Gene transfer strategies in tissue engineering. *J. Cell. Mol. Med.* 11, 206–223. doi: 10.1111/j.1582-4934.2007.00027.x
- Bonvallet, P. P., Culpepper, B. K., Bain, J. L., Schultz, M. J., Thomas, S. J., and Bellis, S. L. (2014). Microporous dermal-like electrospun scaffolds promote accelerated skin regeneration. *Tissue Eng. Part A* 20, 2434–2445. doi: 10.1089/ten.tea.2013.0645
- Broughton, G., Janis, J. E., and Attinger, C. E. (2006). Wound healing: an overview. *Plast. Reconstr. Surg.* 117(7 Suppl.), 1e–S–32e–S. doi: 10.1097/01.prs.0000222562.60260.f9
- Burdick, J. A., Mauck, R. L., and Gerecht, S. (2016). To serve and protect: hydrogels to improve stem cell-based therapies. *Cell Stem Cell* 18, 13–15. doi: 10.1016/j.stem.2015.12.004
- Caley, M. P., Martins, V. L. C., and O'Toole, E. A. (2015). Metalloproteinases and wound healing. *Adv. Wound Care* 4, 225–234. doi: 10.1089/wound.2014.0581
- Campos, P. M. B. G. M., Ricci, G., Semprini, M., and Lopes, R. A. (1999). Histopathological, morphometric, and stereologic studies of dermocosmetic

- skin formulations containing vitamin a and/or glycolic acid. *J. Cosmet. Sci.* 50, 159–70.
- Carswell, L., and Borger, J. (2019). Hypertrophic scarring keloids. *StatPearls*.
- Chen, M., Patra, P. K., Lovett, M. L., Kaplan, D. L., and Bhowmick, S. (2009). Role of electrospun fibre diameter and corresponding specific surface area (SSA) on cell attachment. *J. Tissue Eng. Regen. Med.* 3, 269–279. doi: 10.1002/term.163
- Cheng, G., Yin, C., Tu, H., Jiang, S., Wang, Q., Zhou, X., et al. (2019). Controlled co-delivery of growth factors through layer-by-layer assembly of core-shell nanofibers for improving bone regeneration. *ACS Nano* 13, 6372–6382. doi: 10.1021/acsnano.8b06032
- Chua, K.-N., Chai, C., Lee, P.-C., Tang, Y.-N., Ramakrishna, S., Leong, K. W., et al. (2006). Surface-aminated electrospun nanofibers enhance adhesion and expansion of human umbilical cord blood hematopoietic stem/progenitor cells. *Biomaterials* 27, 6043–6051. doi: 10.1016/j.biomaterials.2006.06.017
- Cole, G., Ali, A. A., McErlean, E., Mulholland, E. J., Short, A., McCrudden, C. M., et al. (2019). DNA vaccination via RALA nanoparticles in a microneedle delivery system induces a potent immune response against the endogenous prostate cancer stem cell antigen. *Acta Biomater.* 96, 480–490. doi: 10.1016/j.actbio.2019.07.003
- Commander, S., Chamata, E., Cox, J., Dickey, R., and Lee, E. (2016). Update on postsurgical scar management. *Semin. Plast. Surg.* 30, 122–128. doi: 10.1055/s-0036-1584824
- Corcione, A., Benvenuto, F., Ferretti, E., Giunti, D., Cappiello, V., Cazzanti, F., et al. (2006). Human mesenchymal stem cells modulate B-cell functions. *Blood* 107, 367–372. doi: 10.1182/blood-2005-07-2657
- Corr, D. T., Gallant-Behm, C. L., Shrive, N. G., and Hart, D. A. (2009). Biomechanical behavior of scar tissue and uninjured skin in a porcine model. *Wound Repair Regen.* 17, 250–259. doi: 10.1111/j.1524-475X.2009.00463.x
- Cui, W., Li, X., Zhou, S., and Weng, J. (2007). Investigation on process parameters of electrospinning system through orthogonal experimental design. *J. Appl. Polym. Sci.* 103, 3105–3112. doi: 10.1002/app.25464
- Darby, I. A., Laverdet, B., Bonté, F., and Desmoulière, A. (2014). Fibroblasts and myofibroblasts in wound healing. *Clin. Cosmet. Investig. Dermatol.* 7, 301–311. doi: 10.2147/CCID.S50046
- Deng, A., Yang, Y., Du, S., and Yang, S. (2018). Electrospinning of *in situ* crosslinked recombinant human collagen peptide/chitosan nanofibers for wound healing. *Biomater. Sci.* 6, 2197–2208. doi: 10.1039/C8BM00492G
- Desmoulière, A., Chaponnier, C., and Gabbiani, G. (2005). Tissue repair, contraction, and the myofibroblast. *Wound Repair Regen.* 13, 7–12. doi: 10.1111/j.1067-1927.2005.130102.x
- Dunn, L., Prosser, H. C. G., Tan, J. T. M., Vanags, L. Z., Ng, M. K. C., Bursill, C. A. (2013). Murine Model of Wound Healing. *J. Vis. Exp.* e50265. doi: 10.3791/50265
- Ehrlich, H. P., Desmoulière, A., Diegelmann, R. F., Cohen, I. K., Compton, C. C., Garner, W. L., et al. (1994). Morphological and immunochemical differences between keloid and hypertrophic scar. *Am. J. Pathol.* 145, 105–113.
- Fang, R. C., and Galiano, R. D. (2008). A review of becaplermin gel in the treatment of diabetic neuropathic foot ulcers. *Biologics* 2, 1–12. doi: 10.2147/BTT.S1338
- Field, C. K., and Kerstein, M. D. (1994). Overview of wound healing in a moist environment. *Am. J. Surg.* 167, S2–S6. doi: 10.1016/0002-9610(94)90002-7
- Fu, X.-B., Sun, T.-Z., Li, X.-K., and Sheng, Z.-Y. (2005). Morphological and distribution characteristics of sweat glands in hypertrophic scar and their possible effects on sweat gland regeneration. *Chin. Med. J.* 118, 186–191.
- Gao, W., Jin, W., Li, Y., Wan, L., Wang, C., Lin, C., et al. (2017). A highly bioactive bone extracellular matrix-biomimetic nanofibrous system with rapid angiogenesis promotes diabetic wound healing. *J. Mater. Chem. B* 5, 7285–7296. doi: 10.1039/C7TB01484H
- Gassner, H. G., Sherris, D. A., and Otley, C. C. (2000). Treatment of facial wounds with botulinum toxin A improves cosmetic outcome in primates. *Plast. Reconstr. Surg.* 105, 1948–1953. doi: 10.1097/00006534-200005000-00005
- Geng, X., Kwon, O., and Jang, J. (2005). Electrospinning of chitosan dissolved in concentrated acetic acid solution. *Biomaterials* 26, 5427–5432. doi: 10.1016/j.biomaterials.2005.01.066
- Ghosh, P., Han, G., De, M., Kim, C. K., and Rotello, V. M. (2008). Gold nanoparticles in delivery applications. *Adv. Drug Deliv. Rev.* 60, 1307–1315. doi: 10.1016/j.addr.2008.03.016
- Goker, F., Larsson, L., Del Fabbro, M., and Asa'ad, F. (2019). Gene delivery therapeutics in the treatment of periodontitis and peri-implantitis: a state of the art review. *Int. J. Mol. Sci.* 20:3551. doi: 10.3390/ijms20143551
- Golecki, H. M., Yuan, H., Glavin, C., Potter, B., Badrossamay, M. R., Goss, J. A., et al. (2014). Effect of solvent evaporation on fiber morphology in rotary jet spinning. *Langmuir* 30, 13369–13374. doi: 10.1021/la5023104
- Grove, G. L., and Kligman, A. M. (1983). Age-associated changes in human epidermal cell renewal. *J. Gerontol.* 38, 137–142. doi: 10.1093/geronj/38.2.137
- Gu, X., Cao, R., Li, Y., Liu, S., Wang, Z., Feng, S., et al. (2019). Three-component antibacterial membrane of poly(butylene carbonate), poly(lactic acid) and chitosan prepared by electrospinning. *Mater. Technol.* 34, 463–470. doi: 10.1080/10667857.2019.1576822
- Hadjizadeh, A., Ghasemkhan, F., and Ghasemzaie, N. (2017). Polymeric scaffold based gene delivery strategies to improve angiogenesis in tissue engineering: a review. *Polym. Rev.* 57, 505–556. doi: 10.1080/15583724.2017.1292402
- Haider, A., Haider, S., and Kang, I.-K. (2015). A comprehensive review summarizing the effect of electrospinning parameters and potential applications of nanofibers in biomedical and biotechnology. *Arab. J. Chem.* 11, 1165–1188. doi: 10.1016/j.arabjc.2015.11.015
- Hajiali, H., Summa, M., Russo, D., Armirotti, A., Brunetti, V., Bertorelli, R., et al. (2016). Alginate-lavender nanofibers with antibacterial and anti-inflammatory activity to effectively promote burn healing. *J. Mater. Chem. B* 4, 1686–1695. doi: 10.1039/C5TB02174J
- He, C.-L., Huang, Z.-M., and Han, X.-J. (2009). Fabrication of drug-loaded electrospun aligned fibrous threads for suture applications. *J. Biomed. Mater. Res. Part A* 89A, 80–95. doi: 10.1002/jbm.a.32004
- He, S., Xia, T., Wang, H., Wei, L., Luo, X., and Li, X. (2012). Multiple release of polyplexes of plasmids VEGF and bFGF from electrospun fibrous scaffolds towards regeneration of mature blood vessels. *Acta Biomater.* 8, 2659–2669. doi: 10.1016/j.actbio.2012.03.044
- He, W., Ma, Z., Yong, T., Teo, W. E., and Ramakrishna, S. (2005). Fabrication of collagen-coated biodegradable polymer nanofiber mesh and its potential for endothelial cells growth. *Biomaterials* 26, 7606–7615. doi: 10.1016/j.biomaterials.2005.05.049
- Hsieh, J. Y., Smith, T. D., Meli, V. S., Tran, T. N., Botvinick, E. L., and Liu, W. F. (2017). Differential regulation of macrophage inflammatory activation by fibrin and fibrinogen. *Acta Biomater.* 47, 14–24. doi: 10.1016/j.actbio.2016.09.024
- Hu, M. S., Cheng, J., Borrelli, M. R., Leavitt, T., Walmsley, G. G., Zielins, E. R., et al. (2018). An improved humanized mouse model for excisional wound healing using double transgenic mice. *Adv. Wound Care* 7, 11–17. doi: 10.1089/wound.2017.0772
- Ignatova, M., Starbova, K., Markova, N., Manolova, N., and Rashkov, I. (2006). Electrospun nano-fibre mats with antibacterial properties from quaternised chitosan and poly(vinyl alcohol). *Carbohydr. Res.* 341, 2098–2107. doi: 10.1016/j.carres.2006.05.006
- Im, J. S., Yun, J., Lim, Y.-M., Kim, H.-I., and Lee, Y.-S. (2010). Fluorination of electrospun hydrogel fibers for a controlled release drug delivery system. *Acta Biomater.* 6, 102–109. doi: 10.1016/j.actbio.2009.06.017
- Jackson, B. A., and Shelton, A. J. (1999). Pilot study evaluating topical onion extract as treatment for postsurgical scars. *Dermatol. Surg.* 25, 267–269. doi: 10.1046/j.1524-4725.1999.08240.x
- Jackson, W. M., Nesti, L. J., and Tuan, R. S. (2012). Mesenchymal stem cell therapy for attenuation of scar formation during wound healing. *Stem Cell Res. Ther.* 3:20. doi: 10.1186/scrt111
- Jeong, K.-J., Song, Y., Shin, H.-R., Kim, J. E., Kim, J., Sun, F., et al. (2017). *In vivo* study on the biocompatibility of chitosan-hydroxyapatite film depending on degree of deacetylation. *J. Biomed. Mater. Res. Part A* 105, 1637–1645. doi: 10.1002/jbm.a.35993
- Jiang, H., Wang, L., and Zhu, K. (2014). Coaxial electrospinning for encapsulation and controlled release of fragile water-soluble bioactive agents. *J. Control Release* 193, 296–303. doi: 10.1016/j.jconrel.2014.04.025
- Ju, H. W., Lee, O. J., Lee, J. M., Moon, B. M., Park, H. J., Park, Y. R., et al. (2016). Wound healing effect of electrospun silk fibroin nanomatrix in burn-model. *Int. J. Biol. Macromol.* 85, 29–39. doi: 10.1016/j.ijbiomac.2015.12.055
- Karami, Z., Rezaeian, I., Zahedi, P., and Abdollahi, M. (2013). Preparation and performance evaluations of electrospun poly(ϵ -caprolactone), poly(lactic acid), and their hybrid (50/50) nanofibrous mats containing thymol as an

- herbal drug for effective wound healing. *J. Appl. Polym. Sci.* 129, 756–766. doi: 10.1002/app.38683
- Kean, T., and Thanou, M. (2010). Biodegradation, biodistribution and toxicity of chitosan. *Adv. Drug Deliv. Rev.* 62, 3–11. doi: 10.1016/j.addr.2009.09.004
- Kiani, M. T., Higgins, C. A., and Almqvist, B. D. (2018). The Hair follicle: an underutilized source of cells and materials for regenerative medicine. *ACS Biomater. Sci. Eng.* 4, 1193–1207. doi: 10.1021/acsbomaterials.7b00072
- Koh, H. S., Yong, T., Chan, C. K., and Ramakrishna, S. (2008). Enhancement of neurite outgrowth using nano-structured scaffolds coupled with laminin. *Biomaterials* 29, 3574–3582. doi: 10.1016/j.biomaterials.2008.05.014
- Kordestani, S. S. (2019). “Wound care management,” in *Atlas of Wound Healing* (Elsevier), 31–47. Available online at: <https://linkinghub.elsevier.com/retrieve/pii/B9780323679688000057>
- Krafts, K. P. (2010). Tissue repair: the hidden drama. *Organogenesis* 6, 225–233. doi: 10.14161/org.6.4.12555
- Kryczka, J., and Boncela, J. (2015). Leukocytes: the double-edged sword in fibrosis. *Mediators Inflamm.* 2015, 1–10. doi: 10.1155/2015/652035
- Lagaron, J. M., Solouk, A., Castro, S., and Echegoyen, Y. (2017). “Biomedical applications of electrospinning, innovations, and products,” in *Electrospun Materials for Tissue Engineering and Biomedical Applications*, eds T. Uyar and E. Kny (Elsevier; Woodhead Publishing), 57–72. doi: 10.1016/B978-0-08-101022-8.00010-7
- Li, B., and Wang, J. H.-C. (2011). Fibroblasts and myofibroblasts in wound healing: force generation and measurement. *J. Tissue Viability* 20, 108–120. doi: 10.1016/j.jtv.2009.11.004
- Li, Z., Wang, H., Yang, B., Sun, Y., and Huo, R. (2015). Three-dimensional graphene foams loaded with bone marrow derived mesenchymal stem cells promote skin wound healing with reduced scarring. *Mater. Sci. Eng. C* 57, 181–188. doi: 10.1016/j.msec.2015.07.062
- Liao, Y., Zhang, L., Gao, Y., Zhu, Z.-T., and Fong, H. (2009). Preparation, characterization, and encapsulation/release studies of a composite nanofiber mat electrospun from an emulsion containing poly (lactic-co-glycolic acid). *Polymer* 49, 5294–5299. doi: 10.1016/j.polymer.2008.09.045
- Lim, X., Tateya, I., Tateya, T., Muñoz-Del-Río, A., and Bless, D. M. (2006). Immediate inflammatory response and scar formation in wounded vocal folds. *Ann. Otol. Rhinol. Laryngol.* 115, 21–29. doi: 10.1177/000348940611501212
- Longaker, M. T., Gurtner, G. C., Werner, S., and Barrandon, Y. (2008). Wound repair and regeneration. *Nature* 453, 314–321. doi: 10.1038/nature07039
- Ma, K., Liao, S., He, L., Lu, J., Ramakrishna, S., and Chan, C. K. (2011). Effects of nanofiber/stem cell composite on wound healing in acute full-thickness skin wounds. *Tissue Eng. Part A* 17, 1413–1424. doi: 10.1089/ten.tea.2010.0373
- Ma, L., Yang, G., Wang, N., Zhang, P., Guo, F., Meng, J., et al. (2015). Trap effect of three-dimensional fibers network for high efficient cancer-cell capture. *Adv. Healthc. Mater.* 4, 838–843. doi: 10.1002/adhm.201400650
- Machula, H., Ensley, B., and Kellar, R. (2014). Electrospun tropoelastin for delivery of therapeutic adipose-derived stem cells to full-thickness dermal wounds. *Adv. Wound Care* 3, 367–375. doi: 10.1089/wound.2013.0513
- Mackool, R. J., Gittes, G. K., and Longaker, M. T. (1998). Scarless healing. The fetal wound. *Clin. Plast. Surg.* 25, 357–365.
- Mahjour, S. B., Fu, X., Yang, X., Fong, J., Sefat, F., and Wang, H. (2015). Rapid creation of skin substitutes from human skin cells and biomimetic nanofibers for acute full-thickness wound repair. *Burns* 41, 1764–1774. doi: 10.1016/j.burns.2015.06.011
- Marshall, C. D., Hu, M. S., Leavitt, T., Barnes, L. A., Lorenz, H. P., and Longaker, M. T. (2018). Cutaneous scarring: basic science, current treatments, and future directions. *Adv. Wound Care* 7, 29–45. doi: 10.1089/wound.2016.0696
- Martinello, T., Gomiero, C., Perazzi, A., Iacopetti, I., Gemignani, F., DeBenedictis, G. M., et al. (2018). Allogeneic mesenchymal stem cells improve the wound healing process of sheep skin. *BMC Vet. Res.* 14:202. doi: 10.1186/s12917-018-1527-8
- Mashhadi, S. A., and Loh, C. Y. Y. (2011). A knotless method of securing the subcuticular suture. *Aesthetic Surg. J.* 31, 594–595. doi: 10.1177/1090820X11411080
- McCarthy, H. O., McCaffrey, J., McCrudden, C. M., Zholobenko, A., Ali, A. A., McBride, J. W., et al. (2014). Development and characterization of self-assembling nanoparticles using a bio-inspired amphipathic peptide for gene delivery. *J. Control Release* 189, 141–149. doi: 10.1016/j.jconrel.2014.06.048
- Mengistu Lemma, S., Bossard, F., and Rinaudo, M. (2016). Preparation of pure and stable chitosan nanofibers by electrospinning in the presence of poly(ethylene oxide). *Int. J. Mol. Sci.* 17:1790. doi: 10.3390/ijms17111790
- Mingozzi, F., and High, K. A. (2013). Immune responses to AAV vectors: overcoming barriers to successful gene therapy. *Blood* 122, 23–36. doi: 10.1182/blood-2013-01-306647
- Mirastschijski, U., Sander, J. T., Zier, U., Rennekampff, H. O., Weyand, B., and Vogt, P. M. (2015). The cost of post-burn scarring. *Ann. Burns Fire Disasters* 28, 215–222.
- Monaco, J. L., and Lawrence, W. T. (2003). Acute wound healing an overview. *Clin. Plast. Surg.* 30, 1–12. doi: 10.1016/S0094-1298(02)00070-6
- Montagna, W., and Yun, J. S. (1964). The skin of the domestic pig. *J. Invest. Dermatol.* 42, 11–21. doi: 10.1038/jid.1964.110
- Mulholland, E. J., Ali, A., Robson, T., Dunne, N. J., and McCarthy, H. O. (2019). Delivery of RALA/siFKBP nanofibers via electrospun bilayer nanofibers: an innovative angiogenic therapy for wound repair. *J. Control Release* 316, 53–65. doi: 10.1016/j.jconrel.2019.10.050
- Nie, H., He, A., Zheng, J., Xu, S., Li, J., and Han, C. C. (2008). Effects of chain conformation and entanglement on the electrospinning of pure alginate. *Biomacromolecules* 9, 1362–1365. doi: 10.1021/bm701349j
- Olden, B. R., Cheng, Y., Yu, J. L., and Pun, S. H. (2018). Cationic polymers for non-viral gene delivery to human T cells. *J. Control Release* 282, 140–147. doi: 10.1016/j.jconrel.2018.02.043
- Orbay, H., Tobita, M., and Mizuno, H. (2012). Mesenchymal stem cells isolated from adipose and other tissues: basic biological properties and clinical applications. *Stem Cells Int.* 2012:461718. doi: 10.1155/2012/461718
- Park, K., Ju, Y. M., Son, J. S., Ahn, K.-D., and Han, D. K. (2007). Surface modification of biodegradable electrospun nanofiber scaffolds and their interaction with fibroblasts. *J. Biomater. Sci. Polym. Ed.* 18, 369–382. doi: 10.1163/156856207780424997
- Persano, L., Camposeo, A., Tekmen, C., and Pisignano, D. (2013). Industrial upscaling of electrospinning and applications of polymer nanofibers: a review. *Macromol. Mater. Eng.* 298, 504–520. doi: 10.1002/mame.201200290
- Prabhakaran, M. P., Venugopal, J., Chan, C. K., and Ramakrishna, S. (2008). Surface modified electrospun nanofibrous scaffolds for nerve tissue engineering. *Nanotechnology* 19:455102. doi: 10.1088/0957-4484/19/45/455102
- Qin, Y. (2016). (Ed.). “Functional wound dressings,” in *Woodhead Publishing Series in Textiles, Medical Textile Materials* (Elsevier; Woodhead Publishing), 89–107. doi: 10.1016/B978-0-08-100618-4.00007-8
- Quinn, J. A., Yang, Y., Buffington, A. N., Romero, F. N., and Green, M. D. (2018). Preparation and characterization of crosslinked electrospun poly(vinyl alcohol) nanofibrous membranes. *Polymer* 134, 275–281. doi: 10.1016/j.polymer.2017.11.023
- Ramachandran, K., and Gouma, P.-I. (2008). Electrospinning for bone tissue engineering. *Recent Pat. Nanotechnol.* 2, 1–7. doi: 10.2174/187221008783478608
- Ramakrishna, S., Fujihira, K., Teo, W.-E., Yong, T., Ma, Z., and Ramaseshan, R. (2006). Electrospun nanofibers: solving global issues. *Mater. Today* 9, 40–50. doi: 10.1016/S1369-7021(06)71389-X
- Ramirez, H., Patel, S. B., and Pastar, I. (2014). The role of TGF β signaling in wound epithelialization. *Adv. Wound Care* 3, 482–491. doi: 10.1089/wound.2013.0466
- Ramotowski, C., Qu, X., and Villa-Diaz, L. G. (2019). Progress in the use of induced pluripotent stem cell-derived neural cells for traumatic spinal cord injuries in animal populations: meta-analysis and review. *Stem Cells Transl. Med.* 8, 681–693. doi: 10.1002/sctm.18-0225
- Redd, M. J., Cooper, L., Wood, W., Stramer, B., and Martin, P. (2004). Wound healing and inflammation: embryos reveal the way to perfect repair. *Philos. Trans. R. Soc. Lond. B Biol. Sci.* 359, 777–784. doi: 10.1098/rstb.2004.1466
- REGGRANEX® (2018). REGGRANEX® (Becaplermin) Gel for Topical Use. Highlights of Prescribing Information.
- Reiber, G. E., Vileikyte, L., Boyko, E. J., del Aguila, M., Smith, D. G., Lavery, L. A., et al. (1999). Causal pathways for incident lower-extremity ulcers in patients with diabetes from two settings. *Diabetes Care* 22, 157–162. doi: 10.2337/diacare.22.1.157
- Ren, G., Zhang, L., Zhao, X., Xu, G., Zhang, Y., Roberts, A. I., et al. (2008). Mesenchymal stem cell-mediated immunosuppression occurs via concerted action of chemokines and nitric oxide. *Cell Stem Cell* 2, 141–150. doi: 10.1016/j.stem.2007.11.014

- Sá, O., Lopes, N., Alves, M., and Caran, E. (2018). Effects of glycine on collagen, PDGF, and EGF expression in model of oral mucositis. *Nutrients* 10:1485. doi: 10.3390/nu10101485
- Sarrazay, V., Billet, F., Micallef, L., Coulomb, B., and Desmoulière, A. (2011). Mechanisms of pathological scarring: role of myofibroblasts and current developments. *Wound Repair Regen.* 19(Suppl. 1), s10–s15. doi: 10.1111/j.1524-475X.2011.00708.x
- Schilling, J. A. (1976). Wound healing. *Surg. Clin. North Am.* 56, 859–874. doi: 10.1016/S0039-6109(16)40983-7
- Seaton, M., Hocking, A., and Gibran, N. S. (2015). Porcine models of cutaneous wound healing. *ILAR J.* 56, 127–138. doi: 10.1093/ilar/ilv016
- Sencadas, V., Ribeiro, C., Nunes-Pereira, J., Correia, V., and Lanceros-Méndez, S. (2012). Fiber average size and distribution dependence on the electrospinning parameters of poly(vinylidene fluoride–trifluoroethylene) membranes for biomedical applications. *Appl. Phys. A* 109, 685–691. doi: 10.1007/s00339-012-7101-5
- Sequeira, R. S., Miguel, S. P., Cabral, C. S. D., Moreira, A. F., Ferreira, P., and Correia, I. J. (2019). Development of a Poly(vinyl alcohol)/Lysine electrospun membrane-based drug delivery system for improved skin regeneration. *Int. J. Pharm.* 570:118640. doi: 10.1016/j.ijpharm.2019.118640
- Shalumon, K. T., Anulekha, K. H., Nair, S. V., Nair, S. V., Chennazhi, K. P., and Jayakumar, R. (2011). Sodium alginate/poly(vinyl alcohol)/nano ZnO composite nanofibers for antibacterial wound dressings. *Int. J. Biol. Macromol.* 49, 247–254. doi: 10.1016/j.ijbiomac.2011.04.005
- Shan, Y.-H., Peng, L.-H., Liu, X., Chen, X., Xiong, J., and Gao, J.-Q. (2015). Silk fibroin/gelatin electrospun nanofibrous dressing functionalized with astragaloside IV induces healing and anti-scar effects on burn wound. *Int. J. Pharm.* 479, 291–301. doi: 10.1016/j.ijpharm.2014.12.067
- Shete, A. S., Yadav, A. V., and Murthy, S. M. (2012). Chitosan and chitosan chlorhydrate based various approaches for enhancement of dissolution rate of carvedilol. *Daru* 20:93. doi: 10.1186/2008-2231-20-93
- Singer, A. J., and Clark, R. A. F. (1999). Cutaneous wound healing. *N. Engl. J. Med.* 341, 738–746. doi: 10.1056/NEJM199909023411006
- Sotiropoulou, P. A., Perez, S. A., Gritzapis, A. D., Baxevanis, C. N., and Papamichail, M. (2006). Interactions between human mesenchymal stem cells and natural killer cells. *Stem Cells* 24, 74–85. doi: 10.1634/stemcells.2004-0359
- Storch, J. E., and Rice, J. (eds.). (2005). *Reconstructive Plastic Surgical Nursing*. Oxford: Blackwell Publishing Ltd. doi: 10.1002/9780470774656
- Tanaka, A., Hatoko, M., Tada, H., Iioka, H., Niitsuma, K., and Miyagawa, S. (2004). Expression of p53 family in scars. *J. Dermatol. Sci.* 34, 17–24. doi: 10.1016/j.jdermsci.2003.09.005
- Tarun, K., and Gobi, N. (2012). Calcium alginate/PVA blended nano fibre matrix for wound dressing. *Indian J. Fibre Text Res.* 37, 127–132.
- Thomas, J. R., and Somenek, M. (2012). Scar revision review. *Arch. Facial Plast. Surg.* 14:162. doi: 10.1001/archfacial.2012.223
- van Zuijlen, P. P. M., Ruurda, J. J. B., van Veen, H. A., van Marle, J., van Trier, A. J. M., Groenevelt, F., et al. (2003). Collagen morphology in human skin and scar tissue: no adaptations in response to mechanical loading at joints. *Burns* 29, 423–431. doi: 10.1016/S0305-4179(03)00052-4
- Venkat, P., Shen, Y., Chopp, M., and Chen, J. (2018). Cell-based and pharmacological neurorestorative therapies for ischemic stroke. *Neuropharmacology* 134, 310–322. doi: 10.1016/j.neuropharm.2017.08.036
- Wakuda, Y., Nishimoto, S., Suye, S., and Fujita, S. (2018). Native collagen hydrogel nanofibers with anisotropic structure using core-shell electrospinning. *Sci. Rep.* 8:6248. doi: 10.1038/s41598-018-24700-9
- Wang, L., Yang, J., Ran, B., Yang, X., Zheng, W., Long, Y., et al. (2017). Small molecular TGF- β 1-inhibitor-loaded electrospun fibrous scaffolds for preventing hypertrophic scars. *ACS Appl. Mater. Interfaces* 9, 32545–32553. doi: 10.1021/acsami.7b09796
- Wang, M., Xiao, Y., Lin, L., Zhu, X., Du, L., and Shi, X. (2018). A microfluidic chip integrated with hyaluronic acid-functionalized electrospun chitosan nanofibers for specific capture and nondestructive release of CD44-overexpressing circulating tumor cells. *Bioconjug. Chem.* 29, 1081–1090. doi: 10.1021/acs.bioconjug.7b00747
- Wang, X., Ge, J., Tredget, E. E., and Wu, Y. (2013). The mouse excisional wound splinting model, including applications for stem cell transplantation. *Nat. Protoc.* 8, 302–309. doi: 10.1038/nprot.2013.002
- Wei, Q., Xu, F., Xu, X., Geng, X., Ye, L., Zhang, A., et al. (2016). The multifunctional wound dressing with core-shell structured fibers prepared by coaxial electrospinning. *Front. Mater. Sci.* 10, 113–121. doi: 10.1007/s11706-016-0339-7
- Werner, S., and Grose, R. (2003). Regulation of wound healing by growth factors and cytokines. *Physiol. Rev.* 83, 835–870. doi: 10.1152/physrev.2003.83.3.835
- White, W., Brody, G. S., Glaser, A. A., Marangoni, R. D., Beckwith, T. G., Must, J. S., et al. (1971). Tensiometric studies of unwounded and wounded skin. *Ann. Surg.* 173, 19–25. doi: 10.1097/00000658-197101000-00003
- Williams, A. R., Suncion, V. Y., McCall, F., Guerra, D., Mather, J., Zambrano, J. P., et al. (2013). Durable scar size reduction due to allogeneic mesenchymal stem cell therapy regulates whole-chamber remodeling. *J. Am. Heart Assoc.* 2:e000140. doi: 10.1161/JAHA.113.000140
- Wu, J., and Hong, Y. (2016). Enhancing cell infiltration of electrospun fibrous scaffolds in tissue regeneration. *Bioact. Mater.* 1, 56–64. doi: 10.1016/j.bioactmat.2016.07.001
- Xie, Q., Jia, L., Xu, H., Hu, X., Wang, W., and Jia, J. (2016). Fabrication of core-shell PEL/pBMP2-PLGA electrospun scaffold for gene delivery to periodontal ligament stem cells. *Stem Cells Int.* 2016, 1–11. doi: 10.1155/2016/3385137
- Yan, D., Jones, J., Yuan, X., Xu, X., Sheng, J., Lee, J. C. M., et al. (2013). Plasma treatment of random and aligned electrospun PCL nanofibers. *J. Med. Biol. Eng.* 33, 171–178. doi: 10.5405/jmbe.1072
- Yang, X., Yang, J., Wang, L., Ran, B., Jia, Y., Zhang, L., et al. (2017). Pharmaceutical intermediate-modified gold nanoparticles: against multidrug-resistant bacteria and wound-healing application via an electrospun scaffold. *ACS Nano* 11, 5737–5745. doi: 10.1021/acsnano.7b01240
- Yang, X. H., Xiao, Y. Y., Tan, T. X., Luo, J. J., Fan, P. J., and Lei, S. R. (2016). C-jun is increased in hypertrophic scar and inhibits apoptosis in fibroblasts. *Int. J. Clin. Exp. Med.* 9, 3132–3138.
- Yang, Y., Xia, T., Chen, F., Wei, W., Liu, C., He, S., et al. (2012). Electrospun fibers with plasmid bFGF polyplex loadings promote skin wound healing in diabetic rats. *Mol. Pharm.* 9, 48–58. doi: 10.1021/mp200246b
- Younes, I., Frachet, V., Rinaudo, M., Jellouli, K., and Nasri, M. (2016). Cytotoxicity of chitosans with different acetylation degrees and molecular weights on bladder carcinoma cells. *Int. J. Biol. Macromol.* 84, 200–207. doi: 10.1016/j.ijbiomac.2015.09.031
- Yuan, T. T., DiGeorge Foushee, A. M., Johnson, M. C., Jockheck-Clark, A. R., and Stahl, J. M. (2018). Development of electrospun chitosan-polyethylene oxide/fibrinogen biocomposite for potential wound healing applications. *Nanoscale Res. Lett.* 13:88. doi: 10.1186/s11671-018-2491-8
- Zamani, M., Prabhakaran, M. P., and Ramakrishna, S. (2013). Advances in drug delivery via electrospun and electrosprayed nanomaterials. *Int. J. Nanomedicine* 8, 2997–3017. doi: 10.2147/IJN.S43575
- Zhang, N., Deng, Y., Tai, Q., Cheng, B., Zhao, L., Shen, Q., et al. (2012). Electrospun TiO₂ nanofiber-based cell capture assay for detecting circulating tumor cells from colorectal and gastric cancer patients. *Adv. Mater.* 24, 2756–2760. doi: 10.1002/adma.201200155
- Zhao, G., Bao, X., Huang, G., Xu, F., and Zhang, X. (2019). Differential effects of directional cyclic stretching on the functionalities of engineered cardiac tissues. *ACS Appl. Biol. Mater.* 2, 3508–3519. doi: 10.1021/acsbm.9b00414
- Ziade, M., Domergue, S., Batifol, D., Jreige, R., Sebbane, M., Goudot, P., et al. (2013). Use of botulinum toxin type A to improve treatment of facial wounds: a prospective randomised study. *J. Plast. Reconstr. Aesthet. Surg.* 66, 209–214. doi: 10.1016/j.bjps.2012.09.012
- Ziyadeh, N., Fife, D., Walker, A. M., Wilkinson, G. S., and Seeger, J. D. (2011). A matched cohort study of the risk of cancer in users of becaplermin. *Adv. Skin Wound Care* 24, 31–39. doi: 10.1097/01.ASW.0000392922.30229.b3

Conflict of Interest: The author declares that the research was conducted in the absence of any commercial or financial relationships that could be construed as a potential conflict of interest.

Copyright © 2020 Mulholland. This is an open-access article distributed under the terms of the Creative Commons Attribution License (CC BY). The use, distribution or reproduction in other forums is permitted, provided the original author(s) and the copyright owner(s) are credited and that the original publication in this journal is cited, in accordance with accepted academic practice. No use, distribution or reproduction is permitted which does not comply with these terms.



Targeting Tunable Physical Properties of Materials for Chronic Wound Care

Yuzhen Wang^{1,2,3,4}, Ubaldo Armato^{5,6} and Jun Wu^{6*}

¹ Research Center for Tissue Repair and Regeneration Affiliated to the Medical Innovation Research Department and 4th Medical Center, PLA General Hospital and PLA Medical College, Beijing, China, ² PLA Key Laboratory of Tissue Repair and Regenerative Medicine and Beijing Key Research Laboratory of Skin Injury, Repair and Regeneration, Beijing, China, ³ Research Unit of Trauma Care, Tissue Repair and Regeneration, Chinese Academy of Medical Sciences, 2019RU051, Beijing, China, ⁴ Department of Burn and Plastic Surgery, Air Force Hospital of PLA Central Theater Command, Datong, China, ⁵ Histology and Embryology Section, Department of Surgery, Dentistry, Pediatrics and Gynecology, University of Verona Medical School Verona, Verona, Italy, ⁶ Department of Burn and Plastic Surgery, Second People's Hospital of Shenzhen, Shenzhen University, Shenzhen, China

OPEN ACCESS

Edited by:

Monica A. Serban,
University of Montana, United States

Reviewed by:

Baolin Guo,
Xi'an Jiaotong University, China
Leila Cuttle,

Queensland University of
Technology, Australia

*Correspondence:

Jun Wu
junwupro@126.com

Specialty section:

This article was submitted to
Biomaterials,
a section of the journal
Frontiers in Bioengineering and
Biotechnology

Received: 19 February 2020

Accepted: 13 May 2020

Published: 11 June 2020

Citation:

Wang Y, Armato U and Wu J (2020)
Targeting Tunable Physical Properties
of Materials for Chronic Wound Care.
Front. Bioeng. Biotechnol. 8:584.
doi: 10.3389/fbioe.2020.00584

Chronic wounds caused by infections, diabetes, and radiation exposures are becoming a worldwide growing medical burden. Recent progress highlighted the physical signals determining stem cell fates and bacterial resistance, which holds potential to achieve a better wound regeneration *in situ*. Nanoparticles (NPs) would benefit chronic wound healing. However, the cytotoxicity of the silver NPs (AgNPs) has aroused many concerns. This review targets the tunable physical properties (i.e., mechanical-, structural-, and size-related properties) of either dermal matrixes or wound dressings for chronic wound care. Firstly, we discuss the recent discoveries about the mechanical- and structural-related regulation of stem cells. Specially, we point out the currently undocumented influence of tunable mechanical and structural properties on either the fate of each cell type or the whole wound healing process. Secondly, we highlight novel dermal matrixes based on either natural tropoelastin or synthetic elastin-like recombinamers (ELRs) for providing elastic recoil and resilience to the wounded dermis. Thirdly, we discuss the application of wound dressings in terms of size-related properties (i.e., metal NPs, lipid NPs, polymeric NPs). Moreover, we highlight the cytotoxicity of AgNPs and propose the size-, dose-, and time-dependent solutions for reducing their cytotoxicity in wound care. This review will hopefully inspire the advanced design strategies of either dermal matrixes or wound dressings and their potential therapeutic benefits for chronic wounds.

Keywords: chronic wounds, stem cells, mechanical properties, structural properties, nanotechnology

INTRODUCTION

Infections, diabetes, or radiation exposures promote chronic wounds. About 1–2% of the population in developed countries suffer from chronic wounds throughout their lifetime (Dovi et al., 2003; Satish et al., 2017). In China, the prevalence rate of chronic wounds was 1.7% among hospitalized patients based on the latest cross-sectional epidemiological survey (Jiang et al., 2011). The feet of diabetic patients usually suffer more as compared with other bodily parts because of further aggravations due to persistent bacterial infections, to sympathetic nerve dysfunctions, and

to the continuous frictions of walking (Akash et al., 2020). Approximately one diabetic patient in six suffers from chronic foot wounds (Bakker et al., 2016). Among them, each year almost one million diabetic patients have to undergo lower limb amputation (Boulton et al., 2005). With the aging of the global population, chronic wounds are becoming a worldwide growing medical burden.

Traditional therapeutic approaches to chronic wounds are unsatisfactory because patients suffer prolonged pain as well as unavoidable upshots such as scarring and physical dysfunctions. Commonly used therapeutic approaches are chemical strategies, such as drugs, growth factors, agonists, or inhibitors of critical signaling pathways. However, recent advances in the fields of stem cells and nanotechnology highlighted some knowledge-updating discoveries of physical properties (i.e., mechanical-, structural-, and size-related properties) in directing endogenous stem cell fates (Jiang et al., 2018) and fighting bacterial resistance (Bhattacharya et al., 2019), which might play major roles in chronic wound healing.

The World Health Organization reported that about 265,000 deaths occur every year caused by burns or lack of appropriate treatments including skin substitutes or wound dressings (Das et al., 2016; Khorasani et al., 2018). Generally, skin substitutes aim at replacing missing tissues with gradually degrading dermal matrixes (Ramanathan et al., 2017), while wound dressings cover wound beds acting as temporary mechanical barriers to prevent bacterial infections and to avoid the loss of water and nutrients (Kalantari et al., 2020). Herein, we respectively discuss how the mechanical and structural properties of dermal matrixes affect stem cell behavior, as well as the application of nanoparticle-based (size-related properties) wound dressings for treating infections of chronic wounds. Moreover, we also discuss some worries about mechanical- and structure-related regulation of stem cells. We also address current biosafety concerns about nanoparticles (NPs) and examine workable solutions to reduce their cytotoxicity.

CHRONIC WOUND HEALING

Endogenous Stem Cells

Concerning acute wounds, healing processes are singled out in stages such as hemostasis, inflammation, novel tissue generation, and remodeling, which successively appear and overlap one after the other. Endogenous stem cells (i.e., endothelial progenitor cells, epidermal stem cells, etc.) can both undergo self-renewal and differentiate into one or multiple lineages to repair tissue losses (Kanji and Das, 2017). However, infection, diabetes or radiation exposure may disrupt the well-orchestrated stem cell behaviors and result in chronic wounds (Figure 1). Even worse, continuing pathological risks (i.e., bacterial infection, high blood glucose levels, local continuous pressure or friction, etc.)

hinder the healing of wounds, which become chronic when they did not show any sign of improved healing after 30 days (Kim et al., 2018).

Endogenous endothelial progenitor cells, which are either resident in wound environments or originate from bone marrow, can promote wound healing via angiogenesis (Kanji and Das, 2017). Angiogenesis involves the sequential occurrence and overlap of various stages, i.e. the activation of endothelial cells, the degradation of the endothelial cells' basement membranes, and the sprouting and ripening of newly-formed vascular structures (Huang et al., 2019). Various alterations of oxygen, nutrients, metabolites' levels, and inflammatory events easily impact on the whole angiogenic process. For example, diabetic wounds easily suffer from hypoxia (or reduced oxygen supply) due to inadequate angiogenesis and a concurring vascular dysfunction and neuropathy. Even more worrying, diabetic wounds usually exhibit higher oxygen consumption rates causing a further lessening of available oxygen *in situ* (Hopf and Rollins, 2007). Concurrently, an inadequate angiogenesis due to an impaired function of endogenous endothelial progenitor cells restricts the proliferation of fibroblasts and their collagen deposition by affecting the hydroxylation of proline and lysine residues, which impacts on scarring's outcomes (Figure 1; Desmet et al., 2018).

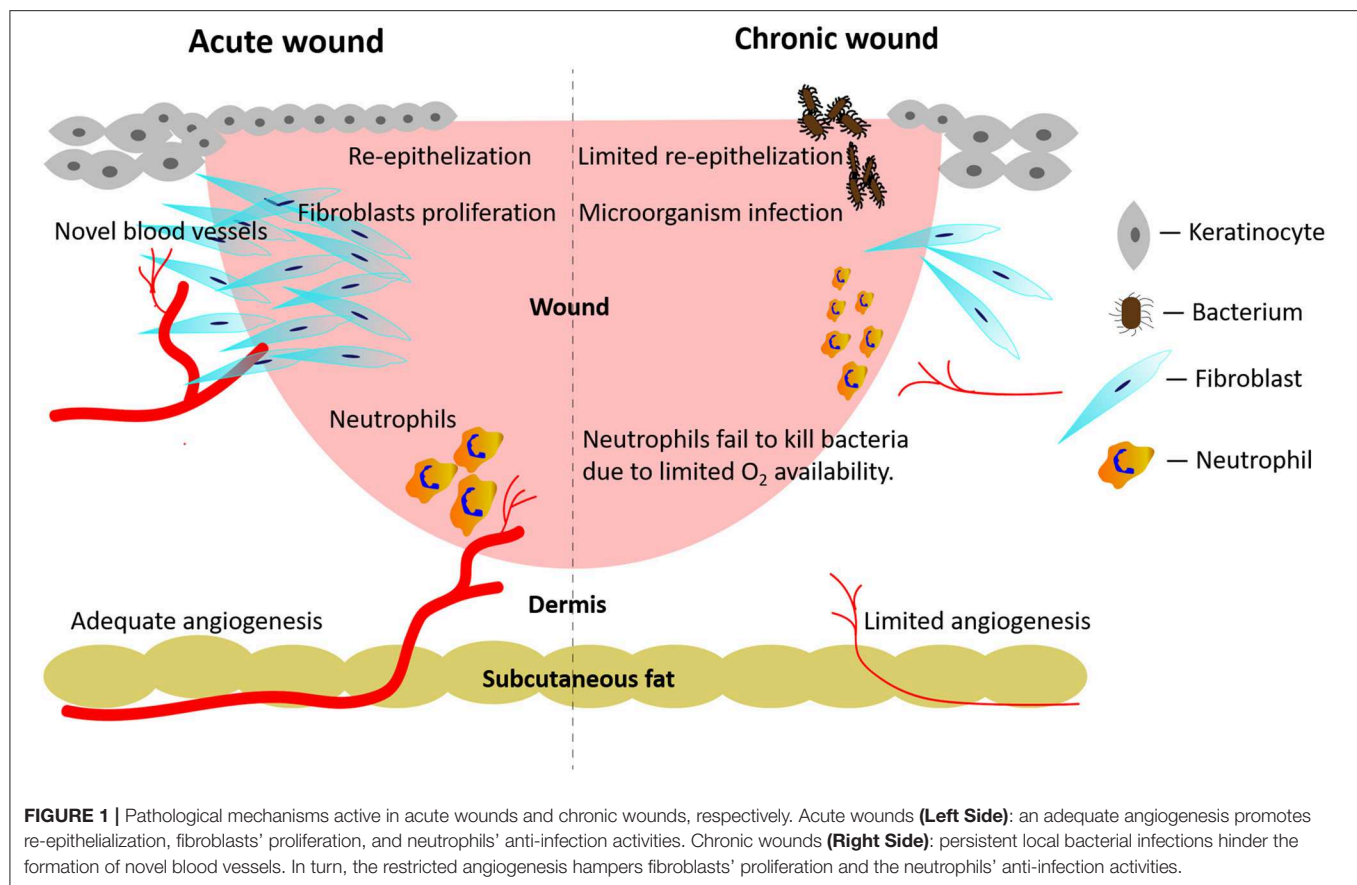
Endogenous epidermal stem cells with different lineages inhabit the basal layers, interfollicular epidermis, sebaceous glands, eccrine sweat ducts, or hair follicles bulges. During wound healing processes, epidermal stem cells are capable of differentiating into multiple lineages and of repopulating other epidermal components (Haensel et al., 2020). In chronic wounds, most epidermal stem cells show a blunted self-renewal or have been destroyed together with the missing deep tissue. In this case, re-epithelialization typically occurs from the peripheral edges of chronic wounds, being mediated by the recruitment of mobilized stem cells from wound-adjacent stem cell sources (Vagnozzi et al., 2015). Therefore, regulating endogenous stem cells behaviors plays a vital role in chronic wound care.

Infection

Persistent infections help bring about chronic wounds, which are all susceptible to a contaminating localization of microorganisms. The proliferation coupled with toxins release of the localized microorganisms causes inflammatory reactions in the host. Microorganisms can form polymicrobial biofilms, which are one of the mechanisms underlying antibiotic resistance. If left untreated, the infected wounds do not heal (Figure 1).

The infecting organisms, most often bacteria, can easily attach to the wound bed and enter into the blood system because the skin barrier is no longer present. *Staphylococcus*, a genus of Gram-positive bacteria which includes more than 40 species, is the most common type of infectious agent found in burn wounds (Dhanalakshmi et al., 2016). The methicillin-resistant *Staphylococcus aureus* (MRSA) is the most common antibiotic-resistant microorganism responsible for hospital-acquired infections (Dantes et al., 2013). Other bacteria genres found in wounds environment are *Pseudomonas aeruginosa*, *Klebsiella pneumoniae*, *Proteus mirabilis*, *Streptococcus faecalis*,

Abbreviations: AgNPs, silver nanoparticles; ARID1A, AT-rich interactive-domain 1A; ELRs, elastin-like recombinamers; MRSA, methicillin-resistant *Staphylococcus aureus*; MSCs, mesenchymal stem cells; NPs, nanoparticles; PLGA, poly(lactic-co-glycolic acid); ROS, reactive oxygen species; SWI/SNF, switch/sucrose non-fermenting; TAZ, transcriptional co-activator with PDZ-binding motif; YAP, yes-associated protein.



and others more. Besides, an alteration of intestinal flora might cause the gut bacteria to trespass into circulating blood; this has become a current research hotspot and has attracted a lot of attention (He et al., 2019).

In chronic wounds, inadequate angiogenesis due to functionally impaired endogenous endothelial progenitor cells might further reduce the innate anti-infection capabilities. When wounds have become infected, the phagocytosis of the involved pathogens by leukocytes will trigger the respiratory burst process resulting in the release of massive amounts of bactericidal reactive oxygen species (ROS). Reportedly, the respiratory burst process consumes about 98% of the oxygen in neutrophils (Bryan et al., 2012). A lack of oxygen in chronic wounds impairs the anti-infection abilities of neutrophils (Figure 1).

Usually, diabetic patients show high blood glucose levels due to reduced autologous insulin secretion or increased insulin resistance, which result in multiple metabolic dysfunctions. Several underlying pathological factors also contribute to the delayed healing of diabetic wounds, such as local persistent bacterial infections coupled with excessive levels of pro-inflammatory cytokines, proteases, ROS (Frykberg and Banks, 2015), and with a worsening vascular dysfunction combined with the cells' inability to respond to pro-reparative stimuli (Kim et al., 2018).

MECHANICAL PROPERTIES

Mechanical properties of dermal matrixes include stiffness, elastic modulus, tensile strength, viscoelasticity, stress stiffening effects, stress-relaxation rate, and more. Recent studies about mechanical-related regulation of stem cells and elastin-based dermal matrixes highlighted the practical solutions for chronic wound care.

Mechanical-Related Regulation During Wound Healing

Clinical practice in wound healing has shown that higher tension sutures of surgical wounds increase scar tissue formation, and that the stress and stiffness of wound fixation could also affect wound healing speed and quality. However, the underlying mechanism is still unclear.

Recently, mechanical signals have increasingly shown an overarching ability to regulate stem cell characteristics and lineages. Among mechanical signals, stiffness-related control of cell fates has been studied extensively. For example, mesenchymal stem cells (MSCs) show distinctive differentiation patterns when cultured in matrixes of tunable stiffness. MSCs changed their lineage specification into neurons, myoblasts or osteoblasts when cultured in polyacrylamide hydrogels with a tunable stiffness gradient varying from 0.1 to 25 kPa (Engler et al., 2006). In

other words, MSCs “felt” matrixes stiffness and then “chose” their direction of differentiation.

Further research showed that the transcriptional co-activator with PDZ-binding motif (TAZ) and Yes-associated protein (YAP) played vital roles in the stiffness-related regulation of stem cell fates (Yang et al., 2014). YAP/TAZ are two highly related downstream readers and transcriptional regulators of mechanotransduction, serving as molecular “beacons” of cellular responses to surrounding mechanical stimuli (Brusatin et al., 2018). Reportedly, the AT-rich interactive domain-containing protein 1A (ARID1A) is located in the chromosome 1p36 region acting as a tumor suppressor gene (Guan et al., 2011). The ARID1A belongs to the switch/sucrose non-fermenting (SWI/SNF) chromatin remodeling complex, which encodes a large nuclear protein involved in chromatin remodeling (Guan et al., 2011). The full activation of YAP/TAZ activity needs to meet two requirements: i.e., both the promotion of YAP/TAZ nuclear accumulation and the inhibition of the ARID1A-containing SWI/SNF complex (Chang et al., 2018). In other words, the ARID1A-containing SWI/SNF complex works as a mechano-regulated inhibitor of YAP/TAZ. In multiple experimental organoids, YAP/TAZ activity modulates stem cells’ stemness and cell fates, which are eventually dictated by the spatio-temporal balance between material stiffness and degradability (Brusatin et al., 2018). Specifically, the stiffness-sensing YAP/TAZ is gradually inactivated due to the “contact inhibition” of cell proliferation; while this happens, the stem cells lose their stemness and choose a specific direction of differentiation. At this very moment, a suitable speed of biomaterial degradation could supply extra inner spaces for cellular proliferation thus preserving cellular stemness for organoid generation. These novel discoveries have highlighted how to spatio-temporally control stem cells differentiation through mechanically related YAP/TAZ activity and biomaterials degradation for best dermal matrixes.

As regards wound healing, experimental work uncovered an interesting “mechanical memory” effect: epithelial cells primed on stiff matrixes exhibited higher capabilities of migration and adhesion even after transfer onto a softer secondary matrixes (Nasrollahi et al., 2017). These interesting results showed that migrating cells can “remember” information from past physical environments and that these “mechanical memories” may be exploited to influence cell fates. As stem cells in chronic wounds show a slow self-renewal and remain uncommitted to differentiation, the tailored control of stem cells is believed to help wound healing.

Moreover, mechanical properties can influence scar formation. Reportedly, aberrant mechanotransduction is regarded as a driver of fibrosis (Brusatin et al., 2018). For chronic wounds, the mechanical signals might either affect extracellular matrixes remodeling through the “stiffness-sensing” capability of fibroblasts (Zhou et al., 2016) or impact the delivery of bioactive agents during the fibroblasts-to-myofibroblasts transdifferentiation, a key pathological process underlying the development of hypertrophic scars (Jiang et al., 2018).

Last but not least, the mechanical signals were also reported to regulate immune responses by influencing the behavior of human

monocyte-derived macrophages (Adlerz et al., 2016), which is related to bacterial resistance in chronic wounds.

Elastin-Based Dermal Matrixes

Due to the huge impact exerted by mechanical signals on the regulation of stem cell differentiation and of mechanotransduction in the course of wound healing, elastin-based dermal matrixes have recently emerged as means to provide elastic recoil and resilience to the wounded dermis and to prevent pathological scar retractions.

Generally, dermal elastic fibers and collagen fibers are responsible for Young’s (elastic) modulus and the tensile strength of human dermis, respectively (Wang et al., 2015). In healthy skin, elastin monomers derive from the tropoelastin precursor and are then further crosslinked into polymeric networks. The latter enable healthy skin to recover its original shape once stretched to a great extent. In wounded skin, as compared to normal, a smaller amount of elastin monomers is produced, while most of the dermal fibers are deposited in an aberrant manner, resulting in a disorderly fibrous and poorly elastic network. Although elastin accounts for only about 2–4% of the human skin dry weight (Rodriguez-Cabello et al., 2018), its significant functional role is attracting a growing attention aimed at improving dermis mechanical properties and at regulating cellular activities during wound healing.

Currently, dermal matrixes trying to mimic the natural elastic properties of human skin are based on either natural tropoelastin or synthetic elastin-like recombinamers (ELRs) (Rodriguez-Cabello et al., 2018).

Tropoelastin-Based Dermal Matrixes

Tropoelastin, which naturally exists in all vertebrates except Cyclostomes, is a 60–72 kDa protein made of 750–800 amino acid residues constituting the dominant building block of the elastic fibers that imbue tissues with elasticity and resilience. Tropoelastin is made up of alternating hydrophilic and hydrophobic domains. The latter show elastic properties while the intercalated hydrophilic lysine-rich domains act as crosslinkers. As recently reported, the established atomic structure of human tropoelastin is an extended molecular body flanked by two protruding legs (Wang et al., 2015). The lysine residues of the hydrophilic domains show a substantial variation in their locations, which might contribute to their greater accessibility and cross-linking capacities (Tarakanova et al., 2019).

The versatile and pliable potentialities of tropoelastin have attracted interest from several biomedical fields. Tropoelastin and silk fibroin were blended to produce electrospun yarns, in which the elasticity of the former is combined with the mechanical strength of the latter. The results of the subcutaneous implantation of such yarns in mice proved their good tolerance and persistence for over 8 weeks, supporting their potential application to tissue engineering (Aghaei-Ghareh-Bolagh et al., 2019). In another study, the engineered tropoelastin-polydopamine-coated tendon scaffolds promoted the tenogenic commitment of human adipose tissue-derived stem cells which remarkably synthesized and deposited elastin in the

generated elastin-rich matrixes *in vitro* (Almeida et al., 2019). Yeo et al. (2019) immobilized tropoelastin on plasma-coated polyurethane films, which significantly promoted the adhesion and proliferation of multipotent adult progenitor cells.

The first *in vivo* study focusing on the therapeutic effects of tropoelastin on full-thickness dermal wounds was recently reported by Mithieux et al. (2018). The implanted pure tropoelastin exhibited superior cell recruiting properties and significantly promoted angiogenesis, resulting in an enhanced healing of full-thickness pig skin wounds. The pure tropoelastin used for the experiments was dissolved, dried, and heated in a stepwise procedure with no addition of other chemicals. Although the regeneration included vessels, rete ridges, and a keratinizing stratified epithelium, no results were reported about the recovery of any degree of elasticity on the part of the tropoelastin-treated wounds.

Although the above discoveries highlighted the potential therapeutic values of tropoelastin as regards wound healing, we still lack *in vivo* evidences in terms of a restored elasticity of regenerated wound tissues during lengthy follow-up observations.

ELRs-Based Dermal Matrixes

ELRs are genetically engineered polypeptides having the repeated elastin sequence valine-proline-glycine-X-glycine (VPGXG), where X can be any amino acid excepting proline. The structures made of engineered ELRs are tunable and offer versatile elastic-tailored applications. Gonzalez de Torre et al. (2018) described the “clickable” properties of ELRs and used electrospinning to prepare bioactive fibers from clickable ELRs with no crosslinking agent added. In another study, Changi et al. (2018) developed thermo-sensitive ELRs which contained bioactive molecules and showed good biocompatibility and limited immunogenicity in BALB/c and C57BL/6 mouse models. Moreover, some functional sequences, such as growth factors, can be attached via chemical reactions to ELRs molecule or can be directly inserted into main sequences of ELRs through recombinant techniques (Flora et al., 2019).

To sum up, mechanical signals can regulate stem cells, scar formation, or immune responses during wound healing. Current studies have shown that both tropoelastin and ELRs exhibit a potential for chronic wound care. However, limited research has been hitherto focused on the recovered elasticity of the regenerated skin. Further experiments need to be carried out to confirm the long-term therapeutic effects of elastin- and ELRs-based dermal matrixes.

STRUCTURAL PROPERTIES

Structure-Related Regulation During Wound Healing

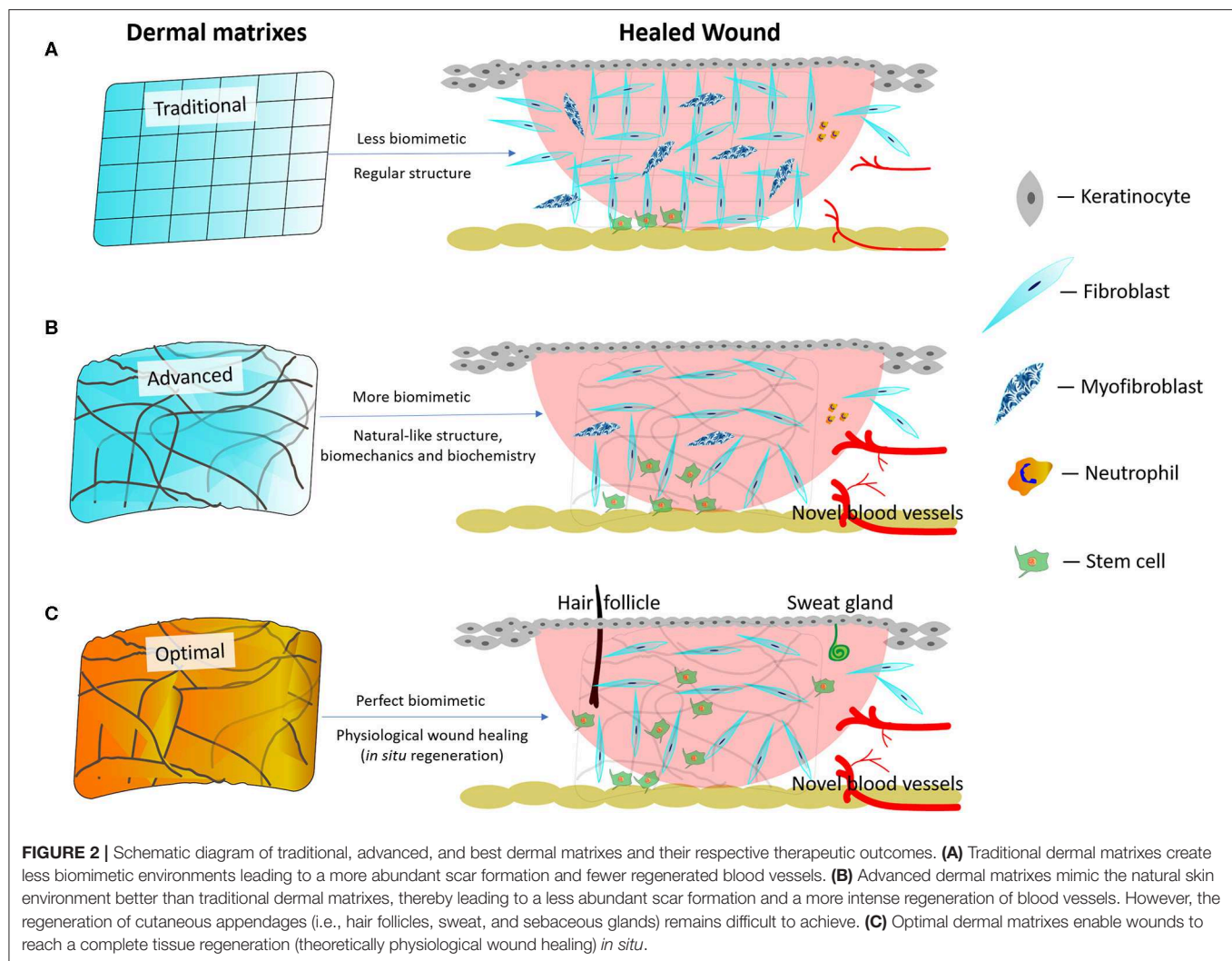
Structural properties of dermal matrixes include pore sizes, porosity, surface topology, organization of inner frames, etc. Among structural properties, pore sizes (Wang et al., 2016) and porosity (i.e. the ratio between the hollow space inside a scaffold and its overall volume; Xu et al., 2016) have been extensively studied. Dermal matrixes presently available in clinical settings

have suitable pore sizes and high degrees of inner connections to allow cell migration as well as nutrients exchange. The Wnt/ β -catenin signaling pathway was recently reported to regulate pore-size-related cell proliferation (Xu et al., 2018). The current consensus is that ideal pore sizes or porosity have yet to be ascertained for the different kinds of matrixes and seeded cells (Xu et al., 2015).

Interestingly, surface topology was found to regulate stem cells mainly via roughness and texture (Xing et al., 2019). Firstly, a rough surface can attract stem cell aggregation. In human skin, stem cells usually gather and undergo self-renewal in “niches,” i.e., the interfollicular epidermis, the basal layers, and the hair follicle bulges (Alonso and Fuchs, 2006). Likewise, stem cells tend to aggregate on rough surfaces endowed with topologically “artificial niches,” such as holes, canyons, grooves, or craters (Cooper et al., 2012). Secondly, surface textures with different shapes further direct stem cell fates. Kilian et al. (2010) patterned the mesenchymal stem cell individually on a substrate and each cell was patterned with a certain shape, i.e. rectangles or pentagonal symmetries (five-pointed star). The mesenchymal stem cells were found to display different adipogenesis and osteogenesis profiles once seeded onto different shapes. Furthermore, the mesenchymal stem cells were then patterned individually onto different rectangles with increasing aspect ratios as well as onto dissimilar pentagonal symmetries with varied subcellular curvatures. Their results showed that changing the cell shapes correspondingly changed the cell lineages. In other words, altering the shapes of stem cells can influence the cell lineages they generate. Therefore, manipulating the roughness and texture of surface topology could enable us to tailor the fate of the individual cell.

Recently, surface micropatterning methods (i.e., nanotechnology, 3D bio-printing, laser photolithography, microcontact transfer method, electron beam etching, etc.) can manipulate the microgeographic structures on matrix surfaces (Bui et al., 2018). Therefore, surface micropatterning methods hold potential to regulate the stem cell fates during wound healing via tailoring the surface topology. In a recent study, a crossed groove/column micropattern was constructed on the surface of bacterial cellulose matrix using low-energy CO₂ laser photolithography. Animal experiments indicated that this micropatterned shape guided a “basket-woven” organization of collagen distribution that may reduce scar formation (Hu et al., 2019).

Anyhow, natural skin environment acts as the blueprint for engineered dermal matrixes. Maximally mimicking the natural skin environment holds potential to achieve a scarless regeneration *in situ* (MacEwan et al., 2017). Traditional dermal matrixes create less biomimetic environments that do not help commit stem cells to differentiation. Consequently, higher numbers of fibroblasts transdifferentiate into myofibroblasts, which possibly leads to hypertrophic scars (Figure 2A; Li Y. et al., 2019). Nowadays, advanced dermal matrixes endowed with more skin-like biomimetic architectures and mechanical properties as well as with the necessary biochemical signals are believed to commit stem cells to differentiation (MacEwan et al., 2017), which further reduces scar formation while



promoting angiogenesis (**Figure 2B**). However, the regeneration of cutaneous appendages (i.e. hair follicles or sweat glands) is not yet satisfactory. Theoretically, optimal dermal matrixes should enable wounds to achieve tissue regeneration (i.e. physiological wound healing) *in situ*, which means that the healed wound has the same morpho-functional features as the natural skin, is devoid of scar tissue, and has concurrently regenerated the cutaneous appendages (i.e. hair follicles or sweat glands; **Figure 2C**). However, it is still beyond our sight what the best dermal matrixes might be and how they would regulate stem cells differentiation.

Further understanding of natural dermal structures might inspire the organization of the inner structures (e.g. random, aligned, gradient, porous, or filamentous) of dermal matrixes. Reportedly, collagen/elastin-based three-dimensional (3D) histological images indicated that the human dermis amounts to a “sandwich” structure with gradient changes in gradual terms of either interstitial spaces or architecture at different dermal depths (Wang et al., 2015). However, no solid conclusion has been hitherto reached whether dermal aligned or gradient

structures are significantly better than random or homogeneous structures. The best patterns of the inner structures of dermal matrixes are yet to be assessed for the different cell types and chemical components.

Concerns Regarding Mechanical and Structural Regulation of Cells

Although mechanical and structural properties of dermal matrixes have shown crucial effects on cell behaviors, we cannot yet reach a solid conclusion concerning one or another specific parameter and its corresponding therapeutic effects. Tunable mechanical and structural properties exert a previously undocumented influence on either the fate of each cell type or the whole wound healing process.

First, it is difficult to decouple the interplay between structural and mechanical properties. When we tune one physical property and study its therapeutic effects, inevitably other properties concurrently change. For example, when we tried to fabricate a series of scaffolds with varied stiffness gradients, the other intrinsic properties (e.g., pore size, porosity, organization of

inner structures, and elastic modulus) changed correspondingly. One study reported that mixtures with different proportions of collagen and hydroxyapatite could be coated on decellularized cancellous bone to vary its stiffness with no statistically significant after-coating changes in the scaffold architecture. Notwithstanding this, the chemical composition and related cell binding sites underwent concomitant changes (Chen et al., 2015). In another study, the cryoprotectant dimethyl-sulfoxide was used to control pore size by regulating ice crystal sizes in 3D freeze-dried porous scaffolds, while the stiffness was regulated by adjusting the degree of cross-linking (Jiang et al., 2019). Although using the above methods achieved an independent control of pore size and stiffness, the decoupling of structural and mechanical properties affecting cellular activities was far from being satisfactory due to variations in chemical inhomogeneity among scaffolds.

Second, it is difficult to observe cellular responses to a single tunable physical property due to the complex and changeable spatio-temporal microenvironments, because so many kinds of cells are involved in wound healing and each cell type is regulated by a specific set of multiple factors. For example, porosity and pore size are two correlated physical properties. On the one hand, smaller pores favor cell adhesion and immigration because of their higher surface area and ligand density. On the other hand, smaller pores are easily subject to clogging when cells grow on their inside, the upshot being a decreased porosity which further reduces permeability to oxygen and nutrients. It seems that we cannot find the “best choice” for a single specific parameter due to the great complexity of cellular microenvironments.

Third, cellular behaviors distinctly differ going from individual cell level to tissue/organ level. Micropatterning technologies (Brusatin et al., 2018) have been intensively used to study individual cell's behaviors with respect to various physical properties in two dimensions (2D). By this way the first evidences and groundbreaking discoveries were mostly gained about mechanical-related cellular responses. However, from what is known about 2D cultures, it is difficult to extrapolate the cellular behaviors in complex 3D environments. Moreover, precisely tuning physical properties of 3D matrixes faces insurmountable difficulties due to the concomitant changes in the other parameters, just as we mentioned above.

Fourth, the confusion about bulk stiffness and local stiffness also causes concerns. Bulk stiffness is usually measured via tensile/compression tests and refers to the scaffolds overall macroscopic features. However, local stiffness is usually measured via atomic force microscopy and is believed to be the only biophysical signal scaffolds-attached cells can sense and respond to. A study using atomic force microscopy indicated that the local stiffness of different sites within acellular fibrotic lungs was very inhomogeneous (Melo et al., 2014). Therefore, when attached cells are migrating through a scaffold, they will experience significantly heterogeneous degrees of local stiffness from their own perspective. There are worrying trends that many studies of cellular mechano-responsiveness only focus on bulk stiffness, yet unintentionally neglect local stiffness. Concerning dermal matrixes, it is still unclear how local stiffness and bulk

stiffness antagonistically regulate stem cell fates during wound healing.

Hopefully, many scientists have started taking heed of this problem. In order to mimic the dynamic microenvironments, a 4D programmable culture system with self-morphing capabilities was developed to regulate the controlled differentiation of neural stem cells (Miao et al., 2020). In addition, mathematical methods also help to solve these problems. Recently, a Bayesian linear regression mathematical model was used to predict the changes of topography-induced gene expression (Cutiongco et al., 2020). In another case, a mathematical model was used to assess the correlation between local and bulk stiffness, i.e., the bulk/local stiffness ratio. The results showed that the local stiffness detected by atomic force microscopy fell within the value ranges predicted via the mathematical model (Jiang et al., 2019).

SIZE-RELATED PROPERTIES

Nanotechnology has become known as an exciting wound treatment tool. Multiple kinds of macroscopic nanobiomaterials (e.g., electrospun nanofibers, nanosheets, nanoemulsions, carbon nanotubes-based, or graphene-based nanocomposites) and nano-sized biomaterials (e.g., NPs, ions, molecules, nucleic acids, functional peptides, proteins, oligosaccharides, or polysaccharides) have exhibited great potential capabilities of modulating vascularization, bacterial resistance, and inflammation during wound healing (Chakrabarti et al., 2019).

In this regard, size-related physical properties targeting chronic wound care are anti-infection outcomes contributed by NPs. Common NPs in use are metals (e.g., Ag, TiO₂, ZnO, MgF₂, CeO₂), lipid-based vesicles (e.g., liposome, exosomes), and polymers. Compared with materials of regular sizes, NPs quite differ in regard to mechanical strengths, melting points, surface areas, optical, and magnetic properties (Das and Baker, 2016).

Metal NPs

The silver NPs (AgNPs) are the most widely used metal NPs in both laboratory and clinical applications. AgNPs ranging from 1 to 100 nm in size or silver nanoclusters with an ultrasamll size (<2 nm) have shown good antimicrobial properties. Solid evidence has been provided that AgNPs can prevent and/or fight microorganism infections and significantly enhance the healing of chronic wounds (Sandri et al., 2019).

Bacterial biofilms are associated with the resistance to an extensive range of antibiotics, contributing to chronic wounds formation. Recent studies have shown that AgNPs exert promising therapeutic effects against the biofilm-forming MRSA (Zhang et al., 2018). Another study also reported the inhibiting ability of AgNPs loaded with thymol and chitosan on the biofilm formation by MRSA with a 10.08 ± 0.06 mm zone of inhibition (ZOI) and a minimum inhibitory concentration of 100 $\mu\text{g mL}^{-1}$ (Manukumar et al., 2017). The AgNPs killing efficacy on biofilms of *Vibrio* species, another group of clinically multi-drug resistant bacteria, was also verified (Satish et al., 2017). Moreover, clinical data further confirmed the effectiveness of AgNPs against biofilm-forming bacteria. Thomas et al. (2014) isolated from clinical samples a series of multidrug-resistant biofilm-forming

coagulase-negative staphylococci, e.g. *S. epidermidis* strains, *S. aureus*, *Salmonella typhi*, and *Salmonella paratyphi*. Surprisingly, AgNPs exerted their antibacterial activity against all the tested strains. A randomized and double-blind pilot clinical trial study also revealed that Nano Silver Fluoride particles can inhibit the formation of *Streptococcus* mutants' biofilms (Freire et al., 2017).

The likely underlying mechanisms of AgNPs' antibacterial properties lie in structurally damaging the cell membranes and in deeply altering the intracellular metabolic activities of the bacteria (Eckhardt et al., 2013). AgNPs also inhibit the activities of bacterial respiratory enzymes (Franci et al., 2015). In addition, other evidences demonstrated that AgNPs control inflammatory processes and modulate cytokines' activities (Rigo et al., 2013), which might be additional mechanisms benefiting chronic wound healing.

Lipid NPs

Liposomes, also known as phospholipid vesicles, are the most widely used lipid NPs for wound dressings (Nasab et al., 2019). In contact with an aqueous solution liposomes can be automatically assembled into enclosed phospholipid bilayers containing a watery core surrounded by a hydrophobic membrane (Ahmed et al., 2019). Reportedly, vancomycin-loaded nanoliposomes coupled with an anti-staphylococcal protein (lysostaphin) can serve as potential antimicrobial formulations for wound infections caused by MRSA, which is resistant to several conventional antibiotics (Hajiahmadi et al., 2019).

The lipid-based NPs versatile capabilities due to their nanoscales, biocompatibility, and high permeability might change our classical views on drugs pharmacokinetics. For example, egg lecithin and soy lecithin liposomes showed superior antioxidant activity *in vitro* and significantly accelerated wound-healing *in vivo* (Nasab et al., 2019). Reportedly, farnesyl-encapsulated liposomes promoted wound healing in a rat model with third-degree burns (Wu et al., 2019). More interestingly, liposomes encapsulating propolis, a natural bee product, showed both antimicrobial and antioxidant activities (Aytekin et al., 2019), which indicated the multiplicity of potential applications of liposomes in pharmacotherapy.

Besides discovering the potential therapeutic effects of new drugs, lipid-based NPs might also enable us to amplify the applications of traditional drugs regarding chronic wound care. Insulin administered by injection is a drug used to regulate blood sugar levels in Internal Medicine. Recently, the promising therapeutic effects of insulin's external administration on chronic wounds were noted, probably because insulin regulates nutrients' metabolism further helping cellular activities during wound healing. However, insulin's external administration is a great technical challenge due to its limited transdermal absorption and its rapid degradation in the wound's bed. To solve this problem, Dawoud et al. (2019) formulated insulin-loaded chitosan NPs liposomes which successfully prolonged the release of insulin.

Moreover, the use of liposomes for intracellular drug delivery is a promising approach to reduce scarring, promote vascularization of ischemic wounds or regulate inflammation in cases of diabetic ulcers and other types of chronic wounds (Choi et al., 2017). Reportedly, glucocorticoid-loaded liposomes

did induce a pro-resolution phenotype in human primary macrophages, which significantly promoted the healing of chronic wounds (Gauthier et al., 2018). Similarly, fibroblast growth factor-encapsulating liposomes advanced wound healing in rats (Xiang et al., 2011). Nunes et al. (2016) developed an usnic acid/liposomes-embedded gelatin-based membrane which is capable of transdermal absorption by skin layers and of controlled drug release. Another intracellular delivery use of liposomes aimed at upregulating growth factor co-receptors in diabetic wounds, which usually heal with difficulty due to growth factor resistance (Das et al., 2014).

Other widely used lipid NPs are exosomes (Chen et al., 2019), solid lipid NPs, and more. Exosomes have diameter sizes ranging from 30 to 100 nm, and are usually released from cells when multivesicular bodies fuse with the plasma membrane (Zarrintaj et al., 2017). Reports indicated that exosomes derived from gene-modified microRNA-126-overexpressing synovium MSCs significantly promoted the proliferation of human dermal microvascular endothelial cells and of human dermal fibroblasts in a dose-dependent manner (Tao et al., 2017). Besides, solid lipid NPs (Eskiler et al., 2019) also exhibited superior capabilities of controlling drugs delivery for potential wound care applications. Moreover, lipid-based NPs partake in emerging applications in relation to several fields, such as cancer therapy, vaccines, dermatological treatments, ocular delivery (Li N. et al., 2019), and post-surgery pain control (Cohen et al., 2019).

Polymeric NPs

Polymeric NPs are usually used to encapsulate drugs, nucleic acids, proteins, macromolecules, and growth factors in order to extend their half-life and improve their bioavailability by physically isolating them from the wound's bed environment, in which multiple kinds of proteases are present. Moreover, the sustained release of drugs at therapeutic concentrations not only can reduce the frequency of drug deliveries but also achieves optimized pharmacokinetics profiles (Kim et al., 2018). Therefore, wound dressings with polymeric NPs have drawn increasing attention due to their intracellular delivery capabilities.

Among them, poly (lactic-co-glycolic acid) (PLGA)-based NPs are widely used for controlled drug releasing due to their versatile degradation kinetics. PLGA biodegradation can also release lactate byproducts further advancing wound healing processes. An endogenous human host defense peptide, LL37, was encapsulated into PLGA NPs to prevent infection and accelerate wound healing (Cherreddy et al., 2014). Karimi Dehkordi et al. (2019) formulated a nanocrystalline cellulose-hyaluronic acid composite embedded with granulocyte-macrophage-colony-stimulating-factor-loaded chitosan NPs to promote wound healing. In the last composite, nanocrystalline cellulose acts as a strengthening agent boosting the mechanical properties of hyaluronic acid.

As biological macromolecular compounds, polymeric NPs exhibit bioactivities that are easily affected by several physical properties, such as sizes, components, surface charges, shapes, etc. Hasan et al. (2019) developed positively- and negatively-charged, respectively, PLGA NPs containing the antibiotic

Clindamycin. Although both kinds of nanoparticles did no detectable harm to healthy fibroblasts, the positively charged NPs elicited significantly better therapeutic outcomes of wound healing in a MRSA-infected mouse model. The different effectiveness in antibacterial activity exhibited by the positively charged vs. the negatively charged polymeric NPs was probably due to their dissimilar capability of adhering to bacteria. To systematically compare the effects of NPs surface charges and shapes on wound healing, Mahmoud et al. (2019) synthesized a series of polymeric hydrogels loaded with gold NPs of differing shapes (rods and spheres) and introduced various surface modifications (neutral, cationic, and anionic charged polymers). Both the inherent parameters (e.g., colloidal stability and release behavior) and therapeutic outcomes (e.g., wound healing, skin re-epithelialization, collagen deposition, inflammation level, and antibacterial activity) were assessed in an animal wound model. Their results showed that hydrogels of gold nanorods constitute a promising nano-platform for wound healing.

Like lipid-based NPs, polymeric NPs might also affect drugs' pharmacokinetics in wound environments, thus enabling us to explore potential off-label uses of current drugs. Jia et al. (2018) developed nanofibrous PLGA incorporating andrographolide-loaded mesoporous silica NPs. Their results showed that the sustained releasing of andrographolide, which is extracted from a Chinese herb, surprisingly reduced inflammation intensity while promoting epidermal cells adhesion. Another kind of Chinese herb, *Aloe vera*, was reported to enhance wound healing when encapsulated inside PLGA NPs to be used in wound dressings (Garcia-Orue et al., 2019). A further recent example comes from the interesting works of Farghaly Aly et al. (2019) who showed that hydrogels containing polymeric NPs loaded with Simvastatin, a cardiovascular drug commonly used to treat serum hyperlipidemia, can benefit wound healing processes. Once encapsulated in chitosan NPs, Phenytoin, an antiepileptic drug, also exhibits a potential capability to accelerate wound healing, a suggestion inspired by recently reported clinical cases of gingival hyperplasia after Phenytoin's oral administration (Cardoso et al., 2019).

Biosafety Concerns of NPs

The biosafety and cytotoxicity of AgNPs have already aroused many concerns. AgNPs seem to be cytotoxic for many species including human beings (Shavandi et al., 2011; Pratsinis et al., 2013). Newly published research showed the toxicity of AgNPs on marine microalgae (Hazeem et al., 2019) and the yeast *Saccharomyces cerevisiae* BY4741 (Kasemets et al., 2019). As regards human beings, prolonged exposures to AgNPs can cause argyria (Richter et al., 2015), whose symptoms include blue gray skin color changes and multiple alterations of bodily functions such as gastrointestinal disorders, spasms, and even death (Rice, 2009). Importantly, AgNPs have produced genotoxicity in the testicles of Sprague Dawley rats (Elsharkawy et al., 2019) and in the embryos of Zebrafish (Chakraborty et al., 2016). As regards human beings, AgNPs have showed genotoxicity in human liver HepG2 and colon Caco2 cells (Sahu et al., 2016). These results revealed a possible reproductive genotoxicity of AgNPs on human offspring especially when AgNPs are used at

high doses and for lengthy periods in patients with large area burns or chronic wounds. Moreover, AgNPs can possibly induce neurotoxicity by crossing the brain blood barrier and penetrating the central nervous system of human beings (Khan et al., 2019).

To test the toxicity when AgNPs are applied on wounds, Pang et al. (2020) applied AgNPs onto the wounds of Zebrafish after the amputation of fins. AgNPs were found to impair epithelialization and blastema formation especially during the first few days, showing that the cytotoxicity of AgNPs is time-dependent and is more obvious at the initial stages of wound healing. Konop et al. (2019) used micellar electro kinetic chromatography to detect the releasing profile of AgNPs from wound dressings. AgNPs at concentration higher than 10 ppm exerted significant ($p < 0.05$) toxicity on the fibroblasts isolated from diabetic mice vs. a murine fibroblasts cell line and a human fibroblasts cell line. Our team also found that an exposure to high concentrations of AgNPs significantly inhibited the proliferation of mice fibroblasts (Liu et al., 2018b). Specially, we noticed that the antibacterial efficiency stopped growing and entered a plateau stage as the AgNPs doses increased, which indicated that an optimized dose range does exist for AgNPs (Liu et al., 2017).

Also, attentions have already been paid to the biosafety and toxicity of other metal NPs, such as TiO_2 , ZnO, magnesium fluoride (MgF_2), cerium oxide (CeO_2), copper, iron oxide, gold, etc. Wang et al. (2018) compared the toxicity of Ag, TiO_2 , and ZnO NPs to human smooth-muscle cells. Their results showed that all the three kinds of metal NPs could induce inflammatory responses. More importantly, ZnO NPs significantly increased intracellular ROS showing a stronger cellular cytotoxicity than that of Ag and TiO_2 NPs. In another case, Filipova et al. (2018) reported a "three-in-one" screening assay to test the toxicity of three kinds of NPs for human umbilical vein endothelial cells. The three NPs are silica NPs (7–14 nm), superparamagnetic iron oxide NPs (8 nm), and carboxylated multiwall carbon nanotubes (60 nm), all of which were tested at the same concentration of 100 $\mu\text{g}/\text{ml}$. Surprisingly, all the NPs types tested exhibited a gradual toxic effect which decreased cell viability.

Solutions to Reduce Cytotoxicity of AgNPs in Wound Care

Reportedly, a general mechanism for AgNPs-mediated intracellular toxicity is that AgNPs can enter human cells either by endosomal uptake or by diffusion (Frohlich and Frohlich, 2016). The cytotoxicity of AgNPs is a size-, dose-, and time-dependent, which means that it is closely related to nanoparticle size, shape, surface charge, oxidation state, agglomeration condition, administration route, and dosage (Liao et al., 2019). Correspondingly, potential solutions to reducing cytotoxicity of AgNPs are focused on the tunable size-, dose-, or time-dependent features of AgNPs.

First, increasing the size of AgNPs can reduce their cytotoxicity, but the antibacterial efficacy is concurrently reduced. Reportedly, AgNPs with sizes below 10 nm exhibited both a higher antibacterial efficiency and cytotoxicity (Gahlawat et al., 2016). Zille et al. (2015) tested the antibacterial efficacy of AgNPs with 10, 20, 40, 60, and 100 nm particle sizes. The

antibacterial inhibition values against *S. aureus* were 19% for the 100 nm-AgNPs and 95% for the 10 nm-AgNPs, showing that antibacterial effectiveness increases with decreasing nanoparticle size. On the other hand, AgNPs of sizes below 10 nm showed to be more cytotoxic than those of other sizes (Recordati et al., 2016). AgNPs of sizes below 3 nm can be deposited within multiple organs of male mice, such as liver, spleen, kidney, heart, lungs, testicles, stomach, and intestine (Yang et al., 2017). Therefore, a balance needs to be achieved between antimicrobial efficiency and biosafety due to the size-dependent cytotoxicity of AgNPs.

Second, combining AgNPs with other antibacterial strategies can reduce the administered doses to lessen the dose-dependent cytotoxicity. For example, antimicrobial peptides (AMPs), which are integral compounds secreted by natural organisms and act as natural immune defenses (Kokel and Torok, 2018), can possibly reinforce AgNPs in terms of killing antibiotic-resistant bacteria. In a recent study, AMPs were included at the peripheral hydrophilic region of polymersomes, while AgNPs were included inside the hydrophobic corona. *In vitro* tests indicated that the AMP/AgNPs polymersomes exhibited a satisfactory bacteriostatic activity as well as a low cytotoxicity toward human dermal fibroblasts (Bassous and Webster, 2019). In other cases, AgNPs-coated zwitterionic hydrogels, which confer superhydrophilic properties to resist bacterial attachment, were reported to promote wound healing (GhavamiNejad et al., 2016). Our team recently used N,N-dimethylformamide-treated poly(vinylidene fluoride), in which the Ag⁺ ions were reduced to elemental silver. The impregnated AgNPs were then generated *in situ* and the surface hydrophobicity was significantly increased. Then, we tried different concentrations of ingredient materials and eventually reduced the cytotoxicity and achieved optimized anti-bacterial capacities against *A. baumannii* and *E. coli* (Menglong Liu et al., 2018).

Third, novel drug delivery system can release AgNPs in a spatio-temporally controlled or stimuli-responsive profile to reduce dosing frequency and amounts. As regards chronic wounds, the stimuli which trigger the release of AgNPs can be pH levels, lactic acid, glucose, proteases, and matrix metalloproteinases, etc. Among all the peculiar stimuli, pH changes play a vital role by revealing pathophysiological alterations occurring during the transformation of acute wounds into chronic wounds due to infection, ischemia, or inflammation. Recently, our team reported the pH-responsive releasing of AgNPs reinforced via a chemo-photothermal therapy targeting chronic wounds with bacterial infections. The infectious wound environment (pH ~ 6.3) can trigger the release of AgNPs, which contributes to lower their cytotoxicity (Liu et al., 2018a).

REFERENCES

- Adlerz, K. M., Aranda-Espinoza, H., and Hayenga, H. N. (2016). Substrate elasticity regulates the behavior of human monocyte-derived macrophages. *Eur. Biophys. J.* 45, 301–309. doi: 10.1007/s00249-015-1096-8
- Aghaei-Ghareh-Bolagh, B., Mithieux, S. M., Hiob, M. A., Wang, Y., Chong, A., and Weiss, A. S. (2019). Fabricated tropoelastin-silk yarns and woven

OVERVIEW

Obviously, stem cell fates are spatio-temporally modulated by concurrent signals from both physical and chemical stimuli. Surface micropatterning methods, especially the nanotechnology, 3D bio-printing, and laser photolithography enable us to precisely tailor the surface topology and biomechanical features to study the behaviors of individual cells. These discoveries highlighted that in some cases physical properties can be the predominating and independent factors that direct stem cell fates (Kilian et al., 2010).

Earlier strategies for the regeneration of cutaneous appendages (i.e., sweat glands and hair follicles) were focused on chemical approaches, which entailed insurmountable difficulties. The physical property-based regulation of stem cells has been tracking down potential solutions. For example, 3D bio-printed dermal matrixes served as “artificial niches” to direct epidermal progenitors (Liu et al., 2016) and MSCs (Yao et al., 2020) into sweat gland differentiation.

Traditional fabrication techniques do not tailor spatial structures or control modeling for the regenerations of human cutaneous appendages. Recently, a microfluidic device, which can manipulate fluids at the submillimeter scale (Sackmann et al., 2014), was ingeniously designed to recapitulate the development of human epiblast and amniotic ectoderm using human pluripotent stem cells (Zheng et al., 2019). This study showed that the guides of biomimetic spatial structures and physical cues play key roles during the regeneration of organoids with complex microstructures and microfluidics technology holds potential for the regenerations of human cutaneous appendages.

AUTHOR CONTRIBUTIONS

YW provided the main concept for this review and wrote the manuscript. UA and JW prepared the figures and improved the language of the manuscript.

FUNDING

This work was supported by High Level Hospital Construction Project of Guangdong Province.

ACKNOWLEDGMENTS

We would like to thank the kind aid and the inspiring ideas about regenerating cutaneous appendages from Dr. Sha Huang in the Medical Innovation Research Department, PLA General Hospital and PLA Medical College, Beijing, China.

textiles for diverse tissue engineering applications. *Acta Biomater.* 91, 112–122. doi: 10.1016/j.actbio.2019.04.029

- Ahmed, K. S., Hussein, S. A., Ali, A. H., Korma, S. A., Lipeng, Q., and Jinghua, C. (2019). Liposome: composition, characterisation, preparation, and recent innovation in clinical applications. *J. Drug Target.* 27, 742–761. doi: 10.1080/1061186X.2018.1527337

- Akash, M. S. H., Rehman, K., Fiayyaz, F., Sabir, S., and Khurshid, M. (2020). Diabetes-associated infections: development of antimicrobial resistance and possible treatment strategies. *Arch. Microbiol.* doi: 10.1007/s00203-020-01818-x. [Epub ahead of print].
- Almeida, H., Domingues, R. M. A., Mithieux, S. M., Pires, R. A., Goncalves, A. I., Gomez-Florit, M., et al. (2019). Tropoelastin-coated tendon biomimetic scaffolds promote stem cell tenogenic commitment and deposition of elastin-rich matrix. *ACS Appl. Mater. Interfaces* 11, 19830–19840. doi: 10.1021/acsami.9b04616
- Alonso, L., and Fuchs, E. (2006). The hair cycle. *J. Cell Sci.* 119, 391–393. doi: 10.1242/jcs.02793
- Aytemkin, A. A., Tuncay Tanriverdi, S., Aydin Kose, F., Kart, D., Eroglu, I., and Ozer, O. (2019). Propolis loaded liposomes: evaluation of antimicrobial and antioxidant activities. *J. Liposome Res.* 30, 107–116. doi: 10.1080/08982104.2019.1599012
- Bakker, K., Apelqvist, J., Lipsky, B. A., Van Netten, J. J., and International Working Group on the Diabetic (2016). The 2015 IWGDF guidance documents on prevention and management of foot problems in diabetes: development of an evidence-based global consensus. *Diabetes Metab. Res. Rev.* 32(Suppl. 1), 2–6. doi: 10.1002/dmrr.2694
- Bassous, N. J., and Webster, T. J. (2019). The binary effect on methicillin-resistant *Staphylococcus aureus* of polymeric nanovesicles appended by proline-rich amino acid sequences and inorganic nanoparticles. *Small* 15:e1804247. doi: 10.1002/smll.201804247
- Bhattacharya, D., Ghosh, B., and Mukhopadhyay, M. (2019). Development of nanotechnology for advancement and application in wound healing: a review. *IET Nanobiotechnol.* 13, 778–785. doi: 10.1049/iet-nbt.2018.5312
- Boulton, A. J., Vileikyte, L., Ragnarson-Tennvall, G., and Apelqvist, J. (2005). The global burden of diabetic foot disease. *Lancet* 366, 1719–1724. doi: 10.1016/S0140-6736(05)67698-2
- Brusatin, G., Panciera, T., Gandin, A., Citron, A., and Piccolo, S. (2018). Biomaterials and engineered microenvironments to control YAP/TAZ-dependent cell behaviour. *Nat. Mater.* 17, 1063–1075. doi: 10.1038/s41563-018-0180-8
- Bryan, N., Ahswini, H., Smart, N., Bayon, Y., Wohler, S., and Hunt, J. A. (2012). Reactive oxygen species (ROS)—a family of fate deciding molecules pivotal in constructive inflammation and wound healing. *Eur. Cell. Mater.* 24, 249–265. doi: 10.22203/eCM.v024a18
- Bui, V. T., Thi Thuy, L., Choi, J. S., and Choi, H. S. (2018). Ordered cylindrical micropatterned Petri dishes used as scaffolds for cell growth. *J. Colloid Interface Sci.* 513, 161–169. doi: 10.1016/j.jcis.2017.11.024
- Cardoso, A. M., de Oliveira, E. G., Coradini, K., Bruinsmann, F. A., Aguirre, T., Lorenzoni, R., et al. (2019). Chitosan hydrogels containing nanoencapsulated phenytoin for cutaneous use: skin permeation/penetration and efficacy in wound healing. *Mater. Sci. Eng. C Mater. Biol. Appl.* 96, 205–217. doi: 10.1016/j.msec.2018.11.013
- Chakrabarti, S., Chattopadhyay, P., Islam, J., Ray, S., Raju, P. S., and Mazumder, B. (2019). Aspects of nanomaterials in wound healing. *Curr. Drug Deliv.* 16, 26–41. doi: 10.2174/1567201815666180918110134
- Chakraborty, C., Sharma, A. R., Sharma, G., and Lee, S. S. (2016). Zebrafish: a complete animal model to enumerate the nanoparticle toxicity. *J. Nanobiotechnol.* 14:65. doi: 10.1186/s12951-016-0217-6
- Chang, L., Azzolin, L., Di Biagio, D., Zanonato, F., Battilana, G., Lucon Xiccato, R., et al. (2018). The SWI/SNF complex is a mechanoregulated inhibitor of YAP and TAZ. *Nature* 563, 265–269. doi: 10.1038/s41586-018-0658-1
- Changi, K., Bosnjak, B., Gonzalez-Obeso, C., Kluger, R., Rodriguez-Cabello, J. C., Hoffmann, O., et al. (2018). Biocompatibility and immunogenicity of elastin-like recombinamer biomaterials in mouse models. *J. Biomed. Mater. Res. A* 106, 924–934. doi: 10.1002/jbma.a.36290
- Chen, B., Sun, Y., Zhang, J., Zhu, Q., Yang, Y., Niu, X., et al. (2019). Human embryonic stem cell-derived exosomes promote pressure ulcer healing in aged mice by rejuvenating senescent endothelial cells. *Stem Cell Res. Ther.* 10:142. doi: 10.1186/s13287-019-1253-6
- Chen, G., Dong, C., Yang, L., and Lv, Y. (2015). 3D scaffolds with different stiffness but the same microstructure for bone tissue engineering. *ACS Appl. Mater. Interfaces* 7, 15790–15802. doi: 10.1021/acsami.5b02662
- Cherredy, K. K., Her, C. H., Comune, M., Moia, C., Lopes, A., Porporato, P. E., et al. (2014). PLGA nanoparticles loaded with host defense peptide LL37 promote wound healing. *J. Control. Release* 194, 138–147. doi: 10.1016/j.jconrel.2014.08.016
- Choi, J. U., Lee, S. W., Pangeni, R., Byun, Y., Yoon, I. S., and Park, J. W. (2017). Preparation and in vivo evaluation of cationic elastic liposomes comprising highly skin-permeable growth factors combined with hyaluronic acid for enhanced diabetic wound-healing therapy. *Acta Biomater.* 57, 197–215. doi: 10.1016/j.actbio.2017.04.034
- Cohen, B., Glosser, L., Saab, R., Walters, M., Salih, A., Zafeer-Khan, M., et al. (2019). Incidence of adverse events attributable to bupivacaine liposome injectable suspension or plain bupivacaine for postoperative pain in pediatric surgical patients: a retrospective matched cohort analysis. *Paediatr. Anaesth.* 29, 169–174. doi: 10.1111/pan.13561
- Cooper, A., Leung, M., and Zhang, M. (2012). Polymeric fibrous matrices for substrate-mediated human embryonic stem cell lineage differentiation. *Macromol. Biosci.* 12, 882–892. doi: 10.1002/mabi.201100269
- Cuttingco, M. F. A., Jensen, B. S., Reynolds, P. M., and Gadegaard, N. (2020). Predicting gene expression using morphological cell responses to nanotopography. *Nat. Commun.* 11:1384. doi: 10.1038/s41467-020-15114-1
- Dantes, R., Mu, Y., Belflower, R., Aragon, D., Dumyati, G., Harrison, L. H., et al. (2013). National burden of invasive methicillin-resistant *Staphylococcus aureus* infections, United States. *JAMA Intern. Med.* 173, 1970–8. doi: 10.1001/jamainternmed.2013.10423
- Das, S., and Baker, A. B. (2016). Biomaterials and nanotherapeutics for enhancing skin wound healing. *Front. Bioeng. Biotechnol.* 4:82. doi: 10.3389/fbioe.2016.00082
- Das, S., Singh, G., and Baker, A. B. (2014). Overcoming disease-induced growth factor resistance in therapeutic angiogenesis using recombinant co-receptors delivered by a liposomal system. *Biomaterials* 35, 196–205. doi: 10.1016/j.biomaterials.2013.09.105
- Das, U., Behera, S. S., Singh, S., Rizvi, S. I., and Singh, A. K. (2016). Progress in the development and applicability of potential medicinal plant extract-conjugated polymeric constructs for wound healing and tissue regeneration. *Phytother. Res.* 30, 1895–1904. doi: 10.1002/ptr.5700
- Dawoud, M. H. S., Yassin, G. E., Ghorab, D. M., and Morsi, N. M. (2019). Insulin mucoadhesive liposomal gel for wound healing: a formulation with sustained release and extended stability using quality by design approach. *AAPS Pharm.* 20:158. doi: 10.1208/s12249-019-1363-6
- Desmet, C. M., Preat, V., and Gallez, B. (2018). Nanomedicines and gene therapy for the delivery of growth factors to improve perfusion and oxygenation in wound healing. *Adv. Drug Deliv. Rev.* 129, 262–284. doi: 10.1016/j.addr.2018.02.001
- Dhanalakshmi, V., Nimal, T. R., Sabitha, M., Biswas, R., and Jayakumar, R. (2016). Skin and muscle permeating antibacterial nanoparticles for treating *Staphylococcus aureus* infected wounds. *J. Biomed. Mater. Res. Part B Appl. Biomater.* 104, 797–807. doi: 10.1002/jbmb.b.33635
- Dovi, J. V., He, L. K., and DiPietro, L. A. (2003). Accelerated wound closure in neutrophil-depleted mice. *J. Leukoc. Biol.* 73, 448–455. doi: 10.1189/jlb.0802406
- Eckhardt, S., Brunetto, P. S., Gagnon, J., Priebe, M., Giese, B., and Fromm, K. M. (2013). Nanobio silver: its interactions with peptides and bacteria, and its uses in medicine. *Chem. Rev.* 113, 4708–4754. doi: 10.1021/cr300288v
- Elsharkawy, E. E., Abd El-Nasser, M., and Kamaly, H. F. (2019). Silver nanoparticles testicular toxicity in rat. *Environ. Toxicol. Pharmacol.* 70:103194. doi: 10.1016/j.etap.2019.103194
- Engler, A. J., Sen, S., Sweeney, H. L., and Discher, D. E. (2006). Matrix elasticity directs stem cell lineage specification. *Cell* 126, 677–689. doi: 10.1016/j.cell.2006.06.044
- Eskiler, G. G., Cecener, G., Dikmen, G., Egeli, U., and Tunca, B. (2019). Talazoparib loaded solid lipid nanoparticles: preparation, characterization and evaluation of the therapeutic efficacy *in vitro*. *Curr. Drug Deliv.* 16, 511–529. doi: 10.2174/1567201816666190515105532
- Farghaly Aly, U., Abou-Taleb, H. A., Abdellatif, A. A., and Sameh Tolba, N. (2019). Formulation and evaluation of simvastatin polymeric nanoparticles loaded in hydrogel for optimum wound healing purpose. *Drug Des. Devel. Ther.* 13, 1567–1580. doi: 10.2147/DDDT.S198413
- Filipova, M., Elhelu, O. K., De Paoli, S. H., Fremuntova, Z., Mosko, T., Cmarko, D., et al. (2018). An effective “three-in-one” screening assay for testing drug and nanoparticle toxicity in human endothelial cells. *PLoS ONE* 13:e0206557. doi: 10.1371/journal.pone.0206557

- Flora, T., de Torre, I. G., Alonso, M., and Rodriguez-Cabello, J. C. (2019). Tethering QK peptide to enhance angiogenesis in elastin-like recombinamer (ELR) hydrogels. *J. Mater. Sci. Mater. Med.* 30:30. doi: 10.1007/s10856-019-6232-z
- Franci, G., Falanga, A., Galdiero, S., Palomba, L., Rai, M., Morelli, G., et al. (2015). Silver nanoparticles as potential antibacterial agents. *Molecules* 20, 8856–8874. doi: 10.3390/molecules20058856
- Freire, P. L. L., Albuquerque, A. J. R., Sampaio, F. C., Galembeck, A., Flores, M. A. P., Stamford, T. C. M., et al. (2017). AgNPs: the new allies against *S. mutans* biofilm - a pilot clinical trial and microbiological assay. *Braz. Dent. J.* 28, 417–422. doi: 10.1590/0103-6440201600994
- Frohlich, E. E., and Frohlich, E. (2016). Cytotoxicity of nanoparticles contained in food on intestinal cells and the gut microbiota. *Int. J. Mol. Sci.* 17:509. doi: 10.3390/ijms17040509
- Frykberg, R. G., and Banks, J. (2015). Challenges in the treatment of chronic wounds. *Adv. Wound Care* 4, 560–582. doi: 10.1089/wound.2015.0635
- Gahlawat, G., Shikha, S., Chaddha, B. S., Chaudhuri, S. R., Mayilraj, S., and Choudhury, A. R. (2016). Microbial glycolipoprotein-capped silver nanoparticles as emerging antibacterial agents against cholera. *Microb. Cell Fact.* 15:25. doi: 10.1186/s12934-016-0422-x
- Garcia-Orue, I., Gainza, G., Garcia-Garcia, P., Gutierrez, F. B., Aguirre, J. J., Hernandez, R. M., et al. (2019). Composite nanofibrous membranes of PLGA/Aloe vera containing lipid nanoparticles for wound dressing applications. *Int. J. Pharm.* 556, 320–329. doi: 10.1016/j.ijpharm.2018.12.010
- Gauthier, A., Fisch, A., Seuwen, K., Baumgarten, B., Ruffner, H., Aebi, A., et al. (2018). Glucocorticoid-loaded liposomes induce a pro-resolution phenotype in human primary macrophages to support chronic wound healing. *Biomaterials* 178, 481–495. doi: 10.1016/j.biomaterials.2018.04.006
- GhavamiNejad, A., Park, C. H., and Kim, C. S. (2016). *In situ* synthesis of antimicrobial silver nanoparticles within antifouling zwitterionic hydrogels by catecholic redox chemistry for wound healing application. *Biomacromolecules* 17, 1213–1223. doi: 10.1021/acs.biomac.6b00039
- Gonzalez de Torre, I., Ibanez-Fonseca, A., Quintanilla, L., Alonso, M., and Rodriguez-Cabello, J. C. (2018). Random and oriented electrospun fibers based on a multicomponent, in situ clickable elastin-like recombinamer system for dermal tissue engineering. *Acta Biomater.* 72, 137–149. doi: 10.1016/j.actbio.2018.03.027
- Guan, B., Mao, T. L., Panuganti, P. K., Kuhn, E., Kurman, R. J., and Maeda, D., et al. (2011). Mutation and loss of expression of ARID1A in uterine low-grade endometrioid carcinoma. *Am. J. Surg. Pathol.* 35, 625–632. doi: 10.1097/PAS.0b013e318212782a
- Haensel, D., Jin, S., Sun, P., Cinco, R., Dragan, M., Nguyen, Q., et al. (2020). Defining epidermal basal cell states during skin homeostasis and wound healing using single-cell transcriptomics. *Cell Rep.* 30, 3932–3947.e6. doi: 10.1016/j.celrep.2020.02.091
- Hajiahmadi, F., Alikhani, M. Y., Shariatifar, H., Arabestani, M. R., and Ahmadvand, D. (2019). The bactericidal effect of lysostaphin coupled with liposomal vancomycin as a dual combating system applied directly on methicillin-resistant *Staphylococcus aureus* infected skin wounds in mice. *Int. J. Nanomedicine* 14, 5943–5955. doi: 10.2147/IJN.S214521
- Hasan, N., Cao, J., Lee, J., Hlaing, S. P., Oshi, M. A., Naeem, M., et al. (2019). Bacteria-targeted clindamycin loaded polymeric nanoparticles: effect of surface charge on nanoparticle adhesion to MRSA, antibacterial activity, wound healing. *Pharmaceutics* 11:236. doi: 10.3390/pharmaceutics11050236
- Hazeem, L. J., Kuku, G., Dewailly, E., Slomianny, C., Barras, A., Hamdi, A., et al. (2019). Toxicity effect of silver nanoparticles on photosynthetic pigment content, growth, ROS production and ultrastructural changes of microalgae *Chlorella vulgaris*. *Nanomaterials* 9:914. doi: 10.3390/nano9070914
- He, W., Wang, Y., Wang, P., and Wang, F. (2019). Intestinal barrier dysfunction in severe burn injury. *Burns Trauma* 7:24. doi: 10.1186/s41038-019-0162-3
- Hopf, H. W., and Rollins, M. D. (2007). Wounds: an overview of the role of oxygen. *Antioxid. Redox Signal.* 9, 1183–1192. doi: 10.1089/ars.2007.1641
- Hu, Y., Liu, H., Zhou, X., Pan, H., Wu, X., Abidi, N., et al. (2019). Surface engineering of spongy bacterial cellulose via constructing crossed groove/column micropattern by low-energy CO₂ laser photolithography toward scar-free wound healing. *Mater. Sci. Eng. C Mater. Biol. Appl.* 99, 333–343. doi: 10.1016/j.msec.2019.01.116
- Huang, X., Sun, J., Chen, G., Niu, C., Wang, Y., Zhao, C., et al. (2019). Resveratrol promotes diabetic wound healing via SIRT1-FOXO1-c-Myc signaling pathway-mediated angiogenesis. *Front. Pharmacol.* 10:421. doi: 10.3389/fphar.2019.00421
- Jia, Y., Zhang, H., Yang, S., Xi, Z., Tang, T., Yin, R., et al. (2018). Electrospun PLGA membrane incorporated with andrographolide-loaded mesoporous silica nanoparticles for sustained antibacterial wound dressing. *Nanomedicine* 13, 2881–2899. doi: 10.2217/nnm-2018-0099
- Jiang, S., Li, S. C., Huang, C., Chan, B. P., and Du, Y. (2018). Physical properties of implanted porous bioscaffolds regulate skin repair: focusing on mechanical and structural features. *Adv. Healthc. Mater.* 7: E1700894. doi: 10.1002/adhm.201700894
- Jiang, S., Lyu, C., Zhao, P., Li, W., Kong, W., Huang, C., et al. (2019). Cryoprotectant enables structural control of porous scaffolds for exploration of cellular mechano-responsiveness in 3D. *Nat. Commun.* 10:3491. doi: 10.1038/s41467-019-11397-1
- Jiang, Y., Huang, S., Fu, X., Liu, H., Ran, X., Lu, S., et al. (2011). Epidemiology of chronic cutaneous wounds in China. *Wound Repair Regen.* 19, 181–188. doi: 10.1111/j.1524-475X.2010.00666.x
- Kalantari, K., Mostafavi, E., Afifi, A. M., Izadiyan, Z., Jahangirian, H., Rafiee-Moghaddam, R., et al. (2020). Wound dressings functionalized with silver nanoparticles: promises and pitfalls. *Nanoscale* 12, 2268–2291. doi: 10.1039/C9NR08234D
- Kanji, S., and Das, H. (2017). Advances of Stem Cell Therapeutics in Cutaneous Wound Healing and Regeneration. *Mediators Inflamm.* 2017:5217967. doi: 10.1155/2017/5217967
- Karimi Dehkordi, N., Minaiyan, M., Talebi, A., Akbari, V., and Taheri, A. (2019). Nanocrystalline cellulose-hyaluronic acid composite enriched with GM-CSF loaded chitosan nanoparticles for enhanced wound healing. *Biomed. Mater.* 14:035003. doi: 10.1088/1748-605X/ab026c
- Kasemets, K., Kaasaar, S., Vija, H., Fascio, U., and Mantecca, P. (2019). Toxicity of differently sized and charged silver nanoparticles to yeast *Saccharomyces cerevisiae* BY4741: a nano-biointeraction perspective. *Nanotoxicology* 13, 1041–1059. doi: 10.1080/17435390.2019.1621401
- Khan, A. M., Korzeniowska, B., Gorshkov, V., Tahir, M., Schroder, H., Skytte, L., et al. (2019). Silver nanoparticle-induced expression of proteins related to oxidative stress and neurodegeneration in an *in vitro* human blood-brain barrier model. *Nanotoxicology* 13, 221–239. doi: 10.1080/17435390.2018.1540728
- Khorasani, M. T., Joorabloo, A., Moghaddam, A., Shamsi, H., and MansooriMoghadam, Z. (2018). Incorporation of ZnO nanoparticles into heparinized polyvinyl alcohol/chitosan hydrogels for wound dressing application. *Int. J. Biol. Macromol.* 114, 1203–1215. doi: 10.1016/j.ijbiomac.2018.04.010
- Kilian, K. A., Bugarija, B., Lahn, B. T., and Mrksich, M. (2010). Geometric cues for directing the differentiation of mesenchymal stem cells. *Proc. Natl. Acad. Sci. U.S.A.* 107, 4872–4877. doi: 10.1073/pnas.0903269107
- Kim, H. S., Sun, X., Lee, J. H., Kim, H. W., Fu, X., and Leong, K. W. (2018). Advanced drug delivery systems and artificial skin grafts for skin wound healing. *Adv. Drug Deliv. Rev.* 146, 209–239. doi: 10.1016/j.addr.2018.12.014
- Kokel, A., and Torok, M. (2018). Recent advances in the development of antimicrobial peptides (AMPs): attempts for sustainable medicine? *Curr. Med. Chem.* 25, 2503–2519. doi: 10.2174/0929867325666180117142142
- Konop, M., Klodzinska, E., Borowiec, J., Laskowska, A. K., Czuwara, J., Konieczka, P., et al. (2019). Application of micellar electrokinetic chromatography for detection of silver nanoparticles released from wound dressing. *Electrophoresis* 40, 1565–1572. doi: 10.1002/elps.201900020
- Li, N., Xie, X., Hu, Y., He, H., Fu, X., Fang, T., et al. (2019). Herceptin-conjugated liposomes co-loaded with doxorubicin and simvastatin in targeted prostate cancer therapy. *Am. J. Transl. Res.* 11, 1255–1269.
- Li, Y., Zhang, J., Zhou, Q., Wang, H., Xie, S., Yang, X., et al. (2019). Linagliptin inhibits high glucose-induced transdifferentiation of hypertrophic scar-derived fibroblasts to myofibroblasts via IGF/Akt/mTOR signalling pathway. *Exp. Dermatol.* 28, 19–27. doi: 10.1111/exd.13800
- Liao, C., Li, Y., and Tjong, S. C. (2019). Bactericidal and cytotoxic properties of silver nanoparticles. *Int. J. Mol. Sci.* 20:449. doi: 10.3390/ijms200420449

- Liu, M., He, D., Yang, T., Liu, W., Mao, L., Zhu, Y., et al. (2018a). An efficient antimicrobial depot for infectious site-targeted chemo-photothermal therapy. *J. Nanobiotechnol.* 16:23. doi: 10.1186/s12951-018-0348-z
- Liu, M., Liu, T., Chen, X., Yang, J., Deng, J., He, W., et al. (2018b). Nano-silver-incorporated biomimetic polydopamine coating on a thermoplastic polyurethane porous nanocomposite as an efficient antibacterial wound dressing. *J. Nanobiotechnol.* 16:89. doi: 10.1186/s12951-018-0416-4
- Liu, M., Luo, G., Wang, Y., He, W., Liu, T., Zhou, D., et al. (2017). Optimization and integration of nanosilver on polycaprolactone nanofibrous mesh for bacterial inhibition and wound healing in vitro and in vivo. *Int. J. Nanomedicine* 12, 6827–6840. doi: 10.2147/IJN.S140648
- Liu, N., Huang, S., Yao, B., Xie, J., Wu, X., and Fu, X. (2016). 3D bioprinting matrices with controlled pore structure and release function guide in vitro self-organization of sweat gland. *Sci. Rep.* 6:34410. doi: 10.1038/srep34410
- MacEwan, M. R., MacEwan, S., Kovacs, T. R., and Batts, J. (2017). What makes the optimal wound healing material? A review of current science, and introduction of a synthetic nanofabricated wound care scaffold. *Cureus* 9:e1736. doi: 10.7759/cureus.1736
- Mahmoud, N. N., Hikmat, S., Abu Ghith, D., Hajeer, M., Hamadneh, L., Qattan, D., et al. (2019). Gold nanoparticles loaded into polymeric hydrogel for wound healing in rats: Effect of nanoparticles' shape and surface modification. *Int. J. Pharm.* 565, 174–186. doi: 10.1016/j.ijpharm.2019.04.079
- Manukumar, H. M., Chandrasekar, B., Rakesh, K. P., Ananda, A. P., Nandhini, M., Lalitha, P., et al. (2017). Novel T-C@AgNPs mediated biocidal mechanism against biofilm associated methicillin-resistant *Staphylococcus aureus* (BAP-MRSA) 090, cytotoxicity and its molecular docking studies. *Medchemcomm* 8, 2181–2194. doi: 10.1039/C7MD00486A
- Melo, E., Cardenes, N., Garreta, E., Luque, T., Rojas, M., Navajas, D., et al. (2014). Inhomogeneity of local stiffness in the extracellular matrix scaffold of fibrotic mouse lungs. *J. Mech. Behav. Biomed. Mater.* 37, 186–195. doi: 10.1016/j.jmbbm.2014.05.019
- Menglong Liu, Y. W., Xiaodong, H., Weifeng, H., Yali, G., Xiaohong, H., Meixi, L., et al. (2018). Janus N-dimethylformamide as a solvent for a gradient porous wound dressing of poly(vinylidene fluoride) and as a reducer for *in situ* nano-silver production: anti-permeation, antibacterial and antifouling activities against multi-drug-resistant bacteria both *in vitro* and *in vivo*. *RSC Adv.* 8, 26626–26639. doi: 10.1039/C8RA03234C
- Miao, S., Cui, H., Esworthy, T., Mahadik, B., Lee, S. J., Zhou, X., et al. (2020). 4D self-morphing culture substrate for modulating cell differentiation. *Adv. Sci.* 7:1902403. doi: 10.1002/advs.201902403
- Mithieux, S. M., Aghaei-Ghareh-Bolagh, B., Yan, L., Kuppan, K. V., Wang, Y., Garces-Suarez, F., et al. (2018). Tropoelastin implants that accelerate wound repair. *Adv. Healthc. Mater.* 7 e1701206. doi: 10.1002/adhm.201701206
- Nasab, M. E., Takzaree, N., Saffaria, P. M., and Partoazar, A. (2019). *In vitro* antioxidant activity and *in vivo* wound-healing effect of lecithin liposomes: a comparative study. *J. Comp. Eff. Res.* 8, 633–643. doi: 10.2217/cer-2018-0128
- Nasrollahi, S., Walter, C., Loza, A. J., Schimizzi, G. V., Longmore, G. D., and Pathak, A. (2017). Past matrix stiffness primes epithelial cells and regulates their future collective migration through a mechanical memory. *Biomaterials* 146, 146–155. doi: 10.1016/j.biomaterials.2017.09.012
- Nunes, P. S., Rabelo, A. S., Souza, J. C., Santana, B. V., da Silva, T. M., Serafini, M. R., et al. (2016). Gelatin-based membrane containing usnic acid-loaded liposomes improves dermal burn healing in a porcine model. *Int. J. Pharm.* 513, 473–482. doi: 10.1016/j.ijpharm.2016.09.040
- Pang, S., Gao, Y., Wang, F., Wang, Y., Cao, M., Zhang, W., et al. (2020). Toxicity of silver nanoparticles on wound healing: a case study of zebrafish fin regeneration model. *Sci. Total Environ.* 717:137178. doi: 10.1016/j.scitotenv.2020.137178
- Pratsinis, A., Hervella, P., Leroux, J. C., Pratsinis, S. E., and Sotiriou, G. A. (2013). Toxicity of silver nanoparticles in macrophages. *Small* 9, 2576–2584. doi: 10.1002/smll.201202120
- Ramanathan, G., Singaravelu, S., Muthukumar, T., Thyagarajan, S., Perumal, P. T., and Sivagnanam, U. T. (2017). Design and characterization of 3D hybrid collagen matrixes as a dermal substitute in skin tissue engineering. *Mater. Sci. Eng. C Mater. Biol. Appl.* 72, 359–370. doi: 10.1016/j.msec.2016.11.095
- Recordati, C., De Maglie, M., Bianchessi, S., Argenti, S., Cella, C., Mattiello, S., et al. (2016). Tissue distribution and acute toxicity of silver after single intravenous administration in mice: nano-specific and size-dependent effects. *Part. Fibre Toxicol.* 13:12. doi: 10.1186/s12989-016-0124-x
- Rice, L. B. (2009). The clinical consequences of antimicrobial resistance. *Curr. Opin. Microbiol.* 12, 476–481. doi: 10.1016/j.mib.2009.08.001
- Richter, A. P., Brown, J. S., Bharti, B., Wang, A., Gangwal, S., Houck, K., et al. (2015). An environmentally benign antimicrobial nanoparticle based on a silver-infused lignin core. *Nat. Nanotechnol.* 10, 817–823. doi: 10.1038/nnano.2015.141
- Rigo, C., Ferroni, L., Tocco, I., Roman, M., Munivra, I., Gardin, C., et al. (2013). Active silver nanoparticles for wound healing. *Int. J. Mol. Sci.* 14, 4817–4840. doi: 10.3390/ijms14034817
- Rodriguez-Cabello, J. C., Gonzalez de Torre, I., Ibanez-Fonseca, A., and Alonso, M. (2018). Bioactive scaffolds based on elastin-like materials for wound healing. *Adv. Drug Deliv. Rev.* 129, 118–133. doi: 10.1016/j.addr.2018.03.003
- Sackmann, E. K., Fulton, A. L., and Beebe, D. J. (2014). The present and future role of microfluidics in biomedical research. *Nature* 507, 181–189. doi: 10.1038/nature13118
- Sahu, S. C., Njoroge, J., Bryce, S. M., Zheng, J., and Ihrle, J. (2016). Flow cytometric evaluation of the contribution of ionic silver to genotoxic potential of nanosilver in human liver HepG2 and colon Caco2 cells. *J. Appl. Toxicol.* 36, 521–531. doi: 10.1002/jat.3276
- Sandri, G., Miele, D., Faccendini, A., Bonferoni, M. C., Rossi, S., Grisoli, P., et al. (2019). Chitosan/glycosaminoglycan scaffolds: the role of silver nanoparticles to control microbial infections in wound healing. *Polymers* 11:1207. doi: 10.3390/polym11071207
- Satish, L., Santhakumari, S., Gowrishankar, S., Pandian, S. K., Ravi, A. V., and Ramesh, M. (2017). Rapid biosynthesized AgNPs from *Gelidiella acerosa* aqueous extract mitigates quorum sensing mediated biofilm formation of *Vibrio* species—an *in vitro* and *in vivo* approach. *Environ. Sci. Pollut. Res. Int.* 24, 27254–27268. doi: 10.1007/s11356-017-0296-4
- Shavandi, Z., Ghazanfari, T., and Moghaddam, K. N. (2011). *In vitro* toxicity of silver nanoparticles on murine peritoneal macrophages. *Immunopharmacol. Immunotoxicol.* 33, 135–140. doi: 10.3109/08923973.2010.487489
- Tao, S. C., Guo, S. C., Li, M., Ke, Q. F., Guo, Y. P., and Zhang, C. Q. (2017). Chitosan wound dressings incorporating exosomes derived from MicroRNA-126-overexpressing synovium mesenchymal stem cells provide sustained release of exosomes and heal full-thickness skin defects in a diabetic rat model. *Stem Cells Transl. Med.* 6, 736–747. doi: 10.5966/sctm.2016-0275
- Tarananova, A., Yeo, G. C., Baldock, C., Weiss, A. S., and Buehler, M. J. (2019). Tropoelastin is a flexible molecule that retains its canonical shape. *Macromol. Biosci.* 19:e1800250. doi: 10.1002/mabi.201800250
- Thomas, R., Nair, A. P., Kr, S., Mathew, J., and Ek, R. (2014). Antibacterial activity and synergistic effect of biosynthesized AgNPs with antibiotics against multidrug-resistant biofilm-forming coagulase-negative staphylococci isolated from clinical samples. *Appl. Biochem. Biotechnol.* 173, 449–460. doi: 10.1007/s12010-014-0852-z
- Vagnozzi, A. N., Reiter, J. F., and Wong, S. Y. (2015). Hair follicle and interfollicular epidermal stem cells make varying contributions to wound regeneration. *Cell Cycle* 14, 3408–3417. doi: 10.1080/15384101.2015.1090062
- Wang, M., Yang, Q., Long, J., Ding, Y., Zou, X., Liao, G., et al. (2018). A comparative study of toxicity of TiO₂, ZnO, and Ag nanoparticles to human aortic smooth-muscle cells. *Int. J. Nanomedicine* 13, 8037–8049. doi: 10.2147/IJN.S188175
- Wang, Y., Xu, R., He, W., Yao, Z., Li, H., Zhou, J., et al. (2015). Three-dimensional histological structures of the human dermis. *Tissue Eng. Part C Methods* 21, 932–944. doi: 10.1089/ten.tec.2014.0578
- Wang, Y., Xu, R., Luo, G., Lei, Q., Shu, Q., Yao, Z., et al. (2016). Biomimetic fibroblast-loaded artificial dermis with “sandwich” structure and designed gradient pore sizes promotes wound healing by favoring granulation tissue formation and wound re-epithelialization. *Acta Biomater.* 30, 246–257. doi: 10.1016/j.actbio.2015.11.035
- Wu, Y. C., Wu, G. X., Huang, H. H., and Kuo, S. M. (2019). Liposome-encapsulated farnesol accelerated tissue repair in third-degree burns on a rat model. *Burns* 45, 1139–1151. doi: 10.1016/j.burns.2019.01.010
- Xiang, Q., Xiao, J., Zhang, H., Zhang, X., Lu, M., Zhang, H., et al. (2011). Preparation and characterisation of bFGF-encapsulated liposomes and evaluation of wound-healing activities in the rat. *Burns* 37, 886–895. doi: 10.1016/j.burns.2011.01.018
- Xing, F., Li, L., Zhou, C., Long, C., Wu, L., Lei, H., et al. (2019). Regulation and directing stem cell fate by tissue engineering functional

- microenvironments: scaffold physical and chemical cues. *Stem Cells Int.* 2019:2180925. doi: 10.1155/2019/2180925
- Xu, R., Bai, Y., Zhao, J., Xia, H., Kong, Y., Yao, Z., et al. (2018). Silicone rubber membrane with specific pore size enhances wound regeneration. *J. Tissue Eng. Regen. Med.* 12, e905–e917. doi: 10.1002/term.2414
- Xu, R., Luo, G., Xia, H., He, W., Zhao, J., Liu, B., et al. (2015). Novel bilayer wound dressing composed of silicone rubber with particular micropores enhanced wound re-epithelialization and contraction. *Biomaterials* 40, 1–11. doi: 10.1016/j.biomaterials.2014.10.077
- Xu, R., Xia, H., He, W., Li, Z., Zhao, J., Liu, B., et al. (2016). Controlled water vapor transmission rate promotes wound-healing via wound re-epithelialization and contraction enhancement. *Sci. Rep.* 6:24596. doi: 10.1038/srep24596
- Yang, C., Tibbitt, M. W., Basta, L., and Anseth, K. S. (2014). Mechanical memory and dosing influence stem cell fate. *Nat. Mater.* 13, 645–652. doi: 10.1038/nmat3889
- Yang, L., Kuang, H., Zhang, W., Aguilar, Z. P., Wei, H., and Xu, H. (2017). Comparisons of the biodistribution and toxicological examinations after repeated intravenous administration of silver and gold nanoparticles in mice. *Sci. Rep.* 7:3303. doi: 10.1038/s41598-017-03015-1
- Yao, B., Wang, R., Wang, Y., Zhang, Y., Hu, T., Song, W., et al. (2020). Biochemical and structural cues of 3D-printed matrix synergistically direct MSC differentiation for functional sweat gland regeneration. *Sci. Adv.* 6:eaz1094. doi: 10.1126/sciadv.aaz1094
- Yeo, G. C., Kosobrodova, E., Kondyurin, A., McKenzie, D. R., Bilek, M. M., and Weiss, A. S. (2019). Plasma-activated substrate with a tropoelastin anchor for the maintenance and delivery of multipotent adult progenitor cells. *Macromol Biosci.* 19:e1800233. doi: 10.1002/mabi.201800233
- Zarrintaj, P., Moghaddam, A. S., Manouchehri, S., Atoufi, Z., Amiri, A., Amirkhani, M. A., et al. (2017). Can regenerative medicine and nanotechnology combine to heal wounds? The search for the ideal wound dressing. *Nanomedicine* 12, 2403–2422. doi: 10.2217/nnm-2017-0173
- Zhang, X., Manukumar, H. M., Rakesh, K. P., Karthik, C. S., Nagendra Prasad, H. S., Swamy, S. N., et al. (2018). Role of BP**C*@AgNPs in Bap-dependent multicellular behavior of clinically important methicillin-resistant *Staphylococcus aureus* (MRSA) biofilm adherence: A key virulence study. *Microb. Pathog.* 123, 275–284. doi: 10.1016/j.micpath.2018.07.025
- Zheng, Y., Xue, X., Shao, Y., Wang, S., Esfahani, S. N., Li, Z., et al. (2019). Controlled modelling of human epiblast and amnion development using stem cells. *Nature* 573, 421–425. doi: 10.1038/s41586-019-1535-2
- Zhou, C., Jin, S., and Willing, R. (2016). Simulation of extracellular matrix remodeling by fibroblast cells in soft three-dimensional bioresorbable scaffolds. *Biomech. Model. Mechanobiol.* 15, 1685–1698. doi: 10.1007/s10237-016-0791-4
- Zille, A., Fernandes, M. M., Francesko, A., Tzanov, T., Fernandes, M., Oliveira, F. R., et al. (2015). Size and aging effects on antimicrobial efficiency of silver nanoparticles coated on polyamide fabrics activated by atmospheric DBD plasma. *ACS Appl. Mater. Interfaces* 7, 13731–13744. doi: 10.1021/acsami.5b04340

Conflict of Interest: The authors declare that the research was conducted in the absence of any commercial or financial relationships that could be construed as a potential conflict of interest.

Copyright © 2020 Wang, Armato and Wu. This is an open-access article distributed under the terms of the Creative Commons Attribution License (CC BY). The use, distribution or reproduction in other forums is permitted, provided the original author(s) and the copyright owner(s) are credited and that the original publication in this journal is cited, in accordance with accepted academic practice. No use, distribution or reproduction is permitted which does not comply with these terms.



Anatomical Characteristics of Cutaneous Branches Extending From the Second Dorsal Metacarpal Artery

Peng Liu[†], Zhongyuan Deng[†], Tao Zhang* and Xiaojian Li*

Department of Burn and Plastic, Guangzhou Red Cross Hospital, Medical College, Jinan University, Guangzhou, China

OPEN ACCESS

Edited by:

Bing Tang,
First Affiliated Hospital of Sun Yat-sen
University, China

Reviewed by:

Qiang Chen,
Southeast University, China
Fatemeh Kabirian,
Materials and Energy Research
Center, Iran

*Correspondence:

Tao Zhang
z.t-1231@163.com
Xiaojian Li
lixj64@163.com

[†]These authors have contributed
equally to this work

Specialty section:

This article was submitted to
Biomaterials,
a section of the journal
Frontiers in Bioengineering and
Biotechnology

Received: 10 April 2020

Accepted: 29 July 2020

Published: 20 August 2020

Citation:

Liu P, Deng Z, Zhang T and Li X
(2020) Anatomical Characteristics
of Cutaneous Branches Extending
From the Second Dorsal Metacarpal
Artery.
Front. Bioeng. Biotechnol. 8:995.
doi: 10.3389/fbioe.2020.00995

Background: A second dorsal metacarpal artery cutaneous branches flap is often used to repair skin defects in the hand. The location of the cutaneous branch of that artery is very critical for the removal of the flap. In this study, we quantitatively analyzed the origin of the cutaneous branches of the second dorsal metacarpal artery and the distribution characteristics of the radial and ulnar side to provide an anatomical basis for designing a flap.

Methods: Sixteen upper limb specimens were perfused with latex. Four specimens were infused with ethyl acetate plus plastic, and four specimens were perfused with red latex to create pellucid specimens. The origin, travel paths, and distribution of the cutaneous branches of the second dorsal metacarpal artery were anatomically observed, and we measured the length of the cutaneous branch from the midpoint of the second web space edge. We also measured the diameters and pedicle lengths of the radial and ulnar distributions of cutaneous branches of the second dorsal metacarpal artery.

Results: The cutaneous branches of the second dorsal metacarpal artery were mainly clustered at three positions, the second cluster point was at 43.9%, the fourth cluster point was at 61.2%, and the fifth cluster point was at 72.1%. The first cluster point was at 30.8% and the sixth cluster point was at 85.6%. The diameter and pedicle length of the sixth cluster point were the largest. There was no significant difference in the distribution of the diameters and pedicle lengths of the cutaneous branch between the radial and ulnar side. The second dorsal metacarpal artery sent out 1–2 cutaneous branches before the tendon joint, and formed a blood vessel anastomosis with other cutaneous branches located further from the tendon joint. The dorsal branch of the radial nerve in the hand extended a nerve branch at the wrist joint and traveled between the cutaneous branches of the second dorsal metacarpal artery to dominate the corresponding skin.

Conclusion: Three clusters in the distal second dorsal metacarpal artery were selected to be the flap pedicle containing a cutaneous nerve for use in repairing a skin defect in the hand and fingers.

Keywords: second dorsal metacarpal artery, cutaneous branches, cluster distribution, skin wound repair, anatomical characteristics

INTRODUCTION

The hand is the most commonly used appendage in daily life and the most vulnerable part of the body. An injured hand is likely to cause physical dysfunction, adversely affect a person's appearance, and produce psychological burden (Masakatsu et al., 2018; Viktor and Max, 2018; Xu et al., 2018). Dorsal metacarpal artery flaps are used to repair hand tissue defects, and especially defects of the fingers. Some advantages of the dorsal metacarpal artery flap include a simple operation, convenient tissue transfer, and similarities in characteristics of tissue cortex, toughness, and elasticity (Isaraj, 2011; Schiefer et al., 2012).

The second dorsal metacarpal artery is relatively anatomically consistent and rarely absent. Therefore, a second dorsal metacarpal artery flap is usually used to cover a hand skin defect. Current research shows that the second dorsal metacarpal skin flap is usually designed so as to allow the second metacarpal dorsal artery to serve as the vascular pedicle when repairing small area skin defects in the hand. However, a disadvantage of that design is that it sacrifices the second dorsal metacarpal artery and injures a large amount of tissue (Wang et al., 2011; Chi et al., 2018; Webster and Saint-Cyr, 2020).

Recent studies have shown that the second dorsal metacarpal artery extends cutaneous branches that interconnect in the superficial fascia to form a rich reticular structure rich in blood vessels. The cutaneous branches arising from the dorsal metacarpal artery are mainly distributed in the distal 1/3 segment, and have a mean diameter > 0.2 mm. A cutaneous branch of the second dorsal metacarpal artery can be used as the vascular pedicle when repairing a small area defect in hand (Da-Ping and Morris, 2001; Guang-Rong et al., 2005; Zhang et al., 2009; Appleton and Morris, 2014). However, it is difficult to use ultrasound to verify the exact positions of the cutaneous branches before surgery due to their lack of distinction. Therefore, a quantitative analysis of the anatomical distribution of cutaneous branches is helpful for designing the flap.

Vascular perfusion is a common method to study vascular construction such as blood vessel traveling, distribution, and anastomosis. Different fillers can be used to perfuse blood vessels, and then the blood vessel travel can be displayed by anatomy, transparency, corrosion and radiography. These fillers are rubber, plastic, gelatin, and oil, etc. Latex is the emulsion before the rubber solidifies. The blood vessel specimens perfused with the red latex are elastic, easy to stretch and not easy to break. This method is suitable for microanatomy observation research. Ethyl acetate and plastic perfusion is a method to make cast specimens. The blood vessels are perfused with ethyl acetate and plastic mixed with staining agent. After ethyl acetate and plastic hardening, the specimens are corroded with acid to leave only the ethyl acetate and plastic model of blood vessels. Compared with the latex perfusion, the cast specimens made of ethyl acetate and plastic perfusion can show three-dimensional blood vessels traveling and distribution.

Although numerous studies have described using cutaneous branches flaps with the dorsal metacarpal artery serving as a pedicle, no quantitative analysis has been performed on

the distribution patterns of the cutaneous branches, including their radial and ulnar distributions. This study used anatomical techniques such as vascular perfusion, casting, and transparency to study the distribution patterns of the cutaneous branches, including their radial and ulnar distributions, to provide an anatomical basis for designing a flap.

MATERIALS AND METHODS

A total of 24 upper limb specimens were legally obtained from the Human Anatomy Department of Southern Medical University in Guangzhou, China. 24 upper limb specimens were amputated at the human elbow joint and immediately the brachial artery was perfused with colored materials. These specimens were placed in a -18°C refrigerator for storage. We performed the anatomical experiments after 1 week. Next, 16 of the specimens were injected with latex for microanatomy examination, four specimens were embedded with ethyl acetate and plastic for use as cast specimens, and four specimens were injected with latex to create transparent specimens. The study protocol was approved by the Institutional Review Board of Guangzhou Red Cross Hospital.

Latex Specimens for Microanatomy

A glass catheter was carefully inserted into the brachial artery, which was filled with a certain amount of red latex. Next, a longitudinal incision was made between the second and third metacarpal bones on the dorsum of the hand, and the skin tissue was elevated from the deep fascia to expose cutaneous branches extending from the second dorsal metacarpal artery. The lengths, diameters, and positions of cutaneous branches extending from the second dorsal metacarpal artery were measured. The distance between the midpoint of the second web space edge and the midpoint of the second metacarpal bone was set as a unit, and



FIGURE 1 | The distance between the midpoint of the second web space edge and the midpoint of the second metacarpal bone was set as the standard unit length (100%).

we measured the distance of all branches to the midpoint of the second web space edge.

Cast Specimens

A glass catheter was carefully inserted into the brachial artery, which was then injected with 10 mL of an ethyl acetate and plastic solution enough to fill the blood vessel; the solution was replenished with a certain amount of ethyl acetate and plastic mixture every 2 h. The mixture was replenished five times in total. The brachial artery was filled with self-setting dental tray material during the final replenishment. After its preparation, the casting specimen was immersed in a 25% hydrochloric acid bath and allowed to slowly corrode in a week. The positions, distribution, and anastomotic connections of cutaneous branches extending from the second dorsal metacarpal artery were observed.

Transparent Specimens for Direct Observation

An appropriate amount of red latex was perfused into the brachial artery. After it solidified in the blood vessels, the specimen was soaked and subsequently fixed in 75% alcohol; after which, it was air-dried in a ventilated location. Finally, the specimen was soaked in glycerol to make it transparent.

Statistical Analysis

All data were analyzed using SPSS Statistics for Windows, Version 17.0 (SPSS, Inc., Chicago, IL, United States). The distance between the midpoint of the second web space edge and the midpoint of the second metacarpal bone was established as the standard unit length (100%) (Figure 1). The distance of each

TABLE 1 | The clusters distribution of cutaneous branches from the second dorsal metacarpal artery in 16 specimens.

Cluster	Cutaneous branches	Relative distance (%)*	Diameter (mm)	The length of pedicle (mm)
1	9	30.8	0.38 ± 0.15	5.93 ± 1.08
2	21	43.9	0.45 ± 0.13	5.62 ± 2.02
3	16	53.4	0.43 ± 0.13	5.57 ± 1.13
4	22	61.2	0.41 ± 0.11	6.47 ± 1.68
5	22	72.1	0.41 ± 0.17	6.46 ± 2.01
6	13	85.6	0.47 ± 0.20	7.41 ± 1.86

*The distance between the midpoint of the second web space edge and the midpoint of the second metacarpal bone was set as the standard unit length (100%). The relative distance is equal to the distance from each cutaneous branches to the midpoint of the second web space edge divided by the standard unit length.

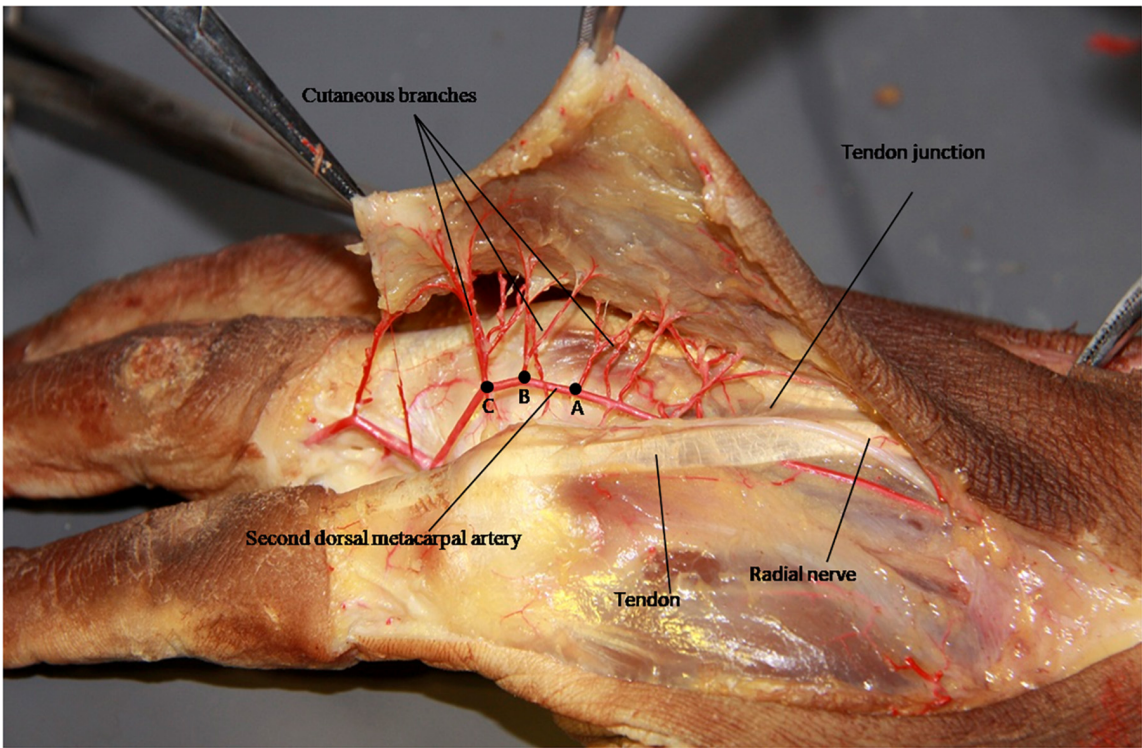


FIGURE 2 | The cutaneous branches from the second dorsal metacarpal artery are mainly clustered at three positions: the second cluster point is at 43.9% (A), the fourth cluster point is at 61.2% (B), and the fifth cluster point was at 72.1% (C).

TABLE 2 | The distribution of the diameter and pedicle length of the cutaneous branches between the radial and ulnar side.

	Radial (<i>n</i> = 55)	Ulnar (<i>n</i> = 48)	<i>t</i>	<i>*p</i>
Diameter (mm)	0.42 ± 0.12	0.43 ± 0.17	−0.443	0.659
The length of pedicle (mm)	6.04 ± 1.64	6.44 ± 1.97	−1.121	0.265

**p* was less than 0.05 means that it was significant difference in the distribution of the diameter and pedicle length of the cutaneous branch between the radial and ulnar side.

cutaneous branch to the midpoint of the second web space edge was recorded. The data were subjected to K-means clustering to quantitatively analyze the origin distribution of the cutaneous branches. The diameters and pedicle lengths of the radial and ulnar distributions of cutaneous branches extending from the second dorsal metacarpal artery were quantitatively analyzed by the independent *t*-test.

RESULTS

Origin Distribution of the Cutaneous Branches From the Second Dorsal Metacarpal Artery

All cutaneous branches extending from the second dorsal metacarpal artery were counted in 16 specimens, and a total of 103 branches were identified. The cutaneous branches were mainly clustered at three positions: the second cluster point was at 43.9%, and included 21 branches, the fourth cluster point was at 61.2%, and included 22 dermal branches, and the fifth cluster point was at 72.1%, and included 22 cutaneous branches. The first cluster point was at 30.8% and the sixth cluster point was

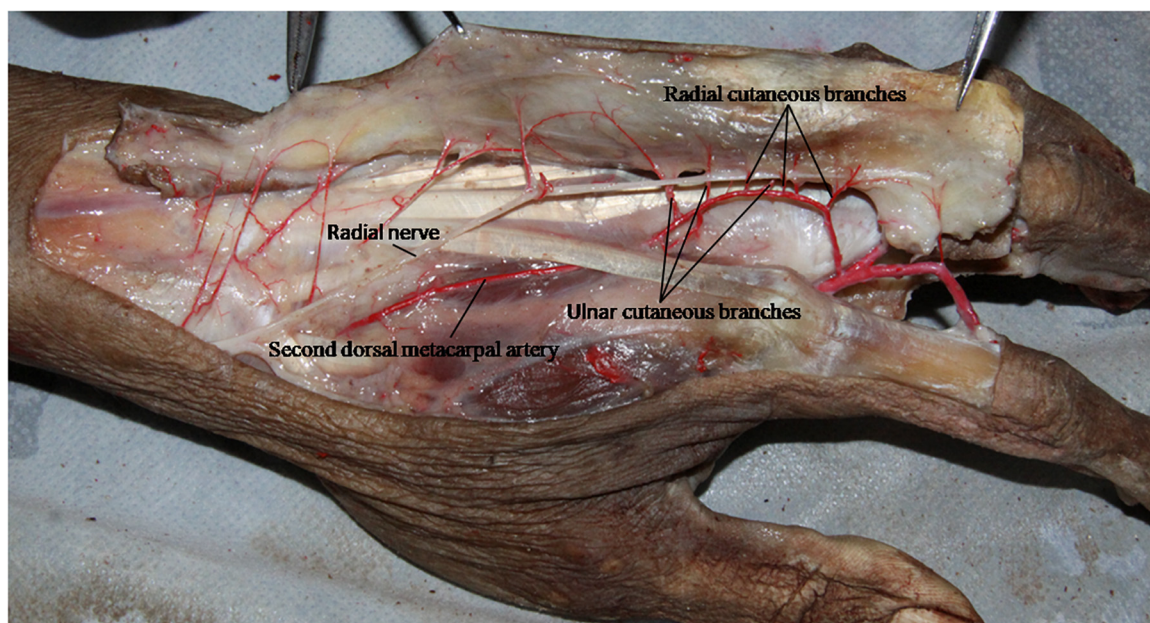
at 85.6%. It was obvious that the cutaneous branches were less distributed at the second cluster point; however, the diameters and pedicle lengths of the branches at the sixth cluster point were the largest (Table 1 and Figure 2).

Distribution Characteristics of the Diameters and Pedicle Lengths of the Radial and Ulnar Distributions of Cutaneous Branches Extending From the Second Dorsal Metacarpal Artery

A total of 55 branches were distributed in the radial side of the second dorsal metacarpal artery and 48 branches were distributed in the ulnar side. There were seven more branches in the radial side than in the ulnar side. The mean diameter of the radial branches was smaller than that of the ulnar cutaneous branches; however, there was no significant difference in the distribution of the diameter of the cutaneous branches in the radial and ulnar sides (*p* = 0.659). The mean pedicle length of the radial branches was significantly less than that of the ulnar branches (*p* = 0.265). Therefore, there was no significant difference in the distribution of the diameters and pedicle lengths of the cutaneous branches in the radial and ulnar side (Table 2 and Figure 3).

The Anatomical Relationship Between Cutaneous Branches and the Dorsal Branches of the Radial Nerve

The second dorsal metacarpal artery travels between the second and third metacarpal bones, and emits numerous cutaneous branches along the way. The cutaneous branches are mainly concentrated in the distal parts of the second and third tendon

**FIGURE 3 |** The distribution of the diameter and pedicle length of the cutaneous branch between the radial and ulnar side was no significant difference.

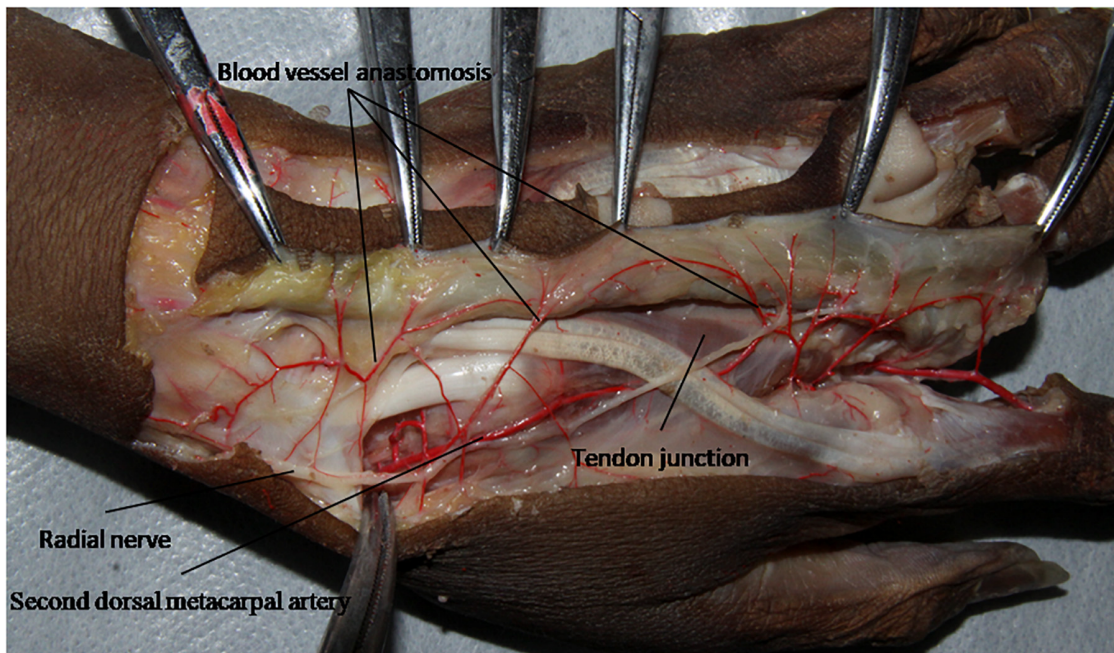


FIGURE 4 | The cutaneous branches extended in the proximal part of the tendon joint, and formed a blood vessel anastomosis with the cutaneous branches farther from the tendon joint.

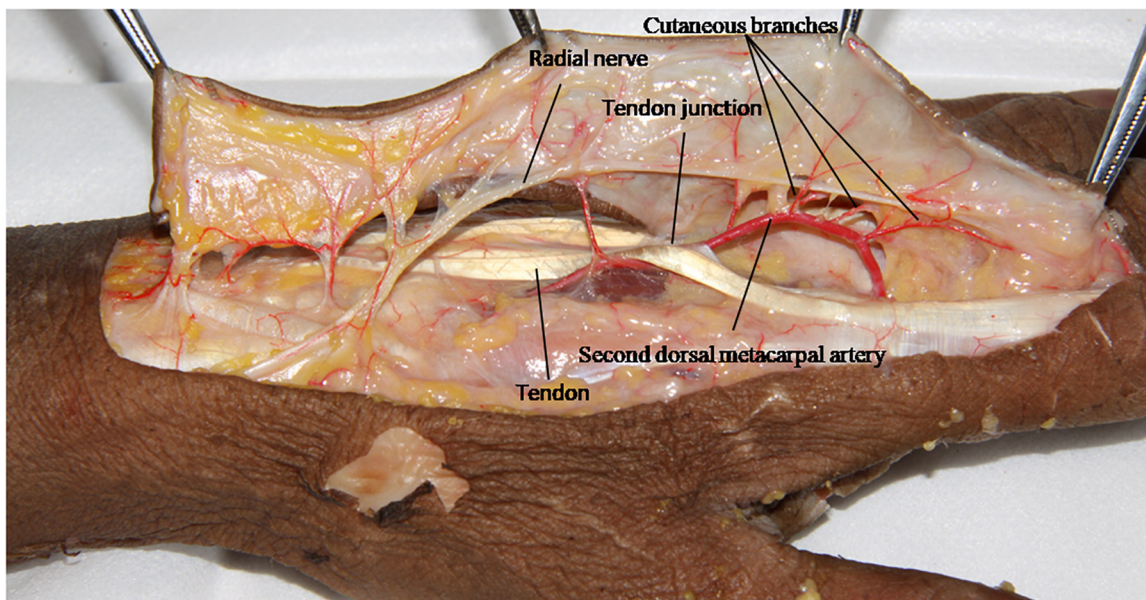
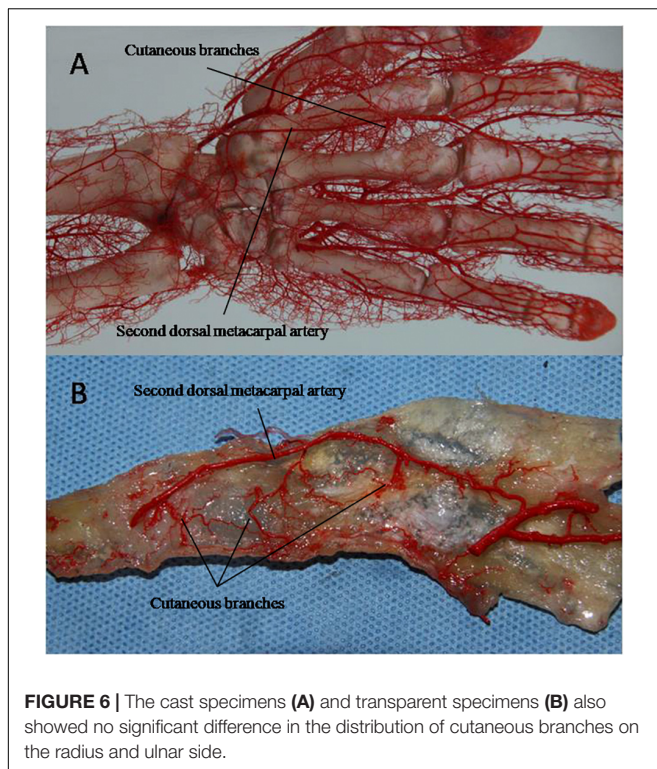


FIGURE 5 | The dorsal branch of the radial nerve in the hand extended a nerve branch at the wrist joint and traveled between the cutaneous branches of the second dorsal metacarpal artery.

joints. However, this anatomical study found that the second dorsal metacarpal artery also emitted 1–2 cutaneous branches prior to the tendon joint, and formed a blood vessel anastomosis with the cutaneous branches located further from the tendon joint. The diameter of the cutaneous branches ranged from 0.31 to 0.47 mm (**Figure 4**). The dorsal branch of the radial

nerve in the hand extended a nerve branch at the wrist joint and traveled between the cutaneous branches of the second dorsal metacarpal artery to dominate the corresponding skin. This anatomical feature can provide an anatomical basis for designing the second dorsal metacarpal artery flap with a sensory nerve (**Figure 5**).



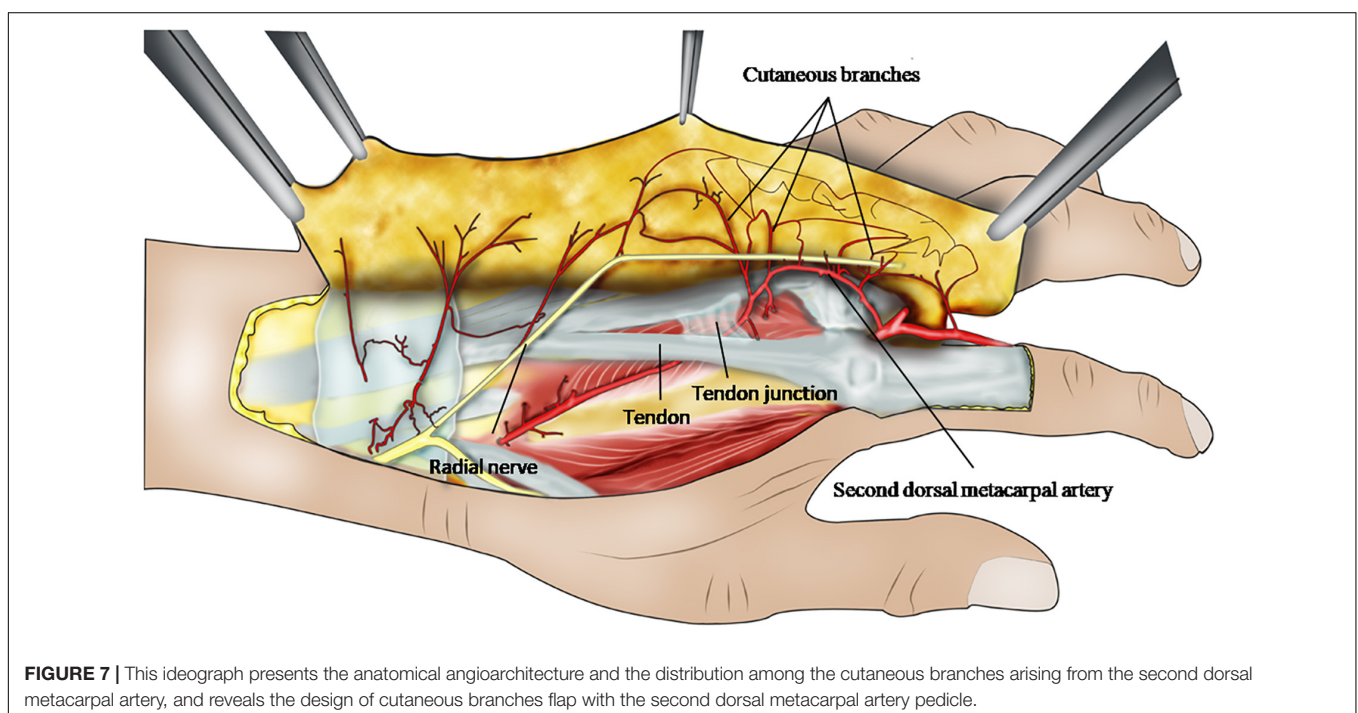
DISCUSSION

The second dorsal metacarpal artery flap is an important flap commonly used to repair skin defects in the hand. Cutaneous branches of the dorsal metacarpal artery form a vascular chain

that supplies blood for the second dorsal metacarpal artery flap. In this study, we analyzed the origin distribution of cutaneous branches and the diameters and pedicle lengths of the radial and ulnar distribution of cutaneous branches extending from the second dorsal metacarpal artery. The three locations of the clustered cutaneous branches were found to be used for clinicians to design cutaneous branches flap and perform operation. The anatomical adjacent relationship between the cutaneous branches and dorsal cutaneous nerve was also observed.

The second dorsal metacarpal artery originates from the radial artery or dorsal carpal artery network. It then travels on the superficial surface of the dorsal interosseous muscles, and emits numerous cutaneous branches along the way that nourish the corresponding skin tissue (Marx et al., 2001; De Rezende et al., 2004; Al-Baz et al., 2019). Our study found that the cutaneous branches of the second dorsal metacarpal artery were mainly distributed in six clusters, of which there were more cutaneous branches distributed at 43.9, 61.2, and 72.1% of the cluster points. A clinician can locate the vascular pedicle prior to surgery in this position. Our statistical analysis showed that an average of 6.4 branches originated from the second dorsal metacarpal artery. Therefore, we conducted a k-mean clustering analysis to establish six categories for better evaluating the cluster characteristics of cutaneous branches, and obtain more information than could be provided by a two-step cluster analysis (Liu et al., 2015).

Clinically, the second dorsal metacarpal artery flap is designed based on the principle of point, line and surface, and usually has a symmetrical design. However, many vascular branches are often anatomically dominant (Schaverien and Saint-Cyr, 2008; Saint-Cyr et al., 2010; Sun et al., 2013). A study of the radial and ulnar distribution of cutaneous branches is helpful for



determining the size and shape of a flap. This study found no significant difference in the distribution of the diameter and pedicle length of the cutaneous branch in the radial and ulnar side (Figure 6).

While most previous studies have focused on the cutaneous branches at the distal part from the tendon joint, there are usually 1–2 cutaneous branches with a diameter of 0.37 ± 0.11 mm before the tendon joint (Yoon et al., 2007; Zhu et al., 2013; Rozen et al., 2015; van Alphen et al., 2016). The cutaneous branches of the distal and proximal parts of the second dorsal metacarpal artery link with each other, which can increase the length of the vascular pedicle of the flap and enlarge its rotational coverage. The dorsal branch of the radial nerve travels between the radial and ulnar cutaneous branches. This anatomical feature can help clinicians to design the second dorsal metacarpal artery flap to include sensory nerves that restore the sensory function of the wound surface and improve the tactile function of the fingertips.

Based on our anatomical observations and statistical studies, the cutaneous branches near or in the cluster points of the second dorsal metacarpal artery were used as the flap pedicle, and the surface projection of the second dorsal metacarpal artery served as the flap axis. A cutaneous branches flap is designed to cut the plane between the shallow and deep fascia (Figure 7). During the surgical procedure, we preserved the fascial tissue around the pedicle as much as possible in order to avoid vascular spasm caused by excessive distortion or rotation of the cutaneous branches. During the process of lifting the flap, it was not necessary to cut the deep fascia so as to protect both the second dorsal metacarpal artery and the original root of the cutaneous branches. After the operation, the patient's index finger and middle finger movement was normal and finger sensory function was good, as judged by a 2 mm two-point discrimination (Delikonstantinou et al., 2011; Figure 8).

However, the diameters of cutaneous branches are small enough that naked branches extremely are prone to vasospasm.

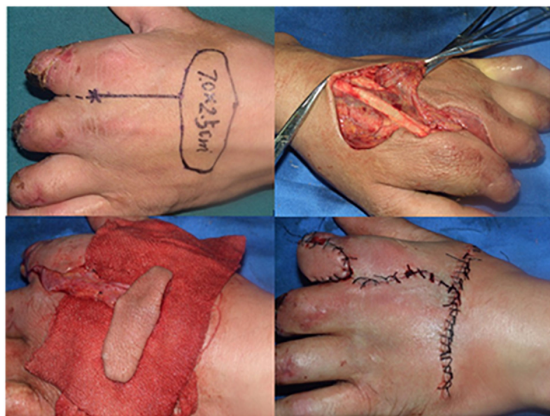


FIGURE 8 | The second dorsal metacarpal artery flap with cutaneous nerve was recovered to repair the skin defect of the hand. After the operation, the patient's finger movement was normal and finger sensory was good due to 2 mm two-point discrimination.

Before the operation it is very important to perform a Doppler exploration. During the operation, it is necessary to pay attention to the anastomosis of cutaneous branches, and to protect the anastomosis linking between the cutaneous branches as much as possible.

CONCLUSION

Cutaneous branches of the second dorsal metacarpal artery were mainly clustered at three positions: 43.9, 61.2, and 72.1% in the distal second dorsal metacarpal artery, which was chosen as the flap pedicle with a cutaneous nerve to repair the skin defect in the hand and fingers of a patient.

DATA AVAILABILITY STATEMENT

All datasets generated for this study are included in the article/supplementary material.

ETHICS STATEMENT

The studies involving human participants were reviewed and approved by the Institutional Review Board of Guangzhou Red Cross Hospital. Written informed consent obtained from the next of kin.

AUTHOR CONTRIBUTIONS

In the beginning of work, XL gave the idea to observe the anastomosis relationship and the distribution of the perforators arising from the second dorsal metacarpal artery. TZ, ZD, and PL dissected carefully the second dorsal metacarpal artery and its perforators, included the linking among the perforators in the superficial fascia and dermis. TZ made the pellucid specimen reveal the course of the perforators and anastomosis between the adjacent branches. In the same time, we measured the diameter and the length of pedicle of the perforators in the course of dissection, then ZD and PL conducted not only a chi-square test to compare the quantities of ulnar and radial branches from second dorsal metacarpal artery in two groups with SPSS 17.0, but also the cluster analysis which was a two-step clustering procedure to observe the integrated distribution of the perforators. ZD and PL design the flap to cover the defect of finger based on the anatomy of second dorsal metacarpal artery perforators. In the whole course, XL provided a great helping for us to complete this research. All authors contributed to the article and approved the submitted version.

FUNDING

This work was supported by research grant 20191A011015 (PL) from General Guidance Project of Guangzhou Municipal Health Committee, research grant A2019273 (PL) from Guangdong

Medical Science and Technology Research Fund, research grant from Guangzhou high-level clinical key specialty construction fund (XL), research grant from 59-special technology project of Guangzhou (XL), research

grant from 2019 Ph.D. Workstation Scientific Research Fund of Guangzhou Red Cross Hospital, and research grant from 2018 Project Funds of Guangzhou Red Cross Hospital.

REFERENCES

- Al-Baz, T., Gad, S., and Keshk, T. (2019). Evaluation of dorsal metacarpal artery perforator flaps in the reconstruction of hand soft-tissue defects. *Menoufia Med. J.* 32, 1256–1261.
- Appleton, S. E., and Morris, S. F. (2014). Anatomy and physiology of perforator flaps of the upper limb. *Hand Clin.* 30, 123–135. doi: 10.1016/j.hcl.2013.12.003
- Chi, Z., Lin, D., and Chen, Y. (2018). Routine closure of the donor site with a second dorsal metacarpal artery flap to avoid the use of a skin graft after harvest of a first dorsal metacarpal artery flap. *J. Plastic Reconstruct. Aesthetic Surg.* 71, 870–875. doi: 10.1016/j.bjps.2018.01.031
- Da-Ping, Y., and Morris, S. F. (2001). Reversed dorsal digital and metacarpal island flaps supplied by the dorsal cutaneous branches of the palmar digital artery. *Ann. Plastic Surg.* 46, 444–449. doi: 10.1097/00000637-200104000-00017
- De Rezende, M. R., Mattar, J. R., and Cho, A. B. (2004). Anatomic study of the dorsal arterial system of the hand. *Rev. Hosp. Clin. Fac. Med. Sao Paulo* 59, 71–76. doi: 10.1590/s0041-87812004000200005
- Delikonstantinou, I. P., Gravvanis, A. I., and Dimitriou, V. (2011). Foucher first dorsal metacarpal artery flap versus littler heterodigital neurovascular flap in resurfacing thumb pulp loss defects. *Ann. Plast. Surg.* 67, 119–122. doi: 10.1097/sap.0b013e3181ef6f6d
- Guang-Rong, Y., Feng, Y., and Shi-Min, C. (2005). Microsurgical second dorsal metacarpal artery cutaneous and tenocutaneous flap for distal finger reconstruction: anatomic study and clinical application. *Microsurgery* 25, 30–35. doi: 10.1002/micr.20077
- Isaraj, S. (2011). Use of dorsal metacarpal artery flaps in post burn reconstruction - two cases report. *Macedonian J. Med. Sci.* 4:11.
- Liu, P., Qin, X., and Zhang, H. (2015). The second dorsal metacarpal artery chain-link flap: an anatomical study and a case report. *Surg. Radiol. Anat.* 37, 349–356. doi: 10.1007/s00276-014-1372-9
- Marx, A., Preisser, P., and Peek, A. (2001). Anatomy of the dorsal mid-hand arteries—anatomic study and review of the literature. *Handchir. Mikrochir. Plast. Chir.* 33, 77–82.
- Masakatsu, H., Takashi, M., and Yoshihito, T. (2018). Functional reconstruction of severely burned hand with osseous blood flow deficiency with immediate surgery using an abdominal bipedicle flap: a case report. *Eplasty* 18:11.
- Rozen, W. M., Katz, T. L., and Hunter-Smith, D. J. (2015). Vascularization of the dorsal base of the second metacarpal bone: implications for a reverse second dorsal metacarpal artery flap. *Plast. Reconstr. Surg.* 135, 231–232.
- Saint-Cyr, M., Mujadzic, M., and Wong, C. (2010). The radial artery pedicle perforator flap: vascular analysis and clinical implications. *Plast. Reconstr. Surg.* 125, 1469–1478. doi: 10.1097/prs.0b013e3181d511e7
- Schaverien, M., and Saint-Cyr, M. (2008). Perforators of the lower leg: analysis of perforator locations and clinical application for pedicled perforator flaps. *Plast. Reconstr. Surg.* 122, 161–170. doi: 10.1097/prs.0b013e3181774386
- Schiefer, J. L., Schaller, H., and Rahmian-Schwarz, A. (2012). Dorsal metacarpal artery flaps with extensor indices tendons for reconstruction of digital defects. *J. Invest. Surg.* 25, 340–343. doi: 10.3109/08941939.2011.640384
- Sun, C., Hou, Z. D., and Wang, B. (2013). An anatomical study on the characteristics of cutaneous branches-chain perforator flap with ulnar artery pedicle. *Plast. Reconstr. Surg.* 131, 329–336. doi: 10.1097/prs.0b013e318277884c
- van Alphen, N. A., Laungani, A. T., and Christner, J. A. (2016). The distally based dorsal metatarsal artery perforator flap: vascular study and clinical implications. *J. Reconstr. Microsurg.* 32, 245–250. doi: 10.1055/s-0035-1554936
- Viktor, M. G., and Max, G. (2018). Wrist scar contracture, hand deviation: anatomy and treatment with trapeze-flap plasty. *Plastic Reconstruct. Surg. Burns* 26, 235–242. doi: 10.1007/978-3-319-78714-5_26
- Wang, P., Zhou, Z., and Dong, Q. (2011). Reverse second and third dorsal metacarpal artery fasciocutaneous flaps for repair of distal- and middle-segment finger soft tissue defects. *J. Reconstr. Microsurg.* 27, 495–502. doi: 10.1055/s-0031-1284235
- Webster, N., and Saint-Cyr, M. (2020). Flaps based on the dorsal metacarpal artery. *Hand Clin.* 36, 75–83. doi: 10.1016/j.hcl.2019.09.001
- Xu, G., Jianli, C., and Ziping, J. (2018). Risk factors for pedicled flap necrosis in hand soft tissue reconstruction: a multivariate logistic regression analysis. *ANZ J. Surg.* 88, 127–131.
- Yoon, S. W., Rebecca, A. M., and Smith, A. A. (2007). Reverse second dorsal metacarpal artery flap for reconstruction of fourth-degree burn wounds of the hand. *J. Burn. Care Res.* 28, 521–523. doi: 10.1097/bcr.0b013e318053daab
- Zhang, X., He, Y., and Shao, X. (2009). Second dorsal metacarpal artery flap from the dorsum of the middle finger for coverage of volar thumb defect. *J. Hand Surg. Am.* 34, 1467–1473. doi: 10.1016/j.jhsa.2009.04.040
- Zhu, H., Zhang, X., and Yan, M. (2013). Treatment of complex soft-tissue defects at the metacarpophalangeal joint of the thumb using the bilobed second dorsal metacarpal artery-based island flap. *Plast. Reconstr. Surg.* 131, 1091–1097. doi: 10.1097/prs.0b013e3182865c26

Conflict of Interest: The authors declare that the research was conducted in the absence of any commercial or financial relationships that could be construed as a potential conflict of interest.

Copyright © 2020 Liu, Deng, Zhang and Li. This is an open-access article distributed under the terms of the Creative Commons Attribution License (CC BY). The use, distribution or reproduction in other forums is permitted, provided the original author(s) and the copyright owner(s) are credited and that the original publication in this journal is cited, in accordance with accepted academic practice. No use, distribution or reproduction is permitted which does not comply with these terms.

Advantages of publishing in Frontiers



OPEN ACCESS

Articles are free to read
for greatest visibility
and readership



FAST PUBLICATION

Around 90 days
from submission
to decision



HIGH QUALITY PEER-REVIEW

Rigorous, collaborative,
and constructive
peer-review



TRANSPARENT PEER-REVIEW

Editors and reviewers
acknowledged by name
on published articles

Frontiers

Avenue du Tribunal-Fédéral 34
1005 Lausanne | Switzerland

Visit us: www.frontiersin.org

Contact us: frontiersin.org/about/contact



REPRODUCIBILITY OF RESEARCH

Support open data
and methods to enhance
research reproducibility



DIGITAL PUBLISHING

Articles designed
for optimal readership
across devices



FOLLOW US

@frontiersin



IMPACT METRICS

Advanced article metrics
track visibility across
digital media



EXTENSIVE PROMOTION

Marketing
and promotion
of impactful research



LOOP RESEARCH NETWORK

Our network
increases your
article's readership